

**Biosphere-Atmosphere Exchange  
of Peroxyacetyl Nitrate:  
Development of a Flux  
Measurement System and its  
Application on a Grassland  
Ecosystem**

A dissertation submitted to the  
FACULTY OF BIOLOGY, CHEMISTRY AND GEOSCIENCES  
UNIVERSITY OF BAYREUTH

to attain to the degree of  
DR. RER. NAT.

presented by  
ALEXANDER MORAVEK  
Dipl.-Geoökol.

January 2014



**Biosphere-Atmosphere Exchange  
of Peroxyacetyl Nitrate:**

**Development of a Flux Measurement  
System and its Application on a  
Grassland Ecosystem**

supervised by  
Prof. Dr. Thomas Foken



Die vorliegende Arbeit wurde in der Zeit von Februar 2009 bis Dezember 2013 in Mainz am Max-Planck-Institut für Chemie, Abteilung für Biogeochemie, unter der Betreuung von Prof. Dr. Thomas Foken und Dr. Ivonne Trebs angefertigt.

Vollständiger Abdruck der von der Fakultät für Biologie, Chemie und Geowissenschaften der Universität Bayreuth genehmigten Dissertation zur Erlangung des akademischen Grades eines Doktors der Naturwissenschaften.

Dissertation eingereicht am: 20.01.2014

Zulassung durch die Promotionskommission: 29.01.2014

Wissenschaftliches Kolloquium: 15.04.2014

Amtierender Dekan: Prof. Dr. Rhett Kempe

Prüfungsausschuss:

Prof. Dr. Thomas Foken (Erstgutachter)

Prof. Dr. Andreas Held (Zweitgutachter)

Prof. Dr. Bernd Huwe (Vorsitz)

Prof. Dr. Christiane Werner



# Summary

Peroxyacetyl nitrate (PAN) is an organic nitrogen species playing an important role in atmospheric chemistry. Being a source of other nitrogen oxides, it promotes for example the formation of aerosol particles and tropospheric ozone (O<sub>3</sub>). It has an impact on air quality, human health, as well as on aquatic and terrestrial ecosystems. Knowledge of the formation and removal of atmospheric PAN is thus important and also essential for the improvement of the chemistry of climate models. While PAN is known to be taken up by vegetation, underlying mechanisms are still not well understood and the role of PAN deposition as a removal process and source of nitrogen to ecosystems is not clear.

This thesis presents a measurement system designed for the determination of biosphere-atmosphere exchange fluxes of PAN. The system was applied on a natural grassland ecosystem with the focus on the performance of the flux measurement system, but also with the aim to contribute to a better understanding of the biosphere-atmosphere exchange of PAN.

The system was designed for the application of two flux measurement techniques, hyperbolic relaxed eddy accumulation (HREA) and the modified Bowen ratio (MBR) method, employing a gaschromatograph with electron capture detection (GC-ECD) for PAN analysis. A keystone in its design was the pre-concentration of PAN by capillary columns, which were used as up- and downdraft reservoirs for the HREA application and enabled simultaneous sampling at two measurement heights, which is an important feature for the MBR method. A major challenge of the design was the resolution of small PAN mixing ratio differences by the analytical unit, which required an optimum choice of operational settings and a detailed error analysis.

The PAN flux measurement system was first applied on a nutrient-poor natural grassland site at the premises of the Mainz-Finthen Airport, Germany, in the period from August to September 2011. The application of the MBR method yielded average daytime PAN fluxes of  $-0.07 \text{ nmol m}^{-2} \text{ s}^{-1}$  with a random flux error of  $\pm 0.03 \text{ nmol m}^{-2} \text{ s}^{-1}$ , which was mainly attributed to the small PAN mixing ratio

differences. Due to both a higher surface resistance and larger uncertainties of the PAN analysis, at the natural grassland site no significant PAN fluxes could be resolved with the HREA method. The thesis demonstrates that above low vegetation, like the studied grassland, the MBR method is in most cases more suitable than the REA technique, while REA is preferably used above high vegetation such as forest canopies.

Due to large errors of the HREA application, this thesis presents a detailed analysis of the effects of an imprecise sampling of up- and downdraft events for REA applications. Especially, the implication of a long inlet tube may introduce a significant lag time error and high frequency attenuation effects. The simulation of REA fluxes of several scalar quantities revealed that REA fluxes might be generally underestimated from less than 5% to about 50% for typically observed lag time errors. The observed effect of high frequency attenuation on REA fluxes is of similar magnitude, ranging between less than 5% to about 30% for typical filter strengths. For both effects a function of the flux loss with the so-called eddy reversal frequency was found, which could be used to correct HREA fluxes at the investigated grassland site or identify their uncertainties. Furthermore, in the Appendix a detailed procedure is provided how to minimize, evaluate and correct lag time and high frequency effects for future REA setups.

In the last part of the thesis, the impact of PAN deposition at the nutrient-poor natural grassland site is investigated. PAN deposition fluxes obtained with the MBR method were partitioned into stomatal and non-stomatal deposition pathways. A significant non-stomatal conductance was found, which was of similar magnitude than the non-stomatal conductance for  $O_3$ , which would imply that currently applied deposition models may significantly underestimate the deposition of PAN. The retrieved information on the stomatal and non-stomatal conductances was used to model the PAN deposition over a 3.5 months period (summer to early autumn). Since the measurement site was situated on the edge of an urban and industrialized region, this allowed the investigation of the influence of local air pollution on the PAN deposition. Although PAN deposition was about twice as large during polluted periods, the results suggest that PAN deposition does not play a critical role as a nitrogen source to the investigated nutrient-poor grassland ecosystem, during both polluted and unpolluted conditions. Instead, PAN deposition was found to contribute to 20–30% of the PAN removal from the atmosphere during daytime. In higher latitudes or during winter, when thermochemical decomposition of PAN is low, PAN deposition is likely to be the predominant sink.

# Zusammenfassung

Peroxyacetylnitrat (PAN) ist eine organische Stickstoffverbindung und spielt für die Chemie der Atmosphäre eine wichtige Rolle. Als Quelle anderer Stickoxide, ist PAN beispielsweise an der Bildung von Aerosolpartikeln oder troposphärischem Ozon (O<sub>3</sub>) beteiligt. Dadurch nimmt es Einfluss auf die Luftqualität und damit die menschliche Gesundheit und wirkt auf terrestrische und aquatische Ökosysteme ein. Die Kenntnis der Quellen und Senken von atmosphärischem PAN ist daher von Bedeutung und zudem ein wichtiger Baustein in der Optimierung chemischer Prozesse in Klimamodellen. Eine bekannte Senke ist die Deposition von PAN an Pflanzenoberflächen, allerdings fehlt das genaue Verständnis über die wichtigsten Mechanismen und die Bedeutung von PAN Deposition als ein wichtiger Senkenprozess ist noch ungeklärt.

Die vorliegende Dissertation beschreibt die Entwicklung eines Messsystems zur Bestimmung des Biosphären-Atmosphärenaustausches von PAN. Das Messsystem fand Anwendung auf einem Trockenrasen-Ökosystem, um im Besonderen die Eignung und Leistung des Systems zu testen, und mit dem Ziel, zu einem besseren Verständnis der Prozesse des PAN-Austausches beitragen zu können.

Das Messsystem wurde für die Anwendung von zwei Ansätzen zur Flussbestimmung entwickelt, der hyperbolischen Relaxed-Eddy-Akkumulations-Methode (HREA) und der modifizierten Bowen-Verhältnis-Methode (MBR), wobei ein Gaschromatograph mit einem Elektroneneinfangdetektor (GC-ECD) für die PAN-Analyse zum Einsatz kam. Eine Grundlage des Messsystems war die Nutzung von Kapillarsäulen, welche als Sammeleinheiten für PAN aus auf- und abwärtsgerichteten Luftmassen (für die HREA-Methode) verwendet wurden und zudem die simultane Messung in zwei Einlasshöhen (für MBR-Methode) ermöglichten. Eine besondere Herausforderung bei der Messsystementwicklung stellte die Auflösung von sehr kleinen PAN-Mischungsverhältnisdifferenzen dar, was eine optimale Abstimmung aller Komponenten erforderte.

Das PAN-Flussmesssystem kam auf einer nährstoffarmen Trockenrasenfläche auf dem Gelände des Flugplatzes in Mainz-Finthen im August und September 2011 zum Einsatz. Mit der MBR-Methode wurden tagsüber PAN-Flüsse von  $-0,07 \text{ nmol m}^{-2} \text{ s}^{-1}$

gemessen, wobei der statistische Fehler von  $\pm 0,03 \text{ nmol m}^{-2} \text{ s}^{-1}$  hauptsächlich auf die geringen PAN-Mischungsverhältnisdifferenzen am Tag zurückzuführen war. Aufgrund eines größeren Oberflächenwiderstandes und einer größeren Messunsicherheit der PAN-Messungen, wurden auf dem Trockenrasengelände mit der HREA-Methode keine signifikanten PAN-Flüsse gemessen. Die Dissertation veranschaulicht, dass die MBR-Methode über niedriger Vegetation eher geeignet ist als die REA-Methode, welche über höherer Vegetation wie etwa Waldbeständen vorzuziehen ist.

Aufgrund der großen Messunsicherheiten bei der Anwendung der HREA-Methode, geht die vorgelegte Dissertation im Detail auf die Auswirkungen einer ungenauen Auftrennung von auf- und abwärtsgerichteten Luftmassen bei der REA-Methode im Allgemeinen ein. Besonders die Verwendung eines langen Ansaugschlauches kann zu erheblichen Fehlern durch eine ungenaue Verzögerungszeit oder Dämpfung hochfrequenter Anteile des Turbulenzspektrums führen. Die Simulation der Flüsse verschiedener skalarer Größen mit der REA-Methode ergab, dass REA-Flüsse für typische Fehler der Verzögerungszeit um weniger als 5 % und bis zu 50 % unterschätzt werden können. Die beobachteten Auswirkungen der Hochfrequenzdämpfung mit typischen Filterstärken sind mit weniger als 5 % und bis zu 30 % ähnlich groß. Beide Probleme konnten als eine Funktion der sogenannten „eddy reversal frequency“ beschrieben werden, mit Hilfe derer die mit der HREA-Methode bestimmten PAN-Flüsse korrigiert wurden oder zumindest ihr Unsicherheitsbereich definiert werden konnte.

Im letzten Teil der Dissertation wird der Einfluss der PAN-Deposition auf das nährstoffarme Trockenrasen-Ökosystem untersucht. Dazu wurden die PAN-Depositionsflüsse, welche mit der MBR-Methode bestimmt wurden, in ihre stomatären und nicht-stomatären Anteile aufgeteilt. Eine erhebliche nicht-stomatäre Leitfähigkeit wurde festgestellt, was bedeuten würde, dass PAN-Deposition in bisherigen Depositionsmodellen deutlich unterschätzt wird. Auf Basis der gewonnenen Erkenntnisse über die stomatäre und nicht-stomatäre Leitfähigkeit wurde die PAN-Deposition für einen 3,5-monatigen Zeitraum (Sommer bis Frühherbst) modelliert. Da sich der Messstandort am Rande des Ballungsgebietes der Rhein-Main-Region befindet, ließ sich der Einfluss von lokaler Luftverschmutzung auf die PAN-Deposition untersuchen. Obwohl die PAN-Deposition unter dem Einfluss von belasteten Luftmassen etwas doppelt so groß war wie bei weniger belasteter Luft, legen die Ergebnisse nahe, dass während beider Szenarien die PAN-Deposition keine entscheidende Stickstoffquelle für den nährstoffarmen Trockenrasenstandort darstellte. Stattdessen, machte die PAN-Deposition tagsüber etwa zwischen 20 und 30 % der atmosphärischen Senken aus. In kälteren Regionen dagegen spielt der thermische Zerfall von PAN nur eine untergeordnete Rolle und es kann daher angenommen werden, dass dort der Depositionsprozess den vorherrschenden Weg zur Austragung von PAN aus der Atmosphäre darstellt.

# List of manuscripts

This dissertation is presented in a cumulative form. It consists of three individual manuscripts. One manuscript is published in a peer-reviewed journal, while a second manuscript has been submitted to a peer-reviewed journal. The third manuscript will be submitted after the second manuscript was accepted for publication.

## Published manuscript

Moravek, A., I. Trebs, and T. Foken (2013), Effect of imprecise lag time and high-frequency attenuation on surface-atmosphere exchange fluxes determined with the relaxed eddy accumulation method, *Journal of Geophysical Research: Atmospheres*, 118(17), 10,210-210,224.

## Submitted manuscript

Moravek, A., T. Foken, and I. Trebs (2014), Application of a GC-ECD for measurements of biosphere-atmosphere exchange fluxes of peroxyacetyl nitrate using the relaxed eddy accumulation and gradient method, *submitted to Atmospheric Measurement Techniques*.

## Manuscript to be submitted

Moravek, A., P. Stella, T. Foken, and I. Trebs (2014), Influence of local air pollution on the deposition of peroxyacetyl nitrate to a natural grassland ecosystem, *to be submitted to Biogeosciences*.

## Publications not included in this thesis

- Oswald, R., T. Behrendt, M. Ermel, D. Wu, H. Su, Y. Cheng, C. Breuninger, A. Moravek, E. Mougín, C. Delon, B. Loubet, A. Pommerening-Roser, M. Sorgel, U. Poschl, T. Hoffmann, M. O. Andreae, F. X. Meixner, and I. Trebs (2013), HONO Emissions from Soil Bacteria as a Major Source of Atmospheric Reactive Nitrogen, *Science*, *341*(6151), 1233-1235.
- Ermel, M., R. Oswald, J. C. Mayer, A. Moravek, G. Song, M. Beck, F. X. Meixner, and I. Trebs (2013), Preparation Methods to Optimize the Performance of Sensor Discs for Fast Chemiluminescence Ozone Analyzers, *Environ Sci Technol*, *47*(4), 1930-1936.
- Foken, T., F. X. Meixner, E. Falge, C. Zetzsch, A. Serafimovich, A. Bargsten, T. Behrendt, T. Biermann, C. Breuninger, S. Dix, T. Gerken, M. Hunner, L. Lehmann-Pape, K. Hens, G. Jocher, J. Kesselmeier, J. Luers, J. C. Mayer, A. Moravek, D. Plake, M. Riederer, F. Rutz, M. Scheibe, L. Siebicke, M. Sorgel, K. Staudt, I. Trebs, A. Tsokankunku, M. Welling, V. Wolff, and Z. Zhu (2012), Coupling processes and exchange of energy and reactive and non-reactive trace gases at a forest site - results of the EGER experiment, *Atmos. Chem. Phys.*, *12*(4), 1923-1950.
- Sörgel, M., I. Trebs, A. Serafimovich, A. Moravek, A. Held, and C. Zetzsch (2011), Simultaneous HONO measurements in and above a forest canopy: influence of turbulent exchange on mixing ratio differences, *Atmos. Chem. Phys.*, *11*(2), 841-855.

# Acknowledgements

First of all, I want to thank my supervisor, Prof. Dr. Thomas Foken, for taking me as a PhD student in the first place and then guiding me to this point – the completion of this thesis. I am most grateful for his expertise on flux measurements leading to the success of this thesis, and I value him as a great teacher in Micrometeorology. Also, I want to thank him for his commitment and always acting in my best interest.

Above all, I am thankful to Dr. Ivonne Trebs, who gave me the opportunity to do my PhD in her group and acted as my daily supervisor at the Max Planck Institute for Chemistry (MPIC). Without her scientific input and guidance I would not have made it so far. Most of all, she gave me the motivation to go on when I was in despair about technical problems in the development of the PAN flux measurement system.

Besides my supervisors, I am indebted to Prof. Dr. Meinrat O. Andreae and Dr. Franz X. Meixner as members of my PhD committee and supporting my scientific career in general. I especially want to thank Franz for initially waking my interest in trace gas measurements and research at the soil-vegetation-atmosphere interface.

At this point, I want express my gratitude to Dr. Matthias Sörgel, who is now leading the research group and is always open for fruitful discussions.

This thesis would not be the same without the assistance of my colleagues at the MPIC. I am thankful to all who were involved in the setup and measurements at the Mainz-Finthen experiment site, mainly Dr. Jens-Christopher Mayer and Michael Welling, but also Stefan Wolff and Daniel Moran, who assisted in the initial phase of the experiment. However, I am especially grateful to Daniel Plake, with whom I conducted the most of the experiment in close co-operation. While through many discussions he inspired me to look at some scientific or technical problem from another angle, I particularly value his friendship.

I am especially indebted to Dr. Patrick Stella, from whom I learned a lot about deposition modelling, and also to Dr. Eva Falge and Shang Sun, who both proofread the Synopsis of this thesis. Also, I want to thank my office mate Robert Oswald and all

## Acknowledgements

---

other colleagues, who contributed to a fruitful research environment at the MPIC. I greatly benefited from the co-operation with Anywhere Tsokankunku, Linda Voß, Guozheng Song from MPIC and Dr. Wolfgang Babel from Bayreuth about issues on the eddy covariance technique. I further want to acknowledge the staff of the MPIC mechanical and electronic workshop for their substantial support during the development of the flux measurement system and the Max Planck Society for the financial support during the time of my PhD.

Finally, the biggest “Thank you!” is for my family, who has always supported me, and without whom the completion of this thesis would have been an impossible task.

# Contents

Summary .....	I
Zusammenfassung .....	III
List of manuscripts .....	V
Acknowledgements .....	VII
Contents .....	IX
1 Introduction .....	1
1.1 The role of PANs within the global nitrogen cycle.....	1
1.2 Background on the biosphere-atmosphere exchange of PAN.....	4
1.3 Objectives of thesis .....	6
2 Methods.....	9
2.1 Methodology for the determination of PAN fluxes .....	9
2.2 Challenges for the determination of PAN fluxes .....	12
2.3 Field experiment .....	13
3 Results.....	15
3.1 Development and performance of the PAN flux measurement system .....	15
3.1.1 Setup .....	15
3.1.2 Performance .....	18
3.1.2.1 Precision of PAN analysis.....	18
3.1.2.2 Flux error during the MBR operation .....	19
3.1.2.3 Flux error during the HREA operation.....	20
3.1.2.4 High frequency attenuation and lag time effects on HREA fluxes ....	20
3.1.3 Method comparison .....	22
3.2 Case study: PAN deposition to the grassland ecosystem .....	24
4 Conclusions .....	27
References .....	31

Appendix A: Individual contributions to the joint publications .....	37
Appendix B: PAN flux measurement system.....	39
Abstract .....	40
1 Introduction .....	40
2 Methods.....	42
2.1 Flux measurement techniques .....	42
2.1.1 Hyperbolic relaxed eddy accumulation (HREA).....	42
2.1.2 Modified Bowen ratio method (MBR) .....	44
2.2 Modification of the PAN GC-ECD .....	45
2.3 Field experiment: Experimental site and general setup .....	46
2.4 Setup of PAN flux measurement system: HREA operation.....	47
2.5 Setup of PAN Flux measurement System: MBR operation .....	50
2.6 Calibration and quality control .....	51
2.6.1 Calibration method .....	51
2.6.2 Determination of PAN mixing ratio difference errors .....	51
2.6.3 Random flux error, flux detection limit and quality control .....	52
2.7 Simulation of expected PAN mixing ratio differences .....	53
3 Results.....	54
3.1 Expected PAN mixing ratio differences .....	54
3.1.1 Effect of HREA dead band .....	54
3.1.2 Diurnal cycle of expected PAN mixing ratio differences.....	55
3.2 Calibration .....	56
3.3 Side-by-side measurements .....	57
3.4 PAN flux measurements .....	58
3.4.1 HREA measurements.....	58
3.4.2 MBR measurements .....	62
4 Discussion .....	64
4.1 Performance of the PAN flux measurement system .....	64
4.1.1 Performance of the GC-ECD .....	64
4.1.2 Effect of HREA timing .....	65
4.1.3 Random flux error under varying meteorological conditions.....	65
4.2 Sources of uncertainties of PAN mixing ratio differences .....	68
4.3 Scalar similarity and influence of chemistry .....	70
4.4 Applicability of HREA and MBR for PAN flux measurements.....	71
5 Summary and conclusions .....	73
Acknowledgements .....	75
References .....	75
Supplementary material .....	80
SM 1 Operation of PAN GC.....	80
SM 1.1 Main settings.....	80
SM 1.2 Design and operation of PCUs.....	80
SM 2 Fast response system design for HREA operation .....	81
SM 2.1 Time response of data transmission, HREA software and splitter valve actuation .....	81
SM 2.2 Time response of splitter valves.....	81
SM 3 Calculation of random errors using Gaussian error propagation .....	82
SM 4 Correction method for PAN mixing ratio differences during HREA operation .....	85
SM 5 Additional figure.....	86
References.....	86

---

Appendix C: Tube effects on REA fluxes .....	87
Abstract .....	88
1 Introduction.....	88
2 Methods .....	92
2.1 Experimental setup .....	92
2.2 Lag time error.....	93
2.3 High frequency attenuation .....	95
2.3.1 Experimental transfer function.....	96
2.3.2 Theoretical transfer function .....	97
2.3.3 Simulating the effect on REA fluxes .....	97
3 Results and Discussion .....	98
3.1 The effect of an imprecisely determined lag time on REA fluxes.....	98
3.1.1 Variations of the lag time.....	98
3.1.2 Lag time effect on REA fluxes.....	101
3.2 The effect of high frequency attenuation on REA fluxes.....	104
3.2.1 Observed high frequency attenuation .....	104
3.2.2 High frequency attenuation effect on REA fluxes .....	107
3.3 Combined effect of imprecisely determined lag time and high frequency attenuation .....	109
3.4 Proposed procedure for future REA applications.....	111
4 Summary and Conclusions .....	113
Acknowledgements .....	115
References.....	115
Appendix D: PAN deposition to a grassland ecosystem .....	119
Abstract .....	120
1 Introduction.....	120
2 Methods .....	122
2.1 Site description .....	122
2.2 Measurements of PAN mixing ratios and fluxes .....	123
2.3 Additional measurements.....	124
2.4 Flux partitioning .....	125
2.5 Determination of PAN loss by thermochemical decomposition .....	126
3 Results and discussions .....	127
3.1 Meteorological conditions: Classification of low and high NO <sub>x</sub> episodes.....	127
3.2 Characterisation of PAN under low and high NO <sub>x</sub> conditions .....	129
3.3 Evaluation of PAN flux measurements.....	130
3.3.1 Deposition fluxes and canopy conductance.....	130
3.3.2 Stomatal uptake.....	132
3.3.3 Non-stomatal deposition .....	132
3.4 PAN deposition strength for low and high NO <sub>x</sub> conditions .....	135
4 Conclusions.....	137
Acknowledgements .....	139
References.....	139
Erklärung.....	143



# 1 Introduction

## 1.1 The role of PANs within the global nitrogen cycle

Nitrogen is a basic component of amino acids and organic matter and, therefore, an essential element for the growth and functioning of plants, animals and humans and an essential element for food security [Erisman *et al.*, 2013]. At the same time nitrogen compounds play a key role in the chemistry of the atmosphere, for example in the formation of tropospheric ozone (O<sub>3</sub>) or aerosols. About 99.96% of the Earth's non-crustal nitrogen is found in the atmosphere in the form of the largely unreactive molecular nitrogen (N<sub>2</sub>) and only a small fraction makes up the amount of nitrogen available for uptake by plant species [Söderlund and Svensson, 1976]. The large part of the natural flow of molecular N<sub>2</sub> into terrestrial or marine systems is linked to biological nitrogen fixation by microorganisms [Fowler *et al.*, 2013]. These are able to reduce N<sub>2</sub> to ammonium compounds, which are subsequently transformed into a wide range of amino acids and oxidized nitrogen compounds. Like this, nitrogen fixation produces so-called reactive nitrogen (N<sub>r</sub>) compounds, which can be used directly or indirectly by plants and other organisms. In the light of a growing world population, the limitation of the natural amount of N<sub>r</sub> and the demand of nitrogen as a fundamental nutrient source led in the last century to the development of synthetic fertilizer with industrial fixation of molecular N<sub>2</sub>. It has been estimated that almost half of the human population at the beginning of the twenty-first century depends on nitrogen from industrially produced fertilizers [Erisman *et al.*, 2008]. Another major anthropogenic source of N<sub>r</sub> to the atmosphere is the combustion of fossil fuels for energy production, transport and industrial processes. Being once created, N<sub>r</sub> is highly mobile and can trigger a cascade of negative environmental effects in sequence [Galloway *et al.*, 2003]. The additional creation of N<sub>r</sub> has a major effect on air quality and, hence, on human health, as well as on aquatic and terrestrial ecosystems and climate change. As a consequence, the challenge for the current century is seen in optimizing the use of nitrogen while minimizing the negative impacts [Galloway *et al.*, 2013]. For these reasons, there is a

general interest in the knowledge of processes of reactive nitrogen species and their fluxes between the atmosphere and terrestrial and marine ecosystems.

In the last decades, the understanding of the nitrogen cycles has improved significantly [Galloway *et al.*, 2013]. However, the role of atmospheric organic nitrogen species is still poorly understood, mainly due to the lack of consistency in sampling and measurements methods and the large number of different compounds [Cape *et al.*, 2011]. Atmospheric organic nitrogen species exist in gaseous, particulate and aqueous phase. While water-soluble organic nitrogen compounds are mainly removed from the atmosphere by precipitation, less soluble gaseous species are subject to chemical transformation in the atmosphere or dry deposition to the surface. Among the gaseous organic nitrogen compounds, peroxyacyl nitrates (PANs) are important compounds in the context of the atmosphere's oxidative capacity [e.g., Fahey *et al.*, 1986]. Furthermore, they are discussed as a source of  $N_r$  to ecosystems and as a reservoir species for  $NO_x$ , the sum of nitric oxide (NO) and nitrogen dioxide ( $NO_2$ ) [Singh, 1987].

Peroxyacyl nitrates (also denoted as acyl peroxy nitrates, APNs, in literature) are formed in the atmosphere via the reaction of  $NO_2$  with peroxyradicals ( $RO_2$ , where R is used here as a short notation for  $R^*(C)O$  with  $R^*$  denoting a hydrocarbon group):



Next to the formation of PAN, another important reaction of  $RO_2$  concurring with R1 is the reduction by NO:



As it is demonstrated in Figure 1,  $RO_2$  compounds may have both anthropogenic and biological volatile organic compounds (VOCs) as precursors [LaFranchi *et al.*, 2009]. Biogenic VOCs, such as isoprene and terpenes are emitted by plants and released into the atmospheric boundary layer in significant amounts. Anthropogenic VOCs originate from combustion processes yielding various alkanes, alkenes or aromatics. VOCs are highly reactive and can be quickly oxidized to carbonyl compounds (RO) such as acetaldehyde, acetone and biacetyl. Mainly in the presence of the hydroxyl radical (OH) and radiation (hv), but also of ammonia ( $NH_3$ ) during nighttime, these can be oxidized to form PANs. While some PANs are oxidation products of biogenic VOCs, others are only formed by the oxidation of anthropogenic VOCs. In contrast, peroxyacetyl nitrate (PAN,  $R = CH_3CO$ ) can have both biogenic and anthropogenic precursors. In addition, it typically comprises 80 to 90% of the speciated budget of PANs [Roberts, 1990] and is therefore of special interest.

PAN was first discovered in the 1950s in the context of photochemical smog conditions in urban areas, providing both high concentrations of anthropogenic hydrocarbons and

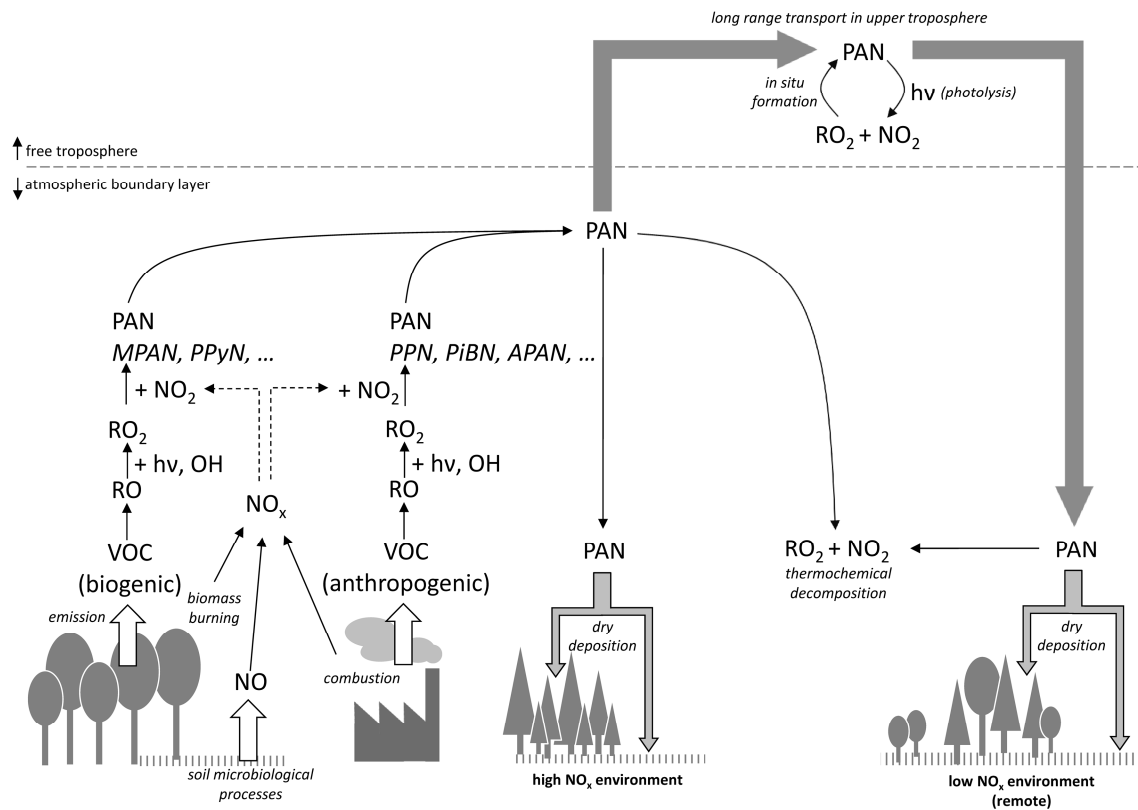


**Figure 1:** Formation, transport and removal of PANs in the troposphere and its link to anthropogenic activity. While most PAN species (highlighted in italics) have

either biogenic or anthropogenic VOCs as precursor, PAN itself is produced via both pathways.

$\text{NO}_x$  together with UV-induced photochemical oxidation [Gaffney and Marley, 2001]. Under these conditions, high PAN mixing ratios can be observed, reaching several tens of ppb or even higher [see Temple and Taylor, 1983, for a compilation of early PAN measurement in urban areas]. At these high mixing ratios a toxic effect on plant tissue and impact on human health was found due to the oxidative nature of PAN [Taylor, 1969; Temple and Taylor, 1983]. Under less extreme conditions, PAN mixing ratios are significantly lower with about 100 ppt in the Northern free troposphere [Singh, 1987], although its abundance is highly variable. In remote areas with low  $\text{NO}_x$  and near tropics mixing ratios in the magnitude of 10 ppt are prevalent [Müller and Rudolph, 1992; Singh et al., 1990].

The importance of PAN is characterized by its relatively long life time and reservoir for both  $\text{RO}_2$  and  $\text{NO}_2$ . Once it is formed in the atmosphere, PAN is primarily subject to three removal pathways: (1) thermochemical decomposition, (2) photolysis and (3) dry deposition to vegetation [Roberts, 1990]. PAN is also oxidized by OH, however, due to its slow reaction rate, this reaction is regarded as unimportant throughout the troposphere [Talukdar et al., 1995]. In addition, due to its low solubility in water [Kames and Schurath, 1995], multiphase reaction in water droplets and wet deposition are considered as insignificant removal processes. In contrast, thermochemical

decomposition of PAN has a major impact on its lifetime. PAN is thermally unstable and decomposes at higher temperatures via the back reaction of R1 and subsequent removal of RO<sub>2</sub> [Orlando *et al.*, 1992]. The latter is mainly removed by reaction with NO (R2) and to some extent also by the reaction with other peroxy radicals. As a result, the life time of PAN due to thermochemical decomposition can be significantly less than an hour at temperatures exceeding 298 K and may be over two days at around 273 K [Singh, 1987]. Due to its stability at cool temperatures along with continued synthesis, PAN can be transported over distances of > 10,000 km in the upper troposphere over several months. Although its life time in the upper troposphere is limited by the UV photolysis, photolysis is considered to be an important process only at heights above 7 km [Talukdar *et al.*, 1995]. As a consequence of its long life time in the upper troposphere, PAN is discussed to be an effective carrier species of N<sub>r</sub> in global atmospheric transport systems [Singh, 1987]. Being then exposed to higher temperatures at the surface, it represents a source of both, NO<sub>2</sub> and RO<sub>2</sub>. In this way, PAN can constitute a significant source of N<sub>r</sub> in remote regions, thereby affecting atmospheric chemistry and ecosystems. Via the pathway of dry deposition, PAN is taken up by vegetation and removed from the atmosphere, while especially nutrient-poor ecosystems might be vulnerable to this additional input of N<sub>r</sub>.

As it was shown, both production and loss of PAN is strongly linked to the surface, by emissions of VOCs or NO<sub>x</sub> on the one hand and thermal decomposition and dry deposition on the other hand. For this reason, biosphere-atmosphere interactions play a key role in understanding the chemistry and processes of PAN and its link to the environmental impact of anthropogenic production of N<sub>r</sub> and perturbation of the nitrogen cycle. In the past a few studies have measured direct biosphere-atmosphere exchange of PAN [Doskey *et al.*, 2004; Schrimpf *et al.*, 1996; Turnipseed *et al.*, 2006; Wolfe *et al.*, 2009]. However, conclusive studies on PAN fluxes are currently very limited, the obtained results differ considerably and the underlying mechanisms are not well understood.

## **1.2 Background on the biosphere-atmosphere exchange of PAN**

The biosphere-atmosphere exchange of trace gases is generally based on both (1) their production and depletion in the atmosphere and (2) their uptake or release by vegetation or other biota such as microorganisms. Depending on the investigated trace gas and ecosystem, the interaction with other inorganic substances at the surface such as thin

water films on leaves or soil minerals may also play a significant role. However, next to atmospheric chemistry and plant physiological processes, the driving mechanism is the transport at the atmosphere-surface interface and in the atmospheric boundary layer (ABL) above, as without transport exchange processes [see e.g., *Foken, 2008; Stull, 1988*] would result in an equilibrium and consequently cease. Within the first millimetres above the surface, in the so-called quasi-laminar boundary layer, transport is characterized by molecular diffusion. Above that layer, turbulent transport is prevalent. Turbulence is characterized by chaotic behaviour and seemingly random motion of fluid parcels. It can be seen as a superimposition of irregular swirls, called eddies, at multiple length scales, which are induced by both shear stress caused by the friction on the surface and buoyant instabilities. The turbulent transport is about five orders of magnitude more efficient than the molecular diffusion and next to convection the major mechanism in transporting trace gases from the surfaces to higher levels in the ABL. As a consequence, studies on the biosphere-atmosphere exchange require a detailed understanding of the structure of the ABL and turbulent transport.

The biosphere-atmosphere exchange of trace gases can be described as a sequence of multiple resistances, which the trace gas encounters when being transported from (emission) or to (deposition) the surface [*Hicks et al., 1987; Wesely and Hicks, 2000*]. While the turbulent transport above the surface is restricted by the aerodynamic resistance, the transport through the thin layer of air in contact of surface elements is restricted by the quasi-laminar boundary layer resistance. Applying a big-leaf approach, the resistance of the surface itself is typically divided into the resistances of the leaf stomata, the leaf cuticle and the soil. In addition, further transport or metabolism processes in the leaf mesophyll are accounted for by the mesophyll resistance. The individual resistances are determined either from direct measurements or are parameterised, and can be used to model biosphere-atmosphere exchange fluxes.

In view of the observed phytotoxic effect of PAN, a deposition of PAN to vegetation was suspected early in course of its discovery. *Hill [1971]* was the first to directly measure deposition of PAN to alfalfa in a flux chamber. *Garland and Penkett [1976]* found in wind tunnel experiments that PAN was substantially deposited to grass and soil, but not to water surfaces. Years later, more detailed chamber experiments [*Okano et al., 1990; Sparks et al., 2003; Teklemariam and Sparks, 2004*] could verify that PAN was taken up largely by plant stomata. A limitation of PAN uptake at high stomatal conductances<sup>1</sup> was found [*Sparks et al., 2003; Teklemariam and Sparks, 2004*], hinting towards the existence of a mesophyll resistance at these conditions, however, the biochemistry for PAN assimilation is not clearly understood [*Doskey et al., 2004*]. A

---

<sup>1</sup> note: the conductance is given by the inverse of the resistance

few studies have measured in situ PAN fluxes above corn [Schrimpf *et al.*, 1996], grassland [Doskey *et al.*, 2004] and pine forest [Turnipseed *et al.*, 2006; Wolfe *et al.*, 2009]. PAN deposition during night time, when leaf stomata are mainly closed, proved the existence of a non-stomatal deposition pathway. E.g., Turnipseed *et al.* [2006] found almost 50% of the daytime deposition to be non-stomatal for a pine forest and suggested it to be the primary deposition pathway in the upper canopy. As a result, Turnipseed *et al.* [2006] found 4–5 times larger daytime deposition velocities than predicted with currently used deposition models. In addition, the role of chemistry above and within the canopy can be significant [Wolfe *et al.*, 2009]. However, conclusive studies on PAN fluxes are currently very limited and the obtained results differ considerably. Especially, the role of wet surfaces – despite the low solubility of PAN – and the relation of PAN to O<sub>3</sub> deposition fluxes are not well understood. As a consequence, the significance of PAN deposition as a removal process from the atmosphere in contrast to its thermochemical decomposition and source of N<sub>r</sub> to ecosystems is not certain.

The lack in the current knowledge on the biosphere-atmosphere exchange of PAN is mainly caused by large uncertainties in the PAN flux measurements on the one hand and the lack of extended flux measurements on the other. While the improvement of current flux measurement techniques is essential to improve the quality of PAN fluxes, reduced costs and user-friendly flux measurements are a long-term objective for flux measurements of nitrogen species, which might allow in the future more extended PAN flux measurements on various ecosystems or even setups with multiple flux measurement systems to investigate problems of advection or flux divergence [Sutton *et al.*, 2007]. For these reasons, the focus of this thesis is the development and detailed evaluation of a flux measurement system for PAN as presented hereafter.

### 1.3 Objectives of thesis

The aim of this thesis is (1) to develop a new system for determining biosphere-atmosphere exchange fluxes of PAN, (2) apply it on a natural grassland ecosystem and (3) thereby contribute to a better understanding of the biosphere-atmosphere exchange of PAN, while the focus is set on the design and performance of the flux measurement system. The used flux methodology and characteristics of the flux measurement system are determined by the main research questions (Q1–Q3), which are:

- Q1: Which factors control the biosphere-atmosphere exchange of PAN and what are the underlying processes?

- Q2: What is the effect of dry deposition of PAN on ecosystems as a source of  $N_r$  under varying environmental conditions?
- Q3: What is the importance of dry deposition of PAN as a removal process for atmospheric  $N_r$  under varying environmental conditions?

The research of these scientific questions requires a flux measurement system which is designed for in situ and long term measurements to capture the effect of varying environmental conditions. Furthermore, to investigate the net effect of PAN deposition on ecosystems, the spatial scale of the flux measurements has to be in the range of the ecosystem scale. These requirements lead to three major cornerstones (C1–C3), on which the design of the flux measurement system is based:

- C1: The system should provide online in situ measurements to investigate the effect of varying environmental conditions.
- C2: The used flux methodology is based on micrometeorological techniques which integrate the trace gas fluxes over the ecosystem scale.
- C3: For the detection of PAN a gas-chromatograph with electron capture detection (GC-ECD) is used. The GC-ECD technique is the standard method for the analysis of PAN and suitable for long term measurements.

The first part of this thesis is the system development, which includes the decision for the appropriate flux measurement technique, its technical realization and testing on a grassland field site. According to the requirements given above, the system is designed for the application of two micrometeorological techniques, the hyperbolic relaxed eddy accumulation method (HREA) and the modified Bowen ratio method (MBR) (details on methods are given in Sect. 2.1). *Moravek et al.* [2014a, Appendix B] describe the design of the system with emphasis on the essential operational settings and a detailed quality assessment of individual components. Also major adaptations that are necessary to meet site specific requirements are given and an extensive error analysis is presented to evaluate the overall performance of the system for both methodological approaches under varying environmental conditions.

A crucial point for the application of the HREA method is a precise timing and damping effects within the inlet line. Since this issue can have a major effect on the obtained fluxes and is thus of general importance for the application of the relaxed eddy accumulation method (REA), *Moravek et al.* [2013, Appendix C] evaluate the new technical methods, that can be implemented to optimize REA systems, and quantify the effect on REA fluxes under varying environmental conditions. The results of this study are used to correct PAN fluxes at the grassland site.

In the second part, PAN fluxes obtained at the grassland site are evaluated to contribute to the understanding of the biosphere-atmosphere exchange of PAN (Q1–Q3). *Moravek et al.* [2014b, Appendix D] investigate the stomatal and non-stomatal deposition pathway of PAN using the PAN fluxes obtained with the MBR method. The PAN deposition is modelled under polluted and non-polluted conditions, to evaluate the effect of local air pollution on the PAN deposition. Finally, the importance of PAN deposition as a sink of  $N_r$  and its impact on the nutrient poor grassland ecosystem are discussed.

## 2 Methods

### 2.1 Methodology for the determination of PAN fluxes

As addressed in Sect. 1.2, the biosphere-atmosphere exchange of trace gases is driven by the vertical turbulent transport in the atmospheric layer above the canopy. Micrometeorological methods, which determine the turbulent exchange near the surface, integrate the trace gas emission or deposition over a footprint area extending several hundred meters and typically cover turbulent eddies with time scales ranging from fractions of a second to up to an hour. Which type of micrometeorological method is the best choice for the determination of PAN fluxes, depends in the first place on the time resolution and precision of the trace gas analysis. Table 1 lists typical specifications of the most common measurement methods for PAN. In the past, measurements of PAN have most often been accomplished using GC-ECD, which is currently still the best developed and proven method. It has a good precision and the limit of detection (LOD) can be improved by pre-concentration or cryofixation of PAN [Vierkorn-Rudolph *et al.*, 1985]. The typical time resolution of several minutes makes it suitable for flux measurements approaches that allow the use of slow sensors such as REA, MBR or the aerodynamic gradient method [AGM, see *Businger*, 1986]. *Schrimpf et al.* [1996] and *Doskey et al.* [2004] have measured PAN fluxes using a GC-ECD with the MBR method. However, in case the potential measurement frequency is high enough (ideally  $> 10$  Hz) with sufficient precision, the eddy covariance method [EC, see *Aubinet et al.*, 2012] is the method of choice for flux measurements. In the last years, *Turnipseed et al.* [2006], *Wolfe et al.* [2009] and *Min et al.* [2012] have implemented the eddy covariance method using thermal dissociation chemical ionization mass spectrometry (TD-CIMS) with a time resolution of 3–4 Hz for the analysis of PAN. The detection limits and instrument response times of the TD-CIMS instruments are excellent, however, interferences with peroxyacetic acid (PAA) can cause a significant background, which increases the flux uncertainties significantly [Phillips *et al.*, 2013; Wolfe *et al.*, 2009]. Furthermore, matrix effects induced by NO or NO<sub>2</sub> and

**Table 1:** Comparison of the most commonly used methods for the analysis of PANs and  $\Sigma$ PAN. The used references represent next to instrumental descriptionsalso results from recent field studies. Precision values for TD-LIF are different to the values in the original publication ( $1\sigma$  and based on 10s).

	Speciation	time resolution	precision ( $1\sigma$ )	LOD ( $3\sigma$ )	Background / Interferences	References
GC-ECD	PAN	1 - 10 min	1 - 3%	2 - 30 ppt	—	1,2,3,4
TD-CIMS	PAN, MPAN, PPN	< 1 s	< 10 %	1 - 8 ppt	PAA, H <sub>2</sub> O, NO, NO <sub>2</sub>	5, 6, 7
TD-LIF	$\Sigma$ PAN	1 s 1 min	16 ppt 2 ppt	—	NO, NO <sub>2</sub>	8, 9
TD-CRDS	$\Sigma$ PAN	1 s 1 min	100/60 ppt 30/20 ppt	—	NO, NO <sub>2</sub>	10 / 11
1	<i>Flocke et al.</i> [2005]	4	<i>Moravek et al.</i> [2014a, Appendix B]	7	<i>Min et al.</i> [2012]	10
2	<i>Zhang et al.</i> [2012]	5	<i>Slusher et al.</i> [2004]	8	<i>Day et al.</i> [2002]	11
3	<i>Fischer et al.</i> [2011]	6	<i>Wolfe et al.</i> [2007]	9	<i>Wooldridge et al.</i> [2010]	<i>Dipayan Paul et al.</i> [2009] <i>D. Paul and Osthoff</i> [2010]

interferences with water vapour can add a significant bias [*Mielke and Osthoff*, 2012] and the operation effort is intensive. Other commonly used techniques measure the sum of all PANs ( $\Sigma$ PAN) after thermal decomposition (TD-) as NO<sub>2</sub>, which might be an alternative for some studies [*Farmer and Cohen*, 2008; *Min et al.*, 2012]. Laser-induced fluorescence (LIF) can be operated with a time resolution in the order of seconds and a reasonable precision [*Day et al.*, 2002], however, they also show interferences with NO and NO<sub>2</sub>. The advantage of instruments using cavity ring down spectroscopy (CRDS) is that they provide an absolute measure of PAN, but their precision is too low to be used for flux measurements [*D. Paul and Osthoff*, 2010].

The flux measurement system presented in this thesis is based on GC-ECD. Due to the absence of interferences, the uncertainties of PAN measurements are lower and GC-ECD might be also more suitable for long term measurements than other techniques. As it was mentioned in the objectives of this thesis (Sect. 1.3), the GC-ECD is used in combination with both the MBR and HREA method, a special case of the REA method. The REA flux ( $F_{REA}$ ) is determined by the difference of two reservoir mixing ratios ( $\Delta\chi$ ), multiplied by a proportionality factor  $b$ , the standard deviation of the vertical wind speed ( $\sigma_w$ ) and the molar density of air  $\rho_m$  [*Businger and Oncley*, 1990]:

$$F_{REA} = b \cdot \sigma_w \cdot \rho_m \cdot (\chi_{w+} - \chi_{w-}) = b \cdot \sigma_w \cdot \rho_m \cdot \Delta\chi \quad (1)$$

Eq. (1) implies that sampled air must be separated into two reservoirs, one for updraft and one for downdraft events during a certain sampling period (typically 30 min). The separation is made with a fast switching valve, which is controlled according to the sign of the vertical wind velocity ( $w$ ) measured by a 3D sonic anemometer. The  $b$ -value is a characteristic of the bivariate joint frequency distribution of the Reynolds fluctuation of the vertical wind velocity ( $w'$ ) and the scalar of interest ( $s'$ ). For an ideal Gaussian frequency distribution, the  $b$ -value is 0.627 [*Wyngaard and Moeng*, 1992]. However, experimental data show that it varies and is on average slightly lower [*Baker*, 2000].

Thus, the  $b$ -value is often derived individually for every sampling interval with a proxy scalar, which can be measured with high frequency to derive an eddy covariance flux [see Eq. (2) in *Moravek et al.*, 2014a, Appendix B].

The HREA method uses a hyperbolic dead band [*Bowling et al.*, 1999], a threshold below which air samples are discarded when the flux is expected to be close to zero, to increase values of  $\Delta\chi$ . The threshold  $H$  is defined according to the flux of a proxy scalar as:

$$H \geq \left| \frac{w' \cdot \chi'_{proxy}}{\sigma_w \cdot \sigma_{\chi_{proxy}}} \right| \quad (2)$$

where  $\chi'_{proxy}$  is the Reynolds fluctuation and  $\sigma_{\chi_{proxy}}$  is the standard deviation of the proxy scalar. If scalar similarity between the scalar of interest and the proxy exists,  $\Delta\chi$  is increased as the threshold is only exceeded when high vertical wind speed fluctuations are accompanied by high fluctuations of the proxy scalar.

The MBR method assumes that the ratio between the molar flux and the vertical concentration difference between two measurement heights is equal for the scalar of interest and a proxy scalar [*Businger*, 1986; *Liu and Foken*, 2001]. The scalar flux  $F_{MBR}$  is then typically estimated by the ratio of concentration differences between the upper and lower measurement height of the scalar and the proxy,  $\Delta c$  and  $\Delta c_{proxy}$ , multiplied by the eddy covariance flux of the proxy ( $F_{EC_{proxy}}$ ):

$$F_{MBR} = F_{EC_{proxy}} \cdot \frac{\Delta c}{\Delta c_{proxy}} \approx F_{EC_{proxy}} \cdot \frac{\Delta\chi}{\Delta\chi_{proxy}} \quad (3)$$

For measurements above the surface, differences in the molar air density between two heights can be often neglected so that mixing ratio differences ( $\Delta\chi$  and  $\Delta\chi_{proxy}$ ) are used instead.

While both HREA and MBR are indirect methods and require reference data from proxy scalars, the HREA might be more suitable under unstable well mixed conditions, where the application of the MBR method is difficult due to very low vertical differences. In return, the technical realization of the HREA method is much more complex and requires a significant effort in the system development.

## 2.2 Challenges for the determination of PAN fluxes

This thesis presents the first REA (and HREA) system for PAN. Typically, REA systems are employed for trace gases which are inert and can be stored over the sampling interval in the reservoir without significant loss. For example, in the past REA systems were often used for volatile organic compounds (VOCs) as they are mostly inert and also emitted in significant amounts from the biosphere [e.g., *Okumura et al.*, 2011; *Park et al.*, 2010]. PAN, however, thermally decomposes (back reaction of R1) and may also react on surfaces as it was reported for Pyrex glass [*Lovelock and Penkett*, 1974; *Singh and Salas*, 1983]. Furthermore, what is known from previous studies [e.g., *Turnipseed et al.*, 2006; *Wolfe et al.*, 2011], PAN fluxes are expected to be significantly lower than those of VOCs. The MBR method has been previously used for PAN by *Schrimpf et al.* [1996]. However, they only determined nighttime fluxes since low mixing ratio differences during daytime could not be resolved. *Doskey et al.* [2004] sampled vertical PAN difference during daytime for the application of the MBR method using temperature as a proxy scalar, however, flux errors were large, ranging from 45 to 450%.

These examples show the difficulties of PAN flux measurements and offer clues to the major challenges that have to be considered in the design and operation of a flux measurement system for PAN with the REA and MBR method, which are:

1. **Small mixing ratio differences.** For both the REA and MBR method, the major challenge is the resolution of low  $\Delta\chi$  values for PAN ( $\Delta\chi_{PAN}$ ) (Eqs. (1) and (3)). Especially, if they rely on a single measurement per sampling period, like for the GC-ECD, the analytical system has to be precise.
2. **Reactivity of PAN.** Thermal decomposition of PAN (Sect. 1.1) increases exponentially with temperature. For example, at 30°C and a NO/NO<sub>2</sub> ratio of 0.5 the life time of PAN is about 45 min. While this might seem long enough for some analysis, it is crucial for flux measurements where small concentration differences have to be resolved. Furthermore, the possible loss of PAN on surfaces requires the use of inert materials.
3. **Accurate sampling of up- and downdraft events during HREA application.** Inaccurate sampling generally reduces the measured concentration differences in the REA reservoirs and, thus, leads to an underestimation of the REA flux. As a consequence, the accurate segregation of air masses into up- and downdraft reservoirs requires a precise timing of the switching of splitter valves according to the vertical wind velocity. In addition, the system might be subject to significant damping of high frequencies (high frequency attenuation) [*Moore*,

1986], which has to be considered in the setup and the evaluation of HREA fluxes.

4. **Scalar similarity.** For both methods, an appropriate proxy scalar has to be found, ideally with a sink and source distribution similar to PAN. As the proxy scalar has to be measured with a high precision at a high frequency ( $> 10$  Hz) for eddy covariance fluxes, the choice is usually limited.

The consideration of these challenges together with the basic requirements stated in the thesis objectives (Sect. 1.3) led to the final design of the PAN flux measurement system as it is presented in Chapter 3.

## 2.3 Field experiment

The PAN flux measurements system was first operated on a nutrient-poor natural grassland ecosystem on the estate of the Mainz-Finthen Airport in Rhineland-Palatinate, Germany ( $49.9685^{\circ}\text{N}$ ,  $8.1481^{\circ}\text{E}$ ). Nutrient-poor habitats might be especially vulnerable to additional nitrogen input via dry deposition of PAN. Also, grassland ecosystems are the third largest land use type in Europe and constitute 41% of global terrestrial surfaces [EUROSTAT, 2011; Suttie *et al.*, 2005].

The system was installed from September 2010 to October 2011, while during the main

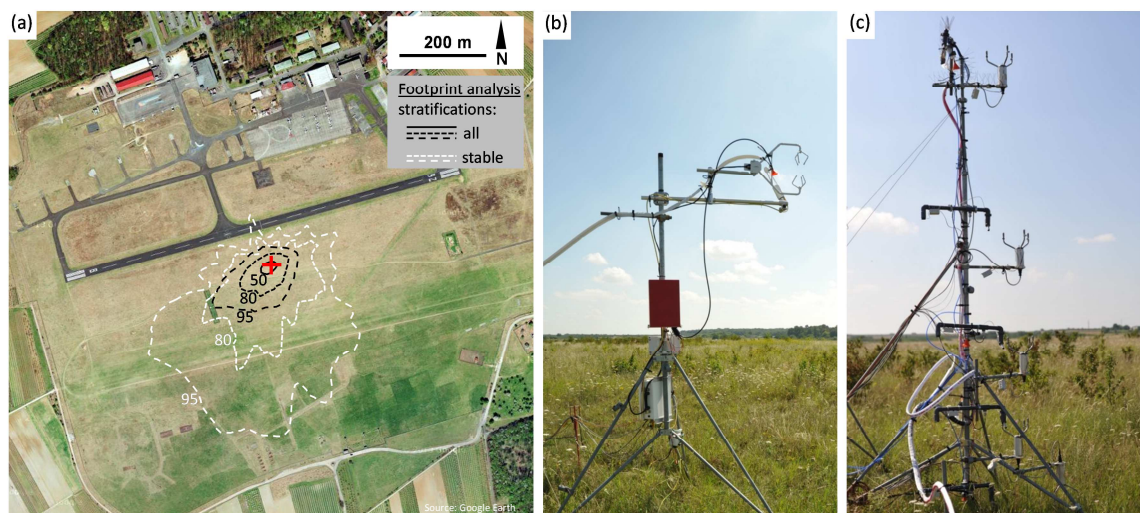


**Figure 2:** (a) Position of the flux measurements (red cross) on the premises of the Mainz-Finthen Airfield including the footprint climatology (white and black lines) for August and September 2011. (b) + (c): Measurement setup of the PAN flux measurement system at the natural grassland site. (b) Inlet of the

HREA system was mounted at 3 m a.g.l. next to the CSAT3 sonic anemometer. The red box is the high frequency analyser for O<sub>3</sub> flux measurements. (c) Inlets for MBR measurements were mounted at the profile mast at 0.8 and 4.0 m a.g.l. together with a vertical profile of temperature, humidity and 2D wind vectors.

part of this period, necessary site specific adaptations and major improvements were made. From 18 August to 4 September 2011 PAN fluxes were measured with the MBR method and from 20 to 26 September with the HREA method.

The natural grassland area of the measurement site extends over an area of 0.7 x 2.0 km, providing good fetch conditions for micrometeorological flux measurements (Figure 2). The ecosystem is primarily unmanaged and the vegetation is characterized by the false oat-grass (*Arrhenatherion elatioris*) plant community on dry and sandy soil with a considerable amount of senescent or dead grass. The site is topographically situated on a plateau 150 m above the Rhine valley and located about 9 km south-west of the city centre of Mainz [see Figure 1 in *Moravek et al.*, 2014b, Appendix D]. Being located on the edge of the industrialized and densely populated Rhine-Main-Area, it is influenced by both polluted and clean air masses and, thus, complies the requirements to study the influence of local air pollution on PAN deposition.

## 3 Results

### 3.1 Development and performance of the PAN flux measurement system

#### 3.1.1 Setup

The setup of REA systems varies significantly, depending on the trace gas of interest, the field conditions and the analytical techniques [for basic concepts see *Delany et al.*, 1991]. Also the sampling at two inlet heights for the application of the MBR technique can be implemented in different ways, i.e. by simultaneous measurements at both heights or by switching systems. For the PAN flux measurement system presented here, two major points determined the design: (1) the necessity of an inlet tubing of 21.5 m and (2) sampling by pre-concentration of PAN on capillary columns.

To allow continuous measurements of PAN fluxes, as it was stated in the objectives of this thesis, the PAN analysis was performed on site by the GC-ECD [Meteorologie Consult GmbH, Germany; modified according to *Moravek et al.*, 2014a, Appendix B], which was installed in an air conditioned container. Since the bulky container had to be located in a distance from the inlets of the PAN flux measurements system in order to prevent flow distortion effects on the flux measurements, a 21.5 m long inlet tubing had to be used. As shown in the very simplified sketch of the system (Figure 3a), in the HREA mode a single inlet tube was used, from which subsamples were drawn into the reservoirs for up- and downdraft events (bypass principle). The splitter valves were switched according to the sign of the vertical wind velocity and the hyperbolic dead band. During the MBR operation two separate inlet tubes were used for measurements at 0.8 and 4 m a.g.l. and sample air from both heights was directed simultaneously into the respective reservoirs (Figure 3b).

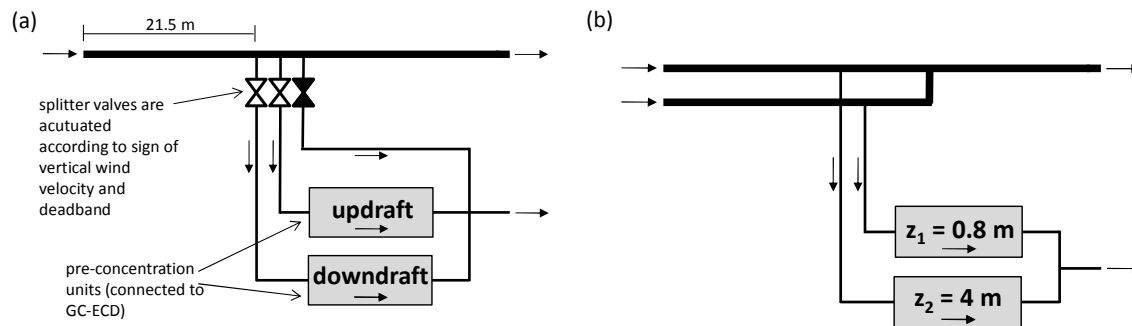


**Figure 3:** Flow scheme of the flux measurement system showing the inlet system and the pre-concentration units for sampling [simplified from Figure 2, *Moravek et al.*, 2014a, Appendix B]. **(a)** Operation in the HREA mode: The system contains one inlet line, and subsamples are drawn according to the sign of the vertical wind velocity into the pre-concentration units acting as reservoirs. The black valve is used for dead

band situations. **(b)** Operation in MBR mode: Two separate inlet lines are employed, and the system is capable to simultaneously sample at two inlet heights and performs subsequent analysis of PAN. **(a) + (b)** The connection of the pre-concentration units to the GC-ECD is shown in Figure 1 in *Moravek et al.* [2014a, Appendix B].

Sampling for both methods was realized by trapping PAN onto two pre-concentration capillary columns over the sampling period (30 min during HREA and 15 min during MBR application) and subsequent analysis by the GC-ECD (15 min). An important feature of the system is that during the pre-concentration method all PAN was trapped by the pre-concentration column, i.e. the frontal zone of PAN would not leave the pre-concentration column during the sampling period [referred to as conservation mode, see *Novak et al.*, 1979], which is important for the application of the REA method. This is in contrast to the commonly applied pre-concentration of PAN on capillary columns, where the equilibrium concentration at the end of the sampling interval is analysed. The used approach demanded (1) a very precise adjustment of flow rates in consideration of the effective sampling time and (2) a customized calibration method for varying sample volumes.

Next to the basic setup of the PAN flux measurement system, the following features were implemented [see *Moravek et al.*, 2014a, Appendix B] to meet the challenges as stated in Sect. 2.2:

1. **Small mixing ratio differences.** The resolution of small mixing ratio differences required the optimum choice of all operational parameters. On the one hand, the use of the hyperbolic dead band during the HREA application increased mixing ratio differences by a factor of about 2.7. For the MBR application, mixing ratio differences were maximised by installing the inlets at 0.8 and 4 m a.g.l, which was the largest applicable vertical difference. On the other hand, flow rates through the pre-concentration columns were adjusted precisely to obtain the maximum amount of PAN.

To improve the precision of the PAN analysis with the GC-ECD the pre-concentration units were optimized to guarantee a precise temperature control of the capillary columns. In addition, the use of special particle filters significantly reduced the pressure drop due to contamination over the measurement period, which is typically observed for membrane filters.

Finally, to account for systematic variations in the PAN analysis, extensive side-by-side measurements of the two pre-concentration units were performed before, during or after the flux measurements.

2. **Reactivity of PAN.** The bypass system (Figure 3) allowed a high flow rate in the main inlet line, thereby reducing the chance of possible thermal decomposition or surface reactions. Furthermore, great attention was paid in using only inert materials (PEEK, PFA, PTFE) for the inlet system. To avoid any loss of PAN, the additional pump of the main inlet line was installed downstream from point where the subsamples were drawn into the reservoirs [see Figure 2 in *Moravek et al.*, 2014a, Appendix B] .
3. **Accurate sampling of up- and downdraft events during HREA application.** The accurate sampling of up- and downdraft events was assured by the REA software program. The software program was designed to perform (a) acquisition of all signals and control of mass flow controllers, (b) coordinate rotation of the wind vector using the double rotation method, (c) hyperbolic dead band calculation, (d) switching of splitter valves and (e) data storage with a frequency of 20 Hz.

The accurate timing of the switching of the splitter valves requires a precise determination of the lag time induced by the residence time of sample air in the inlet tube. To minimize variations in the residence time, the mean volume flow in the inlet tube was continuously regulated. In addition, a new approach, the online cross-correlation method, was used for the lag time determination [*Moravek et al.*, 2013, Appendix C]. For every sample interval the lag time was retrieved by cross-correlation of the vertical wind velocity and the signal of a high frequency CO<sub>2</sub> analyzer, mounted in the main inlet at the position of the splitter valves. During the HREA application the lag time ranged between 1.3 and 1.7 s, while the main variation was attributed to the horizontal separation of the sonic anemometer and the HREA inlet (25 cm). The electronic time lag was less than 20 ms, which was achieved by an optimal interaction between the data acquisition and the HREA software program and the choice of high response splitter valves [*Moravek et al.*, 2013, Appendix C].

Since the high frequency attenuation induced by the 21.5m long inlet tube might be significant, turbulent flow was assured throughout the HREA measurements to minimize the effect [Lenschow and Raupach, 1991]. The high frequency attenuation effect was evaluated experimentally, which was used for corrections of the REA flux (see Sect. 3.1.2.4).

4. **Scalar similarity.** For both the HREA and the MBR method, O<sub>3</sub> was used as a proxy scalar due to its similarity to PAN in the sink and source distribution. On the one hand, the production of both PAN and O<sub>3</sub> is linked to photochemical processes and, on the other hand, both compounds are known to deposit to vegetation. The similarity is also reflected by the strong analogy in their diurnal courses [e.g., Garland and Penkett, 1976]. The signal of a high frequency O<sub>3</sub> analyser (Enviscope GmbH, Germany) was used for both the calculation of eddy covariance fluxes and the online calculation of the HREA dead band. In addition, for the application of MBR method, mixing ratio differences between the two inlet heights were determined with a custom-built differential O<sub>3</sub> analyser [Moravek et al., 2014a, Appendix B].

Further details on the setup and operation of the PAN flux measurement system are presented in Moravek et al. [2014a, Appendix B].

### 3.1.2 Performance

The overall performance of the PAN flux measurements system [see Moravek et al., 2014a, Appendix B] is measured by the performance of the individual components (e.g., the GC-ECD) and the uncertainty of the obtained fluxes. The flux uncertainty itself comprises of the sum of systematic errors and the random flux error. Known systematic errors sources were either minimized by the appropriate design and operation of the flux measurement system (Sect. 3.1.1) or corrected for. Most importantly, this included the systematic differences between the two reservoirs, which were corrected for both the HREA and the MBR method with the results from side-by-side measurements. The random flux error was derived by propagating the random errors of the individual terms in the flux equations (Eqs. (1) and (3)). For both methods, PAN fluxes were defined to be insignificantly different from zero and, thus, below the detection limit when the relative random flux error exceeded 100%.

#### 3.1.2.1 Precision of PAN analysis

The performance of the modified GC-ECD was similar or even better than that of other state-of-the-art GC-ECD systems [see Moravek et al., 2014a, Appendix B]. During calibration experiments, a precision ( $1\sigma$ ) of the GC-ECD of 1.5% in the gradient mode

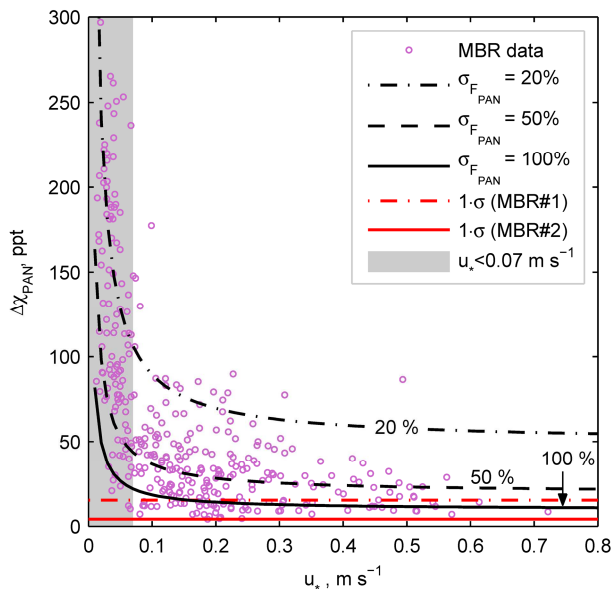


**Figure 4:** PAN mixing ratio differences ( $\Delta\chi_{PAN}$ ) as a function of the friction velocity ( $u_*$ ) during the MBR operation. Black lines show relative random flux errors of 20, 50 and 100%. From *Moravek et al.* [2014a, Appendix B].

and of 3% in the HREA mode was found. The limit of detection was determined as 5 ppt ( $3\sigma$ ). The precision of  $\Delta\chi_{PAN}$  was determined by the side-by-side measurements, performed for both the HREA and MBR method individually. The precision of the gradient system (i.e. MBR) ranged between 4 and 15 ppt. During the HREA application the precision ranged between 18 and 26 ppt after applying a correction for pressure fluctuations. The higher noise in PAN mixing ratios during HREA application was attributed to small pressure changes in the pre-concentration columns caused by the switching of the splitter valves. A simulation analysis revealed that expected daytime  $\Delta\chi_{PAN}$  values at the grassland site for both the MBR and the HREA method were between 15 and 50 ppt. Since these values were not significantly larger than the obtained precision, the error of  $\Delta\chi_{PAN}$  is expected to play a large role in the overall flux error.

### 3.1.2.2 Flux error during the MBR operation

During the period of MBR measurements, the daytime PAN fluxes at the grassland reached on some days up to  $-0.2 \text{ nmol m}^{-2} \text{ s}^{-1}$ , while on other days, when daytime  $\Delta\chi_{PAN}$  values were smaller or not different from zero, PAN fluxes were below the flux detection limit [see *Moravek et al.*, 2014a, Appendix B]. Considering only values above the flux detection limit, daytime PAN deposition was on average  $-0.07 \text{ nmol m}^{-2} \text{ s}^{-1}$  during that period.

As the error analysis revealed, the daytime random flux error (median:  $0.033 \text{ nmol m}^{-2} \text{ s}^{-1}$ ) was on average 50% during the MBR measurement period. This error was attributed to equal amounts to the random errors of  $\Delta\chi_{PAN}$  and  $\Delta\chi_{O_3}$ . Due to the limited turbulent exchange at night,  $\Delta\chi_{PAN}$  values reached up to 400 ppt. However

most nighttime PAN fluxes were negligible (median flux error:  $\pm 0.005 \text{ nmol m}^{-2} \text{ s}^{-1}$ ) or fell below the turbulence criteria, characterized by friction velocities ( $u_*$ ) below  $0.07 \text{ m s}^{-1}$  [Liu and Foken, 2001].

The difference between daytime and nighttime flux errors demonstrates that the flux error does not only depend on the precision of the mixing ratio measurements but also on the turbulence conditions. Figure 4 shows contour lines of the relative flux error ( $\sigma_{F_{PAN}}^{\%}$ ) of 20, 50 and 100% together with the measured  $\Delta\chi_{PAN}$  values during the MBR operation. While for increasing  $u_*$  values  $\sigma_{F_{PAN}}^{\%}$  converges to a constant  $\Delta\chi_{PAN}$  value, below  $u_* = 0.07 \text{ m s}^{-1}$   $\sigma_{F_{PAN}}^{\%}$  of a certain  $\Delta\chi_{PAN}$  value increases rapidly with decreasing  $u_*$ . The study showed that, according to the contour lines in Figure 4 and not considering values below the flux detection limit, 47% of the measured PAN fluxes were associated with a relative random error of between 20 and 50% and 27% between 50 and 100%. Only a few values (8%) showed a relative flux error below 20% and some (18%) above 100%.

### 3.1.2.3 Flux error during the HREA operation

PAN fluxes during the HREA measurement period [see Moravek *et al.*, 2014a, Appendix B] were in most cases below the flux detection limit. Only on one day a deposition flux of up to  $-0.4 \text{ nmol m}^{-2} \text{ s}^{-1}$  was found. For the remaining values above the flux detection limit a median random flux error of  $\pm 0.077 \text{ nmol m}^{-2} \text{ s}^{-1}$  for daytime and  $\pm 0.020 \text{ nmol m}^{-2} \text{ s}^{-1}$  for nighttime was determined. While during nighttime all terms had a similar impact on the total flux uncertainty, the daytime flux errors were mainly attributed to the error of  $\Delta\chi_{PAN}$  with a median error contribution of 50%. Consequently, the larger error during the HREA application was mainly attributed to the higher error of  $\Delta\chi_{PAN}$ . Another cause for the high flux errors during the HREA application are generally lower PAN fluxes due to a reduced PAN uptake by vegetation in the autumn measurement period. Also the meteorological conditions featured weaker turbulence than during the MBR period.

### 3.1.2.4 High frequency attenuation and lag time effects on HREA fluxes

Since the error during the HREA application was large, the effect of an imprecise sampling of up- and downdraft events during the HREA application was investigated in detail for several scalar quantities. This implied the effect of both an erroneous lag time and the high frequency attenuation of the inlet tube on the HREA fluxes. As it is presented in Moravek *et al.* [2013, Appendix C] for the REA method in general, both effects lead to an underestimation of the REA flux, which decreases with higher switching frequencies between the up- and downdraft reservoirs. The switching

frequency, under consideration of the used dead band, is strongly linked to the so-called eddy reversal frequency.

The flux loss due to an imprecisely determined lag time was influenced by both the eddy reversal frequency and the magnitude of the erroneous lag time ( $\Delta t_{lag}$ ). While a quadratic decline of the flux recovery (defined as the ratio of the REA fluxes with and without an additional time lag:  $Rec_{lag} = F_{REA_{lag}}/F_{REA_{ideal}}$ ) with increasing eddy reversal frequencies was found, the flux recovery decreased linearly with  $\Delta t_{lag}$ . For typical lag time errors ( $\Delta t_{lag} = 0.05\text{--}0.4$  s) flux errors may range from  $< 5\%$  at low eddy reversal frequencies up to  $50\%$  at high eddy reversal and a  $\Delta t_{lag}$  value of  $0.4$  s [see Figure 4 in *Moravek et al.*, 2013, Appendix C].

For the high frequency attenuation effect, a dependency of the flux recovery (defined as the ratio of the attenuated and non-attenuated REA fluxes:  $Rec_{HFA} = F_{REA_{HFA}}/F_{REA_{ideal}}$ ) on both the eddy reversal frequency and cut-off frequency of the used low-pass filter ( $f_c$ ) was found. Flux errors due to the high frequency attenuation ( $f_c = 0.5\text{--}10$  Hz) may range from  $< 5\%$  at low eddy reversal frequencies up to  $30\%$  at high eddy reversal and a cut-off frequency of  $0.5$  s. For most scalars the effect on REA fluxes was comparable to the high frequency attenuation effect on eddy covariance fluxes [see Figure 9 in *Moravek et al.*, 2013, Appendix C].

In addition, the interaction between the lag time and high frequency attenuation effect was evaluated, which is important for the correction of REA fluxes. On the one hand, high frequency attenuation reduces the effect of an imprecisely determined lag time. On the other hand, high frequency attenuation introduces a phase lag [*Massman*, 1991; *Massman and Ibrom*, 2008] and, thus, an additional lag time. This link is illustrated in Figure 5 for an eddy reversal frequency of  $3$  Hz. The contour lines show the reduced flux recovery with increasing  $\Delta t_{lag}$  (in positive and negative direction) and larger high frequency attenuation (represented by the cut-off frequency of the low-pass filter). The bending of the contour lines towards positive  $\Delta t_{lag}$  for decreasing  $f_c$  indicates the additional lag time associated with the phase shift of the low-pass filter. The magnitude of this additional lag time is also represented by the lag time determination from the cross-correlation between the low-pass filtered temperature time series and the vertical wind velocity. Another feature of the interaction of both effects is the reduced error made by an erroneous lag time with increased high frequency attenuation. This is illustrated in Figure 5b by the smoother peak of the flux recovery in the cross section for  $f_c = 0.5$  Hz than for  $f_c = 5$  Hz.

Transferring the results from this analysis to the measured HREA flux of PAN, the high frequency attenuation of the inlet tube ( $f_c = 1.2$  Hz) lead to an underestimation of the PAN flux ranging from  $1.8$  to  $31.4\%$  (median:  $11.8\%$ ). As the lag time was determined

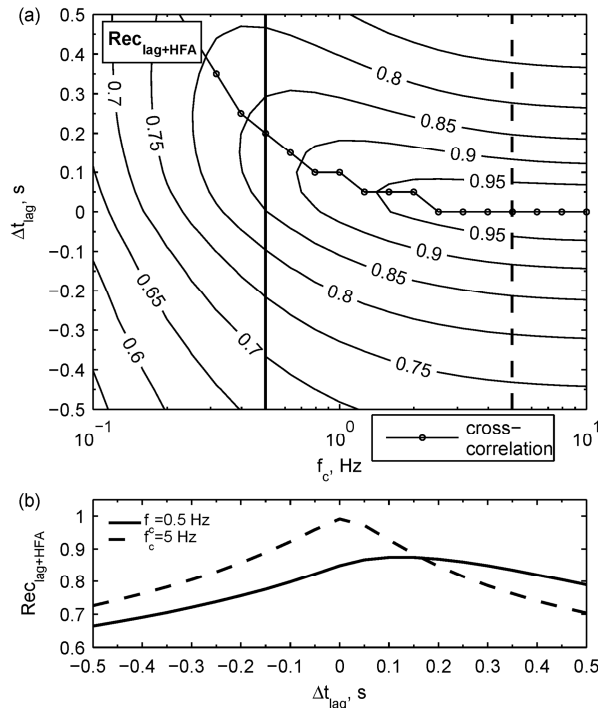


**Figure 5:** The combined flux recovery ( $Rec_{lag+HFA}$ ) for the sensible heat flux due to both an erroneous lag time ( $\Delta t_{lag}$ ) and high frequency attenuation (represented by the cut-off frequency  $f_c$ ). Shown are the results of the REA simulation for an eddy reversal frequency of 3 Hz. **(a)** The contour lines represent the flux recovery as a function of  $\Delta t_{lag}$  and  $f_c$ . The retrieved phase shift due to low-pass filtering is also shown by the results from the cross-correlation between  $w$  and the modified temperature time series. The vertical lines mark the position of **(b)** the cross-section illustrating  $Rec_{lag+HFA}$  as a function of  $\Delta t_{lag}$  for values of  $f_c$  of 0.5 and 5 Hz. From Moravek *et al.* [2013, Appendix C].

with the online cross-correlation method and all other time responses were found negligible, no correction for an erroneous lag time was necessary. However, a random error of the lag time of 0.1 s was found due to the uncertainty of the cross-correlation peak of the vertical wind velocity and the CO<sub>2</sub> signal, which yielded a random flux error ranging between  $\pm 0.6\%$  and  $\pm 9.9\%$  (median:  $\pm 4.0\%$ ).

Since the systematic error of the high frequency attenuation was corrected for in the post-processing and the additional random flux error due to an erroneous lag time was comparatively low, it can be concluded that an imprecise sampling of up- and downdraft events did not have a major impact on the quality of HREA fluxes of PAN. In fact, the precision of the PAN analysis (Sect. 3.1.2.1) and generally lower PAN fluxes (Sect. 3.1.2.3) are the major causes.

### 3.1.3 Method comparison

As the analysis on the performance of the flux measurement system has shown, the applicability of HREA and MBR for PAN flux measurements [see Moravek *et al.*, 2014a, Appendix B] largely depends on the capability of the flux measurements system to resolve small mixing ratio differences ( $\Delta\chi$ ) of PAN. This applies also to other scalar compounds exhibiting small surface-atmosphere exchange fluxes. Next to the magnitude of the flux, the measured mixing ratio differences are influenced by the meteorological conditions and operational settings, such as the size of the dead band

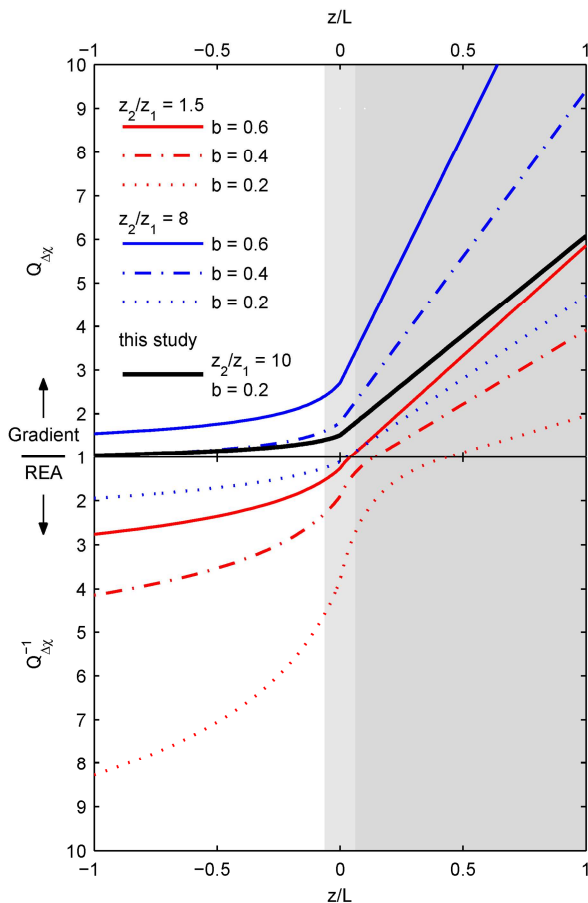


**Figure 6:** Ratio of expected mixing ratio differences of the gradient and REA method versus the stability ( $z/L$ ) for different operational settings. Upper y-axis: The gradient method yields larger mixing ratio differences ( $Q_{\Delta\chi} = \Delta\chi(\text{gradient})/\Delta\chi(\text{REA}) > 1$ ). Lower y-axis (reversed): The REA method yields larger mixing ratio differences ( $Q_{\Delta\chi}^{-1} = \Delta\chi(\text{REA})/\Delta\chi(\text{gradient}) > 1$ ). The red and blue lines represent measurements above low ( $z_2/z_1 = 8$ ) and high ( $z_2/z_1 = 1.5$ ) vegetation, respectively. A  $b$ -value of 0.6 (solid line) represents REA measurements with no dead band. The  $b$ -values of 0.4 (dashed line) and 0.2 (dotted line) represent REA measurements with a small and large dead band, respectively. The black line was derived with the settings used in this thesis. From *Moravek et al.* [2014a, Appendix B].

(HREA or REA in general) and the separation of the inlets (MBR or gradient methods in general).

To evaluate under which conditions either the gradient or the REA approach is favoured, *Moravek et al.* [2014a, Appendix B] examines the ratio of expected mixing ratio differences of both methods. Figure 6 shows the expected ratios of mixing ratio differences as a function of the stability parameter ( $z/L$ ) for different operational settings [for details see Sect. 4.4 in *Moravek et al.*, 2014a, Appendix B]. The results show that above high vegetation ( $z_2/z_1 = 1.5$ ) the REA method has a clear advantage under unstable and also neutral conditions. During stable conditions, the REA method only yields higher mixing ratio differences when choosing a large dead band. Above low vegetation ( $z_2/z_1 = 8$ ) the gradient method yields larger mixing ratio differences under neutral and stable conditions. For unstable conditions, which usually represent daytime fluxes, there is no clear choice for either the REA or gradient method above low vegetation. In the shown example the gradient method yields larger mixing ratio differences when no dead band is chosen, while a large dead band would lead to larger differences with the REA method. Applying the setting used in this study ( $z_2/z_1 = 10$  and  $b = 0.21$ ), larger mixing ratio differences were expected with the MBR method than with the HREA method not only for stable and neutral but also for unstable conditions.

This is in a good agreement with results from a simulation analysis of MBR and HREA measurements and explains – next to the lower precision and expected lower PAN fluxes during the HREA measurements – why PAN fluxes could be resolved with the MBR but not the HREA method.

### 3.2 Case study: PAN deposition to the grassland ecosystem

The PAN flux measurements system was developed to obtain a better understanding of the controlling factors of PAN deposition and its role within the nitrogen cycle. Since no significant PAN fluxes were measured during the HREA measurement period, the results from the MBR flux measurements were used for further evaluations. As it was mentioned in Sect. 3.1.2.2 [for PAN fluxes see also Figure 3 in *Moravek et al.*, 2014b, Appendix D], a mean daytime PAN deposition during the MBR measurements of  $-0.07 \text{ nmol m}^{-2} \text{ s}^{-1}$  was observed, with maximum values during the afternoon reaching up to  $-0.2 \text{ nmol m}^{-2} \text{ s}^{-1}$ .

In a first step, the stomatal and non-stomatal deposition of PAN to the grassland was investigated [see *Moravek et al.*, 2014b, Appendix D]. While the canopy conductance (the inverse of the surface/canopy resistance) was determined from the MBR measurements, the stomatal conductance was derived from the Penman-Monteith equation and corrected for molecular diffusivities of PAN and soil evaporation. Maximum values of the stomatal conductance reached about  $0.26 \text{ cm s}^{-1}$  during daytime. Due to an increased vapour pressure deficit in the afternoon the maximum was skewed towards the morning and occurred at 11:00 CET. The non-stomatal conductance – derived from the residual between the canopy conductance and the stomatal conductance – was considerable and within the magnitude of the stomatal uptake. However, no clear dependency of the non-stomatal conductance for PAN with the diurnal cycle or other quantities was found. The non-stomatal deposition of PAN was also of similar magnitude as the non-stomatal deposition of  $\text{O}_3$ . This is in contrast to currently applied deposition models, which assume the non-stomatal uptake of PAN to be about 10 times smaller due to its lower reactivity [*Simpson et al.*, 2012; *Wesely*, 1989]. Hence, the finding in this study supports the statement by *Turnipseed et al.* [2006] that current deposition models may significantly underestimate PAN non-stomatal deposition.

In a second step, the retrieved information on the stomatal and non-stomatal conductances was used to model the PAN deposition over a 3.5 months period (summer to early autumn) on the grassland site [see *Moravek et al.*, 2014b, Appendix D]. The

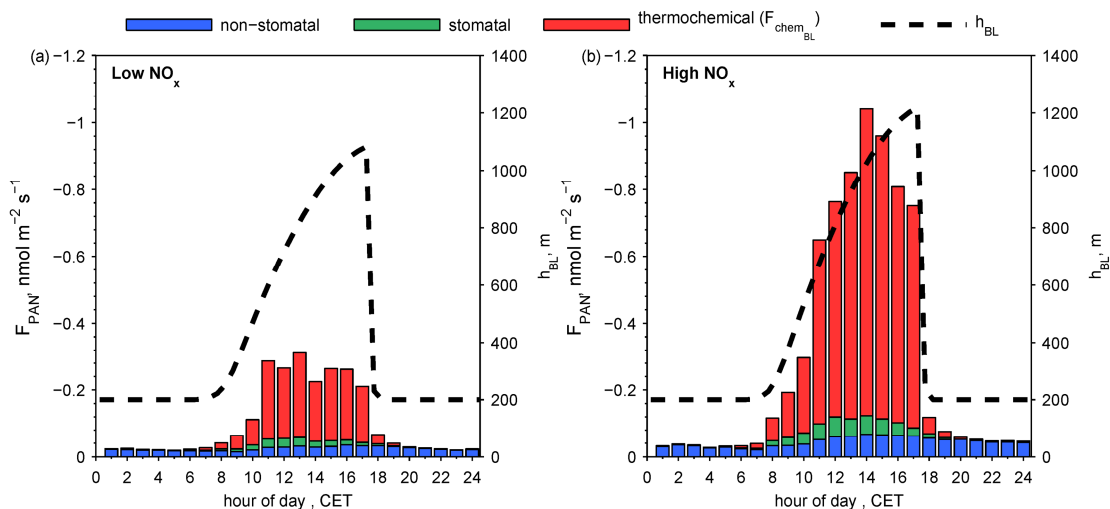


**Figure 7:** Modelled stomatal and non-stomatal PAN deposition fluxes and PAN loss due to thermochemical decomposition for (a) low and (b) high NO<sub>x</sub> periods at the Mainz-Finthen grassland site. The dashed line

marks the theoretical boundary layer height used for the calculation of the PAN decomposition. From Moravek *et al.* [2014b, Appendix D].

PAN deposition at the grassland site was governed by two contrasting pollution regimes, (1) low NO<sub>x</sub> episodes with clean air from south westerly directions and (2) high NO<sub>x</sub> episodes with more polluted air masses from the north eastern sector. PAN mixing ratios showed a clear diurnal cycle with maximum values in the afternoon of 300 ppt (median) during low NO<sub>x</sub> conditions. Under high NO<sub>x</sub> conditions, locally produced PAN from the industrialized region was transported to the site, leading to maximum PAN mixing ratios in the afternoon of on average 600 ppt. Mainly as a result of the differences in the prevailing PAN mixing ratios, the daytime maximum of the modelled PAN deposition flux (stomatal and non-stomatal) was about  $-0.05 \text{ nmol m}^{-2} \text{ s}^{-1}$  during low NO<sub>x</sub> and  $-0.1 \text{ nmol m}^{-2} \text{ s}^{-1}$  during high NO<sub>x</sub> conditions (Figure 7). Considering only daytime values, the contribution of the non-stomatal deposition was of about 70% during low NO<sub>x</sub> and 60% during high NO<sub>x</sub> conditions. As about half of the grassland vegetation was senescing or was already died-off, reaction on plant surfaces may be a reason for the large non-stomatal fraction.

Next to the stomatal and non-stomatal deposition, thermochemical decomposition was a significant removal pathway of PAN from the atmosphere during daytime. During nighttime thermochemical decomposition of PAN was insignificant. Integrating all three removal pathways over the entire day (24 h), the sum of stomatal and non-stomatal deposition made up 32% of the total PAN removal during low NO<sub>x</sub> conditions, while it only accounted for 22% during high NO<sub>x</sub> conditions. The total PAN deposition per day was  $333 \text{ } \mu\text{g m}^{-2} \text{ d}^{-1}$  during low and  $518 \text{ } \mu\text{g m}^{-2} \text{ d}^{-1}$  during high NO<sub>x</sub> conditions. However, these values are much lower than observed deposition rates of other nitrogen compounds at comparable sites, which suggests that PAN deposition did not play a critical role as a source of N<sub>r</sub> to the nutrient-poor grassland ecosystem.



## 4 Conclusions

Up to date very few studies have measured direct PAN deposition to ecosystems. The experiments often cover only a short time period and the obtained results differ considerably. Therefore, the main goal of this thesis was the development of a flux measurement system for PAN and its application on a grassland ecosystem. The system was designed for the use of the HREA method and MBR method in combination with a GC-ECD for PAN analysis. It is the first REA system for PAN and the first system that allowed simultaneous sampling of PAN at two inlet heights for the application of the MBR method. Although it was developed for PAN, some new developments may be also transferred to flux measurement systems of other trace gases.

Following the presented results, the major conclusions from this thesis can be divided into three categories:

1. Conclusions on the development of the PAN flux measurement system and its performance [Moravek *et al.*, 2014a, Appendix B]:
  - Uncertainties in the determination of PAN mixing ratio differences are the most critical issue for a successful application of both the HREA and the MBR method for PAN. This is mainly due to small surface fluxes of PAN and uncertainties in currently used methods for the analysis of PAN. At the investigated natural grassland site, the presented flux measurement system was able to measure PAN deposition fluxes with the MBR method during daytime. However, due to generally lower fluxes and a lower precision the HREA method was not applicable. As an important feature of the quality control, this thesis demonstrated the importance of side-by-side measurements to determine the precision of the flux measurement system under different environmental conditions.
  - As a consequence of the previous point, the applicability of HREA and MBR for PAN flux measurements largely depends on the capability of the flux measurement system to resolve small PAN mixing ratios. The thesis

demonstrated that above low vegetation the gradient method yields larger mixing ratio differences under neutral and stable conditions. For unstable conditions, which usually represent daytime fluxes, there is no clear choice for either the REA or gradient method. Above high vegetation the REA method has a clear advantage under unstable and also neutral conditions, while during stable conditions the REA method only yields higher mixing ratio differences when choosing a large dead band.

- One major characteristic of the flux measurement system is the pre-concentration of PAN on capillary columns as a sampling method. This is possible since a linear relationship was found between the PAN peak area and both the PAN mixing ratio and the sample volume. This allows the system to be used with varying sample volumes, which is a prerequisite for the application of the HREA and REA method. The use of capillary columns as a reservoir for REA applications has not been reported elsewhere and might be a prospective option for REA applications of other reactive compounds. Furthermore, the procedure of simultaneous sampling of PAN with two pre-concentration units and subsequent analysis with the GC-ECD reveals that PAN can be stored at lower temperatures in the pre-concentration units for at least 10 min without significant loss of PAN.

## 2. General conclusions on the application of the REA method [Moravek *et al.*, 2013, Appendix C]:

- An imprecisely determined lag time may lead to a significant reduction of the REA flux, especially in case a long single inlet tube is employed (< 5% to 50% for probable lag time errors of REA systems described in literature). The comparison of different methods for the lag time determination reveals that the online cross-correlation method yields the most accurate results, although it is technically challenging. In case the online cross-correlation is not applied, a horizontal displacement between the sonic anemometer and the REA inlet has to be included in the lag time determination by considering wind direction and speed. For any setup, the flow in the main inlet line should be regulated by the volume flow. In case a systematic error of the lag time is known (e.g., electronic delay or sensor separation effect), the REA flux has to be corrected for, e.g. by using the provided corrections function. In case the lag time method has a random error (e.g., when using the (online) cross-correlation method), the additional random error should be accounted for in the error analysis of the REA fluxes.

- 
- High frequency attenuation due to the employment of a single, long inlet tube may lead to significant reduction of the REA flux (< 5% to 30% for commonly used setups). This thesis shows that the flux recovery decreases linearly with a decreasing cut-off frequency of the low-pass filter and there is a quadratic decline of the flux recovery with increasing eddy reversal frequencies. REA fluxes may be corrected in the post-processing of REA fluxes by using the correction function given in this thesis in case the transfer function of the high frequency attenuation effect is known. Here it has to be considered, that the high frequency attenuation by a long inlet tube is found to be significantly larger than predicted by theoretical functions, which might be attributed to a large extent to the effect of inlet filters.
  - In case both lag time error and high frequency attenuation are significant, the ensemble effect on REA fluxes has to be evaluated. For this, this thesis provides a detailed procedure for validation of REA systems with one single inlet tube. It has to be noted that REA systems with a short single inlet tube or two separate inlets for updraft and downdraft events may also be prone to the discussed uncertainties. Furthermore, in some cases the error due to imprecise conditional sampling can be much less than the error induced by inappropriate chemical analysis. Hence, the knowledge about the potential effect is important for the design of future REA systems, where a compromise in the setup has to be made as it was the case for the presented PAN flux measurement system.
3. Conclusions on the PAN deposition at the natural grassland site [*Moravek et al.*, 2014b, Appendix D]:
- At the natural grassland site, daytime non-stomatal uptake is of similar magnitude as stomatal uptake of PAN and non-stomatal deposition of O<sub>3</sub>. This is in contrast to currently applied deposition models, which assume the non-stomatal uptake of PAN to be about 10 times smaller due to its lower reactivity. Hence, the finding in this thesis supports the statement by Turnipseed et al. (2006) that current deposition models may significantly underestimate PAN non-stomatal deposition.
  - It is likely that PAN deposition does not play a critical role as a source of N<sub>r</sub> to the nutrient-poor grassland ecosystem during both polluted and unpolluted conditions, following the results about the effect of total nitrogen deposition on grassland ecosystems by *Stevens et al.* [2010]. Furthermore, a phytotoxic effect of PAN on grass species can be excluded for any conditions observed at the site.

- Dry deposition of PAN is a significant removal process of PAN from the atmosphere accounting for approximately 20–30% of the PAN removal from the atmosphere during the examined period. In higher latitudes or during winter, when thermochemical decomposition of PAN is low, PAN deposition is likely to be the predominant sink. During nighttime non-stomatal deposition of PAN leads to a distinct decay of PAN mixing ratios in the nocturnal boundary layer and is the predominant removal process for PAN.

This thesis focuses on the development of a PAN flux measurement system and contributes to a more detailed understanding on PAN deposition. To obtain a deeper insight into the importance of PAN deposition and mechanisms of PAN uptake, further PAN flux measurements on different ecosystem types are needed. Ideally, they are performed over a long period, covering more seasons or even annual cycles together with atmosphere-surface fluxes of other  $N_r$  compounds. Laboratory studies pursuing the studies of *Sparks et al.* [2003] and *Teklemariam and Sparks* [2004] are promising to gain further insight into the role of non-stomatal deposition to surfaces and mechanism of PAN uptake by plant tissues. While the PAN flux measurement system in the presented configuration can be used under conditions where PAN fluxes of  $> 0.05 \text{ nmol m}^{-2} \text{ s}^{-1}$  are expected (e.g. above forests ecosystems or intensive grasslands in non-remote regions), flux measurements under low PAN mixing ratios and at sites with a high surface resistance are still a great challenge. While the application of the REA method for PAN requires an extensive effort, the gradient or MBR method with simultaneous sampling at two heights may facilitate a feasible alternative to eddy covariance measurements, especially for long term measurements.

## References

- Ammann, C. (1998), On the application of relaxed eddy accumulation and common methods for measuring trace gas fluxes, *PhD Thesis, ETH Zürich*, pp. 232.
- Aubinet, M., T. Vesala, and D. Papale (2012), *Eddy Covariance: A Practical Guide to Measurement and Data Analysis*, 2012. ed., Springer Netherlands, Dordrecht.
- Baker, J. M. (2000), Conditional sampling revisited, *Agr Forest Meteorol*, 104(1), 59-65.
- Baker, J. M., J. M. Norman, and W. L. Bland (1992), Field-scale application of flux measurement by conditional sampling, *Agr Forest Meteorol*, 62(1–2), 31-52.
- Beverland, I. J., R. Milne, C. Boissard, D. H. Oneill, J. B. Moncrieff, and C. N. Hewitt (1996a), Measurement of carbon dioxide and hydrocarbon fluxes from a sitka spruce forest using micrometeorological techniques, *J. Geophys. Res.-Atmos.*, 101(D17), 22807-22815.
- Bowling, D. R., A. C. Delany, A. A. Turnipseed, D. D. Baldocchi, and R. K. Monson (1999), Modification of the relaxed eddy accumulation technique to maximize measured scalar mixing ratio differences in updrafts and downdrafts, *J. Geophys. Res.-Atmos.*, 104(D8), 9121-9133.
- Businger, J. A. (1986), Evaluation of the Accuracy with Which Dry Deposition Can Be Measured with Current Micrometeorological Techniques, *J Clim Appl Meteorol*, 25(8), 1100-1124.
- Businger, J. A., and S. P. Oncley (1990), Flux Measurement with Conditional Sampling, *J. Atmos. Ocean. Technol.*, 7(2), 349-352.
- Businger, J. A., J. C. Wyngaard, Y. Izumi, and E. F. Bradley (1971), Flux-Profile Relationships in the Atmospheric Surface Layer, *Journal of the Atmospheric Sciences*, 28(2), 181-189.
- Cape, J. N., S. E. Cornell, T. D. Jickells, and E. Nemitz (2011), Organic nitrogen in the atmosphere - Where does it come from? A review of sources and methods, *Atmos. Res.*, 102(1-2), 30-48.
- Day, D. A., P. J. Wooldridge, M. B. Dillon, J. A. Thornton, and R. C. Cohen (2002), A thermal dissociation laser-induced fluorescence instrument for in situ detection of NO<sub>2</sub>, peroxy nitrates, alkyl nitrates, and HNO<sub>3</sub>, *Journal of Geophysical Research: Atmospheres*, 107(D6), ACH 4-1-ACH 4-14.
- Delany, A. C., S. P. Oncley, and J. A. Businger (1991), Adapting the Conditional Sampling Concept for a Range of Different Chemical Species, *Proceeding of the Seventh AMS Symposium on Meteorological Observations and Instrumentation*(New Orleans, La., January 14–18), 22–25.

- Doskey, P. V., V. R. Kotamarthi, Y. Fukui, D. R. Cook, F. W. Breitbeil, and M. L. Wesely (2004), Air-surface exchange of peroxyacetyl nitrate at a grassland site, *J. Geophys. Res.-Atmos.*, *109*(D10), 9, D10310.
- Erisman, J. W., M. A. Sutton, J. Galloway, Z. Klimont, and W. Winiwarter (2008), How a century of ammonia synthesis changed the world, *Nat Geosci*, *1*(10), 636-639.
- Erisman, J. W., J. N. Galloway, S. P. Seitzinger, A. Bleeker, N. B. Dise, A. M. R. Petrescu, A. M. Leach, and W. de Vries (2013), Consequences of human modification of the global nitrogen cycle, *Philosophical Transactions of the Royal Society B: Biological Sciences*, *368*(1621).
- EUROSTAT (2011), Agriculture and fishery statistics: main results 2009-10, edited, p. 152, Publications Office of the European Union, Luxembourg.
- Fahey, D. W., G. Hubler, D. D. Parrish, E. J. Williams, R. B. Norton, B. A. Ridley, H. B. Singh, S. C. Liu, and F. C. Fehsenfeld (1986), Reactive Nitrogen Species in the Troposphere - Measurements of No, No<sub>2</sub>, Hno<sub>3</sub>, Particulate Nitrate, Peroxyacetyl Nitrate (Pan), O<sub>3</sub>, and Total Reactive Odd Nitrogen (Noy) at Niwot Ridge, Colorado, *J. Geophys. Res.-Atmos.*, *91*(D9), 9781-9793.
- Farmer, D. K., and R. C. Cohen (2008), Observations of HNO<sub>3</sub>, Sigma AN, Sigma PN and NO<sub>2</sub> fluxes: evidence for rapid HO<sub>x</sub> chemistry within a pine forest canopy, *Atmos. Chem. Phys.*, *8*(14), 3899-3917.
- Fischer, E. V., D. A. Jaffe, and E. C. Weatherhead (2011), Free tropospheric peroxyacetyl nitrate (PAN) and ozone at Mount Bachelor: potential causes of variability and timescale for trend detection, *Atmos. Chem. Phys.*, *11*(12), 5641-5654.
- Flocke, F. M., A. J. Weinheimer, A. L. Swanson, J. M. Roberts, R. Schmitt, and S. Shertz (2005), On the measurement of PANs by gas chromatography and electron capture detection, *J. Atmos. Chem.*, *52*(1), 19-43.
- Foken, T. (2008), *Micrometeorology*, 306 pp., Springer, Berlin.
- Fowler, D., et al. (2013), The global nitrogen cycle in the twenty-first century, *Philosophical Transactions of the Royal Society B: Biological Sciences*, *368*(1621).
- Gaffney, J. S., and N. A. Marley (2001), Peroxyacetyl nitrate (PAN): Historical perspective, *81st AMS Annual Meeting A Millennium Symposium on Atmospheric Chemistry, January 14-19, 2001*.
- Galloway, J. N., A. M. Leach, A. Bleeker, and J. W. Erisman (2013), A chronology of human understanding of the nitrogen cycle, *Philosophical Transactions of the Royal Society B: Biological Sciences*, *368*(1621).
- Galloway, J. N., J. D. Aber, J. W. Erisman, S. P. Seitzinger, R. W. Howarth, E. B. Cowling, and B. J. Cosby (2003), The nitrogen cascade, *Bioscience*, *53*(4), 341-356.
- Garland, J. A., and S. A. Penkett (1976), Absorption of peroxy acetyl nitrate and ozone by natural surfaces, *Atmos. Environ.*, *10*(12), 1127-1131.
- Hicks, B. B., D. D. Baldocchi, T. P. Meyers, R. P. Hosker, and D. R. Matt (1987), A preliminary multiple resistance routine for deriving dry deposition velocities from measured quantities, *Water Air Soil Poll*, *36*(3-4), 311-330.
- Hill, A. C. (1971), Vegetation - sink for atmospheric pollutants, *Journal of the Air Pollution Control Association*, *21*(6), 341-346.

- Högström, U. (1988), Non-dimensional wind and temperature profiles in the atmospheric surface layer: A re-evaluation, *Boundary-Layer Meteorology*, 42(1-2), 55-78.
- Kames, J., and U. Schurath (1995), Henrys Law and Hydrolysis-Rate Constants for Peroxyacyl Nitrates (Pans) Using a Homogeneous Gas-Phase Source, *J. Atmos. Chem.*, 21(2), 151-164.
- LaFranchi, B. W., et al. (2009), Closing the peroxy acetyl nitrate budget: observations of acyl peroxy nitrates (PAN, PPN, and MPAN) during BEARPEX 2007, *Atmos. Chem. Phys.*, 9(19), 7623-7641.
- Lenschow, D. H., and M. R. Raupach (1991), The attenuation of fluctuations in scalar concentrations through sampling tubes, *J. Geophys. Res.-Atmos.*, 96(D8), 15259-15268.
- Liu, H. P., and T. Foken (2001), A modified Bowen ratio method to determine sensible and latent heat fluxes, *Meteorol. Z.*, 10(1), 71-80.
- Lovelock, J. E., and S. A. Penkett (1974), Pan over Atlantic and Smell of Clean Linen, *Nature*, 249(5456), 434-434.
- Massman, W. J. (1991), The attenuation of concentration fluctuations in turbulent flow through a tube, *J. Geophys. Res.-Atmos.*, 96(D8), 15269-15273.
- Massman, W. J., and A. Ibrom (2008), Attenuation of concentration fluctuations of water vapor and other trace gases in turbulent tube flow, *Atmos. Chem. Phys.*, 8(20), 6245-6259.
- Mielke, L. H., and H. D. Osthoff (2012), On quantitative measurements of peroxy-carboxylic nitric anhydride mixing ratios by thermal dissociation chemical ionization mass spectrometry, *Int J Mass Spectrom*, 310, 1-9.
- Min, K. E., S. E. Pusede, E. C. Browne, B. W. LaFranchi, P. J. Wooldridge, G. M. Wolfe, S. A. Harrold, J. A. Thornton, and R. C. Cohen (2012), Observations of atmosphere-biosphere exchange of total and speciated peroxy nitrates: nitrogen fluxes and biogenic sources of peroxy nitrates, *Atmos. Chem. Phys.*, 12(20), 9763-9773.
- Moore, C. J. (1986), Frequency response corrections for eddy correlation systems, *Boundary-Layer Meteorology*, 37(1-2), 17-35.
- Moravek, A., I. Trebs, and T. Foken (2013, Appendix C), Effect of imprecise lag time and high-frequency attenuation on surface-atmosphere exchange fluxes determined with the relaxed eddy accumulation method, *Journal of Geophysical Research: Atmospheres*, 118(17), 10,210-210,224.
- Moravek, A., T. Foken, and I. Trebs (2014), Application of a GC-ECD for measurements of biosphere-atmosphere exchange fluxes of peroxyacetyl nitrate using the relaxed eddy accumulation and gradient method, *Submitted to Atmospheric Measurement Techniques*.
- Moravek, A., T. Foken, and I. Trebs (2014a, Appendix B), Application of a GC-ECD for measurements of biosphere-atmosphere exchange fluxes of peroxyacetyl nitrate using the relaxed eddy accumulation and gradient method, *submitted to Atmospheric Measurement Techniques*.

- Moravek, A., P. Stella, T. Foken, and I. Trebs (2014b, Appendix D), Influence of local air pollution on the deposition of peroxyacetyl nitrate to a natural grassland ecosystem, *to be submitted to Biogeosciences*.
- Müller, K. P., and J. Rudolph (1992), Measurements of Peroxyacetyl Nitrate in the Marine Boundary Layer over the Atlantic, *J. Atmos. Chem.*, 15(3-4), 361-367.
- Novak, J., J. Janak, and J. Golias (1979), New concepts of quantification in headspace gas analysis by stripping and trapping components in a closed circuit, *in Proceedings of the 9th Materials Research Symposium, April 10-13, 1978, held at NBS, Gaithersburg, MD, NBS Special Publication, No 519, National Bureau of Standards, Washington, DC, 739-746*.
- Okano, K., K. Tobe, and A. Furukawa (1990), Foliar Uptake of Peroxyacetyl Nitrate (PAN) by Herbaceous Species Varying in Susceptibility to this Pollutant, *New Phytol*, 114(1), 139-145.
- Okumura, M., K. Nakagawa, Y. Kominami, T. Miyama, K. Kinoshita, K. Hamotani, S. Tohno, M. Yoneda, and A. Tani (2011), Isoprene flux measurement using relaxed eddy accumulation method in warm-temperate mixed forest in Japan, *Proceedings of Earth Observation for Land-Atmosphere Interaction Science*, 6 pp.-6 pp.6 pp.
- Orlando, J. J., G. S. Tyndall, and J. G. Calvert (1992), Thermal-Decomposition Pathways for Peroxyacetyl Nitrate (Pan) - Implications for Atmospheric Methyl Nitrate Levels, *Atmos Environ a-Gen*, 26(17), 3111-3118.
- Park, C., G. W. Schade, and I. Boedeker (2010), Flux measurements of volatile organic compounds by the relaxed eddy accumulation method combined with a GC-FID system in urban Houston, Texas, *Atmos. Environ.*, 44(21-22), 2605-2614.
- Paul, D., and H. D. Osthoff (2010), Absolute Measurements of Total Peroxy Nitrate Mixing Ratios by Thermal Dissociation Blue Diode Laser Cavity Ring-Down Spectroscopy, *Anal. Chem.*, 82(15), 6695-6703.
- Paul, D., A. Furgeson, and H. D. Osthoff (2009), Measurements of total peroxy and alkyl nitrate abundances in laboratory-generated gas samples by thermal dissociation cavity ring-down spectroscopy, *Review of Scientific Instruments*, 80(11), -.
- Phillips, G. J., N. Pouvesle, J. Thieser, G. Schuster, R. Axinte, H. Fischer, J. Williams, J. Lelieveld, and J. N. Crowley (2013), Peroxyacetyl nitrate (PAN) and peroxyacetic acid (PAA) measurements by iodide chemical ionisation mass spectrometry: first analysis of results in the boreal forest and implications for the measurement of PAN fluxes, *Atmos. Chem. Phys.*, 13(3), 1129-1139.
- Roberts, J. M. (1990), The atmospheric chemistry of organic nitrates, *Atmos Environ a-Gen*, 24(2), 243-287.
- Schrimpf, W., K. Lienaerts, K. P. Muller, J. Rudolph, R. Neubert, W. Schussler, and I. Levin (1996), Dry deposition of peroxyacetyl nitrate (PAN): Determination of its deposition velocity at night from measurements of the atmospheric PAN and (222)Radon concentration gradient, *Geophys. Res. Lett.*, 23(24), 3599-3602.
- Simpson, D., et al. (2012), The EMEP MSC-W chemical transport model - technical description, *Atmos. Chem. Phys.*, 12(16), 7825-7865.
- Singh, H. B. (1987), Reactive Nitrogen in the Troposphere, *Environ Sci Technol*, 21(4), 320-327.

- Singh, H. B., and L. J. Salas (1983), Methodology for the Analysis of Peroxyacetyl Nitrate (Pan) in the Unpolluted Atmosphere, *Atmos. Environ.*, 17(8), 1507-1516.
- Singh, H. B., D. Herlth, D. Ohara, L. Salas, A. L. Torres, G. L. Gregory, G. W. Sachse, and J. F. Kasting (1990), Atmospheric Peroxyacetyl Nitrate Measurements over the Brazilian Amazon Basin during the Wet Season - Relationships with Nitrogen-Oxides and Ozone, *J. Geophys. Res.-Atmos.*, 95(D10), 16945-16954.
- Slusher, D. L., L. G. Huey, D. J. Tanner, F. M. Flocke, and J. M. Roberts (2004), A thermal dissociation-chemical ionization mass spectrometry (TD-CIMS) technique for the simultaneous measurement of peroxyacetyl nitrates and dinitrogen pentoxide, *J. Geophys. Res.-Atmos.*, 109(D19).
- Söderlund, R., and B. H. Svensson (1976), The global nitrogen cycle, in *Nitrogen, Phosphorus and Sulphur - Global Cycles*, edited by B. H. Svensson and R. Söderlund, pp. 23-73.
- Sparks, J. P., J. M. Roberts, and R. K. Monson (2003), The uptake of gaseous organic nitrogen by leaves: A significant global nitrogen transfer process, *Geophys. Res. Lett.*, 30(23).
- Stevens, C. J., et al. (2010), Nitrogen deposition threatens species richness of grasslands across Europe, *Environ Pollut*, 158(9), 2940-2945.
- Stull, R. B. (1988), *An Introduction to Boundary Layer Meteorology*, 666 pp., Springer Netherlands.
- Suttie, J. M., S. G. Reynolds, and C. Batello (2005), *Grasslands of the world*, xxii, 514p. : ill. (mostly col.), figs., maps, tabs. ; 524cm. pp., FAO, Rome.
- Sutton, M. A., et al. (2007), Challenges in quantifying biosphere-atmosphere exchange of nitrogen species, *Environ Pollut*, 150(1), 125-139.
- Talukdar, R. K., J. B. Burkholder, A. M. Schmoltner, J. M. Roberts, R. R. Wilson, and A. R. Ravishankara (1995), Investigation of the Loss Processes for Peroxyacetyl Nitrate in the Atmosphere - Uv Photolysis and Reaction with Oh, *J. Geophys. Res.-Atmos.*, 100(D7), 14163-14173.
- Taylor, O. C. (1969), Importance of Peroxyacetyl Nitrate (PAN) as a Phytotoxic Air Pollutant, *Journal of the Air Pollution Control Association*, 19(5), 347-351.
- Teklemariam, T. A., and J. P. Sparks (2004), Gaseous fluxes of peroxyacetyl nitrate (PAN) into plant leaves, *Plant Cell Environ.*, 27(9), 1149-1158.
- Temple, P. J., and O. C. Taylor (1983), World-wide ambient measurements of peroxyacetyl nitrate (PAN) and implications for plant injury, *Atmospheric Environment (1967)*, 17(8), 1583-1587.
- Turnipseed, A. A., L. G. Huey, E. Nemitz, R. Stickel, J. Higgs, D. J. Tanner, D. L. Slusher, J. P. Sparks, F. Flocke, and A. Guenther (2006), Eddy covariance fluxes of peroxyacetyl nitrates (PANs) and NO<sub>y</sub> to a coniferous forest, *J. Geophys. Res.-Atmos.*, 111(D9), D09304.
- Vierkorn-Rudolph, B., J. Rudolph, and S. Diederich (1985), Determination of Peroxyacetylnitrate (PAN) in Unpolluted Areas, *Int. J. Environ. Anal. Chem.*, 20(1-2), 131-140.
- Wesely, M. L. (1989), Parameterization of surface resistances to gaseous dry deposition in regional-scale numerical-models, *Atmos. Environ.*, 23(6), 1293-1304.

- Wesely, M. L., and B. B. Hicks (2000), A review of the current status of knowledge on dry deposition, *Atmos. Environ.*, *34*(12-14), 2261-2282.
- Wolfe, G. M., J. A. Thornton, R. L. N. Yatawelli, M. McKay, A. H. Goldstein, B. LaFranchi, K. E. Min, and R. C. Cohen (2009), Eddy covariance fluxes of acyl peroxy nitrates (PAN, PPN and MPAN) above a Ponderosa pine forest, *Atmos. Chem. Phys.*, *9*(2), 615-634.
- Wolfe, G. M., J. A. Thornton, V. F. McNeill, D. A. Jaffe, D. Reidmiller, D. Chand, J. Smith, P. Swartzendruber, F. Flocke, and W. Zheng (2007), Influence of trans-Pacific pollution transport on acyl peroxy nitrate abundances and speciation at Mount Bachelor Observatory during INTEX-B, *Atmos. Chem. Phys.*, *7*(20), 5309-5325.
- Wolfe, G. M., et al. (2011), The Chemistry of Atmosphere-Forest Exchange (CAFE) Model - Part 2: Application to BEARPEX-2007 observations, *Atmos. Chem. Phys.*, *11*(3), 1269-1294.
- Wooldridge, P. J., et al. (2010), Total Peroxy Nitrates (&Sigma;PNs) in the atmosphere: the Thermal Dissociation-Laser Induced Fluorescence (TD-LIF) technique and comparisons to speciated PAN measurements, *Atmos. Meas. Tech.*, *3*(3), 593-607.
- Wyngaard, J. C., and C. H. Moeng (1992), Parameterizing turbulent diffusion through the joint probability density *Boundary-Layer Meteorology*, *60*(1-2), 1-13.
- Zhang, G., Y. J. Mu, J. F. Liu, and A. Mellouki (2012), Direct and simultaneous determination of trace-level carbon tetrachloride, peroxyacetyl nitrate, and peroxypropionyl nitrate using gas chromatography-electron capture detection, *J Chromatogr A*, *1266*, 110-115.

# Appendix A

## Individual contribution to the joint publications

This cumulative thesis consists of several manuscripts listed hereafter, which originate from a close collaboration with other researchers. In this section the individual contributions are specified.

## Appendix B

Moravek, A., T. Foken, and I. Trebs (2014), Application of a GC-ECD for measurements of biosphere-atmosphere exchange fluxes of peroxyacetyl nitrate using the relaxed eddy accumulation and gradient method, *submitted to Atmospheric Measurement Techniques*.

- I myself developed the PAN flux measurement system, which involved (1) its initial design and testing in the laboratory and (2) the adjustment and optimization of operational settings on the field site. I conducted the PAN flux measurements and was responsible for the O<sub>3</sub> flux measurements during the experiment. Furthermore, I performed all the data analysis, such as the flux and error calculations. Finally, I developed the idea, the concept of the manuscript and wrote the manuscript.
- Thomas Foken, my supervisor, contributed with important comments on the REA technique and flux measurement. In addition, he gave valuable comments on the manuscript.
- Ivonne Trebs initiated the work on PAN flux measurements. As my day-to-day supervisor she was involved in the major decisions on the design of the flux measurement system. At all stages, she gave valuable comments on the manuscript.

## Appendix C

Moravek, A., I. Trebs, and T. Foken (2013), Effect of imprecise lag time and high-frequency attenuation on surface-atmosphere exchange fluxes determined with the relaxed eddy accumulation method, *Journal of Geophysical Research: Atmospheres*, 118(17), 10,210-210,224.

- I myself developed the idea and concept of the manuscript. I designed and performed the presented experiments and conducted all the data analysis, such as the REA simulation and spectral analysis. Finally, I wrote the manuscript, answered the reviewers' comments and edited the revised version of the manuscript.
- Ivonne Trebs was involved in the discussion of the experiment results. In addition, she gave valuable comments on the manuscript.
- Thomas Foken significantly contributed with his expertise on flux corrections techniques to the manuscript. He was involved in the discussion of the results and gave valuable comments on the manuscript.

## Appendix D

Moravek, A., P. Stella, T. Foken, and I. Trebs (2014), Influence of local air pollution on the deposition of peroxyacetyl nitrate to a natural grassland ecosystem, *to be submitted to Biogeosciences*.

- I myself developed the idea and concept of the manuscript. I performed the PAN mixing ratio and flux measurement. In addition, I was responsible for other EC fluxes measurements at the site and was primarily involved in the installation and setup of the measurement site. I did all data the analysis, which included e.g., the flux calculation, flux partitioning and application of the boundary layer budget approach. Finally, I wrote the manuscript.
- Patrick Stella helped with the flux partitioning and gave inspirations for the concept of the manuscript. He also gave valuable comments on the manuscript.
- Thomas Foken, as my supervisor, was involved at all stages of my research and gave valuable comments on the manuscript.
- Ivonne Trebs, initiated the work on PAN flux measurement. She was involved in the planning of the experiment campaign and in discussion of the presented results. In addition, she gave valuable comments on the manuscript.

## Appendix B

### **Application of a GC-ECD for measurements of biosphere-atmosphere exchange fluxes of peroxyacetyl nitrate using the relaxed eddy accumulation and gradient method**

**A. Moravek<sup>1</sup>, T. Foken<sup>2,3</sup> and I. Trebs<sup>1\*</sup>**

<sup>1</sup> Max Planck Institute for Chemistry, Biogeochemistry Department, Mainz, Germany

<sup>2</sup> Department of Micrometeorology, University of Bayreuth, Bayreuth, Germany

<sup>3</sup> Member of Bayreuth Center of Ecology and Environmental Research (BayCEER), University of Bayreuth, Germany

\* now at: Centre de Recherche Public - Gabriel Lippmann, Department Environment and Agro-biotechnologies, Belvaux, Luxembourg

Correspondence to: A. Moravek (a.moravek@mpic.de)

Published in Atmospheric Measurements Techniques Discussions

Received 13 January 2014 – Accepted 17 February 2014 – Published 26 February 2014.

Published by Copernicus Publications on behalf of the European Geosciences Union.

## Abstract

Peroxyacetyl nitrate (PAN) may constitute a significant fraction of reactive nitrogen in the atmosphere. Current knowledge about the biosphere-atmosphere exchange of PAN is limited and only few studies have investigated the deposition of PAN to terrestrial ecosystems. We developed a flux measurement system for the determination of biosphere-atmosphere exchange fluxes of PAN using both the hyperbolic relaxed eddy accumulation (HREA) method and the modified Bowen ratio (MBR) method. The system consists of a modified, commercially available gas chromatograph with electron capture detection (GC-ECD, Meteorologie Consult GmbH, Germany). Sampling was performed by trapping PAN onto two pre-concentration columns; during HREA operation one was used for updraft and one for downdraft events and during MBR operation the two columns allowed simultaneous sampling at two measurement heights. The performance of the PAN flux measurement system was tested at a natural grassland site, using fast response ozone (O<sub>3</sub>) measurements as a proxy for both methods. The measured PAN fluxes were comparatively small (daytime PAN deposition was on average  $-0.07 \text{ nmol m}^{-2} \text{ s}^{-1}$ ) and, thus, prone to significant uncertainties. A major challenge in the design of the system was the resolution of the small PAN mixing ratio differences. Consequently, the study focuses on the performance of the analytical unit and a detailed analysis of errors contributing to the overall uncertainty. The error of the PAN mixing ratio differences ranged from 4 to 15 ppt during the MBR and between 18 and 26 ppt during the HREA operation, while during daytime measured PAN mixing ratios were of similar magnitude. Choosing optimal settings for both the MBR and HREA method, the study shows that the HREA method did not have a significant advantage towards the MBR method under well mixed conditions as it was expected.

## 1 Introduction

Peroxyacetyl nitrate (PAN,  $\text{CH}_3\text{C}(\text{O})\text{O}_2\text{NO}_2$ ) is an important organic nitrogen compound, whose production is often associated with the anthropogenic emissions of  $\text{NO}_x$  ( $= \text{NO} + \text{NO}_2$ ) and non-methane hydrocarbons (NMHC) [Stephens, 1969]. It is formed through the oxidation of the peroxyacetyl radical (PA) with nitrogen dioxide ( $\text{NO}_2$ ):



The decomposition of PAN is dependent on temperature (back reaction of R1) and also on the reaction of PA with nitrogen monoxide (NO):



Due to its long lifetime at low temperatures PAN can be transported in the upper troposphere over long distances and acts as a reservoir species for  $\text{NO}_x$ . In this way, PAN can alter the ozone ( $\text{O}_3$ ) budget and the oxidative capacity of the atmosphere, especially in unpolluted and  $\text{NO}_x$ -poor environments [Singh and Hanst, 1981]. In addition, the dry deposition of PAN is a source of nitrogen for remote, nutrient-poor ecosystems and, hence, influences carbon sequestration [Magnani et al., 2007].

Besides thermal decomposition, dry deposition is the major removal mechanism of PAN from the atmosphere [Garland and Penkett, 1976; Hill, 1971; Shepson et al., 1992]. However, only very few studies have directly measured the flux of PAN to terrestrial ecosystems [Doskey et al., 2004; Schrimpf et al., 1996; Turnipseed et al., 2006; Wolfe et al., 2009]. The results of these and other indirect studies about PAN deposition fluxes show a large range in the magnitude of PAN fluxes and deposition velocities. The latter varies between around  $0 \text{ cm s}^{-1}$  to  $1.5 \text{ cm s}^{-1}$  for different ecosystem types. Although the difference in the obtained results might be caused by environmental conditions and different uptake mechanisms of plant species, they can also be attributed to relatively large uncertainties in the determined PAN fluxes. Both Turnipseed et al. [2006] and Wolfe et al. [2009] used a chemical ionization mass spectrometer (CIMS) and applied the eddy covariance technique (EC) above a pine forest canopy. They found flux uncertainties of 25% to 65% and 40%, respectively. Doskey et al. [2004] applied the modified Bowen ratio (MBR) method using a gas chromatograph with electron capture detection (GC-ECD) and determined uncertainties of PAN deposition velocities of 45% to 450% during daytime above a grassland ecosystem. These uncertainties are mainly caused by the low precision and accuracy of the concentration measurement, which therefore represents a major challenge in flux measurements of PAN. For instance, Wolfe et al. [2009] report total uncertainty for a single point PAN measurement of  $\pm(21\% + 3 \text{ ppt})$  employing a CIMS at a pine forest site. Recent measurements with GC-ECD achieved a precision ( $1\sigma$ ) of 1 to 3% [Fischer et al., 2011; Mills et al., 2007; G Zhang et al., 2012], while the accuracy is typically below 10% [e.g., Fischer et al., 2011; Flocke et al., 2005]. Schrimpf et al. [1996] derived PAN fluxes from measurements of PAN and  $^{222}\text{Rn}$  concentration gradients only at nighttime when concentration differences were large enough to be resolved by the analysing unit. Other existing studies inferred PAN fluxes using indirect methods such as boundary layer budget models [Garland and Penkett, 1976; Shepson et al., 1992] or chamber studies on leaves [Sparks et al., 2003; Teklemariam and Sparks, 2004]. Mostly, these are also prone to large uncertainties, as they either rely on rough assumptions, or the errors were not derived under field conditions. Hence, our current understanding of the controlling mechanisms and the importance of PAN deposition for

the atmospheric and biogeochemical nitrogen cycles is still very limited. Although PAN and other organic nitrates may constitute more than 50% of  $\text{NO}_y$  (total odd nitrogen compounds), the deposition fluxes of these species as part of the nitrogen cycle are largely unknown [Neff *et al.*, 2002].

We developed a flux measurement system using a GC-ECD for the determination of biosphere-atmosphere exchange fluxes of PAN. The system can be operated to apply both the MBR and the hyperbolic relaxed eddy accumulation (HREA) method. Both methods are favourable when no fast-response gas analyser for the application of the EC method is available. They represent less expensive techniques, potentially applicable also for long-term PAN flux measurements. Particularly at low atmospheric mixing ratios of PAN, a longer integration time or a trapping mechanism is required to resolve very small mixing ratio differences required for flux measurements.

In this study we describe the setup of the PAN flux measurement system and its application on a natural grassland site using  $\text{O}_3$  as a proxy scalar. We present a detailed assessment of the system requirements to resolve the expected PAN fluxes at the site. We additionally evaluate the applicability of HREA and MBR under various environmental conditions. An extensive quality control (detailed systematic and random error analysis) is performed, allowing the investigation of the system performance in relation to the magnitude of the determined PAN fluxes. We find that HREA and MBR are generally applicable to determine PAN fluxes using our GC-ECD setup, but the limitation of the analytical unit to precisely resolve mixing ratio differences remains a major drawback.

## 2 Methods

### 2.1 Flux measurement techniques

#### 2.1.1 Hyperbolic relaxed eddy accumulation (HREA)

Relaxed eddy accumulation (REA) systems are widely used to determine biosphere-atmosphere exchange fluxes of trace gases, in cases when high frequency measurements for the application of the eddy covariance (EC) method are not possible. According to *Businger and Oncley* [1990] the turbulent flux ( $F_{REA}$ ) is determined by the difference of two reservoir mixing ratios ( $\Delta\chi$ ), multiplied by a proportionality factor  $b$ , the standard

deviation of the vertical wind speed ( $\sigma_w$ ) and the molar density of air  $\rho_m$  (conversion of mixing ratio to molar concentration):

$$F_{REA} = b \cdot \sigma_w \cdot \rho_m \cdot (\chi_{w+} - \chi_{w-}) = b \cdot \sigma_w \cdot \rho_m \cdot \Delta\chi \quad (1)$$

Eq. (1) implies that sampled air must be separated into two reservoirs, one for updraft and one for downdraft events during a certain sampling period (typically 30 min). The separation is made with a fast switching valve, which is controlled according to the sign of the vertical wind speed ( $w$ ) measured by a 3D sonic anemometer. The  $b$ -value is determined using a proxy scalar ( $\chi_{proxy}$ ), which can be measured with high frequency:

$$b = \frac{F_{proxy}}{\sigma_w \cdot \rho_m \cdot (\overline{\chi_{proxy}^+} - \overline{\chi_{proxy}^-})} \quad (2)$$

For an ideal Gaussian frequency distribution the  $b$ -value is 0.627 [Wyngaard and Moeng, 1992]. However, experimental data show that it varies and is on average slightly lower [Baker, 2000]. While some studies found the value for  $b$  to be independent of stability [Businger and Oncley, 1990; T. Foken et al., 1995], a slight stability dependence was reported by Ammann and Meixner [2002]. In addition, the  $b$ -value may also vary for different scalars.

Besides the appropriate timing of the valve switching and the choice of the proxy scalar, a major challenge for the application of the REA technique are small values of  $\Delta\chi$ , which must be resolved by the chemical analysis. The value of  $\Delta\chi$  can be increased by the application of a so-called dead band, a threshold below which air samples are discarded when  $w$  is close to zero. The most significant increase of  $\Delta\chi$  is retrieved with the hyperbolic relaxed eddy accumulation (HREA) method (Bowling et al., 1999), which was used in our experiment (Sect. 2.4) since values of  $\Delta\chi_{PAN}$  near the precision of the chemical analysis were expected (see Sect. 3.1). The HREA method defines a threshold  $H$  according to the flux of a proxy scalar as:

$$H \geq \left| \frac{w' \cdot \chi'_{proxy}}{\sigma_w \cdot \sigma_{\chi_{proxy}}} \right| \quad (3)$$

where  $w'$  and  $\chi'_{proxy}$  are the Reynolds fluctuation of  $w$  and  $\chi_{proxy}$ , respectively, and  $\sigma_{\chi_{proxy}}$  is the standard deviation of the proxy scalar. If scalar similarity between the scalar of interest and the proxy exists,  $\Delta\chi$  is maximised since the threshold is only exceeded when high vertical wind speed fluctuations are accompanied by high fluctuations of the proxy scalar.

REA systems are usually designed for inert scalar quantities since air samples are stored in the reservoirs. However, the life time of PAN in the troposphere varies significantly, mainly with temperature and the NO/NO<sub>2</sub> ratio (e.g., at 30°C and a NO/NO<sub>2</sub> ratio of 0.5

the life time of PAN is about 45 min). Hence, its reactivity is a critical point in the design of a REA system for PAN.

### 2.1.2 Modified Bowen ratio method (MBR)

Gradient methods based on the flux-gradient relationship are commonly used for the determination of biosphere-atmosphere exchange fluxes. The MBR method assumes that the ratio between the molar flux ( $F$ ,  $F_{proxy}$ ), in this case normalized by  $\rho_m$ , and the mixing ratio difference ( $\Delta\chi$ ,  $\Delta\chi_{proxy}$ ) of two measurement heights is equal for the scalar of interest and a proxy scalar [Businger, 1986; Liu and Foken, 2001]. This implies that both quantities would be transported with the same transfer velocity ( $v_{tr}$ ):

$$v_{tr} = -\frac{F}{\rho_m \cdot \Delta\chi} = -\frac{F_{proxy}}{\rho_m \cdot \Delta\chi_{proxy}} \quad (4)$$

If  $F_{proxy}$  is determined by eddy covariance, the trace gas flux can be calculated as:

$$F = -v_{tr} \cdot \rho_m \cdot \Delta\chi = F_{proxy} \cdot \frac{\Delta\chi}{\Delta\chi_{proxy}} \quad (5)$$

It is important to note that for the MBR method  $\Delta\chi$  is defined as the mixing ratio difference from the upper minus the lower height ( $\Delta\chi = \chi(z_2) - \chi(z_1)$ ), which yields, for the same sign of  $F$ , the opposite sign of  $\Delta\chi$  than with the REA method. Furthermore, when using mixing ratios instead of concentrations, differences in the molar air density between the two measurement heights are assumed to be negligible.

A major prerequisite for the application of the MBR method is the scalar similarity of the scalar of interest and the proxy scalar. Furthermore, the occurrence of internal boundary layers and chemical transformations within the considered layer violate the application of the gradient approach in general. If the two heights are sampled subsequently and not simultaneously, non-stationarities of the scalar mixing ratios within the sample interval (typically 30 min) are a source of uncertainty, especially for systems with a low temporal resolution.

Like for the HREA method, the major challenge for the successful application of the MBR method for PAN is the accurate determination of small values of  $\Delta\chi$  by the chemical analysis. Especially during daytime, when the boundary layer is well mixed,  $\Delta\chi$  values are expected to be small. For conditions with weak developed turbulence, the transfer velocities determined with the MBR method are expected to be very small and prone to large uncertainties. Hence, Liu and Foken [2001] suggest omitting flux data where the friction velocity ( $u_*$ ) is very low ( $u_* < 0.07 \text{ m s}^{-1}$ ), which mainly concerns nighttime periods.

## 2.2 Modification of the PAN GC-ECD

We used a commercially available gas chromatograph with electron capture detection (GC-ECD) for PAN (Meteorologie Consult GmbH, Germany), which is a further development of the system described by *Volz-Thomas et al.* [2002]. To prevent contamination of the main column, the automatic GC-ECD contains a pre-column, which is back-flushed once all substances of interest have eluted onto the main column (Fig. 1). The chromatogram retrieved by the ECD is automatically integrated by the ADAM32 software program (Meteorologie Consult GmbH, Germany), which is installed on a PC and facilitates the control of the GC-system, the data-acquisition and reduction via a USB-based I/O module (USB-1408FS, Measurement Computing Corp., USA) (for details on GC-ECD analysis see Supplementary Material (SM) 1).

We modified and optimized the GC-ECD for the application of both the HREA and MBR method to determine PAN fluxes. The two reservoirs required for the HREA sampling (see Sect. 2.1.1) can also be used for the simultaneous sampling at two heights and subsequent analysis by the GC-ECD required for the MBR method. Sampling for both methods was realized by trapping PAN onto two pre-concentration capillary columns (MXT-1, Restek, USA; for details see SM 1) over the sampling period and subsequent analysis by the GC-ECD. For this, we modified commercially available pre-concentration units (Meteorologie Consult GmbH, Germany) and implemented them together with two additional multi-port valves (Valco, VICI, Switzerland) in an extended housing of the GC-ECD (Fig. 1). The modifications of the two pre-concentration units (PCU#1, PCU#2) mainly involved improvements on the temperature control and stability as well as a removable housing, which allowed us to exchange the columns easily for maintenance (for details see SM 1). All connections were made of 1/16" OD PEEK tubing (ID 0.050 and 0.075 mm), which was coated with silicon tubes as insulation against temperature changes. During the sampling mode, sample air was drawn through the pre-concentration columns, which were cooled to  $-5^{\circ}\text{C}$  to enhance the pre-concentration efficiency for PAN. The pre-concentration was performed in conservation mode [*Novak et al.*, 1979], i.e. the frontal zone of PAN would not leave the pre-concentration column during the sampling period. Depending on the overall sampling time this required a low flow rate of only a few  $\text{mL min}^{-1}$  (see Sects. 2.4 and 2.5 for details on flow rate and flow control). At the end of the sampling time, PAN was injected from PCU#1 into the separation columns by back-flushing the pre-concentration units (Valco#1, see Fig. 1) and simultaneous heating of the MXT-1 column to  $25^{\circ}\text{C}$  (see SM 1). PCU#2 was injected in the same way 10 min after the injection of PCU#1 by actuation of the 6-port valve (Valco#2, see Fig. 1). After further 5 min, the system was switched back to sampling mode (Valco#1), which lead to a total

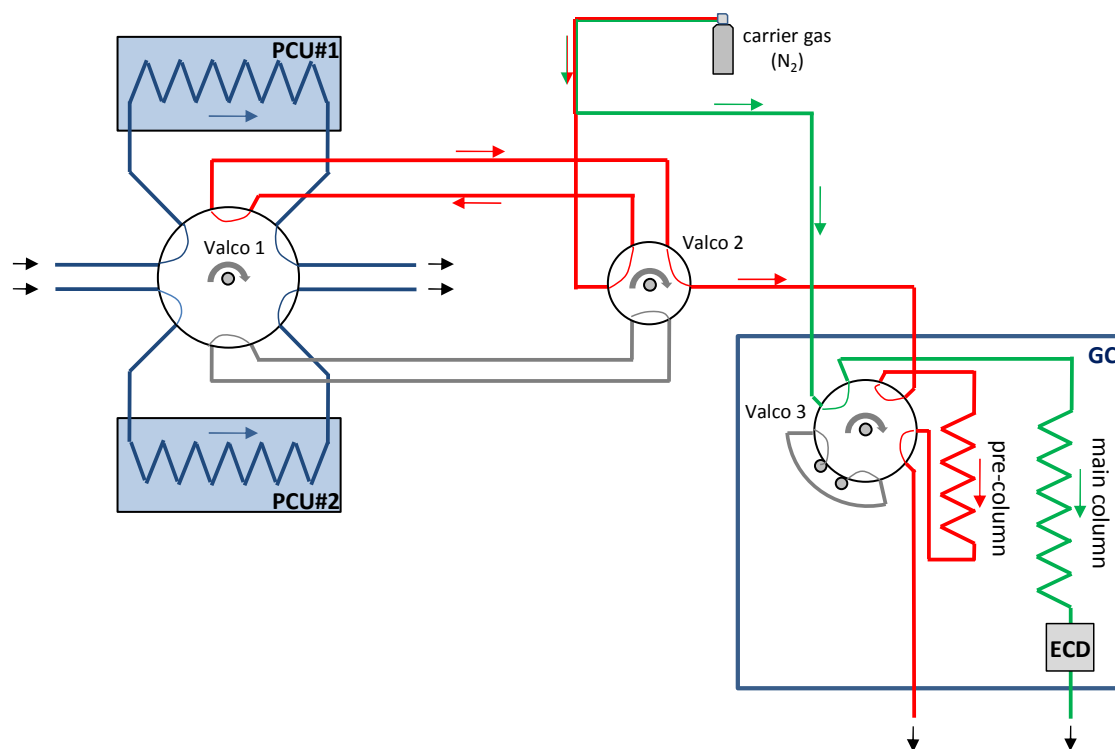


**Figure 1:** Simplified flow scheme of the modified GC-ECD for PAN flux measurements. During the sampling mode (shown in this example) the sample gas is drawn through two pre-concentration units (PCU#1, PCU#2). For the subsequent analysis a 12-port valve (Valco#1) is

actuated, whereas a 6-port valve (Valco#2) switches between the two pre-concentration units (see text for further explanation). The analysis of PAN is performed by a commercially available GC-ECD (Meteorologie Consult GmbH, Germany).

analysing time of 15 min for both PCUs. The in-built pneumatic-actuated 10-port valve (Valco#3, see Fig. 1) was kept from the commercial analyser to connect the pre- and main column in series just before the injection of both PCUs and to back-flush the pre-column 5 min after injection (in case of PCU#1) or just before switching back to the sampling mode (in case of PCU#2).

## 2.3 Field experiment: Experimental site and general setup

The testing, validation and application of the PAN flux measurement system was carried out at a natural grassland site (49.9685°N, 8.1481°E) at the estate of the Mainz-Finthen Airport, Rhineland Palatine, Germany. The vegetation is classified as a nutrient poor steppe-like grassland ecosystem with a mean canopy height of 0.6 m and extends roughly over 0.7 km x 1 km, providing good fetch conditions for flux measurements. The modified GC-ECD was installed in an air-conditioned container, which was located about 20 m north of the eddy covariance complex, a compromise between short inlet tubing and a large distance to reduce flow distortion.

Three dimensional wind vector and temperature were measured by a sonic anemometer (CSAT3, Campbell Scientific Inc., USA) at 3 m a.g.l. and recorded at 20 Hz using a data logger (CR3000, Campbell Scientific Inc., USA). In addition, a fast response open-path CO<sub>2</sub>/H<sub>2</sub>O analyser (LI-7500A, LI-COR, USA) was installed next to the sonic anemometer and sampled by the logger at the same frequency [for details see *Moravek et al.*, 2013]. All turbulent fluxes and stability parameters were calculated using the eddy covariance software TK3.1 [*Mauder and Foken*, 2011].

We chose O<sub>3</sub> as a proxy scalar for both HREA and the MBR method due to its similarity to PAN (see Sect. 4.3 for discussion). For this, a fast response O<sub>3</sub> detector (Enviscope GmbH, Germany) was added to the eddy covariance complex. The sensor discs required for the fast response O<sub>3</sub> measurements were prepared according to *Ermel et al.* [2013] and exchanged every five to eight days. Since the sensitivity of the sensor disc typically decreases with time, the O<sub>3</sub> signal was calibrated by independent O<sub>3</sub> measurements at 4 m a.g.l. using a slow UV-absorption O<sub>3</sub> analyser (49c, Thermo Environmental, USA). The employed analyser was part of a trace gas profile system with inlet heights at 0.2, 0.8 and 4 m a.g.l., with which also NO and NO<sub>2</sub> were measured (CLD 780 TR, Eco-Physics, Switzerland). The profile system was installed on a profile mast located 3 m northwest of eddy covariance complex.

For the application of the modified Bowen ratio technique, we modified a UV-absorption O<sub>3</sub> analyser (49i, Thermo Environmental, USA) to directly measure mixing ratio differences between 0.8 m and 4 m a.g.l. [differential O<sub>3</sub> measurements, see *Cazorla and Brune*, 2010]. To account for systematic errors the instrument was zeroed every 30 min by directing the gas flow of each height through an ozone scrubber for 1.5 min before entering the absorption cells. The O<sub>3</sub> analyser was placed in a water-proof box together with a data logger (CR1000, Campbell Scientific Inc., USA) for instrument control and data acquisition. For the inlet lines opaque 1/4" OD PFA tubes and PTFE membrane particle filters (Pall Corporation, USA) were used.

The PAN flux measurement system was operated in the HREA mode in the period from 20 to 26 September 2011 and in the MBR mode from 18 August to 4 September 2011.

## 2.4 Setup of PAN flux measurement system: HREA operation

The inlet for the HREA system was installed at 3 m a.g.l. at the eddy covariance complex, with a horizontal displacement distance to the CSAT3 of 25 cm. Since a long inlet line from the eddy covariance complex to the air-conditioned container (Sect. 2.3) and a low sample flow through the PCUs (Sect 2.2) were required, we designed a REA

system with a bypass [see *Moravek et al.*, 2013], where subsamples are drawn from the main sample line into the reservoirs (Fig. 2a).

For the main sample line a 21.5 m long opaque PFA tube with ¼" OD was used, equipped with a HDC-II particle filter (ACRO50 LCF, Pall Corporation, USA). This filter type did not cause an increasing pressure drop with time due to contamination, which is typically observed with PTFE-membrane filters. The flow rate through the inlet tube was regulated by a mass flow controller (EL-flow, Bronkhorst High-Tech, Netherlands) and set to a volume flow of 11 L min<sup>-1</sup> to ensure turbulent flow conditions ( $Re \sim 3800$ ). A buffer volume was implemented upstream of the membrane pump (MD 8C, Vacuubrand GmbH, Germany) to ensure a constant performance of the mass flow controller. The volume flow instead of the mass flow was regulated to maintain a constant lag time between the change of sign of the vertical wind speed and the switching of the splitter valves [see *Moravek et al.*, 2013]. The lag time was calculated online by cross-correlation between the vertical wind velocity and the high frequency signal of an in-built high frequency CO<sub>2</sub> analyser, ranging between 1.3 and 1.7 s while the main variation was attributed to the sensor separation effect [see *Moravek et al.*, 2013].

During sampling mode, the splitter valves were switched according to the sign of the vertical wind velocity (Fig. 2a). A third splitter valve was used for dead band situations. The splitter valves were mounted on a PFA manifold, which was installed in the main sample line. We used bi-stationary valves (type 6604, Bürkert, Germany) to reduce the heat development causing a reduction of PAN mixing ratios, which was observed when using other solenoid valves. In addition, the valves were composed of inert materials (PEEK, FFKM) and they feature a low internal volume (35 µl). Tests with a fast pressure sensor revealed that the valves were suitable for a switching frequency of more than 33 Hz (see SM 2).

The subsamples, which were diverted by the splitter valves from the main sample line, were purged through 1/8" OD Nafion dryers (MD-50-12-F, Perma Pure LLC, USA) to prevent the condensation of water at -5°C in the PCUs (Sect. 2.2). To improve the performance of the Nafion dryers, we introduced a by-pass system, which allowed purging the splitter valves and the Nafion dryers with 30 mL min<sup>-1</sup> regulated by a mass flow controller (Fig. 4 in SM 5). The dew point of the sample air in the outflow of the Nafion dryers was constantly monitored with a humidity probe (HMP series, Vaisala, Finland, not shown in Fig. 2a). The average dew point was -14°C and never exceeded -10°C during the experiments. A loss of PAN by Nafion dryers was not observed, which was also found in previous studies [*Mills et al.*, 2007].

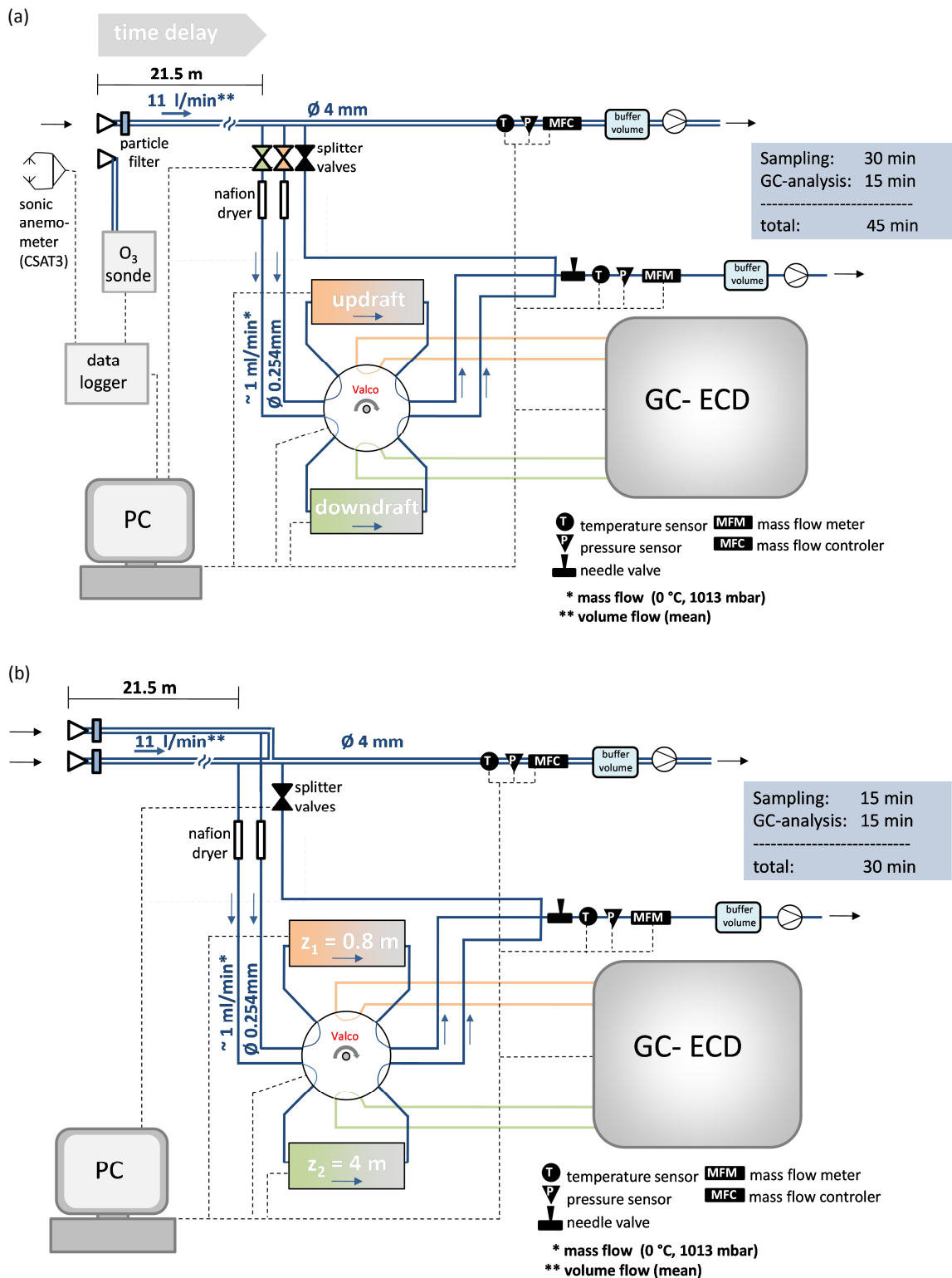


**Figure 2:** Setup of the PAN-flux measurement system showing the inlet system, the pre-concentration units, the GC-ECD for PAN analysis, the data acquisition and control as well as additional measurements. **(a)** Operation in the HREA mode: The system contains one inlet line, and subsamples are drawn according to the sign of the vertical wind velocity into the PCUs acting

as reservoirs. The hyperbolic dead band is calculated using the signal of a high frequency  $\text{O}_3$  analyser. **(b)** Operation in MBR mode: Two separate inlet lines are employed, and the system is capable to simultaneously sample at two inlet heights and performs subsequent analysis of PAN.

The sample air was drawn through the PCUs with a flow rate of  $1 \text{ mL min}^{-1}$  (STP), which was regulated with a needle valve (CNV1A150S1, VICI, Switzerland) and monitored with a mass flow meter (EL-flow, Bronkhorst High-Tech, Netherlands). A pressure sensor (HCX series, Sensortech GmbH, Germany) and a temperature probe were installed upstream of the mass flow meter (Fig. 2a). A buffer volume was employed upstream of the sample pump (NMP 830 KNDC B, KNF Neuberger GmbH, Germany) to exclude an effect of high frequent variations in the pump performance on the flow rate through the PCUs.

During operation of the PAN flux measurement system in the HREA mode the sampling period was set to 30 min. Together with the analysing time of 15 min (Sect. 2.2) a total time resolution of 45 min was achieved.

A PC together with a LabVIEW (National Instruments Corporation, USA) software program was used for the control of the HREA system. The software program was designed to perform (a) acquisition of all signals and control of mass flow controllers, (b) coordinate rotation of the wind vector using the double rotation method, (c) hyperbolic dead band calculation, (d) switching of splitter valves and (e) data storage with a frequency of 20 Hz. Details on the accurate timing of the signal transmission and processing are given in SM 2. Statistical values used for the coordinate rotation and the calculation of the hyperbolic dead band were retrieved by applying a moving average window of 5 min. Furthermore, the LabVIEW program calculated the online cross-correlation for the lag time for the switching of the splitter valves as well as the actual lag of the high frequency  $\text{O}_3$  signal at the end of every sampling interval (i.e. every 45 min) [see *Moravek et al.*, 2013].

## **2.5 Setup of PAN Flux measurement System: MBR operation**

For the application of the MBR method, the setup of the GC-ECD, the flow control and data acquisition was the same as described in Sect. 2.4. However, the inlet system was modified for simultaneous sampling at two measurement heights (Fig. 2b). Two 1/4" OD PFA inlet tubes were installed at the profile mast at 0.8 and 4.0 m a.g.l., respectively. Like for the HREA operation, the inlets were equipped with HDC-II particle filters and had a length of 21.5 m. The combined volume flow rate at the position of the mass flow controller was set to  $11 \text{ L min}^{-1}$  leading to a residence time of  $\sim 3 \text{ s}$ . Subsamples were drawn directly from the inlet tubes, through the Nafion dryers into the PCUs with a total flow rate of  $2 \text{ mL min}^{-1}$  (STP) (Fig. 2b). Since both sample lines and both PCUs were identical in their setup, it was assumed that the flow rate through each PCU was close to  $1 \text{ mL min}^{-1}$ . The sampling time was reduced to 15 min to ensure that the frontal zone of PAN would not leave the pre-concentration column.

With an analysing time of 15 min (Sect. 2.2) the total time resolution during the MBR operation was 30 min.

## 2.6 Calibration and quality control

### 2.6.1 Calibration method

The flux measurement system was calibrated regularly to account for changes in the performance of the PCUs and the increasing sensitivity of the ECD with time. The PAN calibration air was produced using a photolytic calibration unit (Meteorologie Consult GmbH, Germany) as described by Pätz *et al.* [2002]. Hereby, synthetic air (Air Liquide, Germany) was first enriched with acetone in a permeation cell. A known mixing ratio of NO standard gas (Air Liquide, Germany) was then photolyzed in a reaction cell together with the acetone–air mixture to produce PAN. Finally, the calibration air was diluted with zero air that was produced from ambient air aspirated through a membrane pump (N035, KNF Neuberger GmbH, Germany) and purified with active charcoal and Purafil<sup>®</sup>. To obtain the same flow and pressure conditions as during the sampling mode, we aspirated the diluted calibration air through an identical inlet system, consisting of one tube during the HREA operation and two tubes during the MBR operation.

Since the total mass collected by the PCUs varied during HREA sampling, PAN calibration coefficients ( $m, c$ ) were obtained by normalizing the peak integrals ( $Int$ ) with the sampled volume ( $vol$ ), derived from the actual sampling time of each PCU and the flow rate (at STP) through the PCUs. The PAN mixing ratios ( $\chi_{PAN}$ ) were then determined as:

$$\chi_{PAN} = m \cdot \frac{Int}{vol} + c \quad (6)$$

for both PCU#1 and PCU#2 individually.

To obtain a similar amount of sample volume as during the HREA sampling, the splitter valves were switched according to the sign of the vertical wind velocity and with the respective dead band during the HREA calibration. Consequently, the pressure and flow conditions in the PCUs were the same as during sampling, which improved the accuracy of the calibration.

### 2.6.2 Determination of PAN mixing ratio difference errors

For both the HREA and the MBR method, the accuracy and precision of  $\Delta\chi_{PAN}$  is of crucial importance. Uncertainties in  $\Delta\chi_{PAN}$  may be caused for example by slight variations in the sample flow or in the pre-concentration efficiency of the two reservoirs. To account for these systematic and random errors of  $\Delta\chi_{PAN}$ , we performed

side-by-side measurements of the two PCUs before, during or after the flux measurements (the periods are denoted as SBS\_HREA#1, SBS\_HREA#2, SBS\_MBR#1 and SBS\_MBR#2 and comprised for each method at least 50 h in total). Accordingly, we introduced an artificial time delay of 30 s for the switching of the splitter valves for the HREA operation. On the one hand, this should result in  $\Delta\chi_{PAN}$  values to be near zero [Moravek *et al.*, 2013], and, on the other hand, the actual sampling time and the pressure conditions are the same as for the HREA sampling. For the MBR operation, we placed the two trace gas inlets side-by-side at 0.8 m a.g.l..

For both, the HREA and the MBR method, systematic differences between the two reservoirs were corrected for by adjusting PCU#2 to PCU#1 using an orthogonal fit function. The random error (precision) of  $\Delta\chi_{PAN}$  (denoted as  $\sigma_{\Delta PAN}$ ) was defined as the standard deviation of the residuals of the fit according to Wolff *et al.* [2010] (see Sect. 3.3).

### 2.6.3 Random flux error, flux detection limit and quality control

The random flux error ( $\sigma_F$ ) was deduced for both the HREA and the MBR method by combining the random errors of the individual terms in Eqs. (1) and (5), respectively, using Gaussian error propagation (see SM 3), while for the HREA method the  $b$ -value in Eq. (1) was substituted by Eq. (2). The required individual random errors were determined as follows: (a) The random error of the PAN mixing ratio differences ( $\sigma_{\Delta PAN}$ ) was deduced from the side-by-side measurements (Sect. 2.6.2). (b) The random error of mixing ratio differences of the scalar proxy ( $\sigma_{\Delta O_3}$ ) was derived for the HREA method from the calibration. A value of 1% was found and applied as a conservative estimate. For the MBR method,  $\sigma_{\Delta O_3}$  was derived by propagating the standard deviations of the ambient air and zero air measurement of the differential O<sub>3</sub> analyser (Sect. 2.3). (c) The random error of the O<sub>3</sub> flux ( $\sigma_{F_{O_3}}$ ) was calculated by the TK3.1 software program according to Mauder *et al.* [2013] representing the turbulence sampling error. Although it was not directly used for the flux calculation, we derived the random error of the  $b$ -value ( $\sigma_b$ ) by combining the individual random errors in Eq. (2) (see SM 3). For the determination of the random error of  $\sigma_w$  ( $\sigma_{\sigma_w}$ ), we assumed that  $\sigma_{\sigma_w}$  mainly results from the uncertainty of the vertical wind speed measurement, which is given by the manufacturer as 0.5 mm s<sup>-1</sup> (see SM 3).

For all above mentioned quantities, we define values to be insignificant from zero and, thus, below the detection limit when the relative random error (denoted as  $\sigma_x^{\%}$ ) of the quantity ( $x$ ) exceeds 100%. Additionally, PAN fluxes are regarded as below the flux detection limit when  $\Delta\chi_{PAN}$  is below the detection limit (i.e.,  $\sigma_{\Delta PAN}^{\%} > 100\%$ ).

Furthermore, flux values determined with the MBR method which do not meet the turbulence criterion (see Sect. 2.1.2) are considered as insignificant from zero.

For the evaluation of the presented PAN fluxes, we used time periods with sufficient developed turbulence and stationarity [T. Foken and Wichura, 1996], represented by the quality flags 1–6 after Thomas Foken et al. [2004]. Additionally, a footprint analysis and a site specific characterization approach [Göckede et al., 2004; Göckede et al., 2006] was conducted, utilizing a Lagrangian forward stochastic model from Rannik et al. [2000]. We excluded data where the footprint area of the flux measurement included less than 80% of the target area.

## 2.7 Simulation of expected PAN mixing ratio differences

The successful application of both the HREA and the MBR method largely depends on the capability of the analytical system to resolve the mixing ratio differences ( $\Delta\chi_{PAN}$ ). We simulated the expected  $\Delta\chi_{PAN}$  values under various meteorological conditions for the Mainz-Finthen experiment site to define the precision requirements of the analytical system and the optimal configuration for the application of HREA (dead band) and MBR method (measurement heights). Expected  $\Delta\chi_{PAN}$  values were calculated according to Eqs. (1) and (5) with  $O_3$  as a proxy scalar for the data period from 1 August to 30 September 2011.

Whereas  $F_{O_3}$  and  $\Delta\chi_{O_3}(MBR)$  could be retrieved from direct measurements,  $\Delta\chi_{O_3}(HREA)$  was retrieved by simulating the conditional sampling using the measured high frequency time series of  $O_3$  and the vertical wind velocity. To investigate the influence of different dead bands, the simulation was performed using both fixed and hyperbolic dead bands of various sizes. For the dead band calculation and the simulation the same data pre-processing steps as during the real-time REA measurements were performed (Sect. 2.4).

The required estimate for  $F_{PAN}$  was derived by applying the big leaf multiple resistance approach [Hicks et al., 1987; Wesely and Hicks, 2000]. The approach divides the overall resistance against deposition (inverse of the deposition velocity) of a substance into the aerodynamic resistance ( $R_a$ ), the quasi-laminar boundary layer resistance ( $R_b$ ) and the surface resistance ( $R_c$ ) and can be used to describe unidirectional deposition fluxes, which was expected for PAN at the grassland site.  $F_{PAN}$  is then expressed as the ratio of the PAN concentration (PAN mixing ratio multiplied by  $\rho_m$ ) at one height and the resistances against deposition to the ground:

$$F_{PAN} = -\frac{1}{R_a + R_b + R_c} \cdot \rho_m \cdot \chi_{PAN} \quad (7)$$

$R_a$  was calculated according to *Garland* [1977], using the integrated stability correction function of *Businger et al.* [1971] modified by *Högström* [1988].  $R_b$  can be described according to *Hicks et al.* [1987] as a function of  $u_*$ , the Prandtl and Schmidt number. The latter largely depends on the molecular diffusivity ( $D$ ) of the trace gas and was found for PAN according to data of *Hicks et al.* [1987] to be  $\sim 1.72$ . For the  $R_c$  we assumed as a rough estimate that the resistance at the surface for PAN was similar to  $R_c(O_3)$ , which could be determined from the resistance approach since  $F_{O_3}$  was known.

## 3 Results

### 3.1 Expected PAN mixing ratio differences

#### 3.1.1 Effect of HREA dead band

The size and type of the dead band had to be chosen carefully since it influences not only the magnitude of the sampled  $\Delta\chi_{PAN}$  values but also the effective sampling time and the scalar similarity. The results from the HREA simulation analysis (Fig. 3a) shows a steady increase of the relative  $\Delta\chi_{PAN}$  values from a zero dead band (median: 1.4%) to a large hyperbolic dead band of 1.5 (median: 6.3%), whereas at the same time the variability increases with the dead band size. As a result of the increasing  $\Delta\chi_{PAN}$  values, the  $b$ -value decreased exponentially with increasing dead band, starting from

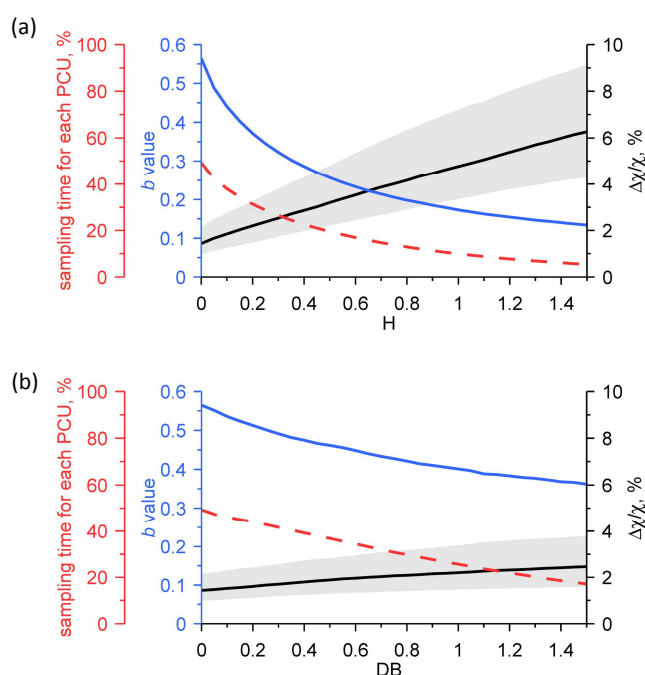


**Figure 3:** Effect of various dead band sizes on the expected relative PAN mixing ratio differences, the  $b$ -value and the sampling time for the application of the REA method. Median values are displayed and the shaded area represents the interquartile range of the expected mixing ratio differences. Variations of the  $b$ -value and the sampling time were only small. Shown are the results from the simulation based on data from the Mainz-Finthen grassland site for the period from 1 August to 30 September 2011 employing (a) a hyperbolic dead band with  $O_3$  as a proxy scalar and (b) a fixed dead band value scaled by  $\sigma_w$  only.

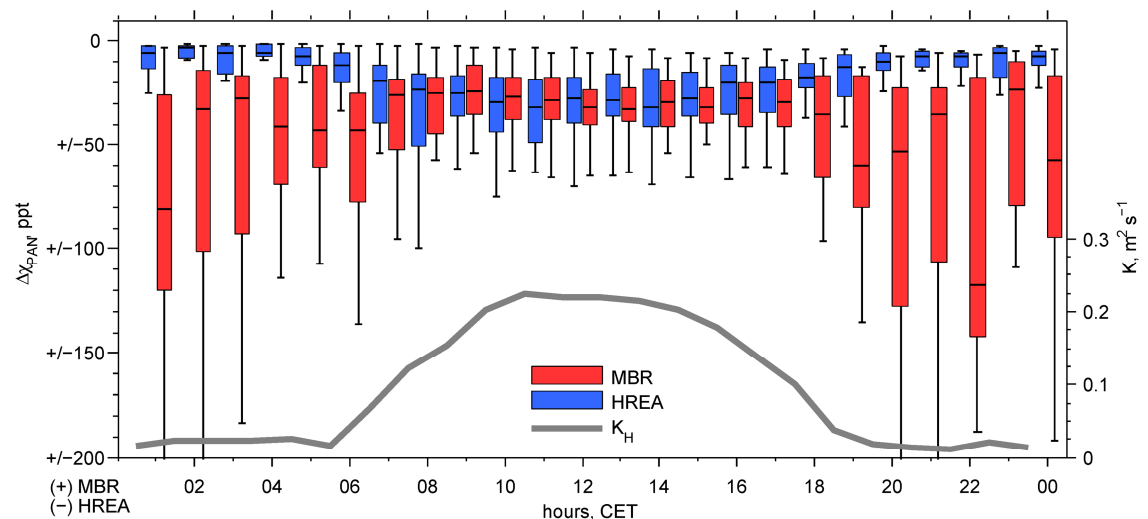
0.56 without dead band to 0.14 for  $H = 1.5$ . In the same way, the effective sampling time for each PCU decreases from 50% of the total sampling time with no dead band to 5.4% at  $H = 1.5$ . In contrast to the relative  $\Delta\chi_{PAN}$  values, both the simulation of the  $b$ -value and the sampling time showed only a very small variability.

Figure 3b shows the results of the simulation for a fixed dead band scaled only by  $\sigma_w$ . The linear increase of relative  $\Delta\chi_{PAN}$  values with increasing dead band is less steep compared to a hyperbolic dead band only resulting in median relative  $\Delta\chi_{PAN}$  values of 2.5% at a dead band of  $1.5 \cdot \sigma_w$ . In return, the effective sample volume per PCU is still 17% at this point.

Since the simulation yielded much higher expected  $\Delta\chi_{PAN}$  with the HREA method, we chose a hyperbolic dead band of  $H = 1.1$  for the further simulation and the experiment. The lower sample volume associated with the hyperbolic dead band could be compensated by using a higher sample flow rate (as given in Sects. 2.4 and 2.5) through the PCUs without reaching the breakthrough of PAN.

### 3.1.2 Diurnal cycle of expected PAN mixing ratio differences

The diurnal course of the expected PAN values is shown in Fig. 4 for both the HREA and MBR method. For the HREA method, expected  $\Delta\chi_{PAN}$  values were very low during nighttime (median values:  $\sim -5$  ppt), whereas absolute  $\Delta\chi_{PAN}$  values increased in the morning together with both the increase of turbulent mixing and the increase of PAN



**Figure 4:** The expected absolute PAN mixing ratio differences using both the HREA and MBR method presented as diurnal cycles using hourly boxplot statistics. Shown are the results from the simulation based on data from the Mainz-Finthen grassland site for the period from 1 August to 30 September 2011. In addition, the median turbulent exchange coefficient  $K_H$  is displayed, which was calculated with the

aerodynamic approach using the universal stability functions for the sensible heat flux of *Businger et al.* [1971] modified by *Högström* [1988]. For most of the nighttime differences for the MBR method the turbulence criterion (i.e.,  $u_* < 0.07 \text{ m s}^{-1}$  according to *Liu and Foken* [2001]) is not fulfilled and the flux calculation is not possible.

mixing ratios (not shown). The average median  $\Delta\chi_{PAN}$  values during the day were around  $-27$  ppt whereas most values ranged between  $-15$  ppt (0.25 percentile) and  $-50$  ppt (0.75 percentile). Lowest absolute values close to zero occurred at high wind speeds under neutral stability conditions. Comparable daytime values were simulated when applying the MBR method. As found for the HREA method, lowest values were reached under neutral conditions. During nighttime, expected  $\Delta\chi_{PAN}$  values were generally larger but also showed a high variability with median values between 23 and 117 ppt.  $\Delta\chi_{PAN}$  values of up to 300 ppt were calculated under conditions with limited turbulent exchange. However, under these conditions fluxes are expected to be very small and might be below the turbulence criterion (Sect. 2.1.2).

### 3.2 Calibration

The aim of the regularly performed calibrations was (a) to determine the point of saturation of the PCUs, which was important for setting the sample flow, (b) to investigate the relationship between peak integral, sample volume and PAN mixing ratio and (c) to determine the precision and limit of detection (LOD) for a single mixing ratio measurement.

Experiments testing different flow rates through the PCUs showed that the time after which the PCU was saturated decreased linearly with an increasing sample flow rate. For a sample flow rate of  $1 \text{ mL min}^{-1}$  (STP), as set during the HREA application, the saturation occurred after  $\sim 12$  min. For the average sampling time per PCU of  $3.83 (\pm 0.77)$  min (with  $H = 1.1$ ) this was sufficient to guarantee that the frontal zone of PAN would not have eluted from the PCUs during sampling. Since the volume (and not mass) flow rate of the sample gas controls the speed of the frontal zone in the PCU, the saturation point is dependent on the pressure in the PCUs. During the HREA operation

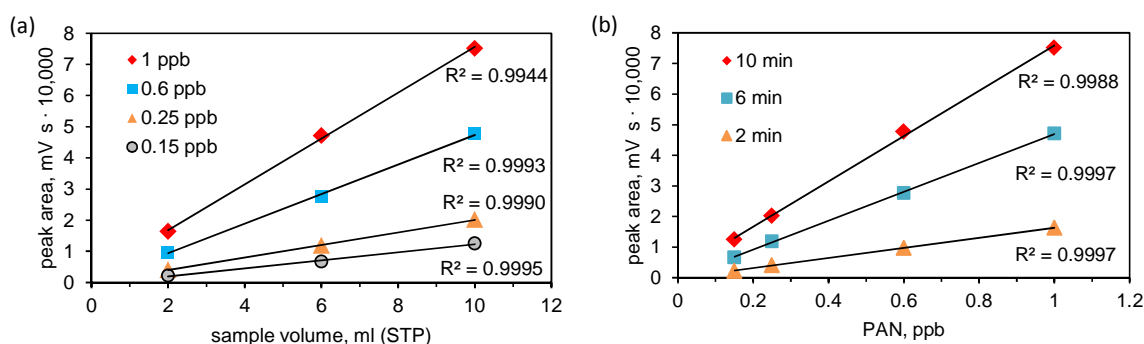


**Figure 5:** Results of a multi-step calibration experiment illustrating the linear relationship between (a) the area of the PAN peak and the sample volume (STP) for various PAN mixing ratios as well as (b) the area of the PAN peak and PAN mixing ratios for different loading

times of the PCUs. Since the flow rate through the pre-concentration unit was regulated by a mass flow controller, both the loading time and the sample volume are linear proportional to the mass of the sampled air volume.

the pressure measured downstream of the PCUs ranged between 718.2 and 739.8 hPa. These variations were mainly caused by the diurnal course in ambient air temperature. The standard deviation of the short-term signal over one sampling period was  $\pm 0.7$  hPa. The mean pressure during the MBR operation was higher ranging between 901.3 and 927.6 hPa ( $\pm 0.5$  hPa), which was due to the employment of two instead of one sample line. This led to a longer time until saturation of the PCU was reached, which allowed us to set the sampling time during MBR operation to 15 min.

We generally found, on the one hand, a linear relationship between the peak integral and the sample volume for different PAN mixing ratios (Fig. 5a), and, on the other hand, between the peak integral and the PAN mixing ratio at different sampling times (Fig. 5b).

### 3.3 Side-by-side measurements

Although all side-by-side measurements were performed during good weather conditions and covered a period of one diurnal cycle or more, the range of prevailing PAN mixing ratios was large (Fig. 6). During both periods, SBS\_HREA#1 and SBS\_MBR#2 PAN mixing ratios below 200 and 400 ppt were measured, respectively. Due to the low mixing ratios during SBS\_HREA#1 we included the results from the calibration with PAN mixing ratios of 1080 ppt ( $\pm 50$  ppt). During SBS\_HREA#2 and SBS\_MBR#1 higher PAN mixing ratios above 200 ppt prevailed reaching up to 700 and 1400 ppt, respectively. For all side-by-side measurements the linear regressions show systematic differences between both PCUs, which were corrected for by using PCU#1 as a reference and adjusting the signals from PCU#2 with the orthogonal fit function.

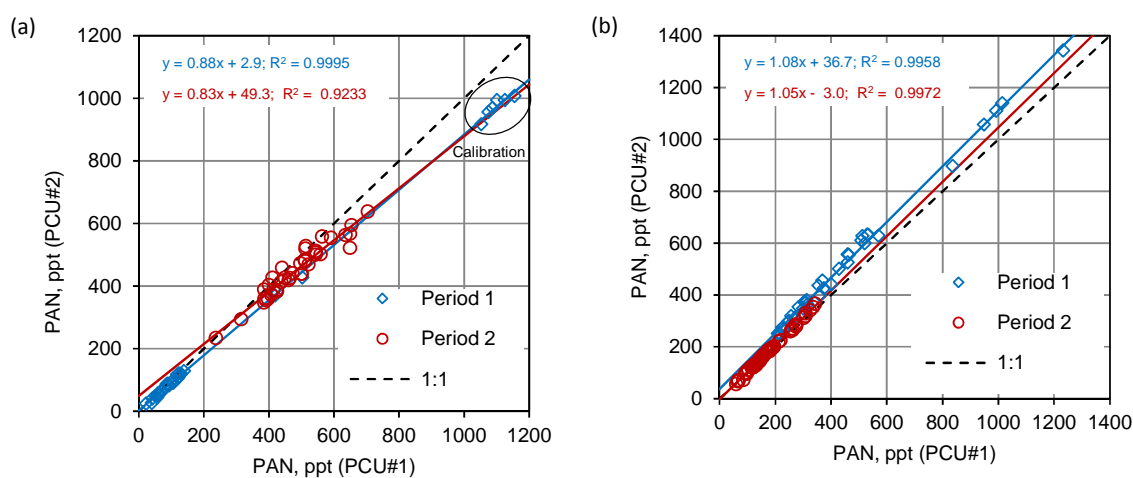


**Figure 6:** Results from side-by-side measurements for two periods during (a) HREA operation after correction for pressure effects (see SM 4) and (b) MBR operation of the PAN flux measurement system, respectively. For

the conversion to PAN mixing ratios, the calibration coefficient from PCU#1 was applied for both PCU#1 and PCU#2 to illustrate the systematic deviation from the 1:1 slope.

**Table 1:** Results from the side-by-side measurements during MBR and HREA operation, showing the parameters of the orthogonal fit functions. The residuals of the regression were used to determine the random error of the PAN mixing ratio differences ( $\sigma_{\Delta PAN}$ ).

	Period	Date	Duration [hrs]	$n$	Slope	Intercept [mV s mL <sup>-1</sup> ]	$R^2$	$\sigma_{\Delta PAN}$ [ppt]
MBR	SBS_MBR#1	18–19 Aug 11	17.75	36	1.08	3294.3	0.9958	15.2
	SBS_MBR#2	29–30 Aug 11	33.25	67	1.05	-298.5	0.9972	4.1
HREA	SBS_HREA#1	19–20 Sep 11	32.0	43 <sup>a</sup>	0.86	142.0	0.9931	32.5
	(corrected)	19–20 Sep 11	32.0	43 <sup>a</sup>	0.88	73.3	0.9995	17.9
	SBS_HREA#2	27–28 Sep 11	29.0	39	0.70	1819.3	0.7707	59.5
	(corrected)	27–28 Sep 11	29.0	39	0.83	1228.8	0.9233	26.1

<sup>a</sup>including calibration data

For the periods between the side-by-side measurements, we linearly interpolated the values for the slope and intercept given in Table 1.

As shown in Table 1, the derived precisions (Sect. 2.6.2) varied between the different experiments. While for the MBR operation the precision was determined as 15.2 ppt before and as 4.1 ppt during the flux measurement experiment, the precision before and after the HREA flux measurements was much lower, namely 32.5 ppt and 59.9 ppt, respectively (Table 1). The significantly larger scatter during the HREA side-by-side measurements was partly corrected for (for details see SM 4 and Sect. 4.2) and the precision was improved by 50%, to 17.9 and 26.1 ppt, respectively (see Table 1 and Fig. 6a). This correction was applied to all data in the post-processing of the HREA measurements.

As defined in Sect. 2.6.3, the precision values presented in Table 1, are considered as the detection limit for  $\Delta\chi_{PAN}$ . This means that  $\Delta\chi_{PAN}$  values below are associated with  $\sigma_{\Delta PAN}^{\%} > 100\%$ .

## 3.4 PAN flux measurements

### 3.4.1 HREA measurements

During the period of the HREA measurements (20 to 26 September 2011) dry and mostly sunny autumn weather conditions prevailed with maximum daytime temperatures of 20 to 25°C and minimum temperatures of 8 to 17°C during the night. While on most days atmospheric conditions were unstable during daytime and stable during nighttime, on 22 and 28 September mostly neutral conditions prevailed on daytime and on 24 September only slightly unstable conditions were encountered. On

these days, the daytime average maximal wind speeds and the average  $u_*$  values (see Fig. 7a) reached  $4.5 \text{ m s}^{-1}$  and  $0.5 \text{ m s}^{-1}$ , respectively, which were much larger in comparison to the other days. The higher turbulent exchange during those days is represented by higher values of  $\sigma_w$  (Fig. 7a), which has an impact on the REA flux (Eq. (1)). During the other days, the mean maximum value of  $\sigma_w$  during daytime was  $0.10 \pm 0.07 \text{ m s}^{-1}$ , which is lower than the respective annual mean for the site ( $\sigma_w = 0.18 \pm 0.15 \text{ m s}^{-1}$ ) and during the period of the MBR measurements ( $\sigma_w = 0.13 \pm 0.11 \text{ m s}^{-1}$ ).

Since  $\text{O}_3$  was used as a proxy scalar for the determination of the HREA dead band and the  $b$ -value, the similarity between PAN and  $\text{O}_3$  mixing ratios is shown in Fig. 7b. On most days both quantities feature a simultaneous increase of their mixing ratios in the morning and a diurnal maximum in the afternoon between 16:00 and 17:00 CET with maximal PAN mixing ratios ranging between 243 and 1172 ppt and  $\text{O}_3$  mixing ratios between 41 and 57 ppb. On 22 September the daytime PAN mixing ratios did not show a significant increase, which was probably caused by both reduced photochemical production due to overcast periods and low  $\text{NO}_x$  conditions, as well as downward transport of PAN-poor air masses due to the enhanced high turbulent mixing.

The values for  $\Delta\chi_{\text{O}_3}$ , calculated from the high frequency  $\text{O}_3$  data with a dead band size of  $H = 1.1$ , were mostly negative and reached minimal values of  $-3$  ppb in the late afternoon, indicating a deposition flux (Fig. 7c). Not considering the  $\Delta\chi_{\text{O}_3}$  values which are below the detection limit ( $\sigma_{\Delta\text{O}_3}^{\%} > 100\%$ ), few positive values were observed during nighttime, which might be caused by limited turbulent exchange and small  $\text{O}_3$  fluxes at night (Fig. 7d). The  $\text{O}_3$  eddy covariance fluxes showed a clear diurnal course with maximal deposition fluxes between  $-5$  and  $-10 \text{ nmol m}^{-2} \text{ s}^{-1}$  during daytime.

The  $b$ -values, which were determined from the  $\text{O}_3$  flux and  $\Delta\chi_{\text{O}_3}$  values, are shown in Fig. 7e. The median was 0.21, which is slightly higher than the median value (0.16) from the simulation analysis with a dead band size of  $H = 1.1$  (Fig. 3a). However, as found by other studies [Beverland et al., 1996a; e.g., Oncley et al., 1993], calculated  $b$ -values may vary significantly (inter-quartile range of 0.19 to 0.30 in this study). The variation was particularly large for conditions with weak turbulence ( $u_* < 0.1 \text{ m s}^{-1}$ ) and small sensible heat fluxes of  $\pm 5 \text{ W m}^{-2}$ . Under these conditions, which occurred mostly during nighttime, both the conditional mixing ratio differences  $\Delta\chi_{\text{O}_3}$  and the  $\text{O}_3$  eddy covariance flux ( $> -0.5 \text{ nmol m}^{-2} \text{ s}^{-1}$ ) changed sign occasionally (Fig. 7c+d) and were also characterized by higher random errors.

Figure 7f shows the measured PAN mixing ratio differences,  $\Delta\chi_{\text{PAN}}$ , between the two PCUs for updraft and downdraft events. Most  $\Delta\chi_{\text{PAN}}$  values did not exceed the

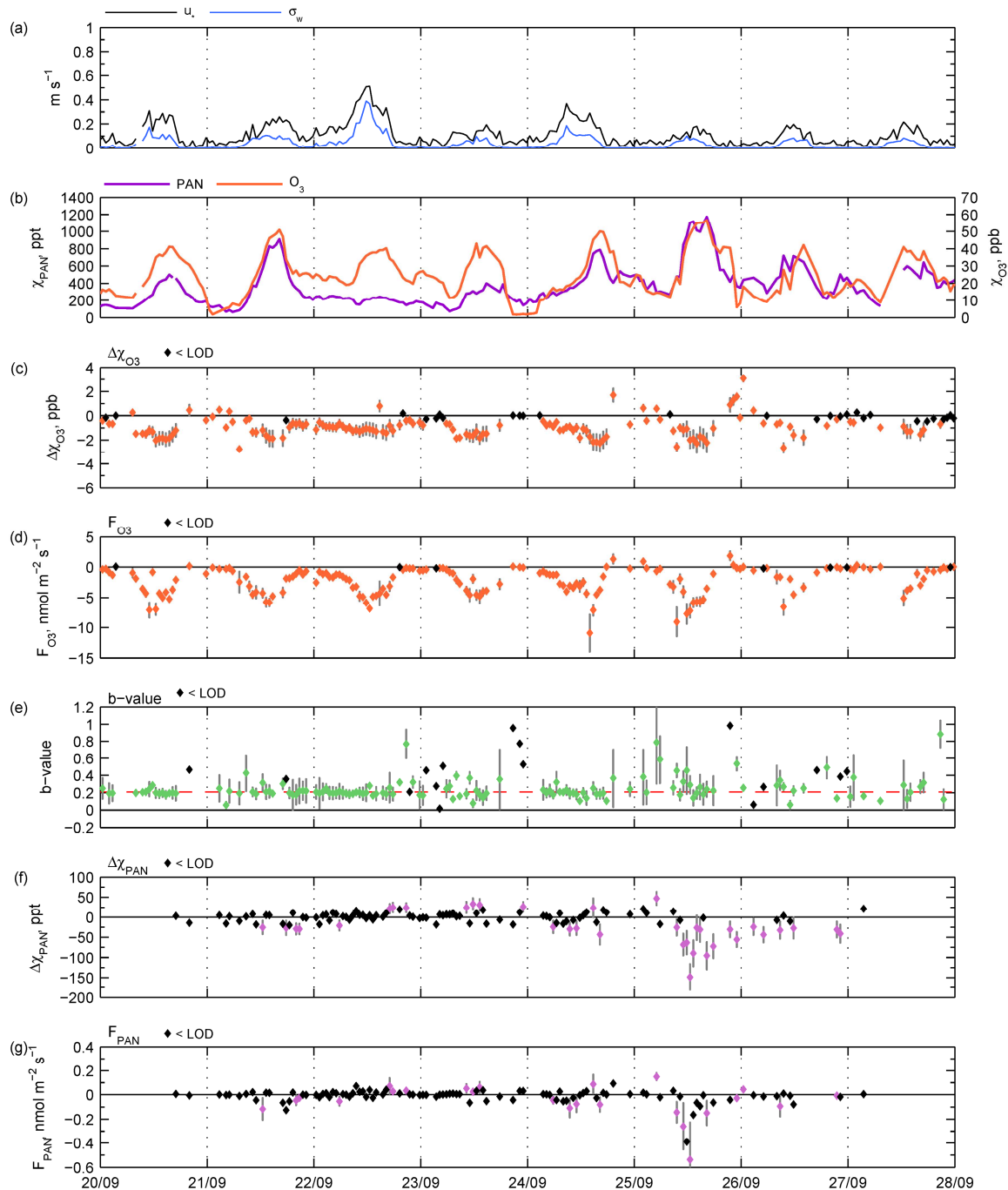


**Figure 7:** Results from the HREA experiment at the Mainz-Finthen grassland site from 19 to 28 September 2011 showing (a)  $u_*$  and  $\sigma_w$ , (b) PAN and  $O_3$  mixing ratios, (c)  $\Delta\chi_{O_3}$ , (d)  $F_{O_3}$ , (e)  $b$ -value, (f)  $\Delta\chi_{PAN}$  and

(g)  $F_{PAN}$ . Grey error bars denote random error. Black data points indicate values below the detection limit (for details see text).

detection limit ( $\sigma_{\Delta PAN}^{\%} > 100\%$ ) determined from the side-by-side measurements (Table 1). The values above the detection limit are randomly distributed throughout the time series and still seem to be within the noise of the mixing ratio measurement. Only on 25 September some significant  $\Delta\chi_{PAN}$  values were detected, which reached up to  $-150$  ppt, indicating a net deposition flux.

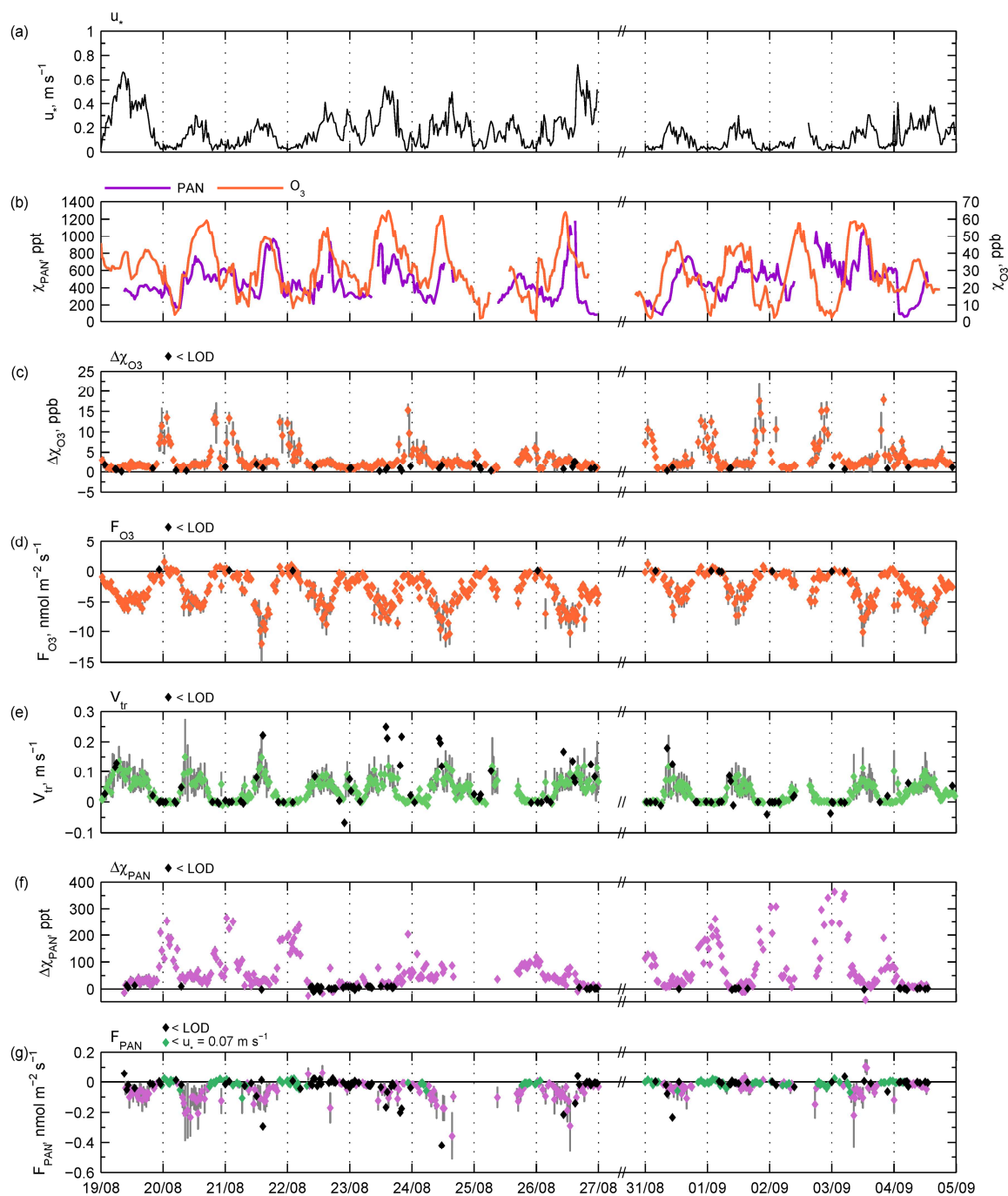


**Figure 8:** Results from the MBR experiment at the Mainz-Finthen grassland site from 18 August to 4 September 2011 showing (a)  $u_*$ , (b) PAN and  $O_3$  mixing ratios (c)  $\Delta\chi_{O_3}$ , (d)  $F_{O_3}$ , (e)  $v_{tr}$ , (f)  $\Delta\chi_{PAN}$  and

(g)  $F_{PAN}$ . Grey error bars denote random error. Black data points indicate values below the detection limit (for details see text). Red data points denote periods where  $u_* < 0.07 \text{ m s}^{-1}$ .

As a consequence of the low  $\Delta\chi_{PAN}$  values, PAN fluxes during the HREA measurement period were in most cases below the flux detection limit (Fig. 7g) as defined in Sect. 2.6.3. Only on 25 September a deposition flux of up to  $-0.4 \text{ nmol m}^{-2} \text{ s}^{-1}$  was found. For the remaining values above the flux detection limit ( $n = 21$ ) a median random flux error of  $\pm 0.078 \text{ nmol m}^{-2} \text{ s}^{-1}$  for daytime and  $\pm 0.020 \text{ nmol m}^{-2} \text{ s}^{-1}$  for

nighttime (Fig. 9a) was determined. The daytime flux errors were mainly attributed to the error of  $\Delta\chi_{PAN}$  with a median error contribution of 50% (Fig. 9b). The magnitude of the covariance term in the error propagation equation (SM 3) was largely governed by the error of  $\Delta\chi_{O_3}$ . During nighttime all terms had a similar impact on the total flux uncertainty.

### 3.4.2 MBR measurements

In general, the weather conditions during the MBR measurements (18 August to 4 September 2011) featured higher temperatures, stronger wind speeds, but also more frequent isolated rain events than during the period of the HREA measurements. The MBR measurements can be divided into two sections (SI+SII) according to the prevailing weather conditions: (SI) from 20 to 26 August was a sunny period with occasional cloud cover and one short rain event on 21 August. Stable stratification at night and unstable stratification during daytime, sometimes leading to free convection, prevailed. Daily maximal temperatures reached up to 34°C, while maximal wind speeds in the afternoon were on average 3.5 m s<sup>-1</sup>. Period SI was terminated by a passing cold front in the late afternoon of 26 August accompanied by rainfall together with a temperature drop and increasing wind speeds. (SII) The period from 30 August to 4 September was a dry period with mostly sunny days under the influence of high pressure systems with increasing temperatures and lower wind speeds (mean diurnal maximum: 2.3 m s<sup>-1</sup>), resulting also in lower  $u_*$  values (Fig. 8a) as during (SI). During that period also stable stratification at night and unstable stratification during daytime, partially leading to free convection, prevailed. The period from 27 to 30 August is not considered here due to the performance of the side-by-side measurements (Sect. 3.3), extended calibrations and maintenance of the GC-ECD in this period.

The effect of the varying weather conditions on O<sub>3</sub> and PAN mixing ratios is shown in Fig. 8b. On most days during period (SI) and (SII) a clear diurnal course of O<sub>3</sub> mixing ratios is visible with maximum values of 65 ppb, while during (SII) the development of strong nocturnal inversion layers lead to nearly complete O<sub>3</sub> depletion at night. The diurnal course of PAN mixing ratios was strongly coupled to that of O<sub>3</sub>, although on some days (e.g., 26 August and early morning of 4 September) the decline of PAN mixing ratios starting in the late afternoon was much stronger. During nights with strong O<sub>3</sub> depletion, PAN mixing ratios of more than 200 ppt prevailed. Daily maxima of PAN mixing ratios ranged from 400 ppt to more than 1200 ppt.

The  $\Delta\chi_{O_3}$  values and the O<sub>3</sub> flux, which were used to calculate the transfer velocity, are displayed in Fig. 8c+d. While during daytime  $\Delta\chi_{O_3}$  values were on average 2.0 ppb ( $\pm 0.6$  ppb) the differences during nighttime were much larger and reached up to 18 ppb during strong stable stratification. During daytime some values were below the

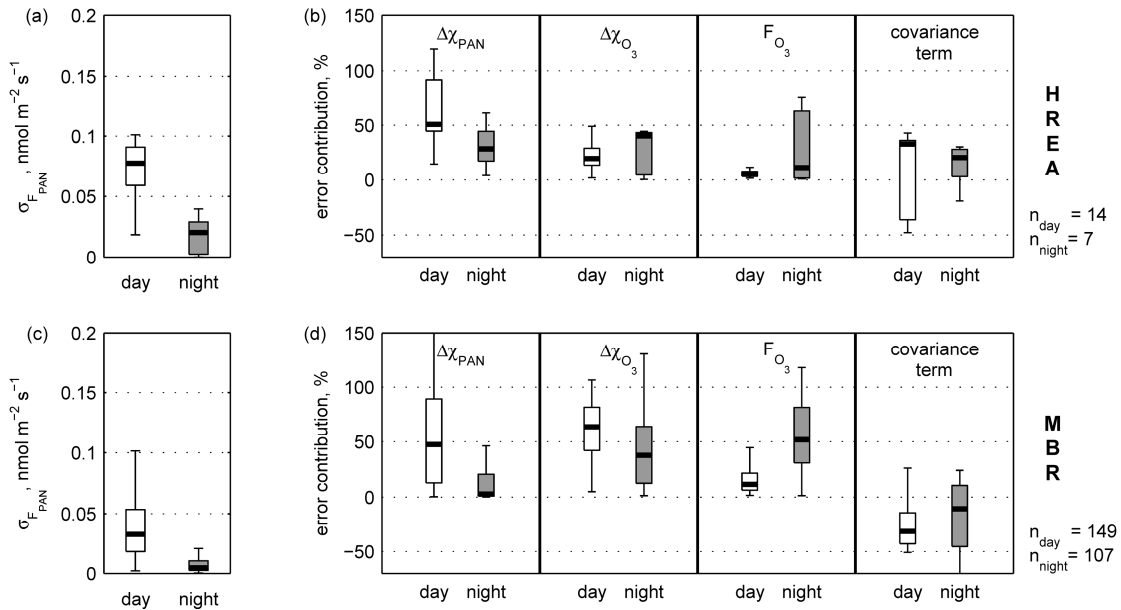


**Figure 9:** Boxplot statistics of random errors for the HREA (upper panel) and MBR (lower panel) measurements during day and nighttime at the Mainz-Finthen grassland site. **(a) + (c):** absolute random errors of the PAN flux; **(b) + (d):** relative contribution to the total random flux error of the individual components

used in the error propagation method (SM 3). The covariance term accounts for a possible correlation of the individual error terms and can be positive or negative. Values below the flux detection limit were not considered, which did not have a significant impact on the displayed boxplot statistics.

detection limit ( $\sigma_{\Delta O_3}^{\%} > 100\%$ ).  $O_3$  deposition fluxes were higher than during HREA measurements and reached during daytime up to  $-12 \text{ nmol m}^{-2} \text{ s}^{-1}$  during daytime, with an average maximum of  $-8 \text{ nmol m}^{-2} \text{ s}^{-1}$ . During nighttime  $O_3$  fluxes were small except on nights with neutral stratification, when fluxes of up to  $-5 \text{ nmol m}^{-2} \text{ s}^{-1}$  prevailed.

The resulting transfer velocity (Fig. 8e) representing the layer between 0.8 and 4.0 m a.g.l. showed average daytime values of  $0.08 \text{ m s}^{-1}$  ( $\pm 0.06 \text{ m s}^{-1}$ ), whereas during nighttime the transfer velocity was close to zero and often below the detection limit ( $\sigma_{v_{tr}}^{\%} > 100\%$ ).

As a result of the limited turbulent exchange at night,  $\Delta\chi_{PAN}$  values reached up to 400 ppt (Fig. 8f). In general, the course of nighttime  $\Delta\chi_{PAN}$  compared well to  $\Delta\chi_{O_3}$  indicating scalar similarity of PAN and  $O_3$ . On average, the daytime  $\Delta\chi_{PAN}$  values were 27 ppt ( $\pm 30$  ppt). While on some days they were clearly different from zero, on other days they were close to zero and did not exceed the detection limit ( $\sigma_{\Delta PAN}^{\%} > 100\%$ ) determined from the side-by-side measurements (Table 1).

On those days with significant daytime  $\Delta\chi_{PAN}$  values also a significant daytime PAN deposition flux was visible and reached up to  $-0.2 \text{ nmol m}^{-2} \text{ s}^{-1}$  (Fig. 8g). On other days, when daytime  $\Delta\chi_{PAN}$  values were smaller or not different from zero, PAN fluxes were below the flux detection limit (for definition see Sect. 2.6.3). Considering only

values above the flux detection limit, daytime PAN deposition was on average  $-0.07 \text{ nmol m}^{-2} \text{ s}^{-1}$  during that period. The corresponding median random flux error was  $\pm 0.033 \text{ nmol m}^{-2} \text{ s}^{-1}$  (Fig. 9c) and mainly consisted of the errors of  $\Delta\chi_{PAN}$  and  $\Delta\chi_{O_3}$  with median error contributions of 52 and 65%, respectively (Fig. 9d). At nighttime PAN fluxes were negligible or fell below the turbulence criteria when  $u_* < 0.07 \text{ m s}^{-1}$  (see Sect. 4.1.3 for discussion). The magnitude of the nighttime random flux error (median:  $\pm 0.005 \text{ nmol m}^{-2} \text{ s}^{-1}$ ) was mainly attributed to the errors of  $\Delta\chi_{O_3}$  and the  $O_3$  flux (median contribution: 38 and 52%, respectively), while the error of  $\Delta\chi_{PAN}$  was insignificant (median contribution: 5%).

## 4 Discussion

### 4.1 Performance of the PAN flux measurement system

#### 4.1.1 Performance of the GC-ECD

The uncertainties in the PAN fluxes were mainly caused by the error of  $\Delta\chi_{PAN}$ , hence, a precision and performance of the GC-ECD analysis is a main criterion for the performance of the flux measurement system. The limit of detection (LOD) of absolute PAN mixing ratios was derived from the height of the residual peak compared to the baseline noise during calibration with zero air and determined as 5 ppt ( $3\sigma$  definition). This value compares well to other GC-ECD systems which employed a capillary column for the pre-concentration of PAN [Jacobi *et al.*, 1999; Mills *et al.*, 2007]. For systems without pre-concentration LODs above 10 ppt [Fischer *et al.*, 2011; Schrimpf *et al.*, 1995] ranging up to 30 ppt or higher [Volz-Thomas *et al.*, 2002; J M Zhang *et al.*, 2009] were reported previously. Flocke *et al.* [2005] and Williams *et al.* [2000] designed their systems for aircraft measurements and achieved a much lower LOD ( $3\sigma$  definition) without pre-concentration, 3 ppt and  $< 5$  ppt, respectively. During calibration experiments with 850 ppt PAN we found a precision ( $1\sigma$ ) of 1.5% in the gradient mode and of 3% in the HREA mode (for discussion see also Sect. 4.2). These values are within the range of other recent GC-ECD systems, which reported a  $1\sigma$  precision for PAN of 1% [G Zhang *et al.*, 2012] or 3% (at 470 ppt) [Fischer *et al.*, 2011].

Although the performance of the GC-ECD was similar or even better than that of other state-of-the-art GC-ECD systems, the derived precision value at a single mixing ratio does not necessarily apply for the whole range of prevailing PAN mixing ratios. In

addition, for the application of the HREA and MBR method the precision of  $\Delta\chi_{PAN}$  is important. As presented in Sect. 3.3, the precision for the  $\Delta\chi_{PAN}$  values derived from the side-by-side measurements ranged between 17.9 and 26.1 ppt for the HREA measurements and between 4.1 and 15.2 ppt for the MBR (Table 1). The precision was largely independent from the prevailing PAN mixing ratios, which is the reason why we applied a constant absolute random error for the whole range of PAN mixing ratios. For the HREA operation the experimentally determined precisions were as high as the simulated daytime differences (Sect. 2.7), which explains the large errors of the PAN flux.

#### 4.1.2 Effect of HREA timing

For the HREA measurements, an accurate conditional sampling of updraft and downdraft air masses into the according PCUs is important, especially at high eddy reversal frequencies [e.g., Baker et al., 1992; Moravek et al., 2013]. Besides a correct online coordinate rotation of the wind vector and the appropriate choice of the dead band size and proxy scalar, this required a precise timing of the switching of the splitter valves and the investigation on high frequency attenuation effects of the inlet tube. As presented in SM 2, the electronic time lag between exceeding the dead band threshold and switching of the splitter valves was less than 20 ms and could be neglected [Moravek et al., 2013]. As shown by Moravek et al. [2013], the application of the online cross-correlation method corrected for the sensor separation effect, but was associated with a random error of  $\pm 100$  ms. The resulting flux error was determined using the relationship between flux loss and the eddy reversal frequency [Moravek et al., 2013]. During the experiment, the eddy reversal frequency ranged from 3.0 to 12.4 Hz (median: 7.6 Hz) for the applied hyperbolic dead band of  $H = 1.1$ . A simulation analysis [Moravek et al., 2013] yielded a random flux error due to the error of the online cross-correlation method between  $\pm 0.6\%$  and  $\pm 9.9\%$  (median: 4.0%), respectively. For the effect of high frequency attenuation a cut-off frequency of 1.2 Hz was determined for the 21.5 m long inlet tube [Moravek et al., 2013], which lead to an underestimation of the PAN flux ranging from 1.8 to 31.4% (median: 11.8%), which was corrected for in the post-processing.

#### 4.1.3 Random flux error under varying meteorological conditions

A main criterion for the performance of the PAN flux measurement system is the random flux error. As presented in Sect. 3.4 and in Fig. 9, the flux errors were large compared to the observed fluxes and were caused to a large extend by the error of  $\Delta\chi_{PAN}$ , but also by the error of  $\Delta\chi_{O_3}$ . This was the case for daytime MBR fluxes, when the standard deviation of  $\Delta\chi_{O_3}$  is large at high  $O_3$  mixing ratios.

The difference between the daytime and nighttime flux error indicates that the flux error does not only depend on the performance of the method but also on the meteorological conditions. Considering the error of  $\Delta\chi_{PAN}$  as the largest fraction of the flux error, we estimate values of  $\Delta\chi_{PAN}$  that would have to be measured with either HREA or MBR to obtain fluxes with a certain minimum precision under varying meteorological conditions.

For the MBR method, the required  $\Delta\chi_{PAN}$  values are obtained for a certain relative random flux errors ( $\sigma_{F_{PAN}}^{\%}$  in %) by

$$\Delta\chi_{PAN}(\sigma_{F_{PAN}}^{\%}) = \frac{\sigma_{F_{PAN}}}{v_{tr}(u_*) \cdot \sigma_{F_{PAN}}^{\%}} \quad (8)$$

where  $\sigma_{F_{PAN}}$  is the absolute flux error derived from the error propagation method. Here,  $v_{tr}$  is determined as a function of  $u_*$  via the aerodynamic approach, using the integrated stability correction functions ( $\Psi$ ) of *Businger et al.* [1971] modified by *Högström* [1988]:

$$v_{tr} = -\frac{\kappa \cdot u_*}{\ln \frac{z_2}{z_1} - \Psi\left(\frac{z_2}{L}\right) + \Psi\left(\frac{z_1}{L}\right)} \quad (9)$$

where  $\kappa$  is the von Kármán constant and  $z_1$  the lower and  $z_2$  the upper height of the gradient system. Finally,  $\Delta\chi_{PAN}(\sigma_{F_{PAN}}^{\%})$  is expressed as a function of  $u_*$ , representing the turbulent and micrometeorological conditions, for different relative random flux errors. Figure 10 shows the hyperbolic fit functions for  $\sigma_{F_{PAN}}^{\%}$  of 20, 50 and 100% together with the measured  $\Delta\chi_{PAN}$  values during the MBR operation. While for higher  $u_*$  the  $\sigma_{F_{PAN}}^{\%}$  values are quite constant for a certain  $\Delta\chi_{PAN}$  value, below  $u_* = 0.07 \text{ m s}^{-1}$  the flux error increases rapidly. The latter value is also given by *Foken* [2008] as a limit for MBR measurements and, hence, was used in the definition of the flux detection limit (Sect. 2.6.3). According to the error lines in Fig. 10 and not considering values below the flux detection limit, we find that 47% of the measured PAN fluxes are associated with a relative random error of between 20 and 50% and 27% between 50 and 100%. Only a few values (8%) showed a relative flux error below 20% and some (18%) above 100%.

Using the same approach for the HREA measurements to determine the influence of the meteorological conditions on  $\sigma_{F_{PAN}}^{\%}$ , was not successful. A clear relationship between the required  $\Delta\chi_{PAN}$  values and  $u_*$  was not found due to the higher scatter of the determined  $\sigma_{F_{PAN}}$  values. For the daytime fluxes, the errors during HREA operation were on average twice as high than during MBR operation (see Fig. 9a+c), which can mainly be attributed to the lower precision of the analysing unit (see Sect. 3.3).

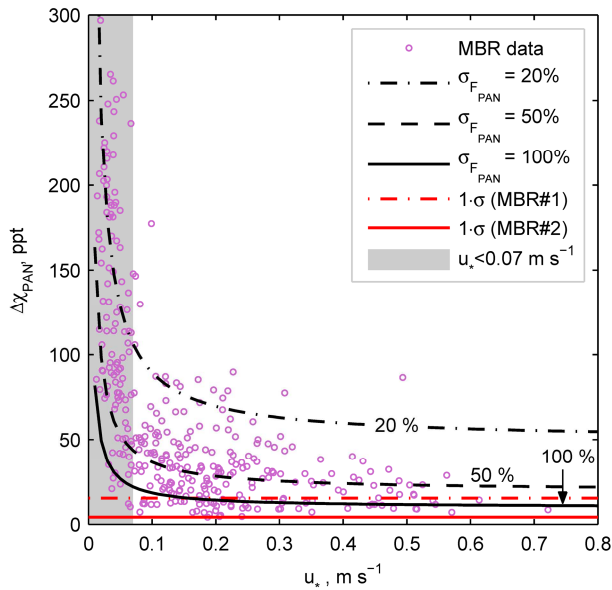


**Figure 10:**  $\Delta\chi_{PAN}$  values during the MBR operation against  $u_*$  (violet circles) are shown together with fitted lines of relative random flux errors of 20, 50 and 100% (black lines) at the Mainz-Finthen grassland site. The red lines mark the precision for the  $\Delta\chi_{PAN}$  measurement determined from side-by-side measurements. Values below this precision were excluded from the plot. The grey area with  $u_* < 0.07 \text{ m s}^{-1}$  indicates fluxes with high relative random errors due to limited turbulent exchange

However, it has to be noted that the HREA measurements took place in September and deposition fluxes to vegetation are lower than during the MBR measurements in August. On the one hand, the surface resistance was higher due to a higher fraction of dead grass species and a reduced stomata opening of the green plant material. On the other hand, during the HREA measurement period  $\sigma_w$  values, which reflect the magnitude of turbulent exchange (Eq. (1)), were below the annual average and also lower than during MBR period. Hence, in general lower fluxes due to the prevailing conditions are an additional obvious reason for the lower quality of the HREA measurements.

As it was outlined in Sect. 1, the flux errors derived by other studies, which measured direct PAN exchange fluxes in the past, are also significant and vary depending on the chosen method. *Doskey et al.* [2004] give a rough estimate of the expected flux errors ranging between 45 and 450% for daytime fluxes. They assume at a deposition velocity of  $1 \text{ cm s}^{-1}$  a vertical mixing ratio difference of 1–10% of the mean mixing ratio and an error of  $\Delta\chi_{PAN}$  of 4.5% determined from the PAN calibration. However, we find that the most reliable method to determine the error of  $\Delta\chi_{PAN}$  are side-by-side measurements at the field site to retrieve the error characteristics over the whole potential range of ambient air PAN mixing ratios. The flux error using the eddy covariance technique with a CIMS [*Turnipseed et al.*, 2006; *Wolfe et al.*, 2009] was found to be less (25–60%), although the uncertainty for a single concentration measurement is larger than with the GC-ECD method and the effect of the background signal on PAN measurements is currently discussed [*Phillips et al.*, 2013].

## 4.2 Sources of uncertainties of PAN mixing ratio differences

As uncertainties in the PAN flux were mainly caused by random errors in the determination of  $\Delta\chi_{PAN}$ , we discuss potential error sources and possibilities for their reduction. Three different parts of the PAN measurement system contribute to the random errors: (a) the inlet tube (b) the pre-concentration step, (c) the peak separation, detection and integration.

- a) Uncertainties due to chemical reactions in the inlet tube could be excluded due to the short sample air residence time of  $\sim 1.5$  s (HREA) and  $\sim 3.0$  s (MBR) and turbulent flow conditions. Experiments employing different inlet tube lengths revealed that the main effect of the sample tube was due to its impact on the pressure conditions in the PCUs, which was accounted for by using the same inlet tube length also during calibration (Sect. 2.6.1).
- b) The use of capillary columns as a reservoir for the REA, MBR or other gradient methods is unique and required the application in conservation mode (Sect. 2.2). Since we determined the saturation point regularly and found a good linear relationship between the PAN mixing ratio and the ratio of peak integral and sampled volume, potential uncertainties associated with the pre-concentration step are not caused by the operation in the conservation mode in general.

However, the higher random errors found during the side-by-side measurement in the HREA mode (Sect. 3.3) suggests that disturbed flow conditions due to fast switching may have an influence on the performance of the PCUs. Apparently, short-term pressure differences induced by the fast switching of the splitter valves or varying sample volumes influence the quality of the PAN measurement. As shown by the developed correction functions for the HREA fluxes (SM 4), we found that larger deviations were correlated with larger sample volume differences between both reservoirs. Large differences in the sample volume are caused by an imbalance of up- and downdraft events during the sampling interval. This is accompanied by an imbalance of the mean duration of up- and downdraft events, which might have an effect on the pressure equilibrium states in the PCUs. Although we did not observe any pressure change downstream of the PCUs induced by the switching of the splitter valves, it might be possible that very small pressure fluctuations inside the PCUs lead to the higher random errors for the HREA operation. Hence, we suggest that future setups should employ capillary columns using zero air when one PCU is not active. However, in our case this would have increased the total sample time for each PCU from around 4 min (Sect. 3.2) to 30 min and required either a much lower sample flow or a longer capillary column to avoid

breakthrough of the PAN frontal zone. Since a much lower sample flow than the one used here ( $\sim 1 \text{ mL min}^{-1}$ ) would cause other problems and is not desired, more efforts should be made to develop PCUs with longer capillary columns. In this case, the quantitative release of all PAN from the column during injection is the major challenge.

Since the pre-concentration efficiency is largely depend on the cooling temperature, small fluctuations of the pre-concentration temperature might also cause random errors. Due to the optimized temperature control of the PCUs, the cooling temperature, which was set to  $-5^\circ\text{C}$ , showed variations of only  $\pm 0.1 \text{ K}$ . Furthermore, temperature measurements at different parts of the capillary column revealed that potential temperature differences along the column were less than  $0.5 \text{ K}$ . We found an increase of the pre-concentration efficiency of around  $4\% \text{ K}^{-1}$  in the temperature range from  $+5$  to  $-5^\circ\text{C}$ . Consequently, larger variations of the cooling temperature would be necessary to have a noticeable effect on the precision of the PAN measurements. In addition, variations of the heating temperature during injection were also small compared to their potential effect. Nevertheless, it cannot be excluded that a significant improvement of the temperature control would reduce the uncertainties.

It was found that contamination of the pre-concentration capillary column was problematic. After some time of operation additional peaks in the chromatogram were observed when heating the pre-concentration capillary column above  $50^\circ\text{C}$  in the injection mode. Hence, we suggest to either clean the column by regularly heating it or exchanging the pre-concentration column from time to time.

- c) The chromatogram of the PAN-GC featured a PAN peak directly preceded by a carbon tetrachloride ( $\text{CCl}_4$ ) peak, which is present at a relatively constant level in the atmosphere [Galbally, 1976] and detected by the ECD due to its electron affinity. Although we achieved a good chromatographic resolution ( $R \sim 1$ ) with the employed operation settings, a small overlap of both peaks leads to potential errors that might be relevant when resolving small differences. We tested this effect by comparing the results from the integration using the ADAM32 software with another independent software program and found a random integration error of only 2%.

Moreover, we found a temperature dependency of the PAN signal which could not be attributed to one single instrument part or process. For slow temperature changes with small diurnal amplitudes the PAN integrals were anti-correlated to the temperature measured inside the instrument and a temperature change of  $2 \text{ K}$  lead to a change of PAN integrals of approximately 5%. During the field experiment the air-conditioning

controlled the air temperature in the measurement container to  $\pm 1$  K with an average periodicity of around 15 min. Since the observed temperature effect was of inertial nature and a slow temperature change would have an effect on the measurement of the PAN from both PCUs, we found the impact of the temperature effect to be insignificant for our results. However, as the potential influence of fast temperature variations could not be determined and cannot be excluded, we suggest for future setups, aiming to resolve small mixing ratio differences, to place the GC in a thermally insulated and temperature controlled compartment [Flocke *et al.*, 2005].

### 4.3 Scalar similarity and influence of chemistry

Scalar similarity is defined as the similarity in the scalar time series throughout the scalar spectra [Kaimal *et al.*, 1972; Pearson *et al.*, 1998]. Since the maximal time resolution of a single PAN measurement with the GC-ECD was 10 min, we could not determine its scalar spectrum over the whole range to obtain a detailed analysis as suggested by other authors [Pearson *et al.*, 1998; Ruppert *et al.*, 2006]. However, the distribution of sources and sinks within the footprint area is an important factor determining scalar similarity. The tropospheric production of O<sub>3</sub> and PAN is strongly coupled to photochemistry and driven by the abundance of hydrocarbons [Roberts, 1990; Seinfeld and Pandis, 2006]. Furthermore, for both quantities downward transport from higher altitudes is an important source to the lower boundary layer [Singh, 1987]. The sink distribution of both O<sub>3</sub> and PAN is strongly linked to dry deposition to the biosphere, in our case the grassland species at the Mainz-Finthen experimental site. Although we can assume that stomatal uptake is the major deposition process for both O<sub>3</sub> [Bassin *et al.*, 2004; Coyle *et al.*, 2009; L M Zhang *et al.*, 2006] and PAN [Okano *et al.*, 1990; Sparks *et al.*, 2003] when stomatal opening is not inhibited, the role of cuticular and mesophyllic uptake processes for PAN [Doskey *et al.*, 2004; Sparks *et al.*, 2003; Teklemariam and Sparks, 2004; Turnipseed *et al.*, 2006] as well as deposition on soil are not well understood (see also Sect. 1), which may be the cause for some divergence from scalar similarity between O<sub>3</sub> and PAN.

In order to investigate whether near ground production, depletion or reaction with other species has an effect on the application of the HREA and MBR method, we analysed the ratio between chemical time scales and turbulent transport times (see Stella *et al.* [2012] for calculation) in the respective layer (Damköhler number ( $Da$ )). For PAN, daytime  $Da$  values were below  $1.0 \cdot 10^{-2}$  and nighttime values below  $0.5 \cdot 10^{-2}$  implying that chemical time scales were much longer than turbulent transport and, thus, did not have an effect on the flux measurements. A similar ratio between turbulent and chemical time scales was found for O<sub>3</sub> ( $Da < 2.0 \cdot 10^{-2}$ ), except between 6:00 and

10:00 CET, when higher NO mixing ratios lead to a faster O<sub>3</sub> depletion. During that time,  $Da$  values of up to 0.25 occurred occasionally (median:  $< 4.0 \cdot 10^{-2}$ ). Consequently, chemical reactions might have had an influence on O<sub>3</sub> flux measurements during these periods.

#### 4.4 Applicability of HREA and MBR for PAN flux measurements

As shown in the previous sections, the applicability of HREA and MBR for PAN flux measurements largely depends on the capability of the flux measurements system to resolve small PAN mixing ratios. Furthermore, the magnitude of the measured mixing ratio differences is influenced by the meteorological conditions, the PAN deposition, as well as the dead band setting (HREA) and the separation of the inlets (MBR).

The simulation analysis revealed that expected daytime  $\Delta\chi_{PAN}$  values were of similar magnitude for both the HREA and MBR method (Sect. 3.1.2, Fig. 4). Prior to the measurements it was assumed that especially under conditions, when strong turbulent mixing results in only small vertical mixing ratio gradients, the application of the REA method might be preferred. However, for the conditions at the Mainz-Finthen grassland site and for the presented setup of inlet heights (Sect. 2.1.2) and dead band settings (Sect. 3.1.1), no significant advantage of the HREA method was found. To evaluate the conditions under which the HREA method may be favoured over the MBR method (higher  $\Delta\chi_{PAN}$  values) for the presented PAN flux measurements, we examine the ratio of the derived mixing ratio differences by the MBR and HREA method. Using the relationships in Eqs. (1) and (4), we obtain a description of this ratio, which is independent of the PAN flux:

$$\frac{\Delta\chi_{PAN}(MBR)}{\Delta\chi_{PAN}(HREA)} = \frac{F_{PAN}}{(-v_{tr})} \cdot \frac{b \cdot \sigma_w}{F_{PAN}} \quad (10)$$

Instead of determining  $v_{tr}$  with a proxy scalar, its aerodynamic representation can be used (see Sect. 4.1.3). Expressing Eq. (10) for any scalar quantity and gradient measurements in general, the ratio of  $\Delta\chi$  from gradient and REA measurements ( $Q_{\Delta\chi}$ ) is then represented by:

$$Q_{\Delta\chi} = \frac{\Delta\chi(Gradient)}{\Delta\chi(REA)} = \frac{b}{\kappa} \cdot \frac{\sigma_w}{u_*} \cdot \left( \ln \frac{z_2}{z_1} - \Psi \left( \frac{z_2}{L} \right) + \Psi \left( \frac{z_1}{L} \right) \right) \quad (11)$$

while  $Q_{\Delta\chi}^{-1}$  is defined as the inverse of  $Q_{\Delta\chi}$ .

Since the  $b$ -value can be considered a constant for a certain dead band size (see Fig. 3 and Fig. 7e),  $Q_{\Delta\chi}$  and  $Q_{\Delta\chi}^{-1}$  are a function of the inlet heights of the gradient measurements, the stability correction function terms and  $\sigma_w/u_*$ . The latter represents

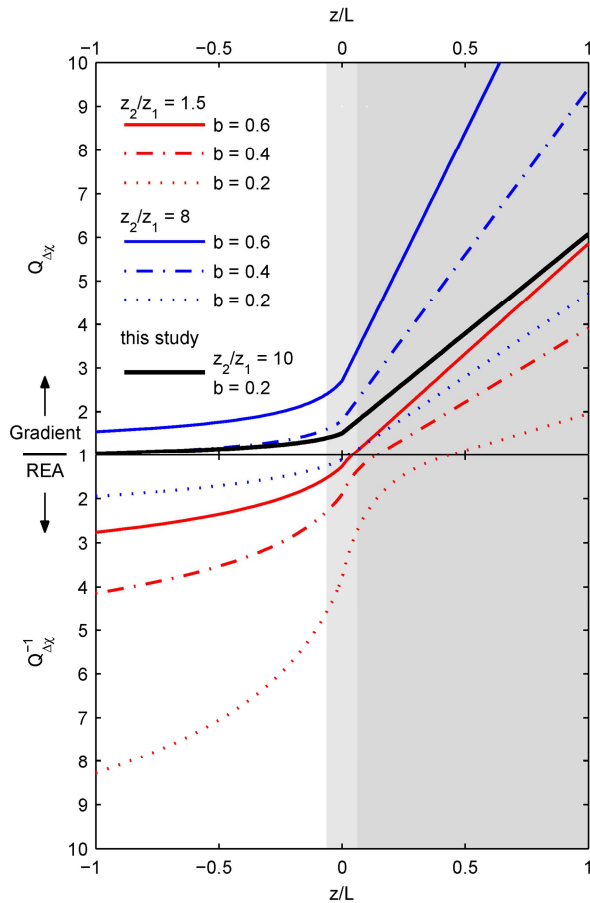


**Figure 11:** Expected  $\Delta\chi(\text{gradient})/\Delta\chi(\text{REA})$  ratio ( $Q_{\Delta\chi}$ ) displayed on the upper y-axis and the  $\Delta\chi(\text{REA})/\Delta\chi(\text{gradient})$  ratio, ( $Q_{\Delta\chi}^{-1}$ ) displayed on the lower y-axis (reversed) versus  $z/L$ . Shown are the ratios determined with Eq.(11) for  $m = z_2/z_1 = 8$  (blue lines) and  $m = z_2/z_1 = 1.5$  (red lines), representing gradient measurements above low and high vegetation, respectively, and  $b$ -values of 0.6 (solid line), 0.4 (dashed line) and 0.2 (dotted line). The black line was calculated with the settings from this study ( $m = (z_2 - d)/(z_1 - d) = 10$  and  $b = 0.21$ ). The upper measurement height of the gradient measurement ( $z_2$ ) was used as reference height for  $z/L$  in Eq. (11) and in the calculation of the integral turbulence characteristics (Eq. (12)). The shaded areas indicate ranges of unstable (white), neutral (light grey) and stable (dark grey) conditions. During the latter, fluxes might be prone to large errors when determined with the gradient method, and a turbulence criterion as for the MBR method (Sect. 2.1.2) should be applied.

the integral turbulence characteristics for  $w$ , which can be parameterized as a function of  $z/L$  [Panofsky *et al.*, 1977]. For the turbulence data at the Mainz-Finthen grassland site we found the best agreement using the parameterization given by Panofsky *et al.* [1977] for  $z/L < 0$ :

$$\frac{\sigma_w}{u_*} = 1.3 \cdot \left(1 - 2 \cdot \frac{z}{L}\right)^{1/3} ; \quad \frac{z}{L} < 0 \quad (12)$$

and for  $z/L \geq 0$  a constant value independent from stability:

$$\frac{\sigma_w}{u_*} = 1.3 ; \quad \frac{z}{L} \geq 0 \quad (13)$$

Inserting the parameterizations in Eq. (11), we derive a function for  $Q_{\Delta\chi}$  which is only dependent on the inlet heights of the gradient system, the REA dead band size and  $z/L$ . In case either  $z_1$  or  $z_2$  is used as the reference level for  $z/L$ , the stability correction term is independent from the absolute inlet heights and only their ratio ( $m = z_2/z_1$ ) has to be given. Figure 11 displays the expected  $Q_{\Delta\chi}$  and  $Q_{\Delta\chi}^{-1}$  values for  $m = 8$  and  $m = 1.5$ , representing gradient measurements above low and high vegetation, respectively. For  $m = 8$  and  $b = 0.6$ , we find under unstable to near neutral conditions  $Q_{\Delta\chi}$  ranging

between 1.5 and 2, i.e. the gradient method yields higher  $\Delta\chi$  values than the REA method. In contrast, when using a REA dead band resulting in a  $b$ -value of 0.2, higher  $\Delta\chi$  values are retrieved with the REA method ( $Q_{\Delta\chi}^{-1} > 1$ ). For  $m = 1.5$ ,  $Q_{\Delta\chi}^{-1}$  values are greater than 2, 3 and 4 for  $b$ -values of 0.6, 0.4 and 0.2, respectively. Hence, above high vegetation the REA method has a clear advantage under unstable and also neutral conditions. During stable conditions, the REA method only yields higher  $\Delta\chi$  values when choosing a dead band above high vegetation. However, for most other settings, the ratio shows a steep linear increase from near neutral to stable conditions in favour of the gradient method, obtaining higher  $\Delta\chi$  values. Since the latter especially prevail under weak turbulence conditions, it has to be noted again that fluxes under stable conditions might still be prone to large errors when determined with the gradient method. Consequently, a turbulence criterion as for the MBR method (Sect. 2.1.2) should be applied.

Applying the setting used in this study ( $m = (z_2 - d)/(z_1 - d) = 10$  and  $b = 0.21$ ), larger  $\Delta\chi$  values are expected with the MBR method than with the HREA method not only for stable and neutral but also for unstable conditions (Fig. 11). During the latter, when highest PAN deposition fluxes are expected,  $Q_{\Delta\chi}$  is nearly unity at  $z/L = -1$ , but increases to about 1.3 at the transition between unstable and neutral conditions. The curve representing this study is in good agreement with the ratios of  $\Delta\chi$  obtained by the simulation analysis of MBR and HREA measurements (Sects. 2.7 and 3.1). This confirms that the presented method can be a simple tool to evaluate the applicability of the REA and gradient approach, especially when small mixing ratio differences are expected, as in our case for PAN.

## 5 Summary and conclusions

We developed a measurement system for the determination of biosphere-atmosphere exchange fluxes using both the HREA and MBR method. It is the first REA system for the determination of PAN fluxes and the system was designed such that it could also be used for simultaneous measurements at two inlet heights for application of the gradient approach. Sampling for both methods was realized by trapping PAN onto two pre-concentration columns over a sampling period of 30 min and subsequent analysis by a GC-ECD. A linear relationship was found between the PAN peak area and both the PAN mixing ratio and the sample volume. This allowed the system to be used with varying sample volumes, which is a prerequisite for the application of the HREA method.

We validated the system and made PAN flux measurements at a natural grassland site at the estate of the Mainz-Finthen Airport, Rhineland Palatine, Germany. For the implementation HREA, the wind vector was adjusted online using the double rotation method. High frequency O<sub>3</sub> measurements were used as a proxy for calculating the hyperbolic dead band ( $H = 1.1$ ) and  $b$ -coefficient ( $\sim 0.21$ ). The application of the hyperbolic dead band reduced the sampling time to about 12% for each reservoir. The setup of the system allowed compensating the resulting reduction of the sample volume by a higher flow rate through the pre-concentration columns. The lag time between the vertical wind speed signal and the splitter valves – a crucial parameter to determine accurate fluxes – was determined continuously online during the measurements and varied by about  $\pm 200$  ms, mainly depending on the prevailing wind direction and the error of the cross-correlation method. High frequency attenuation due to the long intake tube was found to be small and corrected for.

Flux simulations revealed that the uncertainties in measured mixing ratio differences are the most critical issue for a successful application of both the HREA and the MBR method. For the presented natural grassland site, the system should be able to resolve mixing ratio differences of at least 30 ppt for both the MBR and the HREA method to obtain significant daytime fluxes of PAN. The precision of the gradient system was determined by side-by-side measurements and ranged from 4 to 15 ppt. During the HREA application the precision ranged between 18 and 26 ppt after applying a correction for pressure fluctuations. The higher noise in PAN mixing ratios during HREA application were most likely attributed to small pressure changes in the pre-concentration columns caused by the switching of the splitter valves.

We propagated the individual errors of the required quantities for the PAN flux determination and derived median random errors of the daytime PAN fluxes of  $\pm 0.077$  nmol m<sup>-2</sup> s<sup>-1</sup> for the HREA system and of  $\pm 0.033$  nmol m<sup>-2</sup> s<sup>-1</sup> for the MBR system. Most values were below the flux detection limit for the HREA measurements, which was attributed not only to the lower precision but also to the fact that the HREA measurement period took place in autumn (lower fluxes prevailed due to higher surface resistance) and weaker turbulence than during the MBR period. In contrast, significant PAN deposition fluxes could be resolved during the MBR measurement period in summer yielding mean daytime PAN deposition fluxes of  $-0.07(\pm 0.06)$  nmol m<sup>-2</sup> s<sup>-1</sup> with maximal values reaching up to  $-0.2$  nmol m<sup>-2</sup> s<sup>-1</sup> during daytime. During nighttime the fluxes were mostly close to zero or below the detection limit. The range of the obtained PAN differences matched the simulated differences well for both methods, which indicate the plausibility of the PAN fluxes determined by the new system. Damköhler numbers of  $< 0.02$  for most periods revealed that chemical divergence due to thermal decomposition of PAN had no impact on the obtained fluxes.

Our results show that mainly the precision of the mixing ratio measurement by the GC-ECD has to be improved further to reduce the flux uncertainties. Since the largest uncertainties are most likely attributed to the pre-concentration of PAN, the operation of the PCUs should be optimized by adding zero when one reservoir is not active.

In general, the uncertainties are also expected to decrease when the system is applied in ecosystems exposed to higher PAN fluxes (i.e. higher leaf area index and lower surface resistance or higher PAN mixing ratios downwind of urban areas and higher surface roughness) than at the nutrient-poor grassland site.

Finally, we developed a simple method to test the feasibility of the gradient and REA methods for compounds exhibiting small surface-atmosphere exchange fluxes for different meteorological conditions at ecosystems with low and high vegetation. In general, the HREA method is favoured over high vegetation while the MBR is more feasible at low vegetation.

## Acknowledgements

This project was funded by the Max Planck Society. We thank M. Welling for helpful comments on the flux system design as well as J.-C. Mayer and D. Plake for the setup and operation of additional measurements at the field site. We are grateful to H. Gross for the electrical installations at the field site and for logistical support. We thank R. Schmitt for discussions and comments on the modification of the PAN GC-ECD. We are also indebted to the staff of the MPIC mechanical and electronic workshop for their substantial support.

## References

- Ammann, C., and F. X. Meixner (2002), Stability dependence of the relaxed eddy accumulation coefficient for various scalar quantities, *J. Geophys. Res.-Atmos.*, *107*(D7-8).
- Baker, J. M. (2000), Conditional sampling revisited, *Agr Forest Meteorol*, *104*(1), 59-65.
- Baker, J. M., J. M. Norman, and W. L. Bland (1992), Field-scale application of flux measurement by conditional sampling, *Agr Forest Meteorol*, *62*(1-2), 31-52.

- Bassin, S., P. Calanca, T. Weidinger, G. Gerosa, and E. Fuhrer (2004), Modeling seasonal ozone fluxes to grassland and wheat: model improvement, testing, and application, *Atmos. Environ.*, 38(15), 2349-2359.
- Beverland, I. J., R. Milne, C. Boissard, D. H. Oneill, J. B. Moncrieff, and C. N. Hewitt (1996a), Measurement of carbon dioxide and hydrocarbon fluxes from a sitka spruce forest using micrometeorological techniques, *J. Geophys. Res.-Atmos.*, 101(D17), 22807-22815.
- Businger, J. A. (1986), Evaluation of the Accuracy with Which Dry Deposition Can Be Measured with Current Micrometeorological Techniques, *J Clim Appl Meteorol*, 25(8), 1100-1124.
- Businger, J. A., and S. P. Oncley (1990), Flux Measurement with Conditional Sampling, *J. Atmos. Ocean. Technol.*, 7(2), 349-352.
- Businger, J. A., J. C. Wyngaard, Y. Izumi, and E. F. Bradley (1971), Flux-Profile Relationships in the Atmospheric Surface Layer, *Journal of the Atmospheric Sciences*, 28(2), 181-&.
- Cazorla, M., and W. H. Brune (2010), Measurement of Ozone Production Sensor, *Atmos. Meas. Tech.*, 3(3), 545-555.
- Coyle, M., E. Nemitz, R. Storeton-West, D. Fowler, and J. N. Cape (2009), Measurements of ozone deposition to a potato canopy, *Agr Forest Meteorol*, 149(3-4), 655-666.
- Doskey, P. V., V. R. Kotamarthi, Y. Fukui, D. R. Cook, F. W. Breitbeil, and M. L. Wesely (2004), Air-surface exchange of peroxyacetyl nitrate at a grassland site, *J. Geophys. Res.-Atmos.*, 109(D10), 9, D10310.
- Ermel, M., R. Oswald, J. C. Mayer, A. Moravek, G. Song, M. Beck, F. X. Meixner, and I. Trebs (2013), Preparation Methods to Optimize the Performance of Sensor Discs for Fast Chemiluminescence Ozone Analyzers, *Environ Sci Technol*.
- Fischer, E. V., D. A. Jaffe, and E. C. Weatherhead (2011), Free tropospheric peroxyacetyl nitrate (PAN) and ozone at Mount Bachelor: potential causes of variability and timescale for trend detection, *Atmos. Chem. Phys.*, 11(12), 5641-5654.
- Flocke, F. M., A. J. Weinheimer, A. L. Swanson, J. M. Roberts, R. Schmitt, and S. Shertz (2005), On the measurement of PANs by gas chromatography and electron capture detection, *J. Atmos. Chem.*, 52(1), 19-43.
- Foken, T. (2008), *Micrometeorology*, 306 pp., Springer, Berlin.
- Foken, T., and B. Wichura (1996), Tools for quality assessment of surface-based flux measurements, *Agr Forest Meteorol*, 78(1-2), 83-105.
- Foken, T., R. Dlugi, and G. Kramm (1995), On the determination of dry deposition and emission of gaseous compounds at the biosphere-atmosphere interface, *Meteorol. Z.*, 4(3), 91-118118.
- Foken, T., M. Göockede, M. Mauder, L. Mahrt, B. Amiro, and W. Munger (2004), Post-Field Data Quality Control, in *Handbook of Micrometeorology*, edited by X. Lee, W. Massman and B. Law, pp. 181-208, Springer Netherlands.
- Galbally, I. E. (1976), Man-Made Carbon-Tetrachloride in Atmosphere, *Science*, 193(4253), 573-576.

- Garland, J. A. (1977), The dry deposition of sulphur dioxide to land and water surfaces, *Proc. R. Soc. London Ser. A-Math. Phys. Eng. Sci.*, 354(1678), 245-268.
- Garland, J. A., and S. A. Penkett (1976), Absorption of peroxy acetyl nitrate and ozone by natural surfaces, *Atmos. Environ.*, 10(12), 1127-1131.
- Göckede, M., C. Rebmann, and T. Foken (2004), A combination of quality assessment tools for eddy covariance measurements with footprint modelling for the characterisation of complex sites, *Agr Forest Meteorol*, 127(3-4), 175-188.
- Göckede, M., T. Markkanen, C. B. Hasager, and T. Foken (2006), Update of a footprint-based approach for the characterisation of complex measurement sites, *Boundary-Layer Meteorology*, 118(3), 635-655.
- Hicks, B. B., D. D. Baldocchi, T. P. Meyers, R. P. Hosker, and D. R. Matt (1987), A preliminary multiple resistance routine for deriving dry deposition velocities from measured quantities, *Water Air Soil Poll*, 36(3-4), 311-330.
- Hill, A. C. (1971), Vegetation - sink for atmospheric pollutants, *Journal of the Air Pollution Control Association*, 21(6), 341-346.
- Högström, U. (1988), Non-dimensional wind and temperature profiles in the atmospheric surface layer: A re-evaluation, *Boundary-Layer Meteorology*, 42(1-2), 55-78.
- Jacobi, H. W., R. Weller, T. Bluszcz, and O. Schrems (1999), Latitudinal distribution of peroxyacetyl nitrate (PAN) over the Atlantic Ocean, *J. Geophys. Res.-Atmos.*, 104(D21), 26901-26912.
- Kaimal, J. C., Y. Izumi, J. C. Wyngaard, and R. Cote (1972), Spectral characteristics of surface-layer turbulence, *Q. J. R. Meteorol. Soc.*, 98(417), 563-&.
- Liu, H. P., and T. Foken (2001), A modified Bowen ratio method to determine sensible and latent heat fluxes, *Meteorol. Z.*, 10(1), 71-80.
- Magnani, F., et al. (2007), The human footprint in the carbon cycle of temperate and boreal forests, *Nature*, 447(7146), 848-850.
- Mauder, M., and T. Foken (2011), Documentation and Instruction Manual of the Eddy-Covariance Software Package TK3, in *Arbeitsergebnisse*, edited, pp. 60, ISSN 1614-8916, Abteilung Mikrometeorologie, Universität Bayreuth, Bayreuth.
- Mauder, M., M. Cuntz, C. Drüe, A. Graf, C. Rebmann, H. P. Schmid, M. Schmidt, and R. Steinbrecher (2013), A strategy for quality and uncertainty assessment of long-term eddy-covariance measurements, *Agr Forest Meteorol*, 169(0), 122-135.
- Mills, G. P., W. T. Sturges, R. A. Salmon, S. J. B. Bauguitte, K. A. Read, and B. J. Bandy (2007), Seasonal variation of peroxyacetyl nitrate (PAN) in coastal Antarctica measured with a new instrument for the detection of sub-part per trillion mixing ratios of PAN, *Atmos. Chem. Phys.*, 7(17), 4589-4599.
- Moravek, A., I. Trebs, and T. Foken (2013), Effect of imprecise lag time and high-frequency attenuation on surface-atmosphere exchange fluxes determined with the relaxed eddy accumulation method, *Journal of Geophysical Research: Atmospheres*, 118(17), 10,210-210,224.
- Neff, J. C., E. A. Holland, F. J. Dentener, W. H. McDowell, and K. M. Russell (2002), The origin, composition and rates of organic nitrogen deposition: A missing piece of the nitrogen cycle?, *Biogeochemistry*, 57(1), 99-136.

- Novak, J., J. Janak, and J. Golias (1979), in *Proceedings of the 9th Materials Research Symposium, April 10-13, 1978, held at NBS, Gaithersburg, MD, NBS Special Publication, No 519, National Bureau of Standards, Washington, DC, 739-746.*
- Okano, K., K. Tobe, and A. Furukawa (1990), Foliar Uptake of Peroxyacetyl Nitrate (PAN) by Herbaceous Species Varying in Susceptibility to this Pollutant, *New Phytol*, *114*(1), 139-145.
- Oncley, S. P., A. C. Delany, T. W. Horst, and P. P. Tans (1993), Verification of flux measurement using relaxed eddy accumulation *Atmos Environ a-Gen*, *27*(15), 2417-2426.
- Panofsky, H. A., H. Tennekes, D. H. Lenschow, and J. C. Wyngaard (1977), The characteristics of turbulent velocity components in the surface layer under convective conditions, *Boundary-Layer Meteorology*, *11*(3), 355-361.
- Pätz, H. W., A. Lerner, N. Houben, and A. Volz-Thomas (2002), Validation of a new method for the calibration of peroxy acetyl nitrate (PAN)-analyzers, *Gefahrst. Reinhalt. Luft*, *62*(5), 215-219.
- Pearson, R. J., S. P. Oncley, and A. C. Delany (1998), A scalar similarity study based on surface layer ozone measurements over cotton during the California Ozone Deposition Experiment, *J. Geophys. Res.-Atmos.*, *103*(D15), 18919-18926.
- Phillips, G. J., N. Pouvesle, J. Thieser, G. Schuster, R. Axinte, H. Fischer, J. Williams, J. Lelieveld, and J. N. Crowley (2013), Peroxyacetyl nitrate (PAN) and peroxyacetic acid (PAA) measurements by iodide chemical ionisation mass spectrometry: first analysis of results in the boreal forest and implications for the measurement of PAN fluxes, *Atmos. Chem. Phys.*, *13*(3), 1129-1139.
- Rannik, U., M. Aubinet, O. Kurbanmuradov, K. K. Sabelfeld, T. Markkanen, and T. Vesala (2000), Footprint analysis for measurements over a heterogeneous forest, *Boundary-Layer Meteorology*, *97*(1), 137-166.
- Roberts, J. M. (1990), The atmospheric chemistry of organic nitrates, *Atmos Environ a-Gen*, *24*(2), 243-287.
- Ruppert, J., C. Thomas, and T. Foken (2006), Scalar similarity for relaxed eddy accumulation methods, *Boundary-Layer Meteorology*, *120*(1), 39-63.
- Schrimpf, W., K. P. Muller, F. J. Johnen, K. Lienaerts, and J. Rudolph (1995), An Optimized Method for Airborne Peroxyacetyl Nitrate (Pan) Measurements, *J. Atmos. Chem.*, *22*(3), 303-317.
- Schrimpf, W., K. Lienaerts, K. P. Muller, J. Rudolph, R. Neubert, W. Schussler, and I. Levin (1996), Dry deposition of peroxyacetyl nitrate (PAN): Determination of its deposition velocity at night from measurements of the atmospheric PAN and (222)Radon concentration gradient, *Geophys. Res. Lett.*, *23*(24), 3599-3602.
- Seinfeld, J. H., and S. N. Pandis (2006), *Atmospheric chemistry and physics: from air pollution to climate change*, Wiley.
- Shepson, P. B., J. W. Bottenheim, D. R. Hastie, and A. Venkatram (1992), Determination of the relative ozone and PAN deposition velocities at night, *Geophys. Res. Lett.*, *19*(11), 1121-1124.
- Singh, H. B. (1987), Reactive Nitrogen in the Troposphere, *Environ Sci Technol*, *21*(4), 320-327.

- Singh, H. B., and P. L. Hanst (1981), Peroxyacetyl nitrate (PAN) in the unpolluted atmosphere: An important reservoir for nitrogen oxides, *Geophys. Res. Lett.*, 8(8), 941-944.
- Sparks, J. P., J. M. Roberts, and R. K. Monson (2003), The uptake of gaseous organic nitrogen by leaves: A significant global nitrogen transfer process, *Geophys. Res. Lett.*, 30(23).
- Stella, P., et al. (2012), Comparison of methods for the determination of NO-O<sub>3</sub>-NO<sub>2</sub> fluxes and chemical interactions over a bare soil, *Atmos. Meas. Tech.*, 5(6), 1241-1257.
- Stephens, E. R. (1969), *The formation reactions and properties of peroxyacyl nitrates in photochemical air pollution*, 119-146 pp.
- Teklemariam, T. A., and J. P. Sparks (2004), Gaseous fluxes of peroxyacetyl nitrate (PAN) into plant leaves, *Plant Cell Environ.*, 27(9), 1149-1158.
- Turnipseed, A. A., L. G. Huey, E. Nemitz, R. Stickel, J. Higgs, D. J. Tanner, D. L. Slusher, J. P. Sparks, F. Flocke, and A. Guenther (2006), Eddy covariance fluxes of peroxyacetyl nitrates (PANs) and NO<sub>y</sub> to a coniferous forest, *J. Geophys. Res.-Atmos.*, 111(D9), D09304.
- Volz-Thomas, A., I. Xueref, and R. Schmitt (2002), An automatic gas chromatograph and calibration system for ambient measurements of PAN and PPN, *Environ. Sci. Pollut. Res.*, 72-76.
- Wesely, M. L., and B. B. Hicks (2000), A review of the current status of knowledge on dry deposition, *Atmos. Environ.*, 34(12-14), 2261-2282.
- Williams, J., et al. (2000), A method for the airborne measurement of PAN, PPN, and MPAN, *J. Geophys. Res.-Atmos.*, 105(D23), 28943-28960.
- Wolfe, G. M., J. A. Thornton, R. L. N. Yatawelli, M. McKay, A. H. Goldstein, B. LaFranchi, K. E. Min, and R. C. Cohen (2009), Eddy covariance fluxes of acyl peroxy nitrates (PAN, PPN and MPAN) above a Ponderosa pine forest, *Atmos. Chem. Phys.*, 9(2), 615-634.
- Wolff, V., I. Trebs, C. Ammann, and F. X. Meixner (2010), Aerodynamic gradient measurements of the NH<sub>3</sub>-HNO<sub>3</sub>-NH<sub>4</sub>NO<sub>3</sub> triad using a wet chemical instrument: an analysis of precision requirements and flux errors, *Atmos. Meas. Tech.*, 3(1), 187-208.
- Wyngaard, J. C., and C. H. Moeng (1992), Parameterizing turbulent diffusion through the joint probability density *Boundary-Layer Meteorology*, 60(1-2), 1-13.
- Zhang, G., Y. J. Mu, J. F. Liu, and A. Mellouki (2012), Direct and simultaneous determination of trace-level carbon tetrachloride, peroxyacetyl nitrate, and peroxypropionyl nitrate using gas chromatography-electron capture detection, *J Chromatogr A*, 1266, 110-115.
- Zhang, J. M., et al. (2009), Continuous measurement of peroxyacetyl nitrate (PAN) in suburban and remote areas of western China, *Atmos. Environ.*, 43(2), 228-237.
- Zhang, L. M., R. Vet, J. R. Brook, and A. H. Legge (2006), Factors affecting stomatal uptake of ozone by different canopies and a comparison between dose and exposure, *Sci Total Environ*, 370(1), 117-132.

## Supplementary material

### SM 1 Operation of PAN GC

#### SM 1.1 Main settings

During the operation of the GC-ECD the temperature of the Peltier-cooled oven module, which houses both columns, was set to 18°C to prevent thermal decomposition of PAN at higher temperatures. For the same reason, the ECD was heated to only 50°C. We used nitrogen 5.0 (Air Liquide Deutschland GmbH, Germany) as both carrier gas (volume flow 18 mL min<sup>-1</sup>) and make up gas for the ECD (volume flow 16 mL min<sup>-1</sup>). The chosen carrier gas flow rate gave the best compromise to separate the PAN peak (PAN retention time = 243 s) from carbon tetrachloride (CCl<sub>4</sub>, retention time = 203 s) and to minimize the total analysing time. To prevent changes in humidity levels between carrier gas and sample air, the carrier gas was humidified in the GC-ECD by flowing through a thermally-controlled cartridge filled with CuSO<sub>4</sub>·6H<sub>2</sub>O prior to injection [Flocke *et al.*, 2005].

#### SM 1.2 Design and operation of PCUs

The PCUs consist of a 1.15 m capillary column (MXT-1, ID 0.53 mm, film thickness 7.00 µm; Restek, USA) as a trapping material, which is coiled in an insulated circular aluminium (ID 35 mm) housing and cooled by two peltiers (Supercool PE-127-08-25-S, Laird technologies, USA) arranged in series. To optimize the stability of the temperature control, the inner space of the housing was filled by an aluminium cylinder, which could be removed when the column had to be replaced. The temperature of the aluminium housing was monitored by a Pt100 probe and regulated to -5°C. For injections, the capillary column is heated by passing a current through the column using a 12 V DC supply. To prevent a short circuit the MXT-column ( $R = \sim 4.5 \Omega$ ) was coated with 1/16" PFA tubing. The heating of the column was limited to 25°C to prevent thermal decomposition of PAN at higher temperatures, while it was assured that the coil was heated long enough to allow slow substances to evaporate from the column. A balance between the maximum heating temperature, the heating time and the cooling temperature of the aluminium housing had to be found as typically the column temperature declined slowly after heating and had to reach the initial temperature of -5°C before switching to the sampling mode (after 5 min).

## SM 2 Fast response system design for HREA operation

### SM 2.1 Time response of data transmission, HREA software and splitter valve actuation

The PC housing the HREA software program (LabVIEW, National Instruments Corporation, USA) was connected via RS232 with the CR3000 data logger (see Fig. 1a in main article) to receive the high frequency (20 Hz) wind vector, the O<sub>3</sub> signal for calculation of the hyperbolic dead band and the determination of updraft and downdraft events. The signal of the in-built closed-path CO<sub>2</sub> analyser was transmitted for the lag time determination (see Sect. 2.4 in main article). The data was transmitted at a baud rate of 57.6 kBit s<sup>-1</sup> using the four byte floating point (IEEE4) data type which resulted in a time span between the start and end of the data string of about 10 ms. A higher baud rate could not be used due to the length (~20 m) of the RS232 data cable. To assure an accurate timing of the HREA software on the PC, the execution interval (50 ms) was triggered by the incoming string sent from the CR3000. The splitter valves were actuated using a PCI-DAQ card (National Instruments Corporation, USA). To avoid any delays caused by the PC's operation system (Windows XP, Microsoft, USA), the PC's system preferences had to be set to best performance. The elapsed time between the sending of the signal from the CR3000 until the actuation of the splitter valves was measured to be less than 20 ms.

### SM 2.2 Time response of splitter valves

The time response of the splitter valve was tested by recording the signal of a fast response pressure sensor (HCX series, Sensortech GmbH, Germany) mounted in a miniature inlet system (Figure 1) while the valve was opened and closed with different

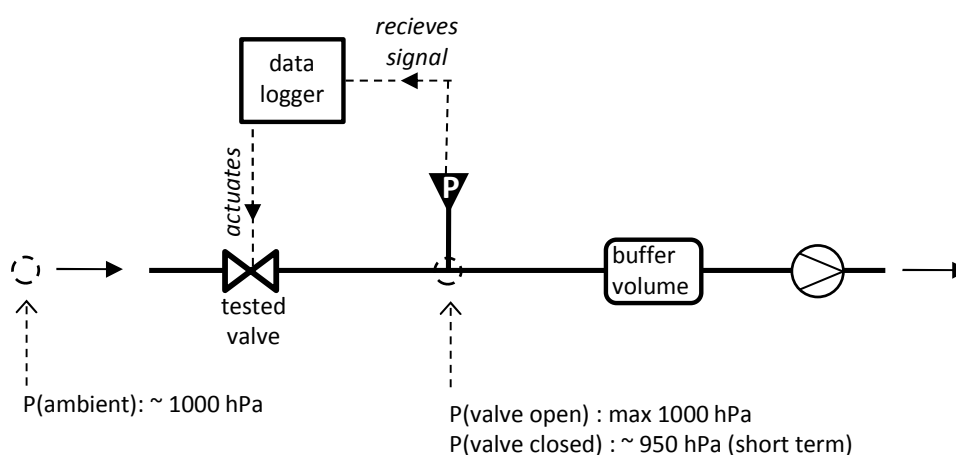


**Figure 1:** Setup used to test the response time of the splitter valves. A data logger actuates the splitter valve with a certain frequency and records the pressure

variation in a miniature inlet tube, induced by the opening and closing of the valve.

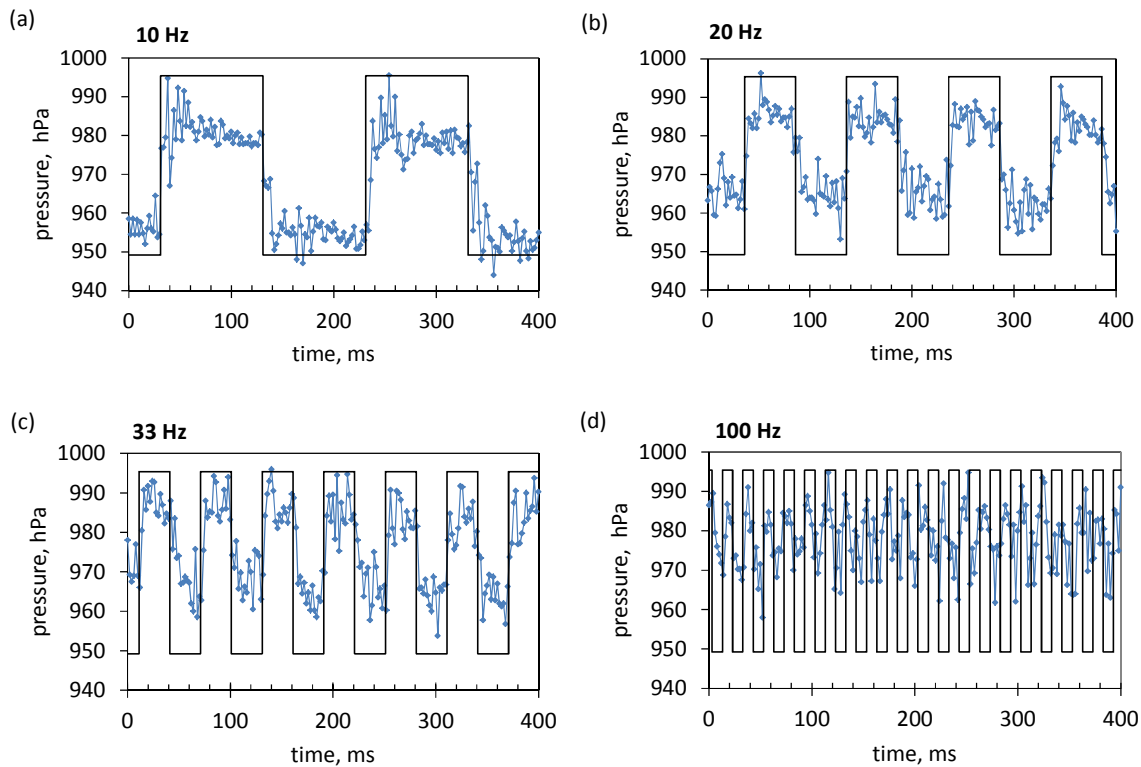


**Figure 2:** Results of the response time test of the used splitter valves. (a-d) Shown are the pressure variations induced by switching frequencies of 10, 20, 33 and 100 Hz.

frequencies. The results are shown in Fig. 2 for switching frequencies of 10, 20, 33 and 100 Hz. Whereas for 10, 20 and 30 Hz the pressure signal still follows the step function of the valve switching, at 100 Hz clear deviations are visible.

### SM 3 Calculation of random errors using Gaussian error propagation

The general form of the Gaussian error propagation equation was used to determine (a) the random flux errors, (b) the random errors of  $\Delta\chi_{O_3(MBR)}$  and (c) the random errors of the  $b$ -value. The variance of a function ( $f$ ) with  $n$  individual quantities ( $x_{i,j}$ ) is described as [e.g., *Bevington and Robinson, 2003*]:

$$\sigma_f^2 = \sum_{i=1}^n \sigma_{x_i}^2 \left( \frac{\partial f}{\partial x_i} \right)^2 + \sum_{i=1}^n \sum_{j=1}^n \left( \left( \frac{\partial f}{\partial x_i} \right) \left( \frac{\partial f}{\partial x_j} \right) \sigma_{x_i} \sigma_{x_j} r(x_i, x_j) \right), \quad i \neq j \quad (1)$$

where  $\sigma_{x_{i,i}}$  denotes the random error of the individual quantities (see Sect. 2.6.3 in main text for their determination) and  $r$  the correlation coefficient between two dependent

quantities  $(x_i, x_j)$ . In case the quantities are uncorrelated the covariance term  $(\sigma_{x_i} \sigma_{x_j} r(x_i, x_j))$  is zero. After solving the partial derivatives of  $f$  and substituting those in Eq. (1), the random error of an individual estimate of  $f$  is determined by the square root of  $\sigma_f^2$ . For the errors (a) – (c)  $f$  is defined as:

(a) for the random error of HREA flux:

$$f_{HREA} := F_{PAN} = \frac{F_{O_3}}{\Delta\chi_{O_3(HREA)}} \cdot \Delta\chi_{PAN} \quad (2)$$

and accordingly for the MBR flux:

$$f_{MBR} := F_{PAN} = \frac{F_{O_3}}{\Delta\chi_{O_3(MBR)}} \cdot \Delta\chi_{PAN} \quad (3)$$

(b) for the random error of  $\Delta\chi_{O_3(MBR)}$ :

$$f_{\Delta\chi_{O_3(MBR)}} := \Delta\chi_{O_3(MBR)} = \Delta S_{O_3}(ambient) - \Delta S_{O_3}(0) \quad (4)$$

where  $\Delta S_{O_3}(ambient)$  and  $\Delta S_{O_3}(0)$  are the calibrated differential signals at ambient and zero air measurements.

(c) Finally, for the random error of the  $b$ -value:

$$f_b := b = \frac{\overline{w'\chi_{O_3}'}}{\sigma_w \cdot \Delta\chi_{O_3(HREA)}} \quad (5)$$

where  $\overline{w'\chi_{O_3}'}$  is the covariance between the vertical wind velocity ( $w$ ) and the  $O_3$  mixing ratios measured by the fast  $O_3$  analyser. The error of  $\sigma_w$ , which is needed for the derivation of  $\sigma_b$  (see Eq. (1)), was determined using the simplified version of Eq. (1) without the covariance term. After expanding the general form of the standard deviation:

$$\sigma_w = \sqrt{\frac{1}{m-1} \sum_{i=1}^m (w_i - \bar{w})^2} \quad (6)$$

we obtain the partial derivative  $(\frac{\partial \sigma_w}{\partial w_i})$  needed in Eq. (1):

$$\frac{\partial \sigma_w}{\partial w_i} = \frac{w_i \cdot (1 - \bar{w})}{\sqrt{\sigma_w} \cdot (m-1)} \quad (7)$$

where  $m$  is the number of measurements per averaging period (i.e.  $m = 36000$  for 30 min at a sample frequency of 20 Hz). Finally, we obtain for the error of  $\sigma_w$ :

$$\sigma_{\sigma_w} = \pm \frac{s_w \cdot (1 - \bar{w})}{\sqrt{\sigma_w} \cdot (m - 1)} \sqrt{\sum_{i=1}^m w_i^2} \quad (8)$$

where  $s_w$  is the random error of a single measurement of  $w$  (given by the manufacturer as  $0.5 \text{ mm s}^{-1}$ , see Sect. 2.6.3 in main text).

The values for the correlation coefficient between the individual quantities are given in Table 1 for the HREA measurement period (for determination of  $\sigma_{F_{PAN}}$  and  $\sigma_b$ ) and Table 2 for the MBR measurement period (for determination of  $\sigma_{F_{PAN}}$ ) separated for daytime and nighttime. The covariance term was not considered for the determination of  $\sigma_{\Delta\chi_{O_3(MBR)}}$  as the correlation between  $\Delta S_{O_3}(\textit{ambient})$  and  $\Delta S_{O_3}(O)$  was not significant during both daytime ( $r = -0.01$ ) and nighttime ( $r = -0.02$ ).

**Table 1:** Matrix of correlation coefficients ( $r$ ) between HREA measurements for daytime/nighttime conditions. dependent quantities ( $x_i, x_j$ ) over the period of the

	$\Delta\chi_{PAN}$	$\Delta\chi_{O_3(HREA)}$	$F_{O_3}$	$\sigma_w$
$\Delta\chi_{PAN}$	1	0.21/0.57	-0.02/0.48	-
$\Delta\chi_{O_3(HREA)}$	-	1	0.18/0.42	-0.25/-0.45
$F_{O_3}$	-	-	1	-0.63/-0.66
$\sigma_w$	-	-	-	1

**Table 2:** Matrix of correlation coefficients ( $r$ ) between MBR measurements for daytime/nighttime conditions. dependent quantities ( $x_i, x_j$ ) over the period of the

	$\Delta\chi_{PAN}$	$\Delta\chi_{O_3(MBR)}$	$F_{O_3}$
$\Delta\chi_{PAN}$	1	0.21/0.57	-0.02/0.48
$\Delta\chi_{O_3(MBR)}$	-	1	0.18/0.42
$F_{O_3}$	-	-	1

## SM 4 Correction method for PAN mixing ratio differences during HREA operation

As demonstrated in the main article, the scatter during HREA operation was significantly larger, which suggests that pressure differences induced by the fast switching of the splitter valves or varying sample volumes may influence the quality of the PAN measurement. Indeed, we found a linear relationship between the ratio of the normalized PAN integrals measured by PCU#1 and PCU#2 and the difference between the sampled gas volumes of both PCUs ( $\Delta vol = vol\#1 - vol\#2$ ) (Figure 3). Using the slope ( $m$ ) of this relationship we could implement a correction of the normalized PAN integrals for PCU#1:

$$\left(\frac{int\#1}{vol\#1}\right)_{mod} = \frac{int\#1}{vol\#1} + \frac{1}{4}\Delta vol \cdot m \cdot \left(\frac{int\#1}{vol\#1} + \frac{int\#2}{vol\#2}\right) \quad (9)$$

and accordingly for PCU#2:

$$\left(\frac{int\#2}{vol\#2}\right)_{mod} = \frac{int\#2}{vol\#2} - \frac{1}{4}\Delta vol \cdot m \cdot \left(\frac{int\#1}{vol\#1} + \frac{int\#2}{vol\#2}\right) \quad (10)$$

Applying the correction for the HREA side-by-side measurements improved the precision by 50%, to 17.9 and 26.1 ppt, respectively. Hence, this correction was applied to all data in the post-processing of the HREA measurements.

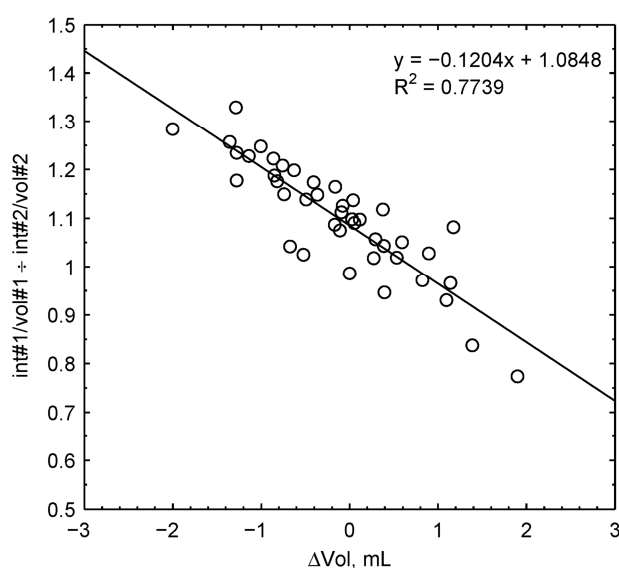


**Figure 3:** Ratio of the normalized PAN integrals measured by PCU#1 and PCU#2 versus the difference between the sampled gas volumes of both PCUs ( $\Delta vol = vol\#1 - vol\#2$ ) during the HREA side-by-side measurements (SBS\_HREA#2). The linear relationship was used to develop a correction function minimizing the random error of the HREA measurements.

## SM 5 Additional figure

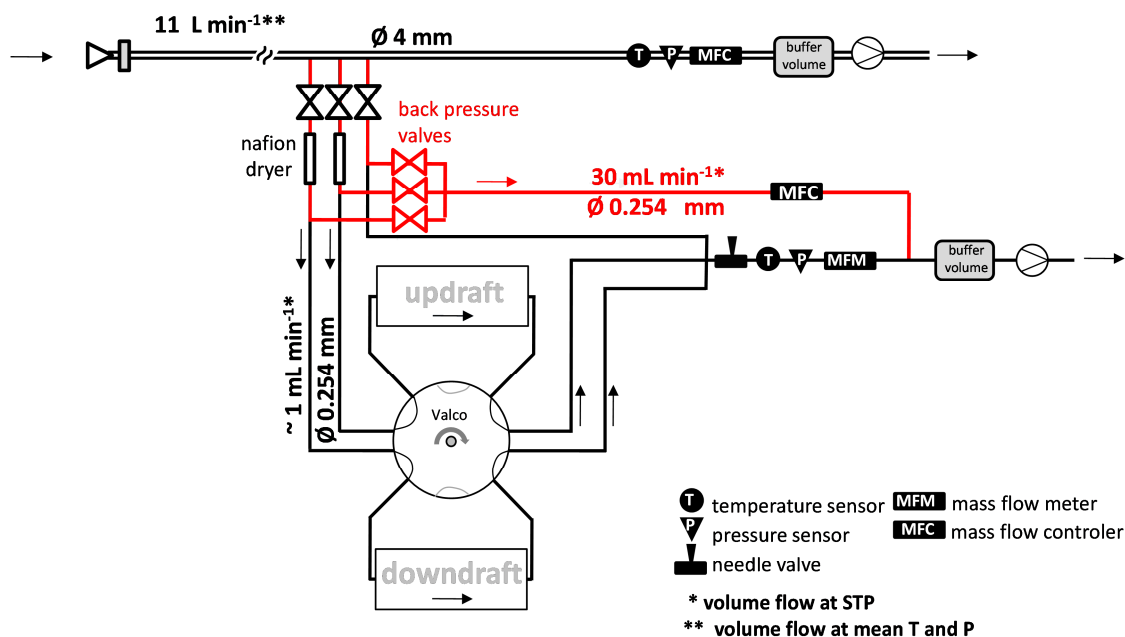


**Figure 4:** Flow scheme of PAN-flux measurement system (shown for the HREA mode), highlighting the implementation of a bypass (marked in red) to enhance the flow rate through the splitter valves and

the Nafion dryers. To prevent back-flushing of sample air into the wrong reservoir three back-pressure valves were employed, which were switched simultaneously with the respective splitter valve.

## References

- Bevington, P. R., and D. K. Robinson (2003), *Data reduction and error analysis for the physical sciences*, McGraw-Hill.
- Flocke, F. M., A. J. Weinheimer, A. L. Swanson, J. M. Roberts, R. Schmitt, and S. Shertz (2005), On the measurement of PANs by gas chromatography and electron capture detection, *J. Atmos. Chem.*, 52(1), 19-43.

# Appendix C

## **Effect of imprecise lag time and high frequency attenuation on surface-atmosphere exchange fluxes determined with the relaxed eddy accumulation method**

**A. Moravek<sup>1</sup>, I. Trebs<sup>1\*</sup> and T. Foken<sup>2,3</sup>**

<sup>1</sup> Max Planck Institute for Chemistry, Biogeochemistry Department, Mainz, Germany

<sup>2</sup> Department of Micrometeorology, University of Bayreuth, Bayreuth, Germany

<sup>3</sup> Member of Bayreuth Center of Ecology and Environmental Research (BayCEER),  
University of Bayreuth, Germany

\* now at: Centre de Recherche Public - Gabriel Lippmann, Department Environment  
and Agro-biotechnologies, Belvaux, Luxembourg

Corresponding author: A. Moravek (a.moravek@mpic.de)

Published in Journal of Geophysical Research Atmospheres

Received 11 December 2012 – Revised 9 August 2013 – Accepted 12 August 2013  
– Published 11 September 2013.

© Wiley 2013. Used with the permission from Wiley.

## Abstract

Relaxed eddy accumulation (REA) systems that employ one single long inlet tube are prone to measurement uncertainties caused by (a) an imprecisely determined lag time between the change of sign in the vertical wind velocity and the switching of the splitter valves and (b) attenuation of high-frequency concentration fluctuations in the tube flow. However, there is currently no commonly applied procedure to address these uncertainties. In this study, we first evaluated the lag time error of the volume flow, mass flow and cross-correlation method (online and offline) and experimentally determined the magnitude of high frequency attenuation for a 21.5 m long inlet tube of an operating REA system. In a second step, we simulated the impact for different artificial lag time errors and low-pass filter strengths on the REA concentration differences and, thus, on the REA flux, using high frequency time series of temperature, O<sub>3</sub>, CO<sub>2</sub> and H<sub>2</sub>O. The reduction of scalar fluxes was mainly correlated with increasing switching frequencies and ranged for typical lag time errors of the investigated REA system between < 5% and 50%, whereas the flux loss due to high frequency attenuation was between < 5% and 30%. The results were very similar for all scalar quantities. Based on our results, we derived empirical correction functions for both imprecise lag times and high frequency attenuation, discuss their potential application to correct fluxes measured with other REA systems and give a general procedure to address the uncertainties in future REA setups.

## 1 Introduction

Despite recent advancements in the development of fast trace gas measurements techniques (e.g., use of laser techniques), the determination of some chemical species still relies on slow-response analytical techniques, such as gas/liquid chromatography or slow-response mass spectrometry with a longer integration time. The time resolution of these techniques is typically lower than 0.1 s, which would be required for the use of the eddy covariance (EC) method. Hence, the relaxed eddy accumulation (REA) technique, where air samples are segregated into up- and downdraft reservoirs according to the sign of the vertical wind velocity ( $w$ ), is still a valuable method for the quantification of surface-atmosphere exchange fluxes. The REA flux is determined as

$$F_{REA} = b \cdot \sigma_w \cdot (\overline{c^+} - \overline{c^-}) = b \cdot \sigma_w \cdot \Delta c \quad (1)$$

where  $\overline{c^+}$  and  $\overline{c^-}$  denote the mean scalar concentrations during positive (updraft) and negative (downdraft) vertical wind direction [Businger and Oncley, 1990]. The respective concentration difference ( $\Delta c$ ) is multiplied by the standard deviation of the vertical wind speed ( $\sigma_w$ ) and a proportional factor ( $b$ ), which is usually determined from eddy covariance measurements of a proxy scalar.

The setup of a REA system may vary significantly, depending on the trace gas of interest and the field conditions as well as on the analytical technique [Delany et al., 1991]. Often, an in situ chemical analysis is required, especially when continuous and not only short term flux measurements are desired or in case the chemical species cannot tolerate prolonged storage. However, the trace gas analyzers often cannot be placed close to the sonic anemometer as (a) they are too bulky and would cause flow distortion, (b) they have to be operated at constant temperature and, hence, installed in an air conditioned container or (c) they require regular maintenance such as daily calibrations. Consequently, inlet lines, ranging from a few meters to several tens of meters are sometimes inevitable, especially when measuring on tall towers with the analyzers being located at the ground [e.g., Park et al., 2010].

In general, two types of REA systems exist; such with separate inlet lines for both up- and downdraft events and such with only one single inlet line. The former have the desirable advantage that air samples are segregated close to the sonic anemometer and should be preferred, if possible. However, depending on the type of reservoir (i.e. sampling bag or adsorption device), the chemical species (reactive or nonreactive) and the type of sample volume requirements of the trace gas analyzer, systems with one single inlet tube may be required [for concept see Delany et al., 1991]. Since these systems usually employ a bypass system, where subsamples are drawn from the main sample line into the reservoirs, the flow rate can be set independently from the type of reservoir and analyzer [e.g., Park et al., 2010]. This is especially important in case a high flow rate in the inlet tube is required (e.g., for reactive species) and, simultaneously, the type of reservoir requires a much lower flow rate. The latter is essential for instance, when the saturation point of an adsorption device is reached after a short time, as in case of the REA system for peroxyacetyl nitrate operated by the authors [Moravek et al., 2014]. Although their inlet line was relatively short, Ren et al. [2011] and Zhang et al. [2012] achieved also a much higher flow rate by using a single inlet with a REA system for nitrous acid, which was necessary to avoid wall reactions. Furthermore, undesired pressure pulses, which are caused by switching of the splitter valves, can be minimized by such an inlet system. These pulses can be particularly large, if the inlet lines of a system with two separate inlet tubes and no zero air addition [Nie et al., 1995] are required to be long and, thus, have a large inner volume. Finally, a

single inlet can serve as a common inlet line for REA measurements and concentration or closed-path EC measurements of other compounds [Park *et al.*, 2010].

A major challenge for all REA systems is the determination of the required lag time between the change of the sign of the vertical wind velocity and the switching of the splitter valves. Thus, the system specific time responses for (A) the detection of the change of sign of the vertical wind velocity by the digital measurement system and (B) signal processing and actuation of splitter valves as well as (C) the response time of the splitter valves have to be known. Hereby, (A), (B) and (C) are known from the manufacturer or can be determined accurately enough as they are usually very constant over time. The longitudinal separation between the sonic anemometer and the trace gas inlet introduces a further time lag (D), providing that the fluctuations of the scalar concentrations at both locations are still correlated, i.e. the eddy travel time has to be small compared to the eddy life time [Kristensen, 1979; Moore, 1986]. However, for systems with one single inlet tube as described above, the time lag created by the inlet tube (E) also has to be known. Depending on the constancy of the sample volume flow rate and on the accuracy of the lag time determination, a long inlet tube may introduce the largest error to the overall lag time determination [Ruppert, 2005], which is critical for the performance of a REA system. In most previous studies, the lag time was estimated from the average volume flow and the tube dimensions [e.g., Ren *et al.*, 2011; Zhang *et al.*, 2012] or by a timed trace gas pulse, that was released at the inlet and analyzed at the other end with a fast response analyzer [e.g., McInnes *et al.*, 1998; Oncley *et al.*, 1993; Schade and Goldstein, 2001]. Ruppert [2005] and Park *et al.* [2010] determined the time lag between the sonic and the splitter valves via cross-correlation [McMillen, 1988] between the vertical wind velocity and measured trace gas concentration, using a built-in, fast trace gas analyzer. While the former approach only accounts for the residence time in the tube (E), the latter includes the time lags (D) and (E). The effect of an erroneous lag time on REA was first discussed by J M Baker *et al.* [1992], who provide a theoretical correction function. Other studies simulated the effect on their REA fluxes using a proxy scalar [Ammann, 1998; B Baker *et al.*, 1999; Beverland *et al.*, 1996a, 1996b; Schade and Goldstein, 2001]. However, these results differ considerably amongst each other and large discrepancies to the function by J M Baker *et al.* [1992] exist. It is often assumed for REA measurements with low switching frequencies, e.g., above forests, that the lag time error has no significant effect on the REA fluxes [Park *et al.*, 2010; Zhang *et al.*, 2012].

Besides the challenge of an accurate lag time determination, the application of a long inlet tube introduces the problem of high frequency attenuation, which reduces the measured concentration differences in the REA reservoirs and, thus, leads to an underestimation of the REA flux. The damping of higher frequencies is due to

differential advection caused by the radial variation of the mean velocity and simultaneous radial diffusion of the sample gas [Lenschow and Raupach, 1991; Taylor, 1953; 1954]. Physical adsorption and desorption at the tube walls as in the case of water vapor lead to an additional high frequency attenuation [e.g., Ammann et al., 2006; Ibrom et al., 2007; Massman and Ibrom, 2008]. Typically, turbulent flow is maintained to minimize these effects [Lenschow and Raupach, 1991]. For post-processing of closed-path eddy covariance data empirical transfer functions are applied to compensate for the damping effect of long tubing [Lenschow and Raupach, 1991; Leuning and Judd, 1996; Massman, 1991], or a correction factor is determined experimentally by the comparison of an attenuated and nonattenuated spectrum [Aubinet et al., 2000; Ibrom et al., 2007; Leuning and King, 1992]. In contrast, for the application of REA systems usually no corrections for high frequency attenuations are applied. It is argued by several authors that the expected effect for their setup would be small [e.g., Ammann, 1998; Park et al., 2010; Schade and Goldstein, 2001; Zhang et al., 2012] or the effect is considered less significant as often fluxes of compounds measured by REA systems are prone to higher uncertainties.

In this study, we discuss the effect of an erroneous lag time and high frequency attenuation on REA fluxes caused by a single long inlet tube. The knowledge of the potential effects is important for choosing the most appropriate design for a REA system, which guarantees accurate conditional sampling and at the same time provides optimal conditions for the chemical analysis of the scalar concentration differences. Many previous studies based their error estimates on rough assumptions or did not address potential uncertainties. Up to date no comprehensive study was performed, which evaluates the effect of lag time errors and high frequency attenuation on REA fluxes when using one single long inlet tube. In addition, the impact of differences between scalar quantities and the role of applying a dead band, a threshold which is applied to increase  $\Delta c$  values for the chemical analysis, has not been studied so far. We used a sophisticated experimental setup to examine first the potential errors of lag times determined with different methods and the high frequency attenuation of the inlet tube. In a second step, we used these results to simulate the impact on the REA concentration differences and, hence, on the determined REA flux. This included the application of different dead band sizes and the investigation of the effect on different scalars. Finally, we provide a general procedure to assess these challenges in future applications of the REA method.

## 2 Methods

### 2.1 Experimental setup

Our analysis is based on the inlet tube of an operating REA system, which was designed for the measurements of trace gas fluxes of peroxyacetyl nitrate and was employed above a natural steppe-like grassland ecosystem (mean canopy height of 0.6 m) in Rhineland-Palatinate (Mainz-Finthen, Germany) in August and September 2011 (a detailed description of the measurement setup will be presented in a subsequent publication). The system used one single inlet tube with a length of 21.5 m and an inner diameter of 4 mm ( $\pm 0.1$  mm tolerance) (Figure 1). The material of the tube was opaque perfluoroalkoxy (PFA), which is suitable to minimize wall effects and photolysis of reactive compounds. The mean volume flow rate was kept constant at  $11 \text{ L min}^{-1}$  by a mass flow controller (Bronkhorst High-Tech, Netherlands), which ensured turbulent flow ( $Re \sim 3800$ ). A LabVIEW (National Instruments, USA) software program regulated the mass flow controller to maintain a constant mean volume flow. Consequently, the mean velocity in the tube was kept constant despite potential pressure or temperature changes, thereby minimizing the variations of the residence time in the tube. Assuming a linear increase of the volume flow due to a linear pressure decrease, the mean volume flow was determined as the average between the volume flow at the inlet and at the position of the splitter valves. For the latter, both a pressure (HCX series, Sensortech GmbH, Germany) and a temperature sensor were connected to the tubing in front of the mass flow controller. The former was derived using ambient air temperature and pressure measurements.

In front of the inlet a HDC-II particle filter (Pall Corporation, USA) was installed. In contrast to commonly used membrane filters, this filter type ensured a lower pressure drop in general and minimized the typically increasing pressure drop with time due to contamination.

The inlet of the tube was mounted next to a CSAT3 (Campbell Scientific Inc., USA) anemometer at 3 m a.g.l., with a horizontal separation distance of 25 cm [Kristensen *et al.*, 1997; Lee and Black, 1994; Moore, 1986]. At the same distance, a fast response open-path  $\text{CO}_2/\text{H}_2\text{O}$  analyzer (LI-7500A, LI-COR, USA) was installed. This sensor was used as a reference for  $\text{CO}_2$  fluxes to study both the lag time and high frequency attenuation. Downstream of the splitter valves a second LI-7500A analyzer was installed, which was equipped with a glass cuvette (ID 1.5 mm, length 117 mm) with two  $\text{CaF}_2$  windows. These are transparent in the infrared absorption bands of  $\text{CO}_2$  and  $\text{H}_2\text{O}$ , such that the LI-7500A could be used as a closed-path analyzer.

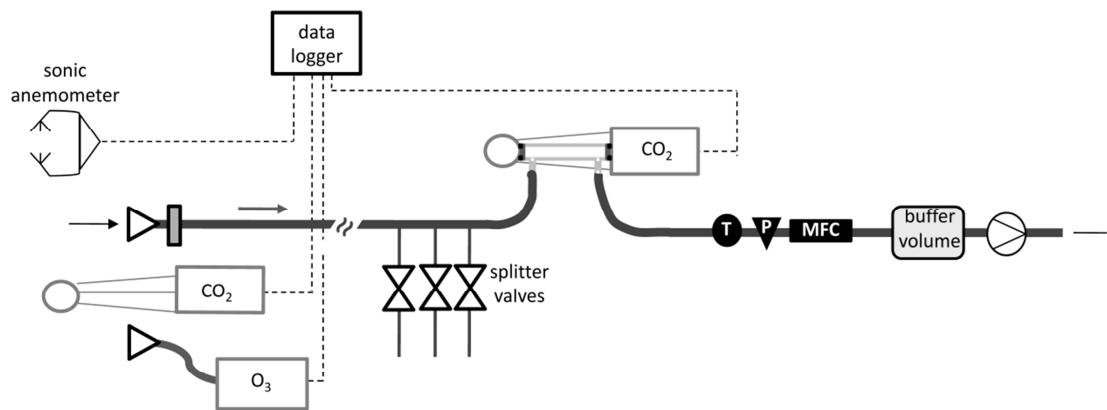


**Figure 1:** Scheme of the experimental setup used for the evaluation of the lag time and high frequency attenuation of a REA system. The sample air is drawn through the 21.5 m long inlet tube and maintained at a constant volume flow by a mass flow controller (MFC), a pressure (P) and temperature (T) sensor. A buffer volume was implemented upstream of the membrane pump to ensure a constant performance of the mass flow controller. Behind the splitter valves (used to separate updraft, downdraft and dead band events

during the REA application) a closed-path high frequency  $\text{CO}_2/\text{H}_2\text{O}$  analyzer is employed. Its  $\text{CO}_2$  signal is compared to the one from the open-path  $\text{CO}_2/\text{H}_2\text{O}$  analyzer mounted next to the inlet. Additionally, a sonic anemometer and a fast response  $\text{O}_3$  detector are mounted next to the inlet, which are used for the determination of updraft and downdraft events and the calculation of the hyperbolic dead band, respectively (see text for more details).

The internal time delay of both LI-7500A analyzers was set to 300 ms. Furthermore, we installed a high frequency ozone ( $\text{O}_3$ ) detector [Enviscope GmbH, Germany; see Zahn *et al.*, 2012] with its 2.5 m long inlet tube positioned at the same lateral distance to the sonic path (25 cm). Cross-correlation analysis revealed a lag time of around 1.3 s and showed a high frequency attenuation of the  $\text{O}_3$  time series by a smoother cross-correlation peak. The signals of all trace gas analyzers and of the CSAT3 were recorded by a CR3000 data logger (Campbell Scientific Ltd., USA) and sampled at a frequency of 20 Hz.

## 2.2 Lag time error

To be able to analyze the effect of an imprecisely determined lag time ( $t_{lag}$ ) on REA fluxes an evaluation of possible errors in the lag time determination and its possible variations over time is required. In this study, we used the volume flow measurements and online cross-correlation to determine the lag time of the REA system. To derive the lag time by the former method, we used the continuously measured actual mean volume flow, which could vary slightly from the set value due to delays in the control mechanism and deviations from the assumed average inner tube diameter of 4.0 mm. Since this method only accounts for the residence time of sampled air in the tube (denoted as (E) in Chapter 1), the time lag between the sonic and the splitter valves was

determined by cross-correlation between the vertical wind velocity and the CO<sub>2</sub> signal from the closed-path LI-7500A analyzer, which accounts mainly for both lag (D) and lag (E). Here, the internal time delay of the CSAT3 (100 ms) and the LI-7500A analyzer (300 ms) had to be considered. The cross-correlation was calculated online before the start of every sampling period on the basis of the last 30 min by the REA software program during the operation of the REA system, from 9 Sep to 28 Sep 2011.

Additionally, we simulated the REA fluxes of sensible and latent heat, CO<sub>2</sub> and O<sub>3</sub> for different shifts in the lag time ( $\Delta t_{lag}$ ). We artificially shifted the 20 Hz time series of the scalars in relation to the vertical wind velocity by 50, 100, 200 and 400 ms (more shifts were made but will not be shown), and then calculated the REA fluxes for these scalars by a simulation analysis. The pre-processing steps of the datasets for the REA simulation were: (1) removal of spikes and outliers, (2) coordinate rotation of the wind vector using the double rotation method [Kaimal and Finnigan, 1994] and (3) correction for the lag time between the vertical wind velocity and the high frequency scalar time series using the cross-correlation method. The sampling period for the REA simulation was set to 30 min.

The ratio between REA flux calculated from the shifted time series ( $F_{REA_{lag}}$ ) and the nonshifted time series ( $F_{REA_{ideal}}$ ) yields the flux recovery

$$Rec_{lag} = \frac{F_{REA_{lag}}}{F_{REA_{ideal}}} = \frac{\Delta c_{lag}}{\Delta c_{ideal}} \quad (2)$$

which equals to unity, when no flux loss is observed. Previous studies have found that the flux recovery  $Rec_{lag}$  decreases with increasing values of the so-called eddy reversal frequency [Ammann, 1998; J M Baker et al., 1992; Beverland et al., 1996a, 1996b]. The latter is the average frequency at which the vertical wind speed changes sign over the sampling period. According to J M Baker et al. [1992], the eddy reversal frequency can be defined by the mean duration of updraft and downdraft events over the sampling period,  $\bar{t}_U$  and  $\bar{t}_D$ :

$$erf = \frac{2}{\bar{t}_U + \bar{t}_D} \quad (3)$$

If no dead band is applied, this eddy reversal frequency also represents the frequency of valve switching during the REA application. The eddy reversal frequency increases with increasing turbulence intensity and smaller eddy sizes and is therefore a function of friction velocity, stability conditions and the measurement height. In our experiment the eddy reversal frequency ranged from 1 to 6 Hz.

Furthermore, we simulated the effect of different dead band sizes by applying the hyperbolic relaxed eddy accumulation (HREA) method [Bowling *et al.*, 1999] to increase  $\Delta c$  with a threshold  $H$  defined as

$$H \geq \left| \frac{w' \cdot c'_{proxy}}{\sigma_w \cdot \sigma_{c_{proxy}}} \right| \quad (4)$$

where  $w'$  and  $c'_{proxy}$  are the Reynolds fluctuation of the vertical wind velocity and a proxy scalar. In our study, we used  $H$  values of 0.4, 0.8 and 1.2 and CO<sub>2</sub> as a proxy scalar for all scalar fluxes, which provided for comparison reasons the same switching pattern for all scalar fluxes.

As part of the data quality control we applied the quality scheme of *Foken and Wichura* [1996] to exclude periods with significant nonstationarity or poor developed turbulence. Furthermore, periods where the EC flux was not significantly different from zero or was within pre-defined limits (sensible heat flux  $\pm 5.8 \text{ W m}^{-2}$ , O<sub>3</sub> flux  $> -0.072 \text{ nmol m}^{-2} \text{ s}^{-1}$ , CO<sub>2</sub> flux  $\pm 0.02 \text{ mmol m}^{-2} \text{ s}^{-1}$ , latent heat flux  $\pm 0.02 \text{ mmol m}^{-2} \text{ s}^{-1}$ ) were omitted. The quality of the cross-correlation was visually checked for each 30 min period, and periods where the maximum correlation coefficient was below 0.1 were removed. Finally, conditions with extreme  $z/L$  values, which were the cause for outliers of the  $b$ -value, were omitted.

### 2.3 High frequency attenuation

To evaluate the effect of high frequency attenuation caused by a long inlet tube for the REA application, we first determined the transfer function of the inlet tube, using both a theoretical and experimental approach. Subsequently, these results were applied to the REA method by simulating the REA sampling with both attenuated and nonattenuated CO<sub>2</sub> time series.

For a closed-path system with an infrared gas analyzer as it was employed in our system setup (Figure 1), the high frequency attenuation of a scalar ( $s$ ) is described by the total transfer function  $T_s(f)$ :

$$T_s(f) = G_s(f) \cdot T_{ps}(f) \cdot T_{ta}(f) \quad (5)$$

where  $T_{ta}(f)$  is the transfer function which accounts for the high frequency loss by the inlet tubing [Moore, 1986].  $G_s(f)$  represents the gain function for the high frequency loss by the scalar sensor according to its time constant, and  $T_{ps}(f)$  is the transfer function for the scalar line averaging due to the path length of the infrared gas analyzer. The effect of the transfer function on the scalar time series can be described in the frequency domain as

$$S_{s_{att}}(f) = S_s(f) \cdot T_s(f) \quad (6)$$

where  $S_{s_{att}}(f)$  denotes the power spectrum of the attenuated and  $S_s(f)$  of the nonattenuated scalar time series.

### 2.3.1 Experimental transfer function

The high frequency attenuation effect of the inlet system was evaluated experimentally by the comparison of attenuated CO<sub>2</sub> power spectra of the closed-path LI-7500A analyzer with the nonattenuated spectra of the open-path CO<sub>2</sub> analyzer (Figure 1). Here, the transfer function  $T_s^{exp}(f)$  is derived experimentally by the ratio of the power spectrum of the attenuated signal ( $S_{s_{cp}}^{exp}$  from the closed-path sensor) and the power spectrum of the nonattenuated signal ( $S_{s_{op}}^{exp}$  from the open-path sensor):

$$T_s^{exp}(f) = \frac{N_{op} \cdot S_{s_{cp}}^{exp}(f)}{N_{cp} \cdot S_{s_{op}}^{exp}(f)} \quad (7)$$

As proposed by Aubinet *et al.* [2000], we normalized the power spectra not by the variance but by a normalization factor  $N$ , which is the integral of the power spectrum excluding the attenuated part of the spectrum. The ratio between the normalization factors of the open-path  $N_{op}$  and the closed-path spectrum  $N_{cp}$  is then defined as

$$\frac{N_{op}}{N_{cp}} = \frac{\int_0^{f'} S_{s_{op}}^{exp}(f) df}{\int_0^{f'} S_{s_{cp}}^{exp}(f) df} \quad (8)$$

where  $f'$  is the limit frequency, which is low enough for the attenuation to be negligible in the integral of the closed-path spectrum. Since  $T_{ps}(f)$  was equal for both the open-path and the closed-path analyzer and assuming a similar time constant of both analyzers, reveals that the experimentally determined function  $T_s^{exp}(f)$  represents only the high frequency attenuation due to the air transport in the tubing as described by  $T_{ta}^{exp}(f)$  (see equation 5)

$$T_s^{exp}(f) = \frac{T_{s_{cp}}(f)}{T_{s_{op}}(f)} = \frac{G_s(f) \cdot T_{ps}(f) \cdot T_{ta}^{exp}(f)}{G_s(f) \cdot T_{ps}(f)} = T_{ta}^{exp}(f) \quad (9)$$

It should be noted that in our setup the  $T_{ta}^{exp}(f)$  also included a possible damping effect of the inlet filter. Furthermore, the time constant of the analyzers represents the electronic time constant, which was equal for both as the same type of analyzer was used, and the response due to the air residence time in the sample volume. The latter was around 80 ms for the closed-path analyzer and ranged between 1.6 and 80 ms for the open-path analyzer depending on the horizontal wind speed. However, a test with two closed-path analyzers, one installed at the inlet downstream of the particle filter and

the other close to the splitter valves, revealed that the influence of the cuvette on the overall damping was negligible.

### 2.3.2 Theoretical transfer function

Besides determining  $T_{ta}(f)$  experimentally, we used a theoretical approach often used for the post-processing of eddy covariance data. The low-pass filtering due to the air transport in the inlet tubing,  $T_{ta}^{theo}(f)$ , was proposed by *Lenschow and Raupach* [1991] and *Leuning and King* [1992]:

$$T_{ta}^{theo}(f) = e^{\frac{-160 \cdot Re^{-1/8} \cdot r \cdot f^2 \cdot L}{\bar{u}^2}} \quad (10)$$

for turbulent flow (i.e.  $Re \geq 2300$ ) where  $Re$  is the Reynolds number,  $r$  the tube radius,  $L$  the tube length and  $\bar{u}$  the mean horizontal wind speed. The Reynolds number is defined as  $Re = \frac{2 \cdot Q}{\pi \cdot r \cdot \nu}$ , in which  $Q$  is the volumetric flow rate in the tube and  $\nu$  the kinematic viscosity.

### 2.3.3 Simulating the effect on REA fluxes

To transfer the high frequency attenuation effect to the REA flux measurements, we used the information provided by both  $T_{ta}^{exp}(f)$  and  $T_{ta}^{theo}(f)$  to low-pass filter the nonattenuated CO<sub>2</sub> signal of the open-path sensor. As suggested by other authors [*Goulden et al.*, 1997; *Ibrom et al.*, 2007], we used a first-order recursive filter. Such a recursive filter accounts in contrast to a symmetric filter for a phase shift under turbulent conditions caused by radial turbulent diffusion and a characteristic radial velocity profile [*Massman*, 1991; *Massman and Ibrom*, 2008] as well as by sorption/desorption processes at the tube walls as demonstrated for nonpassive tracers like H<sub>2</sub>O and O<sub>3</sub> [*Ammann et al.*, 2006; *Massman and Ibrom*, 2008]. The filter is defined in the time domain as

$$c_{att_n} = c_n \cdot A + (1 - A) \cdot c_{att_{n-1}} \quad (11)$$

where  $c$  is the scalar signal,  $c_{att}$  the attenuated scalar signal and  $A$  the dimensionless filter constant. For a given sampling frequency ( $f_s$ ), this constant depends on the so-called cut-off frequency ( $f_c$ ), which is the frequency at which the filter reduces power by a factor of two:

$$A = 1 - e^{-2\pi(f_c/f_s)} \quad (12)$$

Thus, we determined  $f_c$  by fitting the Lorentzian sigmoidal function, that is an approximation of the first order filter function (equation 11) in the frequency domain,

$$T_L = \frac{1}{1 + (f/f_c)^2} \quad (13)$$

to the experimental transfer function  $T_{ta}^{exp}(f)$  [Ibrom *et al.*, 2007]. Hereby, we used the mean values of  $T_{ta}^{exp}(f)$  for several days, after applying quality criteria including stationarity, developed turbulence and the signal to noise ratio of the variance.

Subsequently, we simulated a REA system, using both the filtered and nonfiltered time series of CO<sub>2</sub>, H<sub>2</sub>O, O<sub>3</sub> and temperature and derived a flux recovery as it was provided for the lag time by equation 2:

$$Rec_{HFA} = \frac{F_{REA\_HFA}}{F_{REA\_ideal}} = \frac{\Delta C_{HFA}}{\Delta C_{ideal}} \quad (14)$$

The same data pre-processing steps as for the lag time simulation were applied and the same dead band sizes were used. The sampling period was also set to 30 min.

Another approach to determine the attenuation effect on the REA fluxes would be to directly use the attenuated CO<sub>2</sub> signal of the closed-path sensor for the REA simulation. However, the approach used here has the advantage that it can easily be applied to a long data record, once the tube effects are characterized.

## 3 Results and Discussion

### 3.1 The effect of an imprecisely determined lag time on REA fluxes

#### 3.1.1 Variations of the lag time

The errors of the lag time determined with the online cross-correlation method as well as from continuous volume flow and mass flow measurements were investigated by the identification of both random ( $\sigma$ ) and systematic ( $\delta$ ) errors. As shown in Figure 2a, for all methods the mean lag time varied about 1.5 s, however, we observed significant variations.

#### Errors associated with the online cross-correlation method

The online cross-correlation method yields a much larger variation of the lag time than the volume flow method, ranging from 1.3 to 1.75 s during the investigated time period. Since this method accounts next to the residence time in the tube (E) also for the sensor separation effect (D), wind speed and wind direction have a significant influence on the lag time. Figure 2b shows a linear relationship between the lag time and the cosine of

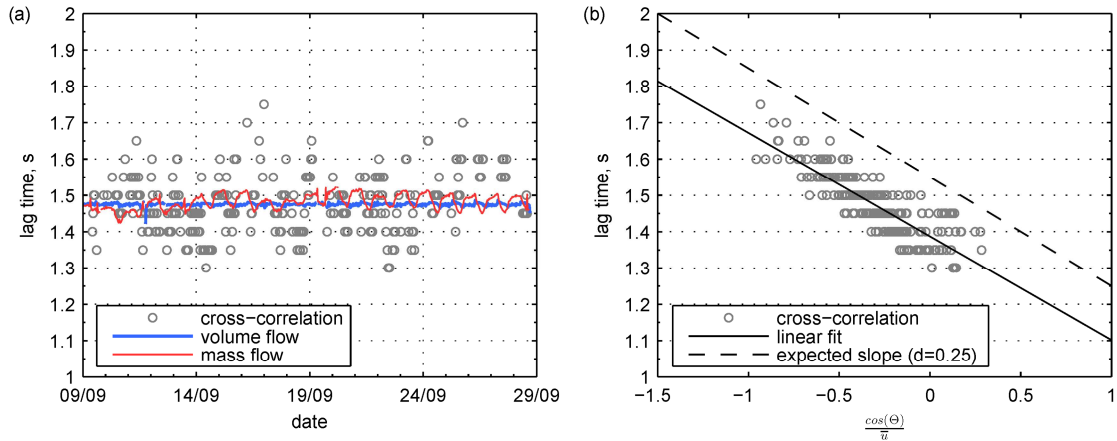


**Figure 2:** **a)** Variations of the lag time determined by cross-correlation, volume flow rate and mass flow over a period of three weeks. **b)** Lag time determined by cross-correlation as a function of the ratio of the angle

between the sonic-inlet axis and the current wind direction ( $\theta$ ) and the mean horizontal wind speed ( $\bar{u}$ ). The dashed line represents the expected slope for a separation distance of 25 cm (see text).

the angle between the sonic-inlet axis and the current wind direction ( $\theta$ ) normalized by the mean horizontal wind speed ( $\bar{u}$ ). The slope of the fit is in very good agreement with the expected slope for a separation distance ( $d$ ) of 25 cm. The expected slope is determined according to equation 16, where the sign depends on the orientation of the coordinate system. However, we observed a variation of the lag time of  $\pm 100$  ms that is not due to the separation effect. Due to the occurrence of dispersion effects in the tubing (Taylor [1954], for discussion see section 3.2.1) the correlation function shows a much wider peak compared to an open-path sensor (Figure 3), which introduces an error to the cross-correlation method. Since the maximum of the average correlation function has a rough width of 200 ms, we can fully attribute the variations around the fit in Figure 2b to the error of the online cross-correlation method. Hence, we can define the error of the lag time, when using the online cross-correlation method, by the standard deviation after subtracting a term for the sensor separation from the lag time ( $t_{lag\_cross}$ ):

$$\sigma_{lag\_cross} = \pm \sigma \left( t_{lag\_cross} - d \cdot \frac{\cos(\theta)}{\bar{u}} \right) \quad (15)$$

Due to the direct measurement of the lag time, the online cross-correlation is not primarily prone to systematic errors.

### Errors associated with the continuous volume and mass flow method

As the flow rate in the tube was regulated according to the mean volume flow, the lag time derived from the volume flow is very constant over time. The random error of the lag time ( $\sigma_{lag\_vol}$ ) is retrieved by the standard deviation and reaches  $\pm 5$  ms. Those fluctuations around the mean are probably caused by the response time of the mass flow controller (1–2 s). The effect of random errors in the pressure and temperature readings,

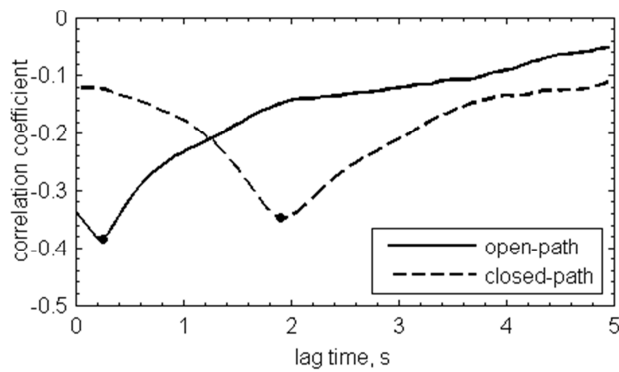


**Figure 3:** Correlation coefficient ( $r$ ) from the cross-correlation analysis between the vertical wind velocity and the CO<sub>2</sub> signals from both the open-path and closed-path CO<sub>2</sub> analyzer. The example is based on data from 12:00 to 12:30 CET at 21 September 2011. The black circles mark the position of the maximum negative correlation as determined online by the REA software.

which were used for the conversion from mass to volume flow, was found to be negligible ( $< 5$  ms).

A significant contribution to the total systematic error ( $\delta_{lag\_vol}$ ) is an erroneous tube radius. In our case the tolerance of  $\pm 0.1$  mm in the tube radius may lead to a systematic error of up to  $\pm 75$  ms, however, the true value was not determined in this study. Another systematic error source is the pressure drop induced by the particle filter, which enhances the volume flow downstream of the filter. Since we used ambient pressure and temperature to calculate the volume flow at the inlet and assumed a linear pressure decrease in the tubing, a large pressure drop induced by the particle filter would lead to a significant underestimation of the lag time. The pressure drop may also be enhanced due to filter contamination and may vary due to humidity effects. Both influences were observed when polytetrafluoroethylene (PTFE) membrane filters were used. However, the HDC-II particle filters applied here induced only a pressure drop of about 10 to 15 mbar, and the constant pressure measured in the tube indicated that errors due to contamination or humidity effects could also be neglected here. REA systems which maintain a constant mass instead of a constant volume flow introduce an additional systematic error to the lag time. This is shown in Figure 2a by the theoretical lag time if the flow rate had been regulated to a constant mass flow. In this case, the lag time shows a clear diurnal cycle and accounts for a systematic error of approximately  $\pm 20$  ms. As both methods, the determination from the volume and the mass flow, do not account for the sensor separation effect, a systematic error of the lag time is described by

$$\delta_{lag\_ss} = d \cdot \frac{\cos(\theta)}{\bar{u}} \quad (16)$$

This systematic error is especially large for low wind speeds and wind direction along the sonic-inlet axis and may account for more than  $\pm 200$  ms in our case.

### 3.1.2 Lag time effect on REA fluxes

Since lag time errors of other REA systems may be larger than the range observed here, we performed simulations of the REA flux with error values up to  $\pm 400$  ms. The REA simulation shows a flux loss when the scalar time series are artificially shifted against the time series of the vertical wind velocity. As it was also found in previous studies, the flux recovery  $Rec_{lag}$  decreased with increasing values of the so-called eddy reversal frequency (Figure 4).

In addition, the flux recovery decreased near-linearly with an increasing lag time. For large lag times shifts the magnitude of the flux reduction is similar for all scalars and reaches up to 30% ( $\Delta t_{lag} = 0.2$  s) and 50% ( $\Delta t_{lag} = 0.4$  s). For small lag time shifts, the effect is most pronounced for the sensible heat flux (Figure 4a), leading to a flux reduction of up to 10% ( $\Delta t_{lag} = 0.05$  s) and 20% ( $\Delta t_{lag} = 0.1$  s). The reduction of the O<sub>3</sub> flux (Figure 4b) is only small ( $< 10\%$ ) for small lag times shifts. This is caused by high frequency attenuation effects of the inlet tube of the O<sub>3</sub> analyzer, which results in a smoother cross-correlation peak, and thus in a reduced effect of an imprecise lag time. A high frequency attenuation effect is also visible for the CO<sub>2</sub> flux (Figure 4c) and the latent heat flux (Figure 4d), and their flux reduction for small lag time shifts is between the one for sensible heat and O<sub>3</sub> flux. Due to the near-linear dependency on the lag time, we could define a quadratic fit function:

$$Rec_{lag} = 1 - a \cdot \Delta t_{lag} \cdot erf^2 \quad (17)$$

where  $a$  is a factor which varies slightly for the different scalars. The best agreement of this general function with the individual fit functions was found for the sensible heat flux ( $a = 7.2 \cdot 10^{-2}$ ). The general fit function for the O<sub>3</sub> flux ( $a = 4.0 \cdot 10^{-2}$ ), which was the most subject to high frequency attenuation, overestimates the effect for small and underestimates it for large lag time shifts. The fit functions for the latent heat and the CO<sub>2</sub> flux are very similar, which is represented by values of  $a$  of  $6.2 \cdot 10^{-2}$  and  $6.1 \cdot 10^{-2}$ , respectively.

Evaluating the shape of the determined fit function, we found that the main reason for the observed quadratic decline is the double dependency of  $Rec_{lag}$  on the eddy reversal frequency. On the one hand, the flux loss is larger for an increased ratio between the time lag and the mean duration of updraft or downdraft events, where the latter is represented by the inverse of the eddy reversal frequency. On the other hand, the flux loss is also larger for scalar time series with a high “periodicity”, which occurs under high eddy reversal frequencies, as they usually show a faster increase or decrease with time after the change of sign of the vertical wind velocity, measured against the mean scalar concentration during the respective updraft or downdraft event. This is illustrated

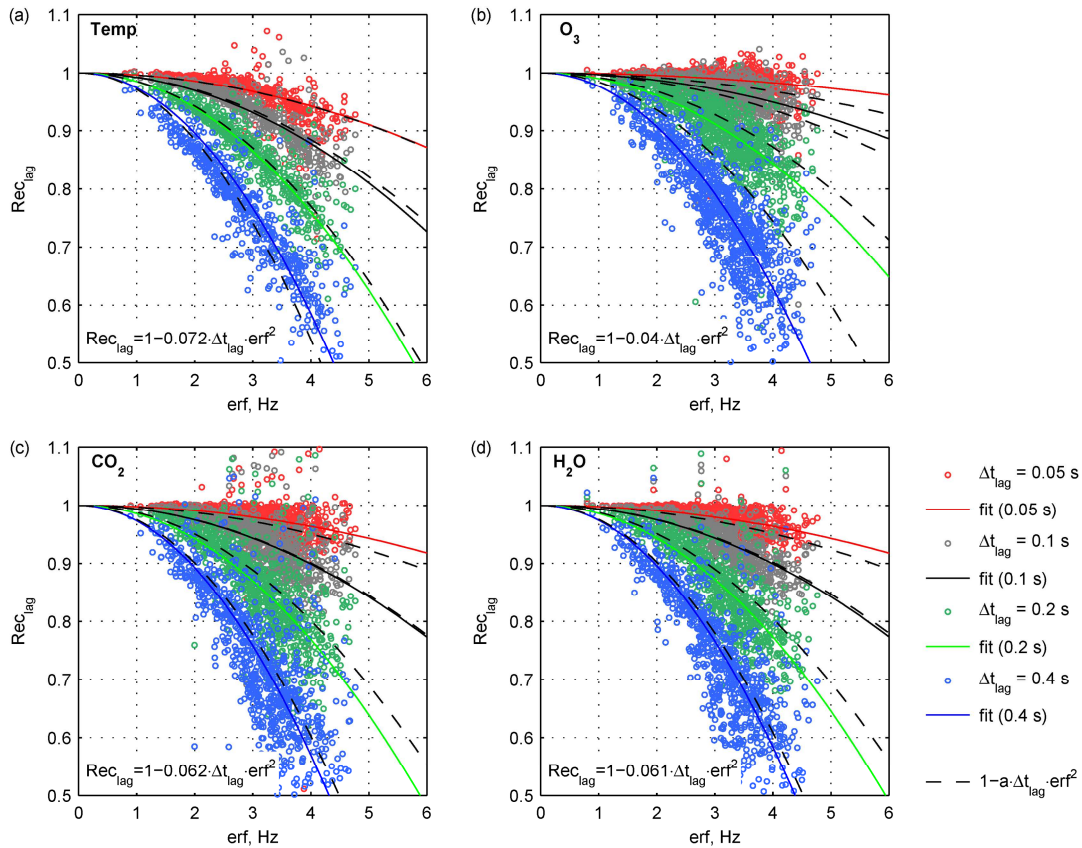


**Figure 4:** Simulated REA flux recovery ( $Rec_{lag}$ ) as a function of the eddy reversal frequency ( $erf$ ) showing the effect of different artificial lag times of 0.05, 0.1, 0.2 and 0.4 s on (a) sensible heat flux, (b)  $O_3$  flux

(c)  $CO_2$  flux and (d) latent heat flux. Evaluated was the time period from 1 to 31 August 2011 at the natural grassland site. Shown are the results without the application of a dead band.

in a conceptual model in Figure 5a, where the scalar time series is simplified by a sine-shaped function of two different periodicities. Comparing our results to the fit functions of *Ammann [1998]* and *Beverland et al. [1996b]* (Figure 5b), we find similar decline of  $Rec_{lag}$  with the eddy reversal frequency, however, their findings suggest a larger effect on the REA fluxes. The linear dependency given by *Beverland et al. [1996a]* for a spruce forest is within the same range, however, it also shows positive values, which could not be explained by the authors. The line by *J M Baker et al. [1992]* is based on a theoretical approach accounting for the concentration change in the reservoirs due to a shift in the lag time. They assume in their model stationarity in the instantaneous concentrations of upward and downward eddies, which is illustrated in Figure 5a by a rectangular function of the scalar concentration over time. As a result, the effect of the eddy reversal frequency on the flux recovery is systematically overestimated compared to the experimentally derived functions. The reasons for the differences between the experimentally derived functions might be different meteorological conditions, site characteristics, measurement setups as well as differences in the source and sink distribution of the used scalar quantities. The latter can be excluded as the flux recovery

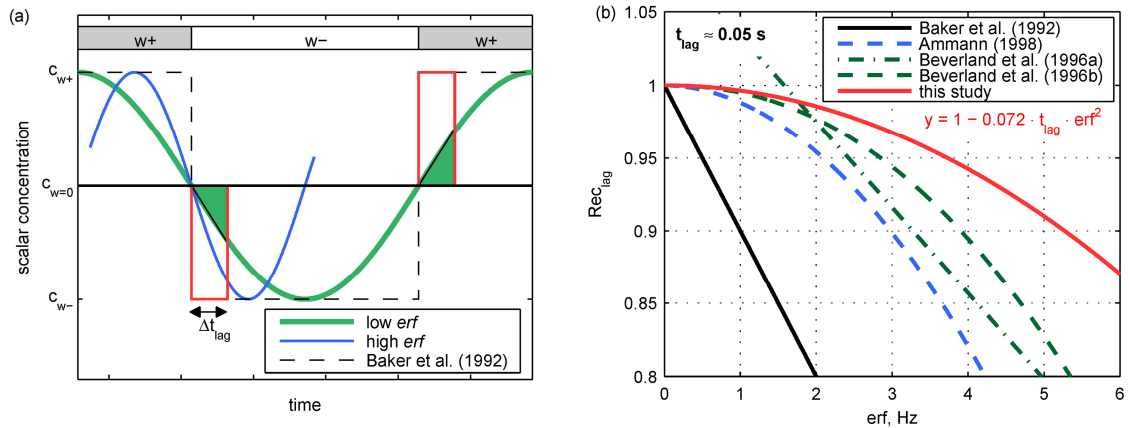


**Figure 5:** (a) Conceptual model illustrating the effect of an erroneous lag time on the conditional sampling for different shapes of an idealized scalar time series, where the red box marks the delayed switching due to an erroneous lag time. As a result, a fixed fraction (green areas below green curve) of the original updraft or downdraft events is sampled into the wrong reservoirs. The effect on the conditional means depends (1) on the ratio of the lag time shift to the mean duration of updraft or downdraft events and (2) on the incline of the green curve within the lag time shift. Hence, for the blue curve, which has a higher periodicity (or eddy reversal frequency in our context)

the steeper incline (2) results in a larger flux loss due to the erroneous lag time as it would be expected by the increase of the ratio of lag time shift and the mean sample time (1). For the same reason, the model by Baker et al. [1992] systematically overestimates the flux loss due to the rectangular shape of the assumed scalar time series. (b) Exponential fit of the sensible heat flux data shown in Figure a for a lag time of 0.05 s compared to the functions of Baker et al. [1992], Beverland et al. [1996a, 1996b] and Ammann [1998]. The quadratic decline of  $Rec_{lag}$  can be explained by the dependency of the effects (1) and (2) in Figure a on the eddy reversal frequency.

from the presented REA simulation shows a similar dependency on the eddy reversal frequency for all scalar quantities (Figure 4a–d). To evaluate the influence of site characteristics and the measurement setup, we additionally simulated the lag time effect on the sensible heat flux with data sets from two other grassland sites in Germany (for site description see Stella et al. [2013] and Mayer et al. [2011]) with a different setup (i.e. measurement height and type of sonic anemometer) and retrieved a fit function (equation 17). The values of  $a$  are  $7.2 \cdot 10^{-2}$  and  $7.8 \cdot 10^{-2}$ , respectively, which compares well to the values for the presented study ( $a = 7.2 \cdot 10^{-2}$ ). We additionally analyzed the sensible heat flux measurement at a forest clearing ( $a = 7.3 \cdot 10^{-2}$ ) and above a spruce forest canopy ( $a = 1.4 \cdot 10^{-1}$ ) at the same experimental site for the same time period [Foken et al., 2012]. The latter differs significantly from the clearing, which suggests that meteorological conditions are not the cause for the observed differences. This indicates that different surface types (e.g., canopy height and structure between the clearing and forest canopy) are responsible for the observed discrepancies, as for the other sites with a low canopy comparable values for  $a$  were derived.

Figure 6 shows the deviations of  $Rec_{lag}$  with different dead bands compared without the application of a dead band. The linear fit function shows that the flux reduction due to an imprecisely determined lag time decreases slightly with an increasing dead band. We found that the relationship in equation 17 still holds for dead band applications

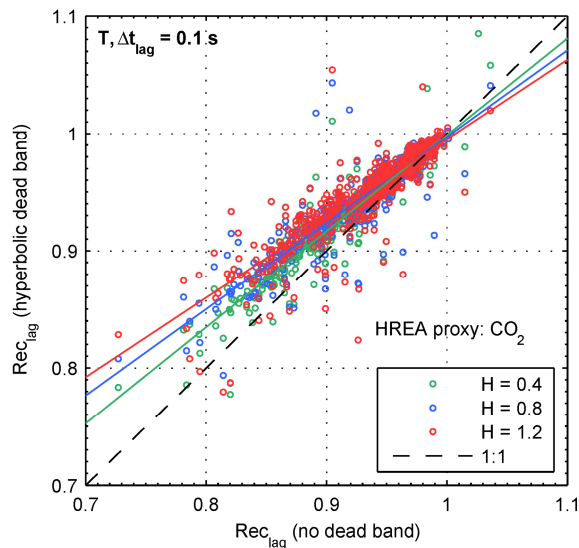


**Figure 6:** Simulated REA flux recovery ( $Rec_{lag}$ ) showing the effect of an artificial lag time of 0.1 s on the sensible heat flux with no dead band application versus different hyperbolic dead bands of  $H = 0.4, 0.8$  and  $1.2$ . Evaluated was the time period from 1 to 31 August 2011 at the natural grassland site.

together with the presented definition of the eddy reversal frequency (equation 3). However, since the sampling time during updraft and downdraft events is reduced by the dead band, the eddy reversal frequency is higher and cannot be considered as a real eddy reversal frequency, but still represents the amount of switching from or to an updraft or downdraft event.

## 3.2 The effect of high frequency attenuation on REA fluxes

### 3.2.1 Observed high frequency attenuation

The spectral energy of both the nonattenuated  $CO_2$  signal of the open-path analyzer and the attenuated  $CO_2$  signal of the closed-path analyzer are presented in

Figure 7 for different stability regimes. In the neutral and unstable cases, the spectra of the open-path analyzer show a fall-off with a slope of about  $-2/3$  which corresponds to Kolmogorov's  $-5/3$  power law in the inertial subrange. For stable conditions, the fall-off is steeper than the expected slope, which suggests an influence of high frequency attenuation due to the time constant and the path length averaging of the open-path LI-7500A analyzer. As the spectral densities under stable stratifications are shifted to higher frequencies [Kaimal and Finnigan, 1994], the impact of the transfer functions  $G_s(f)$  and  $T_{ps}(f)$  on the variance, i.e. the integral of equation 6, is also expected to be larger. The small tailing at the high frequency end can be attributed to aliasing as no low-pass filtering was employed during the measurements to reduce the energy above

the Nyquist frequency. The spectral energy of the closed-path analyzer shows a much steeper fall-off for all stability regimes in comparison to the spectra of the open-path analyzer. This steeper fall-off starts between 0.2 and 0.5 Hz, which would be expected if high frequency attenuation in the tubing was significant. Surprisingly, all spectra show a distinct peak at around 3 Hz and a steep rise towards the Nyquist frequency. The latter can be attributed to some extent to white noise, as the closed-path sensor showed a lower signal-to-noise-ratio caused by the lower pressure (~700 hPa) in the cuvette and possible pressure fluctuations in the tubing of the closed-path system. The possibility that the peak at 3 Hz is due to an effect of pressure or flow alterations caused by the cuvette or the tubing can be excluded since the peaks were not found in the spectra of both the pressure and mass flow signal, which were measured just behind the cuvette. Hence, it is likely that the peak at 3 Hz is an artifact caused by either the LI-7500A or the data acquisition. Since the peak at 3 Hz was absent in an experiment we performed before the presented observation period, we assume that the peak is caused by electronic interferences of other instrumentation, which was additionally installed in the container for the observation period presented here. Unfortunately, we could not identify the

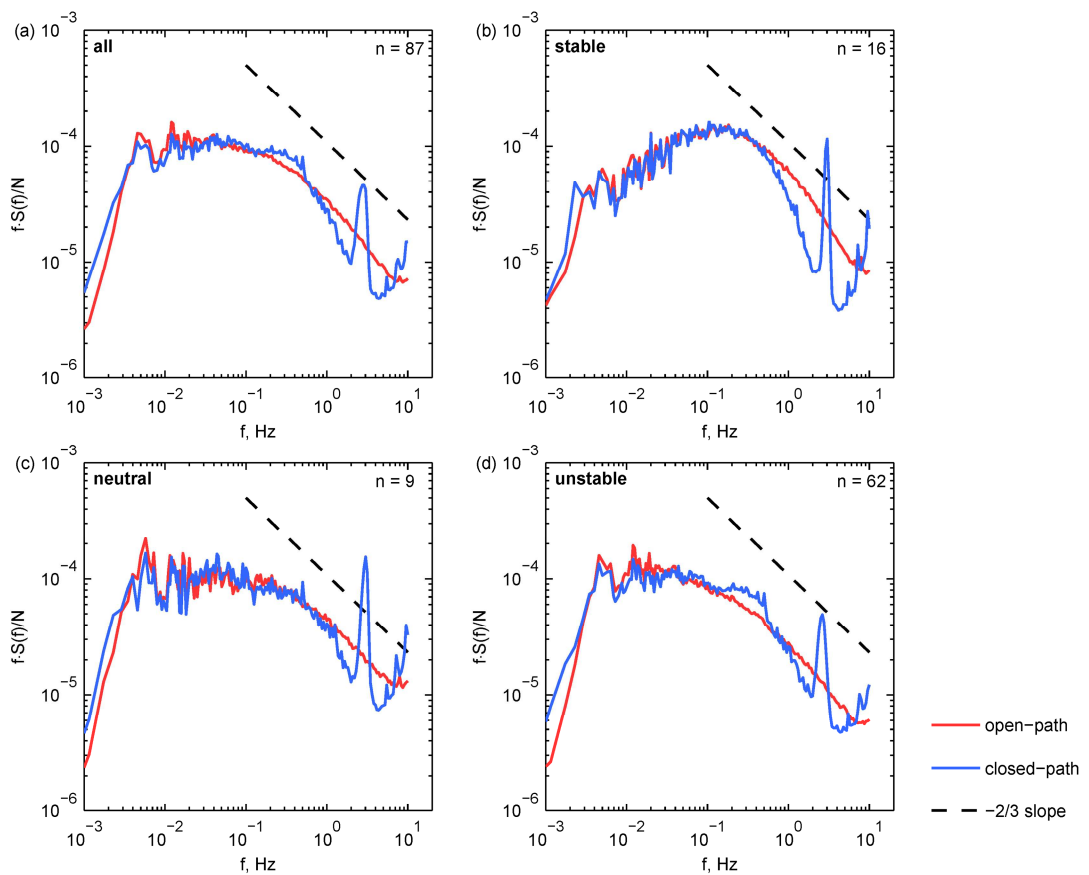


**Figure 7:** Normalized  $\text{CO}_2$  power spectra of the open-path analyzer next to the inlet and the closed-path analyzer mounted 21.5 m downstream in the inlet tube. Shown are the averaged spectra for the period

from 21 to 27 September 2011 at the natural grassland site for **(a)** all data and **(b-d)** for different stability regimes.

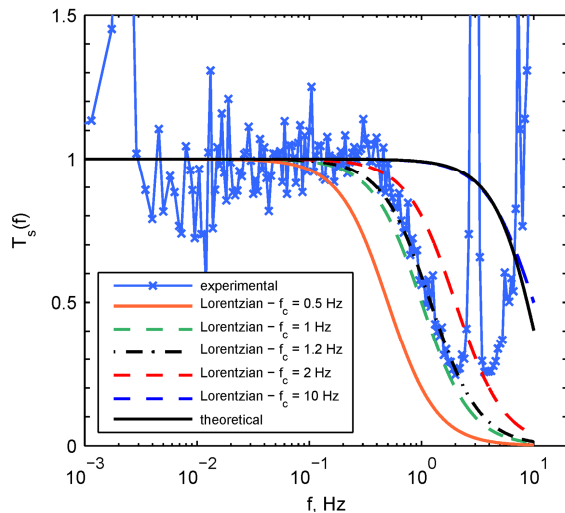


**Figure 8:** Experimentally derived transfer function for the attenuation due to the 21.5 m long inlet tube compared to the theoretical Lorentzian functions (cut-off frequencies of 0.5, 1, 1.2, 2 and 10 Hz) and the theoretical transfer function according to *Massman and Ibrom* [2008].

source of the interferences after the experiment was finished. In the case of unstable stratification, enhanced amplitudes in the spectra were found between 0.1 and 0.5 Hz. This might be due to the increased signal noise of the closed-path LI-7500A or due to other interferences, which would become more apparent at the high frequencies of the spectrum under unstable than under stable conditions. As stable turbulence spectra are shifted to the higher frequencies [*Kaimal and Finnigan*, 1994], the fall-off at the low frequency end is much more profound and associated with less scatter than in the unstable or neutral cases. Thus, the normalization factor can be determined more precisely, which is important for the determination of  $T_{ta}^{exp}(f)$ .

Although for a passive tracer, like  $\text{CO}_2$ ,  $T_{ta}^{exp}(f)$  depends only on the characteristics of the inlet system and not on the meteorological conditions [*Aubinet et al.*, 2001; *Massman and Ibrom*, 2008], Figure 7 would imply that  $T_{ta}^{exp}(f)$  differs for the different stability regimes. Since we could not determine whether these differences were real or a result of the described uncertainties of the spectra under neutral and unstable conditions, we used in our further evaluations only spectra under stable conditions for the derivation of  $T_{ta}^{exp}(f)$ . As shown in Figure 8, the fall-off of  $T_{ta}^{exp}(f)$  is very similar to  $T_L(f)$  derived from the Lorentzian filter function (equation 13) until the start of the peak at 3 Hz, which corroborates the assumption that the peaks are most likely an artifact of the  $\text{CO}_2$  measurements. The half power magnitude of  $T_{ta}^{exp}(f)$  yields a value for  $f_c$  of approximately 1.2 Hz. In contrast, the theoretical approach by *Massman and Ibrom* [2008] shows a smaller attenuation effect with a value for  $f_c$  of approximately 9 Hz. This discrepancy was also found by *Aubinet et al.* [2000], who attribute this significant attenuation effect to the particle filter at the inlet, whereas the theoretical transfer function  $T_{ta}^{theo}(f)$  accounts solely for the effect of the tubing. The setup of our experiment did not allow us to distinguish between the high frequency attenuation of the inlet filter and the effect of the inlet tube itself.

### 3.2.2 High frequency attenuation effect on REA fluxes

To investigate the effect of the high frequency attenuation on the REA fluxes, we low-pass filtered the scalar time series with the Lorentzian filter function (equation 13), using  $f_c$  values of 0.5, 1, 2, and 10 Hz thereby including the range of the experimentally and theoretically derived values. Similar to the lag time simulation, we expected a dependency of  $Rec_{HFA}$  on the eddy reversal frequency as high frequency attenuation would only affect  $\Delta c$  at the point of switching to or from a reservoir. On average, a decrease of  $Rec_{HFA}$  with increasing eddy reversal frequency is observed for all scalar quantities (Figure 9). Using a filter with  $f_c = 1$  Hz, comparable to the value found for the inlet tube system in this study ( $\sim 1.2$  Hz), the REA flux is reduced by up to 20% at high eddy reversal frequencies for the latent, sensible heat and  $CO_2$  flux. Whereas for  $f_c = 0.5$  Hz the REA flux recovery is nearly 30% lower at high eddy reversal frequencies, there is no visible effect on REA fluxes for  $f_c = 10$  Hz. Considering the results for values of  $f_c$  of 0.5, 1, 1.5 (not shown) and 2 Hz, we observe a clear linear dependency of  $Rec_{HFA}$  on  $f_c$ .

Despite the dependency on the eddy reversal frequency, we found that the high frequency attenuation effect is larger for neutral and stable conditions than for unstable conditions. First, this is caused by an enhanced high frequency attenuation effect on the scalar time series (equation 6) for stable conditions due to the shift of the scalar spectrum to higher frequencies [Kaimal *et al.*, 1972]. Second, the eddy reversal frequency generally shows a clear dependency on stability with values increasing from unstable to neutral and stable conditions. The superposition of both effects may lead to the nonlinear decline of  $Rec_{HFA}$  with increasing eddy reversal frequency.

In accordance to equation 17 we derived a fit function representing  $Rec_{HFA}$  as a function of  $f_c$  and the eddy reversal frequency:

$$Rec_{HFA} = 1 - a \cdot f_c \cdot erf^2 \quad (18)$$

For the sensible heat flux we found a value of  $a$  of  $8.8 \cdot 10^{-3}$  and for the  $O_3$  flux of  $5.7 \cdot 10^{-3}$ . For both the  $CO_2$  flux and the latent heat flux  $a$  was  $7.7 \cdot 10^{-3}$ . The attenuation effect on the  $O_3$  flux is smaller (maximal about 10% at  $f_c = 1$  Hz), because the data used for the simulation were already subject to high frequency attenuation induced by the inlet tube. There are a few cases when low-pass filtering lead to a flux increase, of which the majority was removed by the application of the quality criteria. We found that the attenuation of certain harmonics in the time domain can cause an increase of  $\Delta c$  after low-pass filtering and, thus, an increase of the REA flux.

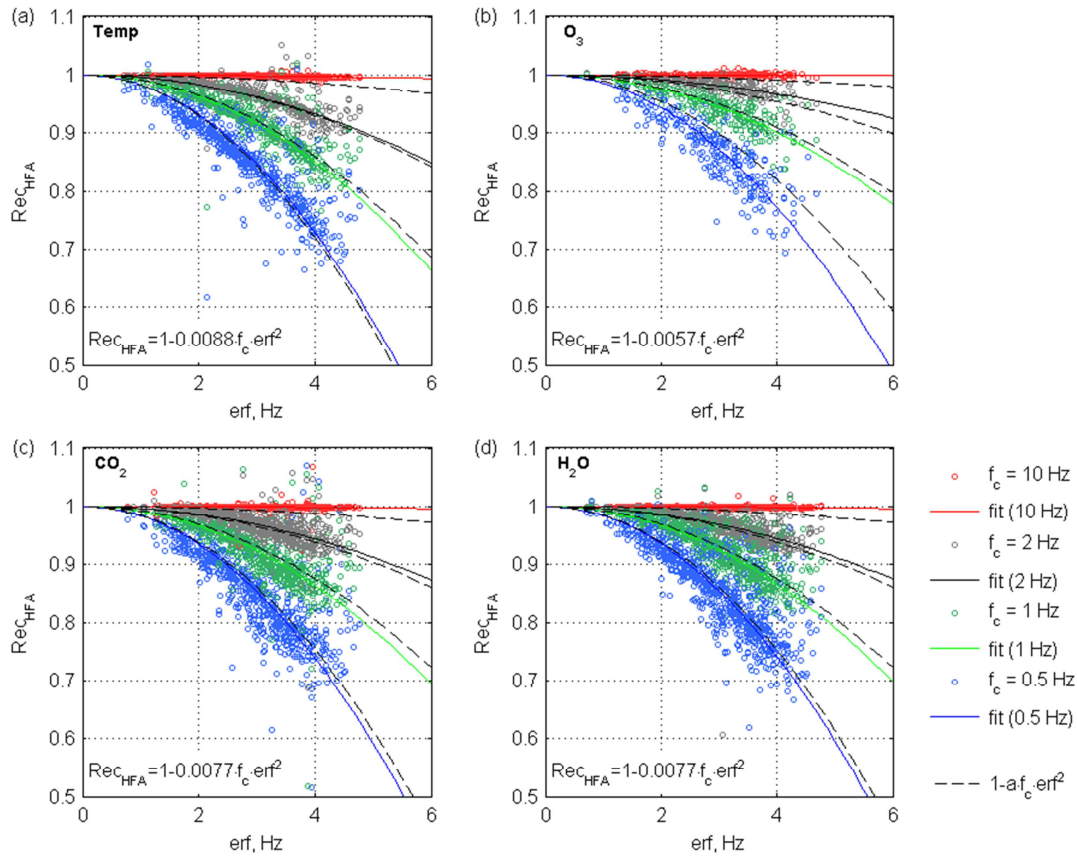


**Figure 9:** Simulated REA flux recovery ( $Rec_{HFA}$ ) as a function of the eddy reversal frequency ( $erf$ ) showing the effect of high frequency attenuation on (a) sensible heat flux, (b)  $O_3$  flux, (c)  $CO_2$  flux and (d) latent heat flux. A low-pass filter with different cut-off frequencies

of 0.5, 1, 1.5 (not shown), 2 and 10 Hz was applied to the 20 Hz scalar time series. Evaluated was the time period from 1 to 31 August 2011 at the natural grassland site. Shown are the results without the application of a dead band.

The implementation of a HREA dead band has no significant effect on simulated REA flux recovery due to high frequency attenuation. As for the lag time, the linear fit functions in Figure 10 show that the flux reduction due to high frequency attenuation decreases slightly with an increasing dead band. The conditional sampling with a hyperbolic dead band is associated with a higher flux of the proxy scalar. Regarding the shape of the turbulent scalar spectra, this implies a shift of the sampled eddies to lower frequencies, which are not affected by the high frequency attenuation. However, the simulation analysis for our data shows that the application of a dead band does not significantly reduce the flux loss caused by high frequency attenuation, which is in contrary to the assumption made by *Schade and Goldstein* [2001] for their REA measurements.

We find that the high frequency attenuation effect on REA fluxes (without dead band) is of similar magnitude as the effect on EC fluxes. The latter was investigated by low-pass filtering the 20 Hz time series of temperature,  $H_2O$  and  $CO_2$  using the same filter as for the REA simulation prior to the flux calculation with the eddy covariance software TK3.1 [Mauder and Foken, 2011]. Applying a filter with the same characteristic as for

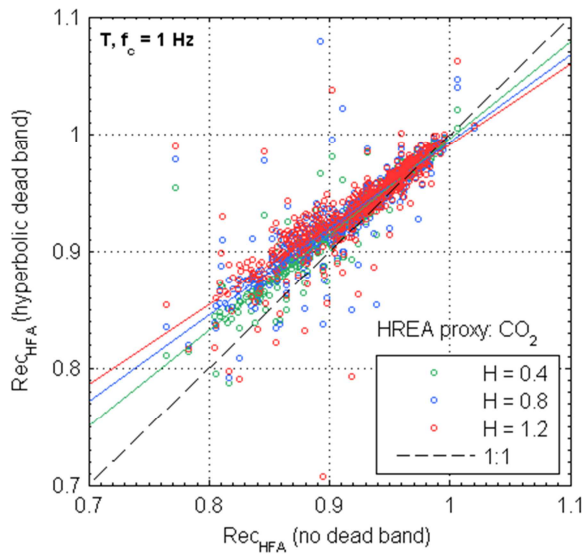


**Figure 10:** Simulated REA flux recovery ( $Rec_{HFA}$ ) showing the effect of high frequency attenuation ( $f_c = 1$  Hz) on the sensible heat flux with no dead band application versus different hyperbolic dead bands of  $H = 0.4, 0.8$  and  $1.2$ . Evaluated was the time period from 1 to 31 August 2011 at the natural grassland site.

the used inlet system in this study ( $f_c = 2$  Hz), the median flux reduction was about 5% for both REA and EC. Using  $f_c = 0.5$  Hz, the median flux reduction was around 15% for REA and ranged between 12% and 20% for EC depending on the scalar quantity. For  $f_c = 10$  Hz no significant reduction of the EC fluxes was observed. However, the presented values do not account for the stability dependency of the high frequency attenuation effect for both REA and EC. At a fixed measurement height under near-neutral and unstable conditions the high frequency attenuation effect on EC fluxes depends only on the horizontal wind velocity ( $u$ ) and the correction factor (inverse of the flux recovery) can be approximated according to *Aubinet et al.* [2001] by  $\varepsilon = 1 + a \cdot u$ , where the proportional factor  $a$  only depends on  $f_c$ . Evaluating this relationship for our data, we find comparable values for  $a$  for both REA and EC, although there is some variation for the different scalars. For the  $CO_2$  flux and with  $f_c = 0.5$  Hz, the flux loss for EC was significantly larger than for REA, reaching occasionally up to more than 50%.

### 3.3 Combined effect of imprecisely determined lag time and high frequency attenuation

As it was discussed in section 3.1.2, the high frequency attenuation may reduce the effect of an imprecisely determined lag time. On the other hand, it was mentioned in section 3.2.2 that a low-pass filter typically introduces a phase lag and, thus, an additional lag time. To simulate the effect of both an erroneous lag time and high frequency attenuation, the time series of the sonic temperature was time-shifted (see section 2.2) and low-pass filtered (see section 2.3) at the same time, using a series of 21

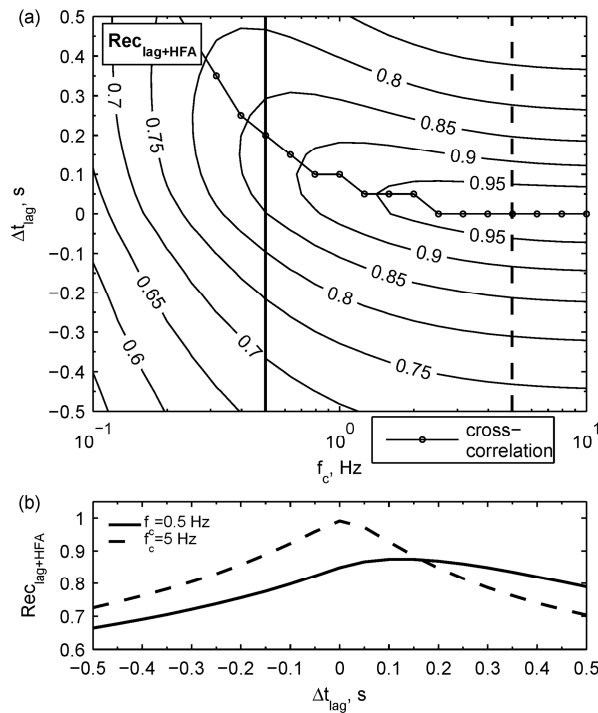


**Figure 11:** The combined flux recovery ( $Rec_{lag+HFA}$ ) for the sensible heat flux due to both an erroneous lag time and high frequency attenuation. Shown are the results of the REA simulation without the application of a dead band for an eddy reversal frequency of 3 Hz. **(a)** Contour lines represent  $Rec_{lag+HFA}$  as a function of  $\Delta t_{lag}$  and  $f_c$ . The retrieved phase shift due to low-pass filtering is also shown by the results from the cross-correlation analysis. The vertical lines mark the position of **(b)** the cross-section illustrating  $Rec_{lag+HFA}$  as a function of  $\Delta t_{lag}$  for values of  $f_c$  of 0.5 and 5 Hz. Evaluated was the time period from 1 to 31 August 2011 at the natural grassland site.

values of both  $\Delta t_{lag}$  (ranging from  $-0.5$  to  $0.5$  s with increments of  $0.1$  s) and  $f_c$  (ranging from  $0.1$  to  $10$  Hz with logarithmic increments). The combined flux recovery ( $Rec_{lag+HFA}$ ) was then obtained from the REA simulation (see also section 2.2). Figure 11 shows the results of  $Rec_{lag+HFA}$  for an eddy reversal frequency of  $3$  Hz. For this, we retrieved a quadratic fit function of  $Rec_{lag+HFA}$  versus the eddy reversal frequency of the same kind as equations 17 and 18 for each combination of  $\Delta t_{lag}$  and  $f_c$ . Figure 11a represents the previously discussed results, namely a reduced flux recovery with increasing  $\Delta t_{lag}$  and high frequency attenuation. The bending of the contour lines towards positive  $\Delta t_{lag}$  for decreasing  $f_c$  indicates the additional lag time associated with the phase shift of the low-pass filter. The magnitude of this additional lag time is also shown in Figure 11a by the results from the cross-correlation analysis between the modified temperature time series and the vertical wind velocity. Additionally, it demonstrates the influence of low-pass filtering on the lag time, which is illustrated in Figure 11b by the cross-sections in Figure 11a at  $0.5$  and  $5$  Hz. Next to the lower flux recovery and the increased phase shift, the error made by an erroneous lag time alone is smaller at lower  $f_c$  values, since the peak of the cross-section is smoother. On the other hand, the positive phase shift of the optimum lag time implies that not accounting for the high frequency attenuation effect would favor to slightly overestimate the actual lag time than to underestimate it. This does not apply when the lag time was determined with the online cross-correlation method, which already accounts for the phase shift introduced by the low-pass filtering effect.

### 3.4 Proposed procedure for future REA applications

In the previous sections we have discussed potential errors of the lag time determination and high frequency attenuation of the inlet system, and we subsequently simulated the effect of the potential errors on the REA fluxes. Since we found a significant effect on REA fluxes for both problems, we propose a procedure for future REA applications with a single long inlet tube including potential corrections methods and error estimates on the REA fluxes (Figure 12).

As a first step, the main sources of lag time errors and high frequency attenuation have to be identified and minimized during the REA application. The magnitude of the lag time error depends on the precision of the lag time determination before or during the REA application, in case the lag time ( $t_{lag}$ ) is expected to be larger than the sample interval ( $t_s$ ). Preferably, the lag time is determined online before the start of every sampling period via cross-correlation, however, this requires a permanently built-in high frequency sensor of an inert scalar species, that shows a significant correlation with the vertical wind speed (e.g., CO<sub>2</sub>). If the cross-correlation is performed offline before the experiment or the lag time is derived from the flow rate, it is recommended to maintain a constant volume flow rate in the tube and consider any longitudinal separation of the inlet and the sonic anemometer by adapting the lag time for each sample period (section 3.1.1).

To evaluate the effect of an erroneous lag time and high frequency attenuation on REA fluxes, the potential lag time errors and low-pass filter transfer function have to be determined, respectively. Systematic errors of the lag time result from an imprecisely determined lag time during the REA application and can be avoided to a large extent by careful assessment of the expected lag time components before the REA measurements. However, when compromises in inlet system setup or the REA application have to be made or some error sources were unknown during the REA application, systematic errors may be determined after the REA experiment. These might include e.g., errors caused by sensor separation, variations in the mean velocity in the tube, an imprecise determination of the tube inner diameter or an unconsidered electronic delay. In contrast to systematic errors, random errors cannot be compensated for during the REA application. Depending on the lag time determination method, random errors might include the random error of the cross-correlation method or random variations of the mean velocity in the tube (section 3.1.1). The high frequency effect of the inlet system is preferably determined experimentally [Aubinet et al., 2000; Ibrom et al., 2007], which requires a built-in high frequency sensor. If this is not possible, the high frequency attenuation effect of the inlet filter (if used) should be tested and added to a

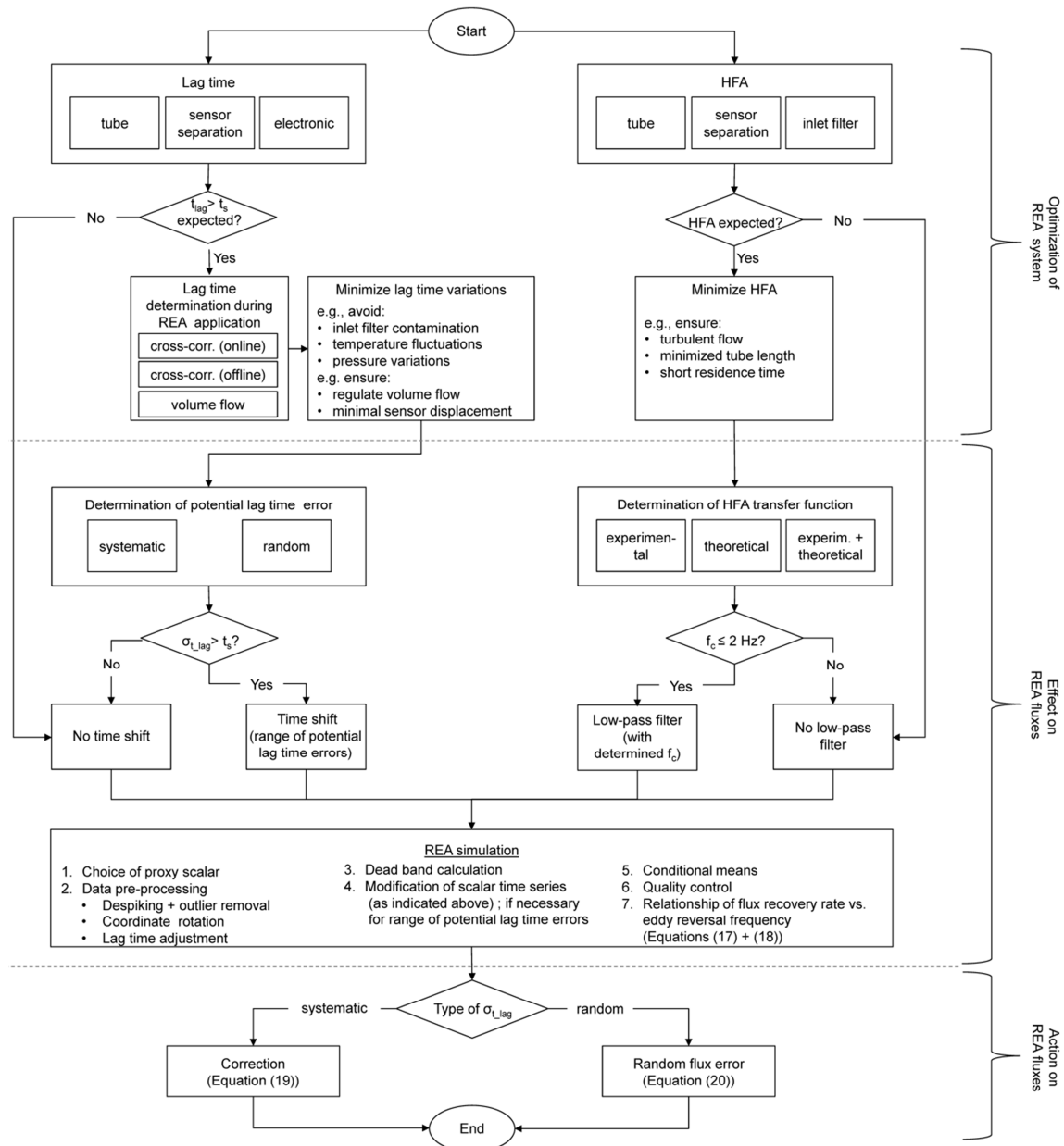


**Figure 12:** Proposed procedure for the validation of a REA system with one long inlet tube, which is prone to flux errors caused by both an imprecisely determined lag time and high frequency attenuation.

theoretical transfer function of the tubing (equation 10). We found in our study that the high frequency attenuation effect is only significant for  $f_c$  values below 2 Hz.

To obtain a site specific relationship between the flux recovery rate and the eddy reversal frequency, a REA simulation has to be performed including the applied dead band. For the REA simulation scalar similarity between the proxy scalar and the compound for which the REA flux is determined should hold (Step 1 of REA simulation in Figure 12). Since for the latter a scalar power spectrum cannot be obtained to prove the similarity, other criteria should be evaluated, such as a similar distribution of sources and sinks [Pearson et al., 1998; Ruppert et al., 2006]. The data pre-

processing steps (Step 2) such as the coordinate rotation as well as the dead band calculation (Step 3) have to be performed in the same way as during the REA application. The scalar time series has to be time-shifted towards the vertical wind velocity for the range of expected lag time errors and low-pass filtered using the determined transfer function (Step 4). The conditional means (Step 5) are created by applying the dead band on the time series of the vertical wind velocity. The quality control (Step 6) involves removal of fluxes which are near zero or do not fulfill the criteria of stationarity or developed turbulence [Foken and Wichura, 1996]. Finally, the flux recovery is calculated according to equations 2 and 14.

Finally, the potential errors of the REA fluxes are corrected or a random flux estimate is provided, depending on whether a systematic or random lag time error was determined, by using the dependency of the flux recovery on the eddy reversal frequency. If the data for the REA simulation covered various meteorological conditions, the function can then be easily applied to a data set over a longer time period. The corrected REA flux is then expressed by:

$$F_{REA\_REC} = b \cdot \sigma_w \cdot \Delta c \cdot \frac{1}{Rec} \quad (19)$$

using  $Rec_{lag}(erf, \Delta t_{lag})$  for the lag time and  $Rec_{HFA}(erf, f_c)$  for the high frequency attenuation effect, or  $Rec_{lag+HFA}(erf, \Delta t_{lag}, f_c)$  when the combined effect was studied. In case a random lag time error was determined, the random error of the REA flux can be described as

$$\sigma_{F\_REA} = F_{REA} \cdot a \cdot erf^2 \cdot |\sigma_{t\_lag}| \quad (20)$$

where  $|\sigma_{t\_lag}|$  accounts for the fact that an error in the lag time results in a flux loss for both positive and negative errors of the lag time.

## 4 Summary and Conclusions

This study demonstrated that an imprecisely determined lag time and high frequency attenuation in a long inlet tube may cause significant errors on fluxes determined with the REA method. For probable lag time errors ( $\Delta t_{lag} = 0.05\text{--}0.4$  s) flux errors may range from  $< 5\%$  at low eddy reversal frequencies up to  $50\%$  at high eddy reversal and a lag time error of  $0.4$  s. Flux errors due to the high frequency attenuation ( $f_c = 0.5\text{--}10$  Hz) may range from  $< 5\%$  at low eddy reversal frequencies up to  $30\%$  at

high eddy reversal and a cut-off frequency of 0.5 s. It is likely that previous studies using REA systems with long inlet tube are prone to these uncertainties.

The observed lag time variations emphasize that the method to determine the lag time is very critical and should be chosen with care. The online cross-correlation method includes the sensor separation, but had a higher random error ( $\pm 0.1$  s) due to the widening of the correlation peak. The lag time derived by the volume flow rate was mainly prone to systematic errors due to the tolerance of the tube diameter (error of  $\pm 0.08$  s) and due to uncertainties in the determination of the average pressure and temperature conditions in the tube. In addition, the horizontal separation distance between the sonic anemometer and the inlet lead to a further systematic error of up to  $\pm 0.25$  s depending on wind speed and wind direction. The flux loss due to an imprecise lag time was correlated with the eddy reversal frequency and the lag time shift. We found that the effect was largest for the sensible heat flux and lowest for the  $O_3$  flux, which could be attributed to the high frequency attenuation effects in the  $O_3$  time series. Furthermore, the simulation showed that the application of a dead band does not have a significant impact on the flux loss compared to measurements without a dead band.

To investigate the effect of high frequency attenuation on REA fluxes, the transfer function of the system has to be known first. For our setup, a large discrepancy between the transfer functions determined by the theoretical and the experimental approach was found. This was due to the fact that the theoretical approach only considers the tubing while the experimental approach also includes other attenuation effects, e.g., those caused by particle filters. Hence, it is suggested to use the experimental approach for the investigation of the effect of high frequency attenuation on REA fluxes. Particularly, when sampling water-soluble sticky trace gases, such as  $NH_3$ ,  $HNO_3$  and  $HNO_2$ , the effect of high frequency attenuation may be even more significant. We found a dependency of the flux recovery on both the eddy reversal frequency and cut-off frequency of the used low-pass filter, which was used to define a fit function for the correction of REA fluxes. The application of a dead band leads only to a minor reduction of the flux loss due to high frequency attenuation.

We demonstrated that both effects are especially large for high eddy reversal frequencies, which are predominantly observed at low measurement heights, under stable conditions and high wind speeds. Hence, for REA measurements at high measurement heights, such as above forest canopies (*erf* usually  $< 1$  Hz), the effect would be less significant and might be neglected [e.g., *Park et al.*, 2010; *Zhang et al.*, 2012]. On the other hand, the proposed corrections and error considerations might be inevitable for nighttime fluxes, when mainly stable conditions prevail and a high accuracy is required as scalar fluxes are generally lower due to reduced turbulent mixing. Since even small errors of the time lag can lead to a significant flux loss, also

REA systems with a short single inlet tube or two separate inlets for updraft and downdraft events are prone to the discussed uncertainties, when e.g. the splitter valves are not switched fast enough due to an electronic delay. Furthermore, our study demonstrates the requirement to account online for lag time variations associated with the sensor separation. This applies for any type of inlet system, where a certain distance between the inlet and the sonic anemometer is kept to prevent flow distortion effects.

## Acknowledgements

The project was funded by the Max Planck Society. We gratefully acknowledge J.-C. Mayer and D. Plake for support during the field measurements. We thank P. Werle for useful comments on the spectral analysis. We additionally thank the anonymous reviewers, who helped to improve the manuscript.

## References

- Ammann, C. (1998), On the application of relaxed eddy accumulation and common methods for measuring trace gas fluxes, *PhD Thesis, ETH Zürich*, pp. 232.
- Ammann, C., A. Brunner, C. Spirig, and A. Neftel (2006), Technical note: Water vapour concentration and flux measurements with PTR-MS, *Atmos. Chem. Phys.*, *6*, 4643-4651.
- Aubinet, M., B. Chermanne, M. Vandenhaute, B. Longdoz, M. Yernaux, and E. Laitat (2001), Long term carbon dioxide exchange above a mixed forest in the Belgian Ardennes, *Agr Forest Meteorol*, *108*(4), 293-315.
- Aubinet, M., et al. (2000), Estimates of the annual net carbon and water exchange of forests: The EUROFLUX methodology, *Advances in Ecological Research*, *Vol 30*, *30*, 113-175.
- Baker, B., A. Guenther, J. Greenberg, A. Goldstein, and R. Fall (1999), Canopy fluxes of 2-methyl-3-buten-2-ol over a ponderosa pine forest by relaxed eddy accumulation: Field data and model comparison, *J. Geophys. Res.-Atmos.*, *104*(D21), 26107-26114.
- Baker, J. M., J. M. Norman, and W. L. Bland (1992), Field-scale application of flux measurement by conditional sampling, *Agr Forest Meteorol*, *62*(1-2), 31-52.
- Beverland, I. J., R. Milne, C. Boissard, D. H. O'Neill, J. B. Moncrieff, and C. N. Hewitt (1996a), Measurement of carbon dioxide and hydrocarbon fluxes from a sitka spruce forest using micrometeorological techniques, *J. Geophys. Res.-Atmos.*, *101*(D17), 22807-22815.

- Beverland, I. J., D. H. O'Neill, S. L. Scott, and J. B. Moncrieff (1996b), Design, construction and operation of flux measurement systems using the conditional sampling technique, *Atmos. Environ.*, 30(18), 3209-3220.
- Bowling, D. R., A. C. Delany, A. A. Turnipseed, D. D. Baldocchi, and R. K. Monson (1999), Modification of the relaxed eddy accumulation technique to maximize measured scalar mixing ratio differences in updrafts and downdrafts, *J. Geophys. Res.-Atmos.*, 104(D8), 9121-9133.
- Businger, J. A., and S. P. Oncley (1990), Flux Measurement with Conditional Sampling, *J. Atmos. Ocean. Technol.*, 7(2), 349-352.
- Delany, A. C., S. P. Oncley, and J. A. Businger (1991), Adapting the Conditional Sampling Concept for a Range of Different Chemical Species, *Proceeding of the Seventh AMS Symposium on Meteorological Observations and Instrumentation*(New Orleans, La., January 14–18), 22–25.
- Foken, T., and B. Wichura (1996), Tools for quality assessment of surface-based flux measurements, *Agr Forest Meteorol*, 78(1-2), 83-105.
- Foken, T., et al. (2012), Coupling processes and exchange of energy and reactive and non-reactive trace gases at a forest site - results of the EGER experiment, *Atmos. Chem. Phys.*, 12(4), 1923-1950.
- Goulden, M. L., B. C. Daube, S. M. Fan, D. J. Sutton, A. Bazzaz, J. W. Munger, and S. C. Wofsy (1997), Physiological responses of a black spruce forest to weather, *J. Geophys. Res.-Atmos.*, 102(D24), 28987-28996.
- Ibrom, A., E. Dellwik, H. Flyvbjerg, N. O. Jensen, and K. Pilegaard (2007), Strong low-pass filtering effects on water vapour flux measurements with closed-path eddy correlation systems, *Agr Forest Meteorol*, 147, 140-156.
- Kaimal, J. C., and J. J. Finnigan (1994), *Atmospheric boundary layer flows: their structure and measurement*, Oxford University Press.
- Kaimal, J. C., Y. Izumi, J. C. Wyngaard, and R. Cote (1972), Spectral characteristics of surface-layer turbulence, *Q. J. R. Meteorol. Soc.*, 98(417), 563-&.
- Kristensen, L. (1979), On longitudinal spectral coherence, *Boundary-Layer Meteorology*, 16(2), 145-153.
- Kristensen, L., J. Mann, S. P. Oncley, and J. C. Wyngaard (1997), How close is close enough when measuring scalar fluxes with displaced sensors?, *J. Atmos. Ocean. Technol.*, 14(4), 814-821.
- Lee, X. H., and T. A. Black (1994), Relating eddy correlation sensible heat flux to horizontal sensor separation in the unstable atmospheric surface layer, *J. Geophys. Res.-Atmos.*, 99(D9), 18545-18553.
- Lenschow, D. H., and M. R. Raupach (1991), The attenuation of fluctuations in scalar concentrations through sampling tubes, *J. Geophys. Res.-Atmos.*, 96(D8), 15259-15268.
- Leuning, R., and K. M. King (1992), Comparison of eddy-covariance measurements of CO<sub>2</sub> fluxes by open- and closed-path CO<sub>2</sub> analysers, *Boundary-Layer Meteorology*, 59(3), 297-311.
- Leuning, R., and M. J. Judd (1996), The relative merits of open- and closed-path analysers for measurement of eddy fluxes, *Glob. Change Biol.*, 2(3), 241-253.

- Massman, W. J. (1991), The attenuation of concentration fluctuations in turbulent flow through a tube, *J. Geophys. Res.-Atmos.*, 96(D8), 15269-15273.
- Massman, W. J., and A. Ibrom (2008), Attenuation of concentration fluctuations of water vapor and other trace gases in turbulent tube flow, *Atmos. Chem. Phys.*, 8(20), 6245-6259.
- Mauder, M., and T. Foken (2011), Documentation and Instruction Manual of the Eddy-Covariance Software Package TK3, in *Arbeitsergebnisse*, edited, pp. 60, ISSN 1614-8916, Abteilung Mikrometeorologie, Universität Bayreuth, Bayreuth.
- Mayer, J. C., A. Bargsten, U. Rummel, F. X. Meixner, and T. Foken (2011), Distributed Modified Bowen Ratio method for surface layer fluxes of reactive and non-reactive trace gases, *Agr Forest Meteorol*, 151(6), 655-668.
- McInnes, K. J., C. S. Campbell, and J. L. Heilman (1998), Separation and dispersion of conditionally sampled eddies through an intake tube, *Agronomy Journal*, 90(6), 845-850.
- McMillen, R. T. (1988), An eddy correlation technique with extended applicability to non-simple terrain, *Boundary-Layer Meteorology*, 43, 231-245.
- Moore, C. J. (1986), Frequency response corrections for eddy correlation systems, *Boundary-Layer Meteorology*, 37(1-2), 17-35.
- Moravek, A., T. Foken, and I. Trebs (2014), Application of a GC-ECD for measurements of biosphere-atmosphere exchange fluxes of peroxyacetyl nitrate using the relaxed eddy accumulation and gradient method, *Submitted to Atmospheric Measurement Techniques*.
- Nie, D., T. E. Kleindienst, R. R. Arnts, and J. E. Sickles (1995), The design and testing of a relaxed eddy accumulation system, *J. Geophys. Res.-Atmos.*, 100(D6), 11415-11423.
- Oncley, S. P., A. C. Delany, T. W. Horst, and P. P. Tans (1993), Verification of flux measurement using relaxed eddy accumulation *Atmos Environ a-Gen*, 27(15), 2417-2426.
- Park, C., G. W. Schade, and I. Boedeker (2010), Flux measurements of volatile organic compounds by the relaxed eddy accumulation method combined with a GC-FID system in urban Houston, Texas, *Atmos. Environ.*, 44(21-22), 2605-2614.
- Pearson, R. J., S. P. Oncley, and A. C. Delany (1998), A scalar similarity study based on surface layer ozone measurements over cotton during the California Ozone Deposition Experiment, *J. Geophys. Res.-Atmos.*, 103(D15), 18919-18926.
- Ren, X., J. E. Sanders, A. Rajendran, R. J. Weber, A. H. Goldstein, S. E. Pusede, E. C. Browne, K. E. Min, and R. C. Cohen (2011), A relaxed eddy accumulation system for measuring vertical fluxes of nitrous acid, *Atmos. Meas. Tech.*, 4(10), 2093-2103.
- Ruppert, J. (2005), ATEM Software for Atmospheric Turbulence Exchange Measurements using Eddy Covariance and Relaxed Eddy Accumulation Systems and Bayreuth whole-air REA system setup, *Arbeitsergebnisse, Abteilung Mikrometeorologie, Universität Bayreuth, Vol. 28*, p. 29, ISSN 1614-8916.
- Ruppert, J., C. Thomas, and T. Foken (2006), Scalar similarity for relaxed eddy accumulation methods, *Boundary-Layer Meteorology*, 120(1), 39-63.

- Schade, G. W., and A. H. Goldstein (2001), Fluxes of oxygenated volatile organic compounds from a ponderosa pine plantation, *J. Geophys. Res.-Atmos.*, *106*(D3), 3111-3123.
- Stella, P., M. Kortner, C. Ammann, T. Foken, F. X. Meixner, and I. Trebs (2013), Measurements of nitrogen oxides and ozone fluxes by eddy covariance at a meadow: evidence for an internal leaf resistance to NO<sub>2</sub>, *Biogeosciences Discuss.*, *10*(3), 4461-4514.
- Taylor, G. (1953), Dispersion of soluble matter in solvent flowing slowly through a tube, *Proceedings of the Royal Society of London Series a-Mathematical and Physical Sciences*, *219*(1137), 186-203.
- Taylor, G. (1954), The dispersion of matter in turbulent flow through a pipe, *Proceedings of the Royal Society of London Series a-Mathematical and Physical Sciences*, *223*(1155), 446-468.
- Zahn, A., J. Weppner, H. Widmann, K. Schlote-Holubek, B. Burger, T. Kuhner, and H. Franke (2012), A fast and precise chemiluminescence ozone detector for eddy flux and airborne application, *Atmos. Meas. Tech.*, *5*(2), 363-375.
- Zhang, N., X. Zhou, S. Bertman, D. Tang, M. Alaghmand, P. B. Shepson, and M. A. Carroll (2012), Measurements of ambient HONO concentrations and vertical HONO flux above a northern Michigan forest canopy, *Atmos. Chem. Phys.*, *12*(17), 8285-8296.

## Appendix D

### **Influence of local air pollution on the deposition of peroxyacetyl nitrate to a nutrient-poor natural grassland ecosystem**

**A. Moravek<sup>1</sup>, P. Stella<sup>1\*</sup>, T. Foken<sup>2,3</sup> and I. Trebs<sup>1\*\*</sup>**

<sup>1</sup> Max Planck Institute for Chemistry, Biogeochemistry Department, Mainz, Germany

<sup>2</sup> Department of Micrometeorology, University of Bayreuth, Bayreuth, Germany

<sup>3</sup> Member of Bayreuth Center of Ecology and Environmental Research (BayCEER), University of Bayreuth, Germany

\* now at: AgroParisTech, UMR INRA/AgroParisTech SAD-APT, Paris, France

\*\* now at: Centre de Recherche Public - Gabriel Lippmann, Department Environment and Agro-biotechnologies, Belvaux, Luxembourg

Correspondence to: A. Moravek (a.moravek@mpic.de)

To be submitted to Biogeosciences

## Abstract

Dry deposition of peroxyacetyl nitrate (PAN) is known to have a phytotoxic impact on plants under photochemical smog conditions, but it may also lead to higher productivity and may threaten species richness of vulnerable ecosystems in remote regions. However, underlying mechanisms or controlling factors for PAN deposition are not well understood and studies on dry deposition of PAN are limited. In this study, we investigate the impact of PAN deposition on a nutrient-poor natural grass land ecosystem situated at the edge of an urban and industrialized region in Germany. PAN mixing ratios were measured within a 3.5 months summer to early autumn period. In addition, for a selected period PAN fluxes were determined with the modified Bowen ratio technique. The evaluation of both stomatal and non-stomatal deposition pathways was used to model PAN deposition over the entire period. We found that air masses at the site were influenced by two contrasting pollution regimes, which lead to median diurnal PAN mixing ratios ranging between 50 and 300 ppt during unpolluted and between 200 and 600 ppt during polluted episodes. The measured PAN fluxes showed a clear diurnal cycle with maximal deposition fluxes of  $\sim -0.1 \text{ nmol m}^{-2} \text{ s}^{-1}$  (corresponding to a deposition velocity of  $0.3 \text{ cm s}^{-1}$ ) during daytime and a significant non-stomatal contribution was found. The ratio of PAN to ozone deposition velocities was found to be  $\sim 0.1$ , which is much larger than assumed by current deposition models. The modelled PAN flux over the entire period revealed that the total PAN deposition over an entire day was  $333 \text{ } \mu\text{g m}^{-2} \text{ d}^{-1}$  under unpolluted and  $518 \text{ } \mu\text{g m}^{-2} \text{ d}^{-1}$  under polluted episodes. Besides, thermochemical decomposition PAN deposition accounted for 32% under unpolluted episodes and 22% under polluted episodes of the total atmospheric PAN loss. However, the impact of PAN deposition as a nitrogen source to the nutrient-poor grassland was estimated to be only minor, under both unpolluted and polluted episodes.

## 1 Introduction

Originating from both anthropogenic and natural sources, peroxyacetyl nitrate ( $\text{CH}_3\text{C}(\text{O})\text{O}_2\text{NO}_2$ , PAN) is primarily known as an atmospheric pollutant. Both, the peroxyacetyl radical ( $\text{CH}_3\text{C}(\text{O})\text{O}_2$ , PA) and nitrogen dioxide ( $\text{NO}_2$ ), which form PAN via



have anthropogenic sources. Due to its thermal instability via the back reaction of R1 and subsequent reaction of PA with nitric oxide (NO),



long range transport of PAN in cold layers of the upper troposphere may constitute a significant source of reactive nitrogen ( $\text{N}_r$ ) in remote regions. Consequently, it affects e.g.; the production of ozone ( $\text{O}_3$ ) and links the atmospheric and biospheric nitrogen cycle through dry deposition [Singh, 1987]. Besides, locally produced PAN may also impact on ecosystems downwind of pollution sources. While high PAN mixing ratios ( $> 15$  ppb), prevailing under strong photochemical smog conditions, PAN is known to be phytotoxic and may harm plant tissues significantly [Temple and Taylor, 1983], the impact of PAN deposition under less extreme conditions and for lower PAN mixing ratios is not yet clear. As a nitrogen source, PAN deposition may lead to higher productivity and may threaten species richness especially in vulnerable ecosystems [Stevens et al., 2010].

Previous studies on surface-atmosphere exchange fluxes of PAN showed that PAN is deposited to vegetation. On the one hand, chamber experiments on PAN uptake [Okano et al., 1990; Sparks et al., 2003; Teklemariam and Sparks, 2004] found a direct relationship between PAN uptake and stomatal conductance. They suggest that stomatal uptake is the major pathway of PAN into leaves. Furthermore, the stomatal uptake of PAN is mainly driven by diffusion across the partial pressure gradient between ambient air and air in the sub-stomatal cavity and controlled by the stomata aperture. On the other hand, previous studies have also shown the existence of non-stomatal deposition of PAN, mainly associated with the uptake by the leaf cuticles [Teklemariam and Sparks, 2004; Turnipseed et al., 2006; Wolfe et al., 2009] While Turnipseed et al. [2006] found almost 50% of the daytime deposition to be non-stomatal for a pine forest and suggest it to be the primary deposition pathway in the upper canopy, Wolfe et al. [2009] attribute between 21 and 35% (for warm and cold periods, respectively) of the deposition flux to non-stomatal pathways for a pine forest site. However, conclusive studies on PAN fluxes are currently very limited and the obtained results differ considerably. The underlying mechanisms or controlling factors for PAN deposition, like the role of wet surfaces, as well as the relation of PAN to  $\text{O}_3$  deposition fluxes are not well understood.

Grassland ecosystems are the third largest land use type in Europe and constitute 41% of global terrestrial surfaces [EUROSTAT, 2011; Suttie et al., 2005]. Moreover, nutrient-poor habitats, where additional nitrogen input via deposition may play a significant role, are often dominated by grass species rather than trees. In this case study, we investigate the influence of polluted and non-polluted air masses on the dry

deposition of PAN at a nutrient-poor natural grassland ecosystem in Central Europe. PAN mixing ratios were measured and analysed over a three months period under two contrasting pollution regimes. For a selected period, we also derived PAN fluxes with the flux-gradient approach, employing a newly developed flux measurements system for PAN [Moravek *et al.*, 2014]. In addition, fluxes of O<sub>3</sub>, which has similarities to PAN and thus is important for model applications, were estimated by eddy covariance. Based on our approaches, we estimate the contribution of stomatal and non-stomatal deposition pathways for PAN and compare these results to those obtained for O<sub>3</sub>.

## 2 Methods

### 2.1 Site description

The study was conducted at a nutrient-poor natural grassland ecosystem on the estate of the Mainz-Finthen Airport in Rhineland-Palatinate, Germany (49.9685°N, 8.1481°E). The natural grassland area of the measurement site extends over an area of 0.7 x 2.0 km (in mainly east western direction), providing good fetch condition for micrometeorological flux measurements. The ecosystem is primarily unmanaged and

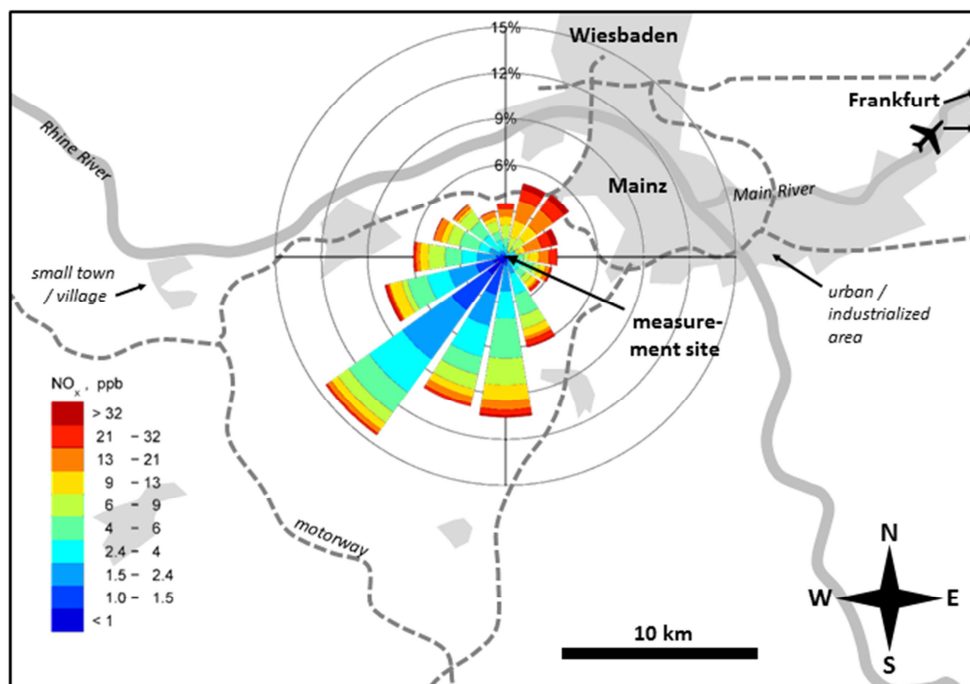


**Figure 1:** Location of the Mainz-Finthen grassland site situated at the edge of the industrialized Rhine-Main-Area in Germany. The wind rose, centred at the

measurement site, indicates unpolluted (low NO<sub>x</sub>) air masses from the south west sector and more polluted (high NO<sub>x</sub>) air masses from north easterly directions.

the vegetation is characterized by the false oat-grass (*Arrhenatherion elatioris*) plant community on dry and sandy soil with a considerable amount of senescent or died-off grass. Small bushes were occasionally removed and parts of the grassland were grazed by sheep once a year. The soil nitrate content was very low ( $\sim 0.7 \text{ mg kg}^{-1}$  in the upper 5 cm) and, hence, ammonium was most likely the largest source of plant available nitrogen from soil ( $\sim 20 \text{ mg kg}^{-1}$  in the upper 5 cm) [Oswald et al., 2013]. The mean canopy height during the field campaign was 0.6 m and the bulk LAI for both green and brown grass was on average 4.8. A roughness length ( $z_0$ ) of 0.1 m and a zero plane displacement ( $d$ ) of 0.45 m were estimated using the approach of De Bruin and Moore [1985] for canopies with increased roughness.. The site is topographically situated on a plateau 150 m above the Rhine valley and located about 9 km south-west of the city centre of Mainz (Fig. 1). The plateau is part of region Rhenish Hesse, which extends to the south and south west and is characterized by agricultural land use (mainly vineyards, orchards and crops) and smaller villages. In contrast, the industrialized and densely populated Rhine-Main-Area extends to northerly and easterly directions. Two motorways bypass closely to the north and east of the site in a distance of 2 and 4 km, respectively.

## 2.2 Measurements of PAN mixing ratios and fluxes

PAN mixing ratios on the site were measured for a 3.5 months period in summer and early autumn 2011 (29 June to 21 October 2011) using a gas chromatograph with electron capture detection (GC-ECD, see Moravek et al. [2014] for detailed description). The GC-ECD was placed in an air-conditioned container and regularly calibrated with air from a photolytic calibration source.

In addition, during the period from 19 August to 4 September we performed gradient measurements at 0.8 and 4.0 m a.g.l. to determine biosphere-atmosphere exchanges fluxes via the modified Bowen ratio (MBR) technique [Businger, 1986]. The PAN flux ( $F_{MBR_{PAN}}$ ) was estimated by the ratio of the PAN and  $O_3$  mixing ratio difference between the upper and lower measurement height,  $\Delta c_{PAN}$  and  $\Delta c_{O_3}$ , multiplied by the eddy covariance flux of  $O_3$  ( $F_{EC_{O_3}}$ ):

$$F_{MBR_{PAN}} = F_{EC_{O_3}} \cdot \frac{\Delta c_{PAN}}{\Delta c_{O_3}} \approx F_{EC_{O_3}} \cdot \frac{\Delta \chi_{PAN}}{\Delta \chi_{O_3}} \quad (1)$$

We used  $O_3$  as a proxy scalar due to its similarity to PAN in the sink and source distribution. On the one hand, the production of both PAN and  $O_3$  is linked to photochemical processes and, on the other hand, both compounds are known to deposit to vegetation. Instead of using concentration differences in Eq. (1), we used the mixing

ratio differences of PAN ( $\Delta\chi_{PAN}$ ) and O<sub>3</sub> ( $\Delta\chi_{O_3}$ ) since the differences in the molar air density between the two heights were negligible. PAN fluxes were corrected for the loss by thermochemical decomposition of PAN as presented in Sect. 2.5. The storage term (see e.g., *Rummel et al.* [2007]) of PAN was estimated using a logarithmically interpolated vertical profile of PAN and was found to be negligible. Further details on the flux measurements, including necessary modifications of the GC-ECD and the inlet system, and an extensive error analysis are given in *Moravek et al.* [2014]. Flux values with random errors larger than 100% were regarded as below the flux detection limit. Furthermore, under conditions with low friction velocities ( $u_* < 0.07 \text{ m s}^{-1}$ ) the application of the MBR methods is prone to larger errors [*Liu and Foken*, 2001].

## 2.3 Additional measurements

For the determination of O<sub>3</sub> eddy covariance fluxes, required for the application of the MBR method, a closed-path fast response O<sub>3</sub> detector (Enviscope GmbH, Germany) was employed together with a sonic anemometer (CSAT3, Campbell Scientific Inc., USA) at  $z_{ref} = 3 \text{ m a.g.l.}$  (see *Moravek et al.* [2014] for details on eddy covariance set up and O<sub>3</sub> calibration). In addition, CO<sub>2</sub> and latent heat fluxes were determined with an open-path CO<sub>2</sub>/H<sub>2</sub>O analyser (LI-7500A, LI-COR, USA). All turbulent fluxes were calculated using the eddy covariance software TK3.1 [*Mauder and Foken*, 2011], applying state-of-the-art corrections methods as listed in *Thomas Foken et al.* [2012]. Additionally, the O<sub>3</sub> flux was corrected for high frequency loss of the 2.5 m long inlet tube [*Moravek et al.*, 2013], for the storage effect and for chemical production from NO<sub>2</sub> photolysis and loss by reaction with NO [*Rummel et al.*, 2007]. The quality scheme of *Foken and Wichura* [1996] was used to exclude periods with significant non-stationarity or poor developed turbulence. Data for which the footprint area of the flux measurement (calculated with a Lagrangian forward stochastic model from *Rannik et al.*, 2000) included less than 80% of the natural grassland area were omitted.

The mixing ratio difference of O<sub>3</sub> between 4.0 and 0.8 m a.g.l. was determined using a differential UV absorption O<sub>3</sub> analyser (49i, Thermo Environmental, USA, modified according to *Cazorla and Brune* [2010]; see *Moravek et al.* [2014] for details on operation). Absolute O<sub>3</sub> mixing ratios at both heights were derived from a vertical profiles system, which also measured NO and NO<sub>2</sub> mixing ratios (O<sub>3</sub> analyser: 49i, Thermo Environmental, USA; NO/NO<sub>2</sub> analyser: CLD 780 TR, Eco-Physics, Switzerland). A vertical profile of temperature, humidity and wind speed was retrieved at 0.2, 0.8, 1.5, 2.5 and 4.0 m a.g.l..

Meteorological parameters used in this study are global radiation (CNR1, Kipp&Zonen, Netherlands), NO<sub>2</sub> photolysis frequency ( $j_{NO_2}$ ) (Meteorology Consult GmbH, Germany), rainfall (AGR100, Environmental Measurements) and surface wetness (Campbell Scientific Inc., USA). All additional measurements were performed during the entire experiment period from 29 June to 21 October 2011.

## 2.4 Flux partitioning

As PAN and O<sub>3</sub> are depositing the PAN and O<sub>3</sub> flux can be partitioned into deposition to leaf stomata ( $F_s$ ) and to non-stomatal surfaces ( $F_{ns}$ ):

$$F = F_s + F_{ns} \quad (2)$$

Following the big leaf multiple resistance approach [Hicks *et al.*, 1987; Wesely and Hicks, 2000] the overall canopy conductance ( $g_c$ , sum of the stomatal ( $g_s$ ) and non-stomatal ( $g_{ns}$ ) conductances) was obtained for both PAN and O<sub>3</sub> from the measured deposition velocity ( $v_D$ , i.e. the flux normalized by the concentration at  $z_{ref}$ ) and the estimated aerodynamic ( $R_a$ ) and quasi-laminar boundary layer ( $R_b$ ) resistances (see Garland [1977] and Hicks *et al.* [1987], respectively):

$$g_c = g_s + g_{ns} = \left( \frac{1}{v_D} - R_a - R_b \right)^{-1} \quad (3)$$

Following e.g., Lamaud *et al.* [2009] and Stella *et al.* [2011],  $g_{sPAN}$  and  $g_{sO_3}$  were derived from the stomatal conductance for water vapour via the Penman-Monteith equation ( $g_{sPM}$ ) corrected for the ratio of their molecular diffusivities to the molecular diffusivity of water vapour. Due to its longer molecular structure, the diffusivity of PAN is lower ( $D_{PAN} \sim 0.87 \cdot 10^{-5} \text{ m}^2 \text{ s}^{-1}$ ) than for O<sub>3</sub> ( $D_{O_3} \sim 1.40 \cdot 10^{-5} \text{ m}^2 \text{ s}^{-1}$ ), which results in  $g_{sPAN}/g_{sO_3} = 0.62$  [derived from Hicks *et al.*, 1987]. Since the measured H<sub>2</sub>O flux, on which Penman-Monteith equation is based, originated not only from transpiration through the plant stomata but also from water evaporation from other sources such as soil pores or liquid water on diverse surfaces, we only used dry conditions with relative humidities (RH) < 60% to compute  $g_{sPM}$ . Under these conditions liquid water on surfaces is assumed to be fully evaporated. Soil evaporation was excluded from  $g_{sPM}$  according to Stella *et al.* [2011]. The final  $g_{sPM}$  values were determined as a function of the corrected  $g_{sPM}$  values against the gross primary production (GPP).

Finally,  $g_{ns}$ , representing all non-stomatal deposition pathways, e.g., to leaf cuticles, soil or water surfaces, was derived by the difference between  $g_c$  and  $g_s$  (Eq. (3)).

The findings on  $g_{nSPAN}$  from the partitioning of  $F_{MBR_{PAN}}$  were used to model PAN deposition fluxes for the entire period from 29 June to 21 October. Applying the restive scheme given in Eq. (3), the modelled PAN flux ( $F_{model_{PAN}}$ ) was derived as

$$F_{model_{PAN}} = - \left( R_a + R_{b_{PAN}} + \frac{1}{g_{SPAN} + g_{nSPAN}} \right)^{-1} \cdot \rho_m \cdot \chi_{PAN} \quad (4)$$

where  $R_a$ ,  $R_{b_{PAN}}$  and  $g_{SPAN}$  were determined as described above over the entire period. Here,  $\rho_m$  and  $\chi_{PAN}$  represent the molar air density and the PAN mixing ratio, respectively, at the height of the eddy covariance measurements ( $z_{ref}$ )

## 2.5 Determination of PAN loss by thermochemical decomposition

Next to dry deposition process, other sink terms impact the measured surface PAN mixing ratios. While PAN photolysis and reaction with the hydroxyl radical (OH) are expected to be very low at altitudes below 7 km [Talukdar *et al.*, 1995], thermochemical decomposition of PAN (back reaction of R1) has to be considered. Thermochemical decomposition of PAN increases exponentially with temperatures and is more efficient at high NO/NO<sub>2</sub> ratios as PA reacts faster with NO instead with NO<sub>2</sub> to reform PAN. Hence, the time scale of PAN towards thermochemical decomposition ( $\tau_{chem}$ ) is given by [Orlando *et al.*, 1992; Shepson *et al.*, 1992] as

$$\tau_{chem}(PAN) = \frac{1}{k_{1r}} \left( 1 + \frac{k_{1f}[NO_2]}{k_2[NO]} \right) \quad (5)$$

To evaluate whether PAN loss significantly impacted the MBR fluxes (Sect. 2.2), the chemical flux divergence between  $z_{ref}$  and  $z_0$  due to thermochemical decomposition of PAN ( $F_{chem_{surf}}$ ) was determined according to Doskey *et al.* [2004] by numeric integration of the thermochemical PAN loss as

$$F_{chem_{surf}} = \int_{z_0}^{z_{ref}} \frac{\rho_m(z) \cdot \chi_{PAN}(z)}{\tau_{chem}(z)} dz \quad (6)$$

The height dependent functions of  $\chi_{PAN}(z)$  and  $\tau_{chem}(z)$  were approximated by logarithmic interpolation between the available measurement heights of the required parameters and  $\rho_m(z)$  was assumed to be constant with height (see Sect. 2.2).

The thermochemical PAN loss over the entire atmospheric boundary layer, represented as a flux ( $F_{chem_{BL}}$ ), was obtained by integrating Eq. (6) from zero level to the height of the boundary layer ( $h_{BL}$ )

$$F_{chemBL} = \int_0^{h_{BL}} \frac{\rho_m(z) \cdot \chi_{PAN}(z)}{\tau_{chem}(z)} dz \quad (7)$$

Assuming a well-mixed boundary layer, the measured PAN concentration and NO/NO<sub>2</sub> ratio were taken as an average value for the whole boundary layer. As  $\tau_{chem}$  is very sensitive to temperature, we assumed a dry adiabatic lapse rate of temperature with height. The height of the nocturnal boundary layer was estimated from the nocturnal decline of O<sub>3</sub> and the corresponding measured  $v_{DO_3}$  from the relation given by [Shepson et al., 1992] (see also Sect. 3.3.3) as

$$h_{BL_{night}} = 2 \cdot v_{DO_3} \cdot \ln \frac{\chi_{O_3}(t_0)}{\chi_{O_3}(t_1)} \quad (8)$$

where  $\chi_{O_3}(t_0)$  and  $\chi_{O_3}(t_1)$  are the O<sub>3</sub> mixing ratios at the start and end of the considered time interval, respectively. Since  $h_{BL_{night}}$  was determined from a boundary layer budget approach, it might not agree well with the real boundary layer height, as the nocturnal boundary layer might be significantly stratified. Instead,  $h_{BL_{night}}$  represents the theoretical depth of a mixed boundary layer, which was required in Eq. (7) to assume constant trace gas mixing ratios with height. The development of the diurnal boundary layer ( $h_{BL_{day}}$ ) after dawn was modelled using the measured sensible heat surface flux and a simple encroachment approach implemented in the mixed layer model MXLCH [Vilà-Guerau de Arellano et al., 2011].

## 3 Results and discussions

### 3.1 Meteorological conditions: Classification of low and high NO<sub>x</sub> episodes

The field experiment was dominated by wind directions from south west. These air masses were associated with relatively low levels of NO<sub>x</sub> (= NO + NO<sub>2</sub>) (ranging mainly between 1 and 10 ppb). In contrast, air masses from north easterly directions were much less frequent, but were often enriched with NO<sub>x</sub> with values ranging mainly between 10 and 30 ppb (Fig. 1). This enrichment was mainly caused by advection from NO<sub>x</sub> sources originated from the City of Mainz, nearby motor ways or other sources in the densely populated and industrialised Rhine-Main region. In contrast, the south west sector is dominated by farming without major industrial activity, thus representing an

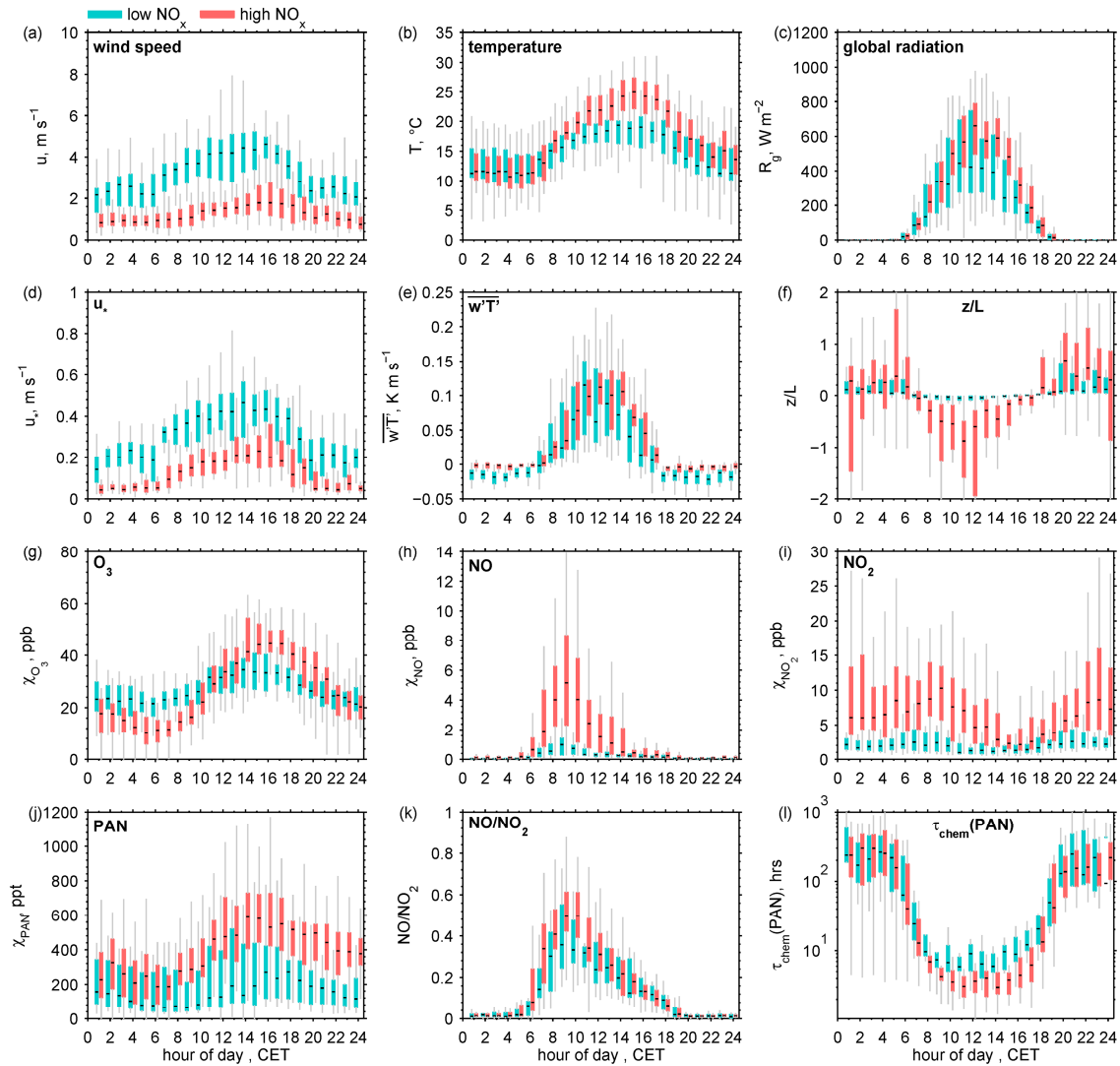


**Figure 2:** Diurnal boxplot statistics for the period from 29 June to 21 October 2011 at the Mainz-Finthen grassland site, characterising low and high  $\text{NO}_x$  periods according to the prevailing meteorological conditions:

(a-f) mixing ratios of the  $\text{O}_3$ -NO- $\text{NO}_2$  triad (g-i) and PAN mixing ratios including the NO/ $\text{NO}_2$  ratio used for the calculation of  $\tau_{chem}$  (j-l).

area with much less air pollution. Consequently, the occurrence of low and high  $\text{NO}_x$  situations during the field experiment was directly coupled to the wind direction and could be attributed to two contrasting synoptic conditions:

- (1) Episodes under deep pressure influence and south westerly wind directions yielded low  $\text{NO}_x$  conditions. They were characterized by higher wind speeds, frequent cloud coverage, a mainly neutrally stratified boundary layer and typically lasted from 2 to 5 days.
- (2) Sunny, convectively driven episodes with low wind speeds and, therefore, also varying wind directions resulted in high  $\text{NO}_x$  conditions, in cases when the wind direction was not from the south west sector. In contrast to the low  $\text{NO}_x$

conditions, these periods occurred sometimes as very isolated events and were associated with an unstable boundary layer during daytime and a stable stratification during nighttime.

For the further evaluation, entire days were selected and classified according to wind speed and wind direction. In total 20 days were classified as low NO<sub>x</sub> and 27 days as high NO<sub>x</sub> conditions. The diurnal averages of the meteorological conditions and micrometeorological characteristics during these days are displayed in Fig. 2a–f and mixing ratios of O<sub>3</sub>, NO and NO<sub>2</sub> are shown in Fig. 2g–i. For both low and high NO<sub>x</sub> conditions photolysis of NO<sub>2</sub> contributed to the steady increase of NO mixing ratios after sunrise, which peaked between 8:00 and 10:00 and then declined with the growth of the daytime boundary layer. During high NO<sub>x</sub> conditions both advection of freshly emitted NO from nearby sources and generally higher NO<sub>2</sub> levels lead to high NO mixing ratios exceeding sometimes 10 ppb. Biogenic NO emission from the grassland ecosystem, determined with the dynamic chamber method, were found to be insignificant [Plake *et al.*, 2013]. NO<sub>2</sub> mixing ratios showed a high variability during high NO<sub>x</sub> conditions also indicating local sources. The daytime NO<sub>2</sub> decline was caused by both dilution due to the growing boundary layer and photolysis. It was anti-correlated with the increase of O<sub>3</sub> mixing ratios. The development of a shallow nocturnal inversion layer during high NO<sub>x</sub> conditions caused increased O<sub>3</sub> removal rates. As a result, nighttime O<sub>3</sub> mixing ratios were lower than during low NO<sub>x</sub> conditions. During daytime, both the higher insolation and the presence of pollutants under high NO<sub>x</sub> conditions resulted in higher O<sub>3</sub> mixing ratios during the afternoon.

### 3.2 Characterisation of PAN under low and high NO<sub>x</sub> conditions

The diurnal cycle of PAN mixing ratios was closely linked to the diurnal cycle of O<sub>3</sub>. As for O<sub>3</sub>, PAN mixing ratios increase after dawn to the maximum in the afternoon, with median values of 300 ppt under low and of 600 ppt under high NO<sub>x</sub> conditions, respectively (Fig. 2j). The maximum is followed by a steady decrease over night to median values just before dawn of about 50 ppt under low NO<sub>x</sub> and 200 ppt under high NO<sub>x</sub> conditions.

The major reason for the much higher PAN levels during high NO<sub>x</sub> conditions, are the elevated NO<sub>2</sub> mixing ratios, which occurred especially at nighttime and declined with the onset of photolysis after dawn and the clearing of the nocturnal boundary layer. Comparing the diurnal evolution of PAN and O<sub>3</sub> mixing ratios, we find a higher PAN/O<sub>3</sub> ratio under high NO<sub>x</sub> conditions at all times throughout the diurnal cycle. During peak PAN and O<sub>3</sub> mixing ratios in the afternoon, the PAN/O<sub>3</sub> ratio was 0.003 and 0.006 during low and high NO<sub>x</sub> conditions, respectively. Since photolytic

production of  $O_3$  from  $NO_2$  was similar for both conditions, a large PAN/ $O_3$  ratio implies a higher abundance of PA as a precursor of PAN [J M Zhang *et al.*, 2009]. Although no direct measurements of PA were available, a very low abundance of volatile organic compounds at the site suggests that these higher levels of PA during high  $NO_x$  conditions primarily originated from anthropogenic non-methane hydrocarbons (NMHCs). Hence, PAN mixing ratios at the site were mainly influenced by advection from nearby pollution sources from north easterly directions.

The timescale for thermochemical decomposition of PAN,  $\tau_{chem}$ , ranged for both low and high  $NO_x$  conditions mainly between 4 and 20 days at night (Fig. 2k). During daytime,  $\tau_{PAN}$  ranged between 2 h and nearly one day (median  $\sim 5$  h) for low  $NO_x$  conditions, but were significantly lower during high  $NO_x$  conditions (ranging between 30 min and 5 h; median  $\sim 2$  h) caused by both on average higher  $NO/NO_2$  ratios in the morning and higher temperatures in the afternoon.

### 3.3 Evaluation of PAN flux measurements

#### 3.3.1 Deposition fluxes and canopy conductance

During the period of the PAN flux measurement mainly high  $NO_x$  conditions prevailed. The PAN fluxes showed a clear diurnal cycle with maximum deposition fluxes at midday and very small fluxes during nighttime (Fig. 3). Although the random flux errors were large compared to the observed fluxes (median  $\pm 0.035$   $nmol\ m^{-2}\ s^{-1}$ , see Moravek *et al.* [2014]) a daytime PAN deposition was clearly visible on most days. The gaps in the time series are due to extended instrument calibrations and maintenance of the GC-ECD. For the further evaluation PAN fluxes below the flux detection limit (34% of data, see Sect. 2.2 for definition) were neglected, despite data where  $u_* < 0.07$   $m\ s^{-1}$  (28% of data) as this criterion would have eliminated most of the nighttime values.

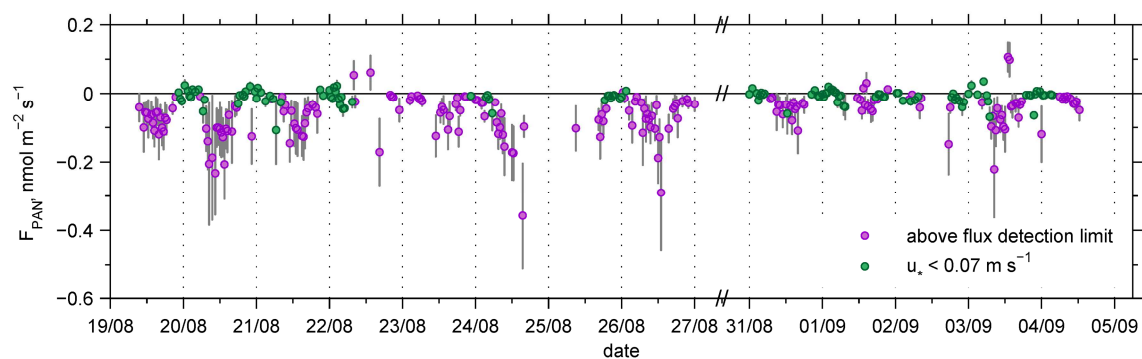


**Figure 3:** Overview of PAN flux measurements using the MBR method from 19 August to 4 September 2011 at the Mainz-Finthen grassland site after applying

quality criteria as described in Moravek *et al.* [2014]. Error bars represent the random flux error and green values mark periods with weak turbulent exchange

**Table 1:** Comparison of PAN fluxes and deposition velocities at the Mainz-Finthen grassland with previous studies. All field experiments were performed in the mid-latitudes of the northern hemisphere within the period of late spring to early autumn.

Method	Vegetation /location	LAI (one sided)	Flux ( $\text{nmol m}^{-2} \text{s}^{-1}$ )		$v_D$ ( $\text{cm s}^{-1}$ )		$v_{D_{PAN}}/v_{D_{O_3}}$ (-)		Study
			day	night	day	night	day	night	
EC (CIMS)	pine forest	3.5	-0.35	-0.05	~0.7	~0.3	-	> 1	<i>Turnipseed et al.</i> [2006]
	pine forest	5.1	-0.04	-0.03	0.30	0.10	1.25	0.5	<i>Wolfe et al.</i> [2009] <sup>†</sup>
Gradient /MBR	corn field	-	-	-	-	0.54	-	-	<i>Schrimpf et al.</i> [1996]
	grassland	-	-	-	0.13	-	0.2- 0.3	-	<i>Doskey et al.</i> [2004] <sup>‡</sup>
	grassland	4.8	-0.07	-0.01	0.30	0.06	1.03	1.25	this study
NBLB	n.s.	-	-	-	-	-	-	0.31	<i>Garland and Penkett</i> [1976] <sup>‡</sup>
	forest, agric.	-	-	-	-	-	-	2.38	<i>Shepson et al.</i> [1992] <sup>‡</sup>
	rural, sea-side	-	-	-	-	-	-	1.1- 6.2	<i>McFadyen and Cape</i> [1999] <sup>‡</sup>
	grassland	4.8	-	-	-	-	-	1.75	this study (see Sect. 3.3.3)
Laboratory	alfalfa	-	-	-	-	-	0.37	-	<i>Hill</i> [1971]
	grass	-	-	-	-	0.25	-	0.5	<i>Garland and Penkett</i> [1976]
	trees, crops	-	-0.02 - -0.06	-	-	0.00 - 1.50	-	-	<i>Sparks et al.</i> [2003]
	trees, herb.	-	-0.01 - -0.02	-	-	0.11 - 0.34	-	-	<i>Teklemariam and Sparks</i> [2004]

<sup>†</sup> net flux; in-canopy production of PAN was observed

<sup>‡</sup> O<sub>3</sub> flux not was not measured directly

The diurnal median values of the PAN and O<sub>3</sub> fluxes are shown in Fig. 4a–b. A diurnal course of the PAN flux is observed with maximal deposition fluxes of  $\sim -0.1 \text{ nmol m}^{-2} \text{ s}^{-1}$  during daytime, which corresponds to  $v_{D_{PAN}}$  at  $z_{ref}$  of  $\sim 0.3 \text{ cm s}^{-1}$ . The visible short-term peaks are mostly attributed to the low number of data values ( $\sum n = 255$ ) and also caused by the flux error of the MBR method. For O<sub>3</sub>, this feature was much less pronounced due to the higher number of data points used ( $\sum n = 639$ ). Both measured PAN fluxes and  $v_{D_{PAN}}$  values were between the observations by *Wolfe et al.* [2009] (midday averages  $-0.04 \text{ nmol m}^{-2} \text{ s}^{-1}$ ;  $v_D \approx 0.1 \text{ cm s}^{-1}$ ) and fluxes by *Turnipseed et al.* [2006] (midday averages  $\sim -0.35 \text{ nmol m}^{-2} \text{ s}^{-1}$ ;  $v_D \approx 1 \text{ cm s}^{-1}$ ) measured at two different pine forest sites in the USA during summer (Table 1). Daytime flux measurements at a grassland site by *Doskey et al.* [2004] resulted in an average  $v_{D_{PAN}}$  of  $0.13 \text{ cm s}^{-1}$ . The magnitude of the midday PAN flux at our site was about two orders of magnitude lower than the O<sub>3</sub> flux, yielding an average  $v_{D_{PAN}}/v_{D_{O_3}}$  ratio of 0.1. Comparison with experimentally derived PAN fluxes in the past (Table 1) reveals that  $v_{D_{PAN}}/v_{D_{O_3}}$  ratios vary considerably, which might be attributed to a large extent to the error of the applied measurement methods and the assumptions made.

The chemical flux divergence between  $z_{ref}$  and  $z_0$  due to thermochemical decomposition of PAN (Eq. (6)) was found to be very small with the highest median value of  $0.007 \text{ nmol m}^{-2} \text{ s}^{-1}$  at noon (Fig. 4a). In contrast, for the O<sub>3</sub> flux, the loss term due to reaction with NO and the production by NO<sub>2</sub> photolysis were significantly higher

between 6:00 and 11:00 CET and led to a small net production of O<sub>3</sub> during daytime, which was corrected for in the presented fluxes.

The overall canopy conductance for PAN ( $g_{cPAN}$ ), representing the flux normalized by the concentration at  $z_0$ , shows a mean diurnal cycle with its maximum during daytime (Fig. 4c–d). The midday median values were around 0.4 cm s<sup>-1</sup> and were similar to  $g_c$  values observed for O<sub>3</sub>.

### 3.3.2 Stomatal uptake

During nighttime  $g_{sPAN}$  values were zero due to stomata closure (Fig. 4c). With the onset of radiation in the morning  $g_{sPAN}$  increases and reaches its maximum of 0.26 cm s<sup>-1</sup> at 11:00 CET. As both  $g_{sPAN}$  and  $g_{sO_3}$  differ only by the PAN and O<sub>3</sub> diffusivities (see Sect. 2.4), they show the same pattern, while  $g_{sO_3}$  is larger by a factor of 1.6 due to the faster diffusivity of O<sub>3</sub>. Due to an increased vapour pressure deficit in the afternoon the maximum values of  $g_{sPAN}$  and  $g_{sO_3}$  are slightly skewed towards the morning.

The existence of a mesophyllic resistance limiting the stomatal uptake of PAN, as it was found by *Teklemariam and Sparks* [2004] or by *Sparks et al.* [2003] at high stomatal conductance, cannot be validated from our data. Only if the modelled  $g_{sPAN}$  values exceeded the measured  $g_{cPAN}$  values, a limitation could be suspected. It is suggested that the mesophyllic uptake of PAN is lower than for O<sub>3</sub>, as there are less reaction sites for PAN within the plant cell and its reaction with proteins is slower, although the mesophyll biochemistry for PAN assimilation is not clearly understood [Doskey et al., 2004].

### 3.3.3 Non-stomatal deposition

According to the MBR flux measurements at our site, the non-stomatal sink played a major role with median midday  $g_{nsPAN}$  values ranging between 0.05 and 0.4 cm s<sup>-1</sup>, corresponding to a non-stomatal resistance ( $R_{ns} = g_{ns}^{-1}$ ) of 2000 and 240 s m<sup>-1</sup>, respectively. The nighttime  $g_{nsPAN}$  values are very low, but have to be treated with caution due to the uncertainties of the MBR method at night. The peaks in  $g_{nsPAN}$  are mainly associated with the uncertainties of  $g_{cPAN}$  caused by the limited data set (see Sect. 3.3.1). For O<sub>3</sub>, we observed a clear diurnal cycle with lowest values in the afternoon. The diurnal cycle could be well reproduced as a function of relative humidity multiplied by LAI, despite elevated values between 06:00 and 10:00 CET, where surface humidity is still very high and the NO<sub>x</sub> advection might lead to a greater uncertainty of the chemical production and loss of terms (Sect. 3.3.1).

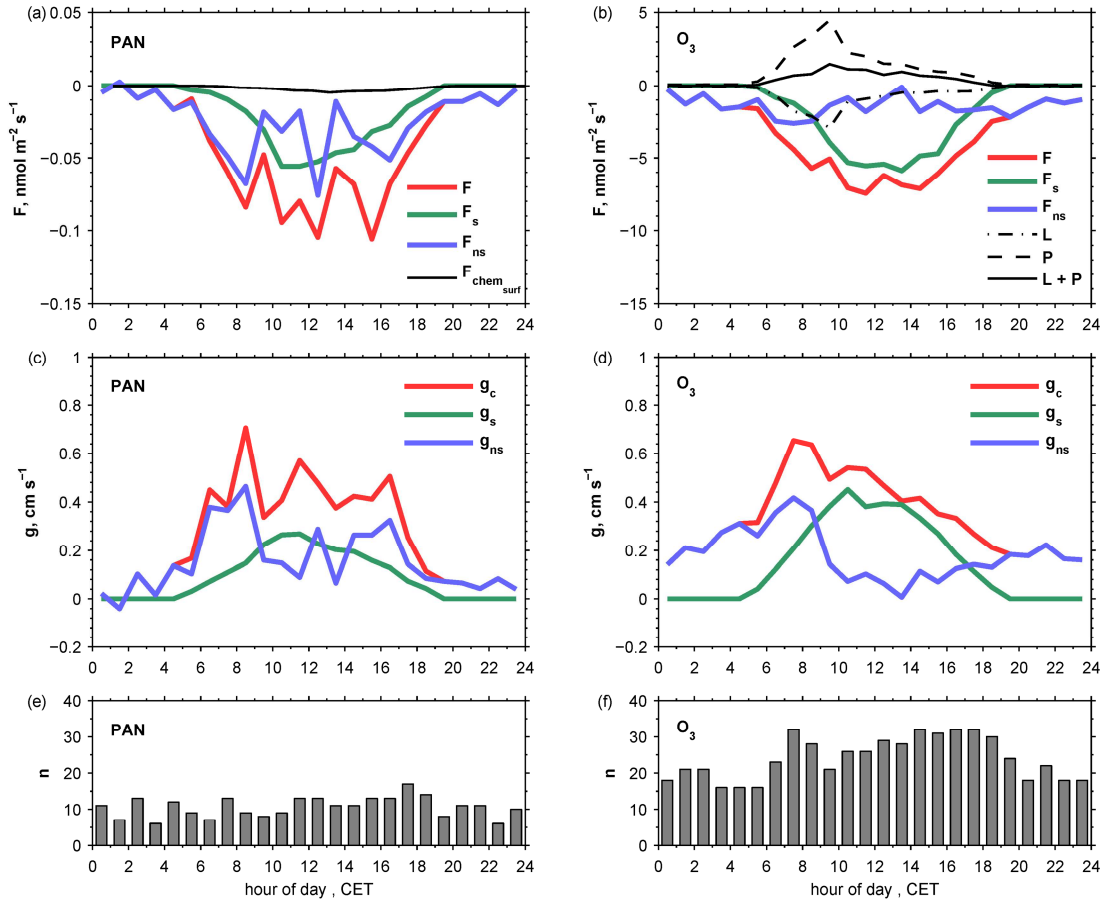


**Figure 4:** Flux partitioning of PAN (left column) and  $O_3$  (right column) deposition into stomatal and non-stomatal pathways at the Mainz-Finthen grassland site. Shown are diurnal median values for the period from 19 August to 4 September 2011. (a) and (b) indicate

the deposition fluxes including the thermochemical flux term ( $F_{chem_{surf}}$ ) for PAN and the loss (L) and production (P) terms for  $O_3$ . (c) and (d) give the respective conductances, while (e) and (f) show the number data points used for every hourly interval.

Since uncertainties in the  $O_3$  flux impact the PAN flux directly, we discarded data with large  $NO_x$  values in the evaluation of  $g_{nsPAN}$  as well as values where  $u_* < 0.07 \text{ m s}^{-1}$ . We could not identify any significant dependency of the individual data point of  $g_{ns}$  on temperature, relative humidity or surface wetness. This contradicts the assumption of *Shepson et al.* [1992], who suspected that  $g_{nsPAN}$  would decrease with higher surface wetness due to the low deposition on water surfaces [*Kames et al.*, 1991]. *Turnipseed et al.* [2006] explained a maximum of  $v_{DPAN}$  after sunrise with increased deposition to leaf surface water of a pine forest canopy and hypothesize the existence of a reactive uptake process within the leaf water. However, our findings support the results by *Schrimpf et al.* [1996], who did not observe a relationship of  $g_{nsPAN}$  with relative humidity.

For the determination of  $F_{modelPAN}$  over the entire measurement period (see Sect. 2.4) an estimate or parameterisations of  $g_{nsPAN}$  is required. Since from our data, no significant dependency was found and nighttime values are uncertain, we assume a

constant value of  $g_{nsPAN}$ . Hence, we derived a bulk  $g_{nsPAN}$  value by correlating the measured PAN fluxes with a modelled PAN flux using a series of different  $g_{nsPAN}$  values in Eq. (2). The smallest root mean square error determined an optimal  $g_{ns}$  value for the whole dataset of  $0.28 \text{ cm s}^{-1}$ , which corresponds to  $R_{nsPAN} = 360 \text{ s m}^{-1}$ . This resistance value is in the range of findings by other studies, e.g., *Turnipseed et al.* [2006] observed a median value of  $244 \text{ s m}^{-1}$  under dry and  $125 \text{ s m}^{-1}$  under wet conditions, although there was a great variability.

To obtain another independent estimate of the non-stomatal deposition, we employed the nocturnal boundary layer budget (NBLB) method according to *Shepson et al.* [1992], which compares the nocturnal PAN decay to that of  $\text{O}_3$  and yields a ratio of PAN to  $\text{O}_3$  deposition velocities. The main assumption, that the decline of both PAN and  $\text{O}_3$  mixing ratio during nighttime was only due to deposition, is valid as chemical reactions at night for both PAN (see Fig. 21) and  $\text{O}_3$  (no photolysis and low NO mixing ratios) are negligible. We analysed in total 16 nights, where a clear logarithmic decline of both PAN and  $\text{O}_3$  mixing ratios was observed and where the main wind direction came from the “clean” sector in the south west. Using only nights with a good correlation between both PAN and  $\text{O}_3$  decline ( $R^2 > 0.7$ ), we obtain an average value for  $v_{DPAN}/v_{DO_3}$  of 1.75, which is similar to the average value obtained by *Shepson et al.* [1992]. As stomatal uptake is assumed to be zero at night, we obtained according to Eq. (3) a bulk  $g_{nsPAN}$  of  $0.5 \text{ cm s}^{-1}$  ( $R_{nsPAN} = 200 \text{ s m}^{-1}$ ). This value of  $g_{nsPAN}$  is slightly larger than the value obtained from the MBR measurement.

In currently applied deposition models [e.g., *Simpson et al.*, 2012],  $g_{nsPAN}$  is often derived according to *Wesely* [1989] as a composite between the non-stomatal conductance of sulphur dioxide ( $g_{nsSO_2}$ ) and  $g_{nsO_3}$

$$g_{nsPAN} = 10^{-5} \cdot H_{PAN}^* \cdot g_{nsSO_2} + f_{0PAN} \cdot g_{nsO_3} \quad (9)$$

$\text{SO}_2$  represents a very soluble substance (effective Henry constant  $H_{SO_2}^* = 10^5 \text{ M atm}^{-1}$ ) and  $\text{O}_3$  a compound that reacts fast with substances in the leave cuticles such as protein thiols [*Mudd*, 1982]. Due to the poor solubility of PAN in water ( $H_{PAN}^* = 4.1 \text{ M atm}^{-1}$ , see *Kames and Schurath* [1995]) the first term of the right side of Eq. (9) can be neglected and only the reactivity index,  $f_0$ , is of significant importance. According to *Wesely* [1989]  $f_{0PAN} = 0.1$ , which suggests the non-stomatal deposition of PAN would be about one order of magnitude lower than for  $\text{O}_3$ . *L Zhang et al.* [2002] suggest a  $f_{0PAN} = 0.6$  based on first studies on PAN deposition by *Hill* [1971] and *Garland* [1977]. This contradicts our findings by both the MBR and the NBLB method, which observed at least equal or even higher non-stomatal deposition for PAN than for  $\text{O}_3$ , and supports

the statement by Turnipseed et al. (2006) that current deposition models may significantly underestimate PAN non-stomatal deposition.

### 3.4 PAN deposition strength for low and high NO<sub>x</sub> conditions

To evaluate the PAN deposition under both low and high NO<sub>x</sub> conditions as well as its potential influence on the natural grassland ecosystem and its role for the atmospheric N<sub>r</sub> budget, the PAN deposition flux for the entire period from 29 June to 21 October was modelled (see Sect. 2.4). For this, we used the bulk value for  $g_{nSPAN}$  of  $0.28 \text{ cm s}^{-1}$  (Sect. 3.3.3) for both low and high NO<sub>x</sub>, as we found this to be the best estimate from our data. The values for  $g_{SPAN}$  were determined as described in Sect. 2.4. The obtained median diurnal cycles of  $F_{modelPAN}$  for low and high NO<sub>x</sub> conditions (Fig. 5) reveal that the total deposition (i.e. stomatal + non-stomatal) was more than twice as high during high NO<sub>x</sub> ( $\sim -0.1 \text{ nmol m}^{-2} \text{ s}^{-1}$ ) than during low NO<sub>x</sub> ( $\sim -0.05 \text{ nmol m}^{-2} \text{ s}^{-1}$ ) conditions, which is mainly attributed to the higher PAN mixing ratios during high NO<sub>x</sub> conditions. Median midday deposition velocities were very similar during both episodes ( $v_{DPAN} \approx 0.5 \text{ cm s}^{-1}$ ). As already discussed in Sect. 3.3.3, the non-stomatal pathway was significant, which is reflected by a daytime fraction of  $g_{nSPAN}/g_{CPAN}$  of 0.7 during low NO<sub>x</sub> and 0.6 during high NO<sub>x</sub> conditions. As about half of the grassland vegetation was senescing or was already dead, reaction on plant surfaces may be a reason for the large non-stomatal fraction.

The importance of PAN deposition as a loss process of PAN from the atmosphere is determined by comparison to the magnitude of the thermochemical decomposition of

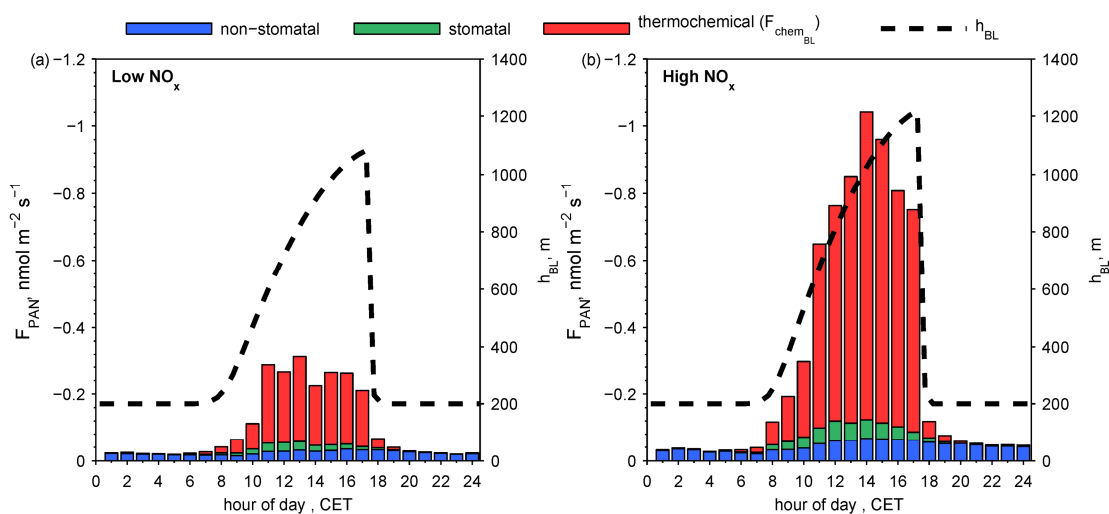


**Figure 5:** Modelled stomatal and non-stomatal PAN deposition fluxes and PAN loss due to thermochemical decomposition for (a) low and (b) high NO<sub>x</sub> periods at the Mainz-Finthen grassland site. The dashed line

marks the theoretical boundary layer height used for the calculation of the PAN decomposition (for details see text).

**Table 2:** Modelled PAN deposition and thermochemical loss for low and high NO<sub>x</sub> conditions at the Mainz-Finthen grassland site. The description of the shown parameters is given in the text.

	PAN (ppt)	T (°C)	NO/NO <sub>2</sub> (-)	h <sub>BL</sub> (m)	τ <sub>dep</sub> (d)	τ <sub>chemBL</sub> (d)	k <sub>dep</sub> (s <sup>-1</sup> )	k <sub>chemBL</sub> (s <sup>-1</sup> )	L <sub>dep</sub> (μg m <sup>-2</sup> d <sup>-1</sup> )	L <sub>chemBL</sub> (μg m <sup>-2</sup> d <sup>-1</sup> )	L <sub>dep</sub> (%)
Low NO <sub>x</sub>											
daytime	182	17.6	0.18	567	1.50	0.88	1.8 · 10 <sup>-4</sup>	3.2 · 10 <sup>-4</sup>			
nighttime	147	13.6	0.01	200	0.42	16.08	6.7 · 10 <sup>-4</sup>	0.17 · 10 <sup>-4</sup>			
all									333	698	32
High NO <sub>x</sub>											
daytime	405	20	0.23	641	1.54	0.54	1.8 · 10 <sup>-4</sup>	5.1 · 10 <sup>-4</sup>			
nighttime	334	15.9	0.01	200	0.83	12.67	3.3 · 10 <sup>-4</sup>	0.21 · 10 <sup>-4</sup>			
all									518	1840	22

PAN in the boundary layer (Eq. (7)). Due to the lower temperatures and the lack of NO at night, the nocturnal thermochemical loss was insignificant during both low and high NO<sub>x</sub> conditions. Using the boundary layer budget approach (Eq. (8)), we found  $h_{BL\_night}$  to be on average 200 m (Fig. 5). In contrast, during daytime the thermochemical loss constituted the largest PAN sink, during both low and high NO<sub>x</sub> conditions. After dawn,  $h_{BL\_day}$  grew during high NO<sub>x</sub> conditions on average up to 1200 m, whereas its development was slightly suppressed during low NO<sub>x</sub> conditions. The modelled boundary layer height was compared for selected days to the boundary layer height obtained from a WRF model. The WRF model yielded slightly higher daytime maximum values ranging from 1100 up to 1700 m. When the boundary was well mixed (11-17 CET), the thermochemical loss during high NO<sub>x</sub> conditions was about 3.5 times higher than during low NO<sub>x</sub> conditions. This was caused by a combination of (a) the higher PAN mixing ratios (effect: 59%), (b) the reduced reaction time scale due to higher temperatures and larger NO to NO<sub>2</sub> ratios (effect: 34%) and to some extent also by (c) the higher boundary layer (effect: 7%). A summary of the relevant parameters for nighttime and daytime conditions is given in Table 2, where the timescales for PAN deposition is given by  $\tau_{dep} = \rho_m \cdot \chi_{PAN} \cdot F_{modelPAN}^{-1} \cdot h_{BL}$ . The reaction rates towards PAN deposition ( $k_{dep}$ ) and thermochemical decomposition over the entire boundary layer height ( $k_{chemBL}$ ) are the inverse values of  $\tau_{dep}$  and  $\tau_{chemBL}$ , respectively.

Integrating  $F_{modelPAN}$  and  $F_{chemBL}$  over the entire diel cycle yields the total mass of PAN removed per unit area by dry deposition ( $L_{dep}$ ) and thermochemical decomposition ( $L_{chemBL}$ ), respectively [McFadyen and Cape, 1999; Turnipseed et al., 2006]. As presented in Table 2, during low NO<sub>x</sub> conditions dry deposition made up 32%

of the diurnal PAN removal, whereas under high  $\text{NO}_x$  conditions 22%. These values are slightly lower as the ones given by *McFadyen and Cape* [1999], who suggest equal PAN loss via both processes. Although they claim very low  $\text{NO}/\text{NO}_2$  ratios at the site to be a major reason for the low chemical loss, an overestimation of the PAN deposition in their study is possible, since it was not measured directly. Accounting for a temperature decrease with height, *Turnipseed et al.* [2006] estimated a maximal contribution of dry deposition of 10%. *Wolfe et al.* [2009] found that dry deposition accounted only for 3% of the total PAN loss during warm and 13% during cool periods.

To evaluate its significance as a source of  $\text{N}_r$  to the grassland ecosystem, PAN deposition has to be evaluated in relation to other  $\text{N}_r$  sources. *Dennis et al.* [2013] estimate a contribution of dry deposition of PANs of about 3.5% to the total dry and wet nitrogen annual deposition in the continental USA. However, their values are based on the parameterisation by *L Zhang et al.* [2002], which might significantly underestimate dry deposition of PAN as found e.g. by *Turnipseed et al.* [2006] and in this study. *Stevens et al.* [2010] evaluated the effect of total inorganic nitrogen deposition on grasslands across Europe and found that species richness decreased with sites that were subject to higher nitrogen deposition. The observed PAN removal via dry deposition (i.e.,  $L_{dep}$ ) over one entire day was in this study  $333 \mu\text{g m}^{-2} \text{d}^{-1}$  during low and  $518 \mu\text{g m}^{-2} \text{d}^{-1}$  during high  $\text{NO}_x$  conditions (Table 2). This is much lower than the total nitrogen deposition observed at the sites reported by *Stevens et al.* [2010] ranging between  $4.7$  and  $104.2 \text{ mg m}^{-2} \text{d}^{-1}$  (equivalent to  $2$  and  $44 \text{ kg N ha}^{-1} \text{a}^{-1}$ ), which suggests that PAN deposition under both low and high  $\text{NO}_x$  does not play a critical role on plant species richness at our site. Also, PAN mixing ratios observed at our site were significantly below the threshold given for phytotoxic effect on plants, which is given by *Temple and Taylor* [1983] between 15 and 25 ppb.

## 4 Conclusions

Up to date very few studies have measured direct PAN deposition to ecosystems. The experiments often cover only a short time period and obtained results differ considerably. In particular, the relation between PAN and  $\text{O}_3$  deposition has remained inconclusive. Based on the MBR method, we find in this study considerable non-stomatal uptake of PAN ( $g_{nSPAN} = 0.28 \text{ cm s}^{-1}$ ). This resulted in an equal or even higher non-stomatal conductance for PAN than for  $\text{O}_3$ , most likely suggesting an underestimation of PAN deposition by current models. We did not find a relation of the non-stomatal conductance for PAN with other quantities, such as relative humidity.

However, it cannot be fully excluded that this may also be attributed to the limited PAN flux data above the flux detection limit. The modelled stomatal uptake did not exceed the overall deposition, suggesting that stomatal uptake is not limited by further, not-considered resistances.

PAN deposition at our measurement site was governed by two contrasting pollution regimes, (1) low NO<sub>x</sub> episodes with clean air from south westerly directions and (2) high NO<sub>x</sub> episodes with more polluted air masses from the north eastern sector. Under high NO<sub>x</sub> conditions, locally produced PAN from the industrialized region was transported to the site, leading to PAN mixing ratios which were a factor of two to four higher than under low NO<sub>x</sub> conditions. Hence, PAN deposition during these episodes was larger with daytime maxima of  $-0.1 \text{ nmol m}^{-2} \text{ s}^{-1}$ . However, as also found in previous studies, the largest fraction of PAN loss during daytime was due to thermochemical decomposition of PAN. For clean conditions dry deposition accounted for about 32% of the daytime PAN loss, while it only accounted for 22% during polluted conditions. The higher thermochemical PAN loss during polluted episodes was mainly associated with different meteorological conditions and only to some extent caused by larger NO/NO<sub>2</sub> ratios, due to freshly emitted NO by nearby sources. During nighttime non-stomatal PAN deposition was the only significant PAN sink.

Comparing PAN deposition at the site to other deposition pathways of atmospheric reactive nitrogen, suggests that PAN deposition only played a minor role as a potential nitrogen source to the nutrient-poor natural grassland ecosystems in this study. However, up to date still little is known about the direct uptake of PAN by vegetation and the effect on their metabolism. Furthermore, studies which performed direct PAN flux measurements are limited to only a few types of ecosystems and conditions and are often prone to large uncertainties. As it was suggested by other studies in the past, PAN deposition might be the dominant removal process in winter at lower temperatures. However, up to date in situ PAN flux measurements only cover late spring to early autumn periods in the northern hemisphere. Hence, both in situ flux measurements of PAN during different seasons and for a larger variety of ecosystems, as well as detailed studies on the role of non-stomatal uptake mechanisms to improve current deposition models are desirable tasks for future research on PAN deposition.

## Acknowledgements

This project was funded by the Max Planck Society. J.-C. Mayer and D. Plake contributed to the setup and operation of additional measurements at the field site. L. Smoydzin applied the WRF model for the estimation of the boundary layer height. We thank C. Ammann and D. Plake for discussion on the flux divergence and chemical correction methods.

## References

- Businger, J. A. (1986), Evaluation of the Accuracy with Which Dry Deposition Can Be Measured with Current Micrometeorological Techniques, *J Clim Appl Meteorol*, 25(8), 1100-1124.
- Cazorla, M., and W. H. Brune (2010), Measurement of Ozone Production Sensor, *Atmos. Meas. Tech.*, 3(3), 545-555.
- De Bruin, H. A. R., and C. J. Moore (1985), Zero-Plane Displacement and Roughness Length for Tall Vegetation, Derived from a Simple Mass Conservation Hypothesis, *Boundary-Layer Meteorology*, 31(1), 39-49.
- Dennis, R. L., D. B. Schwede, J. O. Bash, J. E. Pleim, J. T. Walker, and K. M. Foley (2013), Sensitivity of continental United States atmospheric budgets of oxidized and reduced nitrogen to dry deposition parametrizations, *Philos T R Soc B*, 368(1621).
- Doskey, P. V., V. R. Kotamarthi, Y. Fukui, D. R. Cook, F. W. Breitbeil, and M. L. Wesely (2004), Air-surface exchange of peroxyacetyl nitrate at a grassland site, *J. Geophys. Res.-Atmos.*, 109(D10), 9, D10310.
- EUROSTAT (2011), Agriculture and fishery statistics: main results 2009-10, edited, p. 152, Publications Office of the European Union, Luxembourg.
- Foken, T., and B. Wichura (1996), Tools for quality assessment of surface-based flux measurements, *Agr Forest Meteorol*, 78(1-2), 83-105.
- Foken, T., R. Leuning, S. Oncley, M. Mauder, and M. Aubinet (2012), Corrections and Data Quality Control, in *Eddy Covariance*, edited by M. Aubinet, T. Vesala and D. Papale, pp. 85-131, Springer Netherlands.
- Garland, J. A. (1977), The dry deposition of sulphur dioxide to land and water surfaces, *Proc. R. Soc. London Ser. A-Math. Phys. Eng. Sci.*, 354(1678), 245-268.
- Garland, J. A., and S. A. Penkett (1976), Absorption of peroxy acetyl nitrate and ozone by natural surfaces, *Atmos. Environ.*, 10(12), 1127-1131.
- Hicks, B. B., D. D. Baldocchi, T. P. Meyers, R. P. Hosker, and D. R. Matt (1987), A preliminary multiple resistance routine for deriving dry deposition velocities from measured quantities, *Water Air Soil Poll*, 36(3-4), 311-330.

- Hill, A. C. (1971), Vegetation - sink for atmospheric pollutants, *Journal of the Air Pollution Control Association*, 21(6), 341-346.
- Kames, J., and U. Schurath (1995), Henrys Law and Hydrolysis-Rate Constants for Peroxyacyl Nitrates (Pans) Using a Homogeneous Gas-Phase Source, *J. Atmos. Chem.*, 21(2), 151-164.
- Kames, J., S. Schweighoefer, and U. Schurath (1991), Henrys Law Constant and Hydrolysis of Peroxyacetyl Nitrate (Pan), *J. Atmos. Chem.*, 12(2), 169-180.
- Lamaud, E., B. Loubet, M. Irvine, P. Stella, E. Personne, and P. Cellier (2009), Partitioning of ozone deposition over a developed maize crop between stomatal and non-stomatal uptakes, using eddy-covariance flux measurements and modelling, *Agr Forest Meteorol*, 149(9), 1385-1396.
- Liu, H. P., and T. Foken (2001), A modified Bowen ratio method to determine sensible and latent heat fluxes, *Meteorol. Z.*, 10(1), 71-80.
- Mauder, M., and T. Foken (2011), Documentation and Instruction Manual of the Eddy-Covariance Software Package TK3, in *Arbeitsergebnisse*, edited, pp. 60, ISSN 1614-8916, Abteilung Mikrometeorologie, Universität Bayreuth, Bayreuth.
- McFadyen, G. G., and J. N. Cape (1999), Physical and chemical influences on PAN concentrations at a rural site, *Atmos. Environ.*, 33(18), 2929-2940.
- Moravek, A., I. Trebs, and T. Foken (2013), Effect of imprecise lag time and high-frequency attenuation on surface-atmosphere exchange fluxes determined with the relaxed eddy accumulation method, *Journal of Geophysical Research: Atmospheres*, 118(17), 10,210-210,224.
- Moravek, A., T. Foken, and I. Trebs (2014), Application of a GC-ECD for measurements of biosphere-atmosphere exchange fluxes of peroxyacetyl nitrate using the relaxed eddy accumulation and gradient method, *Submitted to Atmospheric Measurement Techniques*.
- Mudd, J. B. (1982), Effects of oxidants on metabolic function, in *Effects of Gaseous Air Pollution in Agriculture and Horticulture*, edited by M. H. Unsworth and D. P. Ormrod, pp. 189-203, Butterworth-Heinemann, Woburn, Mass.
- Okano, K., K. Tobe, and A. Furukawa (1990), Foliar Uptake of Peroxyacetyl Nitrate (PAN) by Herbaceous Species Varying in Susceptibility to this Pollutant, *New Phytol*, 114(1), 139-145.
- Orlando, J. J., G. S. Tyndall, and J. G. Calvert (1992), Thermal-Decomposition Pathways for Peroxyacetyl Nitrate (Pan) - Implications for Atmospheric Methyl Nitrate Levels, *Atmos Environ a-Gen*, 26(17), 3111-3118.
- Oswald, R., et al. (2013), HONO Emissions from Soil Bacteria as a Major Source of Atmospheric Reactive Nitrogen, *Science*, 341(6151), 1233-1235.
- Plake, D., P. Stella, A. Moravek, J.-C. Mayer, C. Ammann, A. Held, and I. Trebs (2013), Comparison of ozone fluxes measured with the dynamic chamber and the eddy covariance method and partitioning between stomatal and non stomatal deposition, *submitted to Agricultural and Forest Meteorology*.
- Rannik, U., M. Aubinet, O. Kurbanmuradov, K. K. Sabelfeld, T. Markkanen, and T. Vesala (2000), Footprint analysis for measurements over a heterogeneous forest, *Boundary-Layer Meteorology*, 97(1), 137-166.

- Rummel, U., C. Ammann, G. A. Kirkman, M. A. L. Moura, T. Foken, M. O. Andreae, and F. X. Meixner (2007), Seasonal variation of ozone deposition to a tropical rain forest in southwest Amazonia, *Atmos. Chem. Phys.*, 7(20), 5415-5435.
- Schrimpf, W., K. Lienaerts, K. P. Muller, J. Rudolph, R. Neubert, W. Schussler, and I. Levin (1996), Dry deposition of peroxyacetyl nitrate (PAN): Determination of its deposition velocity at night from measurements of the atmospheric PAN and (222)Radon concentration gradient, *Geophys. Res. Lett.*, 23(24), 3599-3602.
- Shepson, P. B., J. W. Bottenheim, D. R. Hastie, and A. Venkatram (1992), Determination of the relative ozone and PAN deposition velocities at night, *Geophys. Res. Lett.*, 19(11), 1121-1124.
- Simpson, D., et al. (2012), The EMEP MSC-W chemical transport model - technical description, *Atmos. Chem. Phys.*, 12(16), 7825-7865.
- Singh, H. B. (1987), Reactive Nitrogen in the Troposphere, *Environ Sci Technol*, 21(4), 320-327.
- Sparks, J. P., J. M. Roberts, and R. K. Monson (2003), The uptake of gaseous organic nitrogen by leaves: A significant global nitrogen transfer process, *Geophys. Res. Lett.*, 30(23).
- Stella, P., et al. (2011), Predicting and partitioning ozone fluxes to maize crops from sowing to harvest: the Surf atm-O-3 model, *Biogeosciences*, 8(10), 2869-2886.
- Stevens, C. J., et al. (2010), Nitrogen deposition threatens species richness of grasslands across Europe, *Environ Pollut*, 158(9), 2940-2945.
- Suttie, J. M., S. G. Reynolds, and C. Batello (2005), *Grasslands of the world*, xxii, 514p. : ill. (mostly col.), figs., maps, tabs. ; 524cm. pp., FAO, Rome.
- Talukdar, R. K., J. B. Burkholder, A. M. Schmoltner, J. M. Roberts, R. R. Wilson, and A. R. Ravishankara (1995), Investigation of the Loss Processes for Peroxyacetyl Nitrate in the Atmosphere - Uv Photolysis and Reaction with Oh, *J. Geophys. Res.-Atmos.*, 100(D7), 14163-14173.
- Teklemariam, T. A., and J. P. Sparks (2004), Gaseous fluxes of peroxyacetyl nitrate (PAN) into plant leaves, *Plant Cell Environ.*, 27(9), 1149-1158.
- Temple, P. J., and O. C. Taylor (1983), World-wide ambient measurements of peroxyacetyl nitrate (PAN) and implications for plant injury, *Atmospheric Environment (1967)*, 17(8), 1583-1587.
- Turnipseed, A. A., L. G. Huey, E. Nemitz, R. Stickel, J. Higgs, D. J. Tanner, D. L. Slusher, J. P. Sparks, F. Flocke, and A. Guenther (2006), Eddy covariance fluxes of peroxyacetyl nitrates (PANs) and NO<sub>y</sub> to a coniferous forest, *J. Geophys. Res.-Atmos.*, 111(D9), D09304.
- Vilà-Guerau de Arellano, J., E. G. Patton, T. Karl, K. van den Dries, M. C. Barth, and J. J. Orlando (2011), The role of boundary layer dynamics on the diurnal evolution of isoprene and the hydroxyl radical over tropical forests, *Journal of Geophysical Research: Atmospheres*, 116(D7), D07304.
- Wesely, M. L. (1989), Parameterization of surface resistances to gaseous dry deposition in regional-scale numerical-models, *Atmos. Environ.*, 23(6), 1293-1304.
- Wesely, M. L., and B. B. Hicks (2000), A review of the current status of knowledge on dry deposition, *Atmos. Environ.*, 34(12-14), 2261-2282.

- Wolfe, G. M., J. A. Thornton, R. L. N. Yatawelli, M. McKay, A. H. Goldstein, B. LaFranchi, K. E. Min, and R. C. Cohen (2009), Eddy covariance fluxes of acyl peroxy nitrates (PAN, PPN and MPAN) above a Ponderosa pine forest, *Atmos. Chem. Phys.*, 9(2), 615-634.
- Zhang, J. M., et al. (2009), Continuous measurement of peroxyacetyl nitrate (PAN) in suburban and remote areas of western China, *Atmos. Environ.*, 43(2), 228-237.
- Zhang, L., M. D. Moran, P. A. Makar, J. R. Brook, and S. Gong (2002), Modelling gaseous dry deposition in AURAMS: a unified regional air-quality modelling system, *Atmos. Environ.*, 36(3), 537-560.

# Erklärung

(§ 5 Nr. 4 PromO)

Hiermit erkläre ich, dass keine Tatsachen vorliegen, die mich nach den gesetzlichen Bestimmungen über die Führung akademischer Grade zur Führung eines Doktorgrades unwürdig erscheinen lassen.

(§ 8 S. 2 Nr. 5 PromO)

Hiermit erkläre ich mich damit einverstanden, dass die elektronische Fassung meiner Dissertation unter Wahrung meiner Urheberrechte und des Datenschutzes einer gesonderten Überprüfung hinsichtlich der eigenständigen Anfertigung der Dissertation unterzogen werden kann.

(§ 8 S. 2 Nr. 7 PromO)

Hiermit erkläre ich eidesstattlich, dass ich die Dissertation selbständig verfasst und keine anderen als die von mir angegebenen Quellen und Hilfsmittel benutzt habe.

Ich habe die Dissertation nicht bereits zur Erlangung eines akademischen Grades anderweitig eingereicht und habe auch nicht bereits diese oder eine gleichartige Doktorprüfung endgültig nicht bestanden.

(§ 8 S. 2 Nr. 9 PromO)

Hiermit erkläre ich, dass ich keine Hilfe von gewerblichen Promotionsberatern bzw. -vermittlern in Anspruch genommen habe und auch künftig nicht nehmen werde.